3D MICROPATTERNABLE HYDROGEL SYSTEMS TO EXAMINE CROSSTALK EFFECTS BETWEEN MESENCHYMAL STEM CELLS, OSTEOBLASTS, AND ADIPOCYTES

A Dissertation
Presented to
The Academic Faculty

by

Taymour Marwan Hammoudi

In Partial Fulfillment
of the Requirements for the Degree
Doctor of Philosophy in the
Department of Biomedical Engineering

Georgia Institute of Technology
December 2012

3D MICROPATTERNABLE HYDROGEL SYSTEMS TO EXAMINE CROSSTALK EFFECTS BETWEEN MESENCHYMAL STEM CELLS, OSTEOBLASTS, AND ADIPOCYTES

Approved by:

Dr. Johnna S. Temenoff, Advisor
Department of Biomedical Engineering
Georgia Institute of Technology

Dr. Michael E. Davis
Department of Biomedical Engineering
Georgia Institute of Technology

Dr. Hang Lu, Advisor
School of Chemical & Biomolecular Engineering
Georgia Institute of Technology

Dr. Jason M. Hansen
Department of Pediatrics
Emory University School of Medicine

Dr. Todd C. McDevitt
Department of Biomedical Engineering
Georgia Institute of Technology

Dr. Alexandra Peister
Department of Biology
Morehouse College

Date Approved: August 8, 2012

To Mom, Dad, and Tarek
for their love, support, and encouragement that knows no bounds

ACKNOWLEDGEMENTS

I acknowledge and sincerely thank everyone who contributed to this work and supported me during my time as a graduate student. First, I wish to thank my committee members – Todd McDevitt, PhD, Mike Davis, PhD, Jason Hansen, PhD, and Alexandra Peister, PhD – for their valuable feedback, guidance, and insights over the course of my graduate career. They always challenged me to see further than the immediate scope of my project and to think in a much more nuanced way about the mechanisms underlying my experimental observations. Additionally, Dr. Davis has been a great advocate and advisor for me as a member of the MD/PhD Executive Committee. Dr. Peister provided valuable insight and expertise into mechanisms of MSC clonogenicity and differentiation, and was a great help during my initial foray into studying how these outcomes might be tested and thinking about various mechanisms. I sincerely appreciated the opportunity to learn redox biology from scratch through working with Dr. Hansen, in addition to gaining the experience of co-writing two grant applications that have provided me with a valuable experience as I further pursue my scientific career. I would especially like to acknowledge and thank Dr. McDevitt, along with his students and post-docs past and present, for their experimental advice and sharing their lab resources, and for teaching me to think about and use stem cells in new and exciting ways. I've thoroughly enjoyed my brainstorming sessions with Todd and Ken Sutha about the broader implications of our work and possible future directions. Todd and members of his lab have been great partners and fantastic neighbors to have, and am grateful to have some of my work contribute to a growing collaboration between our research groups. Furthermore, I owe a special thanks to Drs. Melissa Kemp and Catherine Rivet, who opened me up to the

world of systems biology and were instrumental in helping me to learn and understand methods of multivariate analysis that enabled me to appreciate the complexity and nuance of the platforms I developed as part of this dissertation. Dr. Kemp encouraged me to present my work at the Systems Biology of Human Disease International Conference, and this experience will undoubtedly influence the vein of research that I will pursue during my career. I would also like to acknowledge Dr. Brani Vidakovic for valuable expertise with statistical interpretation and consultation. Finally I would like to acknowledge my undergraduate academic advisor, Dr. Susan Blanchard, as well as my undergraduate research mentors Dr. Herman Staats, Dr. Celia LaBranche, Dr. David Weiner, Dr. Elizabeth Loboa, Dr. Marian McCord, and Dr. Lola Reid for cultivating my enthusiasm for teaching and research that propelled me to pursue a career as a physician scientist.

I wish to thank everyone in the Coulter Department of Biomedical Engineering and the Petit Institute for Bioengineering and Bioscience for their help and support. Shannon Sullivan, Sally Gerrish, Beth Bullock, and Penelope Pollard in BME have been invaluable resources and I will always appreciate their warmth and kindness that is so instrumental to making the BME community thrive. I have thoroughly enjoyed working with the BME Graduate Student Advisory Board with my colleagues as well as Shannon and Dr. Gilda Barabino to provide a student voice in striving to build and maintain our program as the best in the country. I wish to thank Franklin Bost and Marc McJunkin for allowing me the opportunity to TA their sophomore design lab for two semesters, which provided me with a great deal of training as a teacher that I will carry forth in my future career. They both taught me how to think out of the box and how to approach my project

from a design as well as an engineering perspective. I deeply appreciate the tremendous work that Steve Woodard, Aqua Asberry, Andrew Shaw, Jonafel Crowe, and Nadia Boguslavsky in maintaining our and operating our core facilities. I would especially like to acknowledge Aqua for her help in developing our new protocol that allowed us to successfully cryosection hydrogels and which is now used by several labs at Georgia Tech. I would also like to thank Megan McDevitt, Colly Mitchell, James Goddard, Janice Russell, and Alyceson Andrews in IBB for their tireless work in organizing numerous seminars and events and especially Colly for her work with the Petit Scholars program.

I owe a huge debt of gratitude to the Emory MD/PhD program for training me as a future physician scientist. I would especially like to thank: Dr. Chuck Parkos, our program director, who saw the potential and enthusiasm in me when I first interviewed for the MD/PhD program back in 2005; Mary Horton, our co-director and program "mom," for her tireless work and involvement in cultivating the community within our program, for checking in on me and providing emotional support when I needed it most, and for her involvement with the student leadership in recruitment and administration of the program; and Dr. Marie Csete, our former co-director and one of my rotation advisors, who constantly encouraged me to break down barriers and reach for the heavens as a scientist. I would like to thank Sabrina Mallett, Rebecca Sandidge, Maxine Wright-Thompson, and Barbara Powley for their administrative work both in and behind the scenes to make sure that our program runs like a well-oiled machine. I also wish to acknowledge the current senior students and graduates of the program for their mentorship and advice in negotiating the ups and downs of graduate school and life as an MD/PhD student.

To my advisors, Johnna and Hang, I cannot thank you enough for all your help and support over the years. I truly couldn't have asked for two better mentors than both of you and I will be forever grateful. You have pushed me to reach for the stars and to break boundaries with my research. I thank you for having faith in me, even when at times I didn't have faith in myself, and for pulling me back to planet Earth when I needed it most and keeping me grounded. Without you both, my graduate career would have been fraught with uncertainty and strife and I probably would have burned out and not made it through. You have cultivated my passions and turned me into a true multidisciplinary engineer and scientist, provided me with the skills and wherewithal to function as a professional researcher and mentor, and I thank you for giving me the freedom to explore new avenues with my research and for sharing your ideas. I don't think I could feel more prepared than I am now for what's to come and I look forward to continuing our work together in the future.

To my all my labmates, past and present, you have truly felt like a second family to me. Through thick and thin, you have always been more than just colleagues or fellow graduate students, and you have been the best friends I could ask for along this long and arduous journey that is grad school. I will always treasure your support, cooperation, and companionship. The friendship and the memories we shared mean more to me than you will ever know. To Kwanghun Chung, Matt Crane, Alison Paul, Ed Park, Jeff Stirman, and Catherine Rivet I thank you for providing the foundation on which the Lu lab now rests. Your passions were truly reflected in your work and I will always be grateful for the inspiration and guidance that you provided over the years. Ed, I continue to miss our early morning breakfasts and chats. Jeff, you were always a great person to have a beer

with and I appreciate your frankness and wearing your heart on your sleeve. Catherine, I will be forever grateful for your insights and training that helped take this work to new heights. Your passion is something I will always continue to emulate. Ivan Cáceres, I will always enjoy your humor and wit, and I continue to envy your ability to do great science while having such a productive social life outside of work. I can always count on you as the person in the know about how to have a good time. Mel Li, your smile is contagious and your heart is reflected in everything you do. Mei Zhan, you are a rock I have always appreciated your sharp wit and your laughter. Jan Krajniak and Loice Chingoza, we started in the Lu lab together and it's been a pleasure to have you both as wingmen throughout our tenure in the lab. Maria Elena Casas, you've been a great presence in the lab with your constant smile, great attitude and warm heart. To Derek Doroski and Kelly Brink, I will always appreciate the foundation you laid for the rest of us in the Temenoff Lab. Derek, you were the bedrock of the lab, and I will always appreciate our deep discussion and the ways in which you challenged me during your time here. Your leadership and warmth were always apparent and will leave an indelible mark on the culture of the lab. Kelly, I will always appreciate your laughter and kindness and it was great to have your welcoming presence in the lab when I started. While I'm still not sure if Harry Potter is a fad or phenomenon, I still appreciate you and the rest of the lab for introducing me to it nonetheless. Peter Yang, Jeremy Lim, Song Seto and Jen Lei have been great companions over the years. Peter, I will always appreciate hearing your stories and I missed having our daily interruptions as soon as you left the lab. I admire your passion, your style, and your appetite for life (and good food). Your self-awareness, tireless work, and insight have served as a useful guide. Jeremy, I have enjoyed sharing

the ‘bro cave’ with you these last few months, and you have truly been a ‘bro’ in every sense of the word. Your sense of humor always brightened my day, and you have always been a fantastic listener when anyone has needed an ear. Song, at times I feel you know me better than I know myself, and I have always been humbled by your maturity and sense of self. It’s been a lot of fun hanging out with you (and Masa) over these last few years. Jen, I’ve always enjoyed your bright and boisterous personality, as well as your love for all things puppies and Maryland, though I still refuse to cheer for any of your sports teams. Your laughter and passion have been an inspiration. To Torri and Melissa, while we only had a year together in the lab, you guys have still managed to teach me a lot about approaching science and reminded me about all the lessons I have occasionally failed to recall from my early years in grad school. I am especially thankful to Torri for all her invaluable help with the data collection and analysis that helped to solidify a story for the last chapter of this dissertation, and which I think will lead to a great manuscript in the near future. I would like to thank Dr. Sharon Hamilton for her friendship and mentorship during her tenure as a post-doc in the Temenoff and Lu labs. Without her expertise, I am not sure that the polymer chemistry and synthesis arms of my projects over the years would have ever taken off. Lastly, but certainly not least, I owe immeasurable thanks to Nathan Bloodworth, the first student I have ever mentored. Nathan’s knack for problem solving and his intellectual drive were another primary reason for the building success of this work, as well as a few independent projects that are still in development in the lab. Nathan, you have taught me as much as Johnna and Hang about being a great mentor. I am proud to count you as a colleague and a friend, and I wish you continued growth and success as a future physician-scientist.

Finally, I owe tremendous thanks to my mother, father, and my brother, Tarek. It is primarily because of your love and faith in me that I've been able to reach this long-awaited milestone. I almost quit, and if not for you, I likely would never have made it this far, and I will forever be grateful. Thanks for raising me right, for always pushing me to strive for my best, for teaching me to work hard (and to take a break every once in a while), for serving as great role models, for showing me how to open doors and take advantage of every opportunity, and for always providing an ear, a hug, and an occasional shoulder to cry on. Your unwavering support and encouragement provided the necessary foundation for my current and future success. I love you unfathomably, and I hope that I continue to make you all proud.

TABLE OF CONTENTS

Page

ACKNOWLEDGEMENTS iv

LIST OF TABLES vii

LIST OF FIGURES ix

LIST OF ABBREVIATIONS xii

LIST OF SYMBOLS xviii

SUMMARY xix

CHAPTER

1 INTRODUCTION 1

1.1 Motivation 1

1.2 Research Objectives 2

1.3 Significance and Scientific Contributions 7

2 BACKGROUND AND LITERATURE REVIEW 9

2.1 Overview 9

2.2 Mesenchymal Stem Cells and Their Fate 10

2.2.1 Self-Renewal and Clonogenicity 10

2.2.2 Differentiation Potential and Plasticity 11

2.2.3 Reciprocally Regulated Programs of Osteogenesis and Adipogenesis 12

2.3 Co-Dependence and Homeostatic Control of Bone Remodeling and Energy Metabolism 13

2.3.1 Physiological Observations 13

2.3.2 Clinical Correlates of Energy Metabolism and Skeletal Health 14

2.3.3 Knowledge of Feedback Loops Gained from Mechanistic Studies in Animal Models 18

2.3.4 Potential Roles of MSCs 19

2.4 Patterning of Hydrogels and Encapsulated Cells 20

2.4.1 Hydrogels as Biomaterials for Modeling Microenvironments 20

2.4.2 Micropatterning of Hydrogels and Encapsulated Cells 23

2.5 Co-Cultures to Examine Interactions between MSCs, Osteoblasts, and Adipocytes 28

2.5.1 Studies with Conditioned Medium 28

2.5.2 Co-Culture of Two Cell Types 29

2.6 Approaches Using Systems Biology to Understand Cell Fate and Applications to Tissue Engineering 30

2.7 Summary 32

3 LONG-TERM SPATIALLY DEFINED CO-CULTURE WITHIN THREE-DIMENSIONAL PHOTOPATTERNED HYDROGELS 33

3.1 Introduction 33

3.2 Materials and Methods 36

3.3 Results 43

3.4 Discussion 50

3.5 Conclusions 53

4 3D *IN VITRO* TRI-CULTURE PLATFORM TO INVESTIGATE EFFECTS OF CROSSTALK BETWEEN MESENCHYMAL STEM CELLS, OSTEOBLASTS AND ADIPOCYTES 55

4.1 Introduction 55

4.2 Materials and Methods 58

4.3 Results 65

4.4 Discussion 75

4.5 Conclusions 80

5 MESENCHYMAL STEM CELLS DISPLAY UNIQUE GENETIC AND PHENOTYPIC RESPONSES TO GLUCOSE PERTURBATION UNDER DIFFERENT MONO-, CO-, AND TRI-CULTURE CONDITIONS 81

5.1 Introduction 81

5.2 Materials and Methods 85

5.3 Results 94

5.4 Discussion 112

5.5 Conclusions 122

6 CONCLUSIONS AND FUTURE DIRECTIONS 124

6.1 Summary 124

6.2 Conclusions 127

6.3 Future Directions 134

APPENDIX A: DESIGN AND SCREENING OF CONJUGATED POLYMERS FOR HYDROGEL DEGRADABILITY, CYTOCOMPATIBILITY, AND CELL SPREADING 142

APPENDIX B: ADAPTED METHOD FOR CRYOPRESERVATION AND CRYOSECTIONING OF HYDROGELS 153

APPENDIX C: GUIDE TO MULTIVARIATE MODELING 158

REFERENCES 166

LIST OF TABLES

Page

Table 4.1: Library of lineage-specific mRNA transcripts for gene expression analysis 62

Table 5.1: Custom primers used for qPCR analysis of mRNA expression 91

Table A.1: Peptide criteria for successful conjugation and gelation using free-radical polymerization 145

Table A.2: Summary of peptides chosen for conjugation 146

LIST OF FIGURES

Page

Figure 2.1: A number of regulators control MSC fate. 13

Figure 2.2: Several distinct intercellular signaling networks that link bone and fat. 18

Figure 3.1: OPF hydrogels can be photolithographically patterned into a variety of three-dimensional shapes in a controllable, high fidelity manner at the micron to millimeter scale 44

Figure 3.2: Patterning fidelity of OPF hydrogels is enhanced under a nitrogen atmosphere, enabling fabrication of constructs with highly tunable aspect ratios. 46

Figure 3.3: Spatially controlled, tissue scale co-culture of multiple cell types can be realized through serial photo-crosslinking and lamination of hydrogels into templated patterns. 48

Figure 3.4: Primary tendon/ligament fibroblasts and marrow stromal cells remain viable during long-term culture after photopatterning. 50

Figure 4.1: Sample fabrication and study design. 60

Figure 4.2: Co-culture and tri-culture differentially affect expression dynamics of osteoblastic (*RUNX2* and *Osteocalcin*) and adipocytic (*PPARγ2* and *Leptin*) genes in adipocytes but does not affect triglyceride storage with time. 66

Figure 4.3: Co-culture and tri-culture differentially affect expression dynamics of osteoblastic (*RUNX2* and *Osteocalcin*) and chondrogenic (*SOX9*) genes in osteoblasts, in addition to alkaline phosphatase activity persistence with time. 67

Figure 4.4: Co- and tri-culture differentially affect expression levels of several lineage-specific transcription factors (but not terminal differentiation markers) in MSCs, while only causing scant and transient alkaline phosphatase expression in MSCs from osteoblast-containing cultures. 69

Figure 4.5: Statistical modeling based on covariance of the expression of several mesenchymal lineage genes yields two latent variables that are able to distinguish MSCs from adipocytes and osteoblasts, respectively, and elucidates the correlation structure of the gene expression at various time points with each cell type present. 71

Figure 4.6: PLS-DA models of single cell types can robustly separate cell samples derived from different culture conditions and describe the important gene expression variables that correlated with each response to co- or tri-culture. 74

Figure 5.1: Sample fabrication and construct design. 87

Figure 5.2: Study design. 89

Figure 5.3: Cell viability of hMSCs in mono-, co-, and tri-culture under different glucose conditions. 95

Figure 5.4: Varying glucose content differentially modulates gene expression responses in hMSCs from each culture type. 96

Figure 5.5: Mono-, co-, and tri-culture differentially modulate gene expression of mesenchymal lineage marks and glucose-responsive transcription factors in response to varying glucose content. 100

Figure 5.6: Mono-, co-, and tri-culture interact with glucose condition to alter clonogenicity of hMSCs. 102

Figure 5.7: Statistical modeling based on maximum variance of the gene expression data set yields three principle components that indicate most of the variance arises from differences in culture type and elucidates the correlation structure of the gene expression at various time points. 104

Figure 5.8: Statistical modeling based on covariance of the gene expression data yields three latent variables that distinguish hMSCs from each culture type and elucidates its correlation structure with gene expression at various time points. 105

Figure 5.9: PCA within each culture type demonstrates that more than 60% of the variance between samples may be explained by differences from exposure to normal or high glucose. 107

Figure 5.10: PLS-DA models of individual culture types can robustly distinguish hMSC samples cultured under different glucose conditions and describe the important gene expression variables that correlate with response to glucose level. 109

Figure 5.11: Statistical modeling based on covariance of hMSC gene expression data with colony formation yields two latent variables that are able to distinguish hMSCs from different culture types and glucose conditions and elucidates that correlation structure of gene expression and colony formation. 112

Figure A.1: Alginate and Factor Xa-sensitive gels are cytocompatible but demonstrate differences in MSC cell spreading over 7 days in culture. 150

Figure A.2: Mono-cultured adipocytes, osteoblasts, and MSCs demonstrate adequate cell viability when encapsulated in collagenase sensitive gels and no observable cell spreading after 7 days in culture. 151

LIST OF ABBREVIATIONS

2D	two-dimensional
3D	three-dimensional
A/A	antibiotic/antimycotic
AAA	Culture type: hAd-hAd-hAd
αMEM	Minimal Essential Medium - Alpha
AcCl	acryloyl chloride
Acrl-PEG-SVA	acryl-poly(ethylene glycol)-succinimidyl valerate
ACTB	actin, beta
ADIPOQ	adiponectin
ALPL	alkaline phosphatase, liver/bone/kidney; or alkaline phosphatase, tissue-nonspecific isozyme
AMA	Culture type: hAd-hMSC-hAd
ATF2	activating transcription factor-2
ANOVA	analysis of variance
bFGF	basic fibroblast growth factor
BGLAP	bone γ-carboxyglutamate (gla) protein (see also *OCN*)
BMP	bone morphogenetic protein
bMSCs	bovine marrow stromal cells
Ca^{2+}	divalent calcium
CD45	protein tyrosine phosphatase, receptor type, C (PTPRC); or leukocyte common antigen (LCA)
CD146	melanoma cell adhesion molecule (MCAM); or cell surface glycoprotein MUC18

cDNA	complementary DNA
CEBPB	CCAAT/enhancer binding protein (C/EBP), beta
CFU-F	colony-forming unit-fibroblast
CMFDA	carboxymethyl fluorescein diacetate
CMRA	5-(((4-chloromethyl)benzoyl)amino)tetramethyl rhodamine
COL1A2	collagen alpha-2(I) chain
CO_2	carbon dioxide
D2959	Darocur 2959
DAPI	4',6-diamidino-2-phenylindole
DCM	dichloromethane
dH_2O	distilled water
DM	diabetes mellitus
DMEM	Dulbecco's Modified Eagle Medium
DMSO	dimethyl sulfoxide
DNA	deoxyribonucleic acid
DNase I	deoxyribonuclease-1
dNTP	deoxyribonucleotide triphoshphate
dsDNA	double-stranded DNA
DXA (formerly DEXA)	dual-energy X-ray absorptiometry
ECM	extracellular matrix
EDTA	ethylenediaminetetraacetic acid
EthD-1	ethidium homodimer-1
ex/em	excitation/emission

FBS	fetal bovine serum
FEP	fluorinated ethylene propylene
FOXO1	forkhead box O1
FuCl	fumaryl chloride
G-CSF	granulocyte colony-stimulating factor
gla	γ-carboxyglutamic acid
GPC	gel permeation chromatography
GRGDS	glycine-arginine-glycine-aspartic acid-serine polypeptide
HA	hyaluronic acid
hAd	human adipocyte
HCl	hydrochloride (salt)
HEPES	4-(2-hydroxyethyl)-1-piperazineethanesulfonic acid
hMSC	human mesenchymal stem cell
hOb	human osteoblast
HOMA-2	Homeostasis Model Assessment-2
HSC	haematopoietic stem cell
IBMX	3-isobutyl-1-methylxanthine
^{1}H-NMR	proton nuclear magnetic resonance
^{3}[H]-thymidine	tritiated thymidine
Ibsp	integrin-binding sialoprotein (or bone sialoprotein, BSP)
JUN	jun proto-oncogene
K_2CO_3	potassium carbonate
LEP	leptin

LEPR	leptin receptor
LPL	lipoprotein lipase
LV	latent variable
Mg^{2+}	divalent magnesium
$MgSO_4$	magnesium sulfate
MMM	Culture type: hMSC-hMSC-hMSC
MMP	matrix metalloproteinase
mRNA	messenger ribonucleic acids
MW	molecular weight
$NaHCO_3$	sodium bicarbonate
NEAA	non-essential amino acids
NFKB1	nuclear factor of kappa light polypeptide gene enhancer in B-cells 1
OCN	osteocalcin (see also *BGLAP*)
OCT	optimal cutting temperature compound
$Oligo(dT)_{15}$	$oligo(deoxy\text{-}thymine)_{15}$
OMA	Culture type: hOb-hMSC-hAd
OMO	Culture type: hOb-hMSC-hOb
OOO	Culture type: hOb-hOb-hOb
OPF	oligo(poly(ethylene glycol) fumarate)
OPG	osteoprotegerin
Opn	osteopontin
OSX	osterix
PBS	phosphate-buffered saline

PC	principle component
PCA	principle component analysis
PDMS	poly(dimethyl siloxane)
PEG	poly(ethylene glycol)
PEG-DA	poly(ethylene glycol)-diacrylate
PLS	partial least squares/projections to latent structures; or partial least squares regression (PLSR)
PLS-DA	partial least squares discriminant analysis
PPARG2	peroxisome proliferator-activated receptor-γ, isoform 2
PSN	penicillin, streptomycin, neomycin
PTH	parathyroid hormone
qPCR	quantitative reverse transcription polymerase chain reaction
ROS	reactive oxygen species
RPS18	ribosomal protein S18
RUNX2	runt-related transcription factor 2
s.d.	standard deviation
SEM or (s.e.m.)	standard error of the mean
SFL	stop-flow lithography
T1DM	type I diabetes mellitus (also insulin-dependent DM, IDDM)
T2DM	type II diabetes mellitus (also non-insulin-dependent DM, NIDDM)
TCF/LEF1	lymphocyte enhancer-binding factor 1
TCPS	tissue-culture polystyrene
TEA	triethylamine
Tris	tris(hydroxymethyl)aminomethane

UV	ultraviolet
XXX_Norm/High_#	Culture Type_ Glucose_Sample Number
YIGSR	tyrosine-isoleucine-glycine-serine-arginine polypeptide

LIST OF SYMBOLS

c	weight of Y-variable on LV a
C_t	cycle threshold
E	PCR efficiency
$\overline{E}$	mean PCR efficiency
K	number of X-variables
M (or m)	number of classes or response variables (Y-variables)
n	sample number
N	number of observations
N_0	starting amplicon number
N_t	amplicon number at cycle threshold t
p	probability-value threshold for statistical significance
p_a	loading of variable on PC a
Q^2	model predictive quality
R^2X	coefficient of determination for model of $\boldsymbol{X}$
R^2Y	coefficient of determination for model of $\boldsymbol{Y}$
t_a	score on PC or LV a
w_a^*	weight of X-variable on LV a
$\mathbf{X}$	$N \times K$ matrix of observations and variables
$\mathbf{Y}$	$N \times M$ matrix of observations and response variables or classes

SUMMARY

Poor skeletal health results from aging and metabolic diseases such as obesity and diabetes and involves impaired homeostatic balance between marrow osteogenesis and adipogenesis. Tissue engineering provides researchers with the ability to generate improved, highly controlled and tailorable in vitro model systems to better understand mechanisms of homeostasis, disease, and healing and regeneration. Model systems that allow assembly of modules of MSCs, osteoblasts, and adipocytes in a number of configurations to engage in signaling crosstalk offer the potential to study integrative physiological aspects and complex interactions in the face of changes in local and systemic microenvironments. Thus, the overall goal of this dissertation was to examine integrative physiological aspects between MSCs, osteoblasts, and adipocytes that exist within the marrow microenvironment.

To investigate the effects of intercellular signaling in different microenvironmental contexts, methods were developed to photolithographically pattern and assemble cell-laden PEG-based hydrogels with high spatial fidelity and tissue-scale thickness for long-term 3D co-culture of multiple cell types. This platform was applied to study effects of crosstalk between MSCs, osteoblasts and adipocytes on markers of differentiation in each cell type. Additionally, responses of MSCs to systemic perturbations in glucose concentration were modulated by mono-, co-, and tri-culture with these cell types in a model of diabetes-induced skeletal disease. Together, these studies provided valuable insight into unique and differential effects of intercellular signaling within the niche environment of MSCs and their terminally differentiated

progeny during homeostatic and pathological states, and offer opportunities further study of integrative physiological interactions between mesenchymal lineage cells.

CHAPTER 1

INTRODUCTION

1.1 Motivation

Osteopenia and osteoporosis are the most common metabolic disorders of bone formation and remodeling that are exceedingly prevalent in young and adult populations, affecting 200 million individuals worldwide [1, 2]. They constitute the most common cause of fractures (> 1.5 million/year) in the United States [3, 4]. These fractures lead to more than 500,000 hospitalizations, over 800,000 emergency room encounters, more than 2.6 million physician office visits, and the placement of nearly 180,000 individuals into nursing homes [4]. Caring for these fractures is expensive: annual direct care expenditures for osteoporotic fractures range from $12-18 billion/year and indirect costs (e.g., lost productivity for patients and caregivers) likely add billions more to this figure [4, 5]. By 2020, one in two Americans over age 50 is expected to have or be at risk of developing osteoporosis of the hip; even more will be at risk of developing osteoporosis at any site in the skeleton [4, 5]. Available treatment options are supportive rather than curative and oftentimes are associated with persistent patient morbidity, further fractures, and eventually mortality [5, 6].

Primary causes of osteoporosis include age and estrogen deficiency arising from menopause, while secondary osteoporosis can result as a consequence of disorders of energy metabolism such as anorexia nervosa, obesity, and diabetes mellitus [7-11] that are accompanied by their own exorbitantly high prevalence, costs, and morbidities [12-17]. These individuals experience varying degrees of an imbalance between bone deposition and bone resorption, resulting in progressive loss of bone mineral density and skeletal fragility. These changes are accompanied by excess marrow adipogenesis beyond that which develops during the peak time of bone acquisition. Osteoblasts and adipocytes together represent the result of divergent, reciprocally regulated differentiation programs of a common multipotent precursor within the marrow stroma: mesenchymal stem cells

(MSCs). Previous research suggests that there is paracrine signaling between osteoblasts and adipocytes *in vivo* that may affect these divergent, reciprocally regulated MSC differentiation programs [2, 10, 18]. Additionally, elegant work in mouse models has demonstrated that there exists a significant integrative crosstalk between bone and energy metabolisms controlled through neural and endocrine mechanisms and that osteoblasts and adipocytes participate in this crosstalk through secretion of soluble mediators [19-27].

However, due to a dearth of *in vitro* models to study effects of multidirectional crosstalk between MSCs, osteoblasts, and adipocytes, it is not clear to what extent paracrine signaling from nearby cells may direct differentiation and stemness properties of multipotent MSCs, particularly in the context of diseases that result in excess adipogenesis and impaired osteogenesis. This lack of knowledge hinders the development of systemic therapies to regulate formation of adipose stores, restore normal metabolic functions and glucose homeostasis, and rescue the normal osteopoietic environment that balances bone deposition with resorption. Additionally, this hampers the ability to harness the healing potential of endogenous MSCs for treating a variety of musculoskeletal injuries. MSC lineage allocation along with neural and endocrine homeostatic control of their differentiated counterparts balances the process of bone deposition and energy storage as fat to support an energy-intensive remodeling process. Examining the interplay between MSCs, osteoblasts, and adipocytes is therefore crucial to understanding the pathophysiology of osteoporosis and metabolic disorders and development of targeted systemic molecular and cytotherapies.

1.2 Research Objectives and Specific Aims

Thus, the goal of this project is to design and implement a 3D *in vitro* tri-culture system to examine integrative physiological aspects between multiple cell types that exist within the marrow microenvironment. This research will elucidate the roles of osteoblasts

and adipocytes in priming MSC fate and simultaneously evaluate the temporal effects of MSCs on osteoblast-adipocyte crosstalk. This project will use PEG-based hydrogels as a 3D scaffolding platform to model a portion of the marrow microenvironment and study aspects of the integrative MSC, osteoblast, and adipocyte interactions that may govern bone metabolism. The rationale for this project is that by patterning and laminating hydrogel modules containing different cell types into a single structure, this system may be used simultaneously to interrogate paracrine signaling effects of multiple cell types on each other and retain the ability to separate cells after the tri-culture period for analyses of individual cell types. The **central hypothesis** of this work is that this tri-culture system will allow us to demonstrate how MSC lineage allocation and differentiation are affected by osteoblasts and adipocytes, and how MSCs in turn are affected by their neighboring cell types in response to pathophysiological levels of glucose as a model for diabetes. This hypothesis will be investigated in the following three specific aims:

Hypothesis I: 3D laminated hydrogel modules will facilitate culture of multiple cell types in tandem for a specified time, after which cell types may be isolated and separately analyzed for genotypic and phenotypic characteristics.

Specific Aim I: Design and develop methods for photopatterning cell-laden, 3D hydrogel constructs for spatially controlled long term co-culture and subsequent separation of multiple cell types.

Spatiotemporally controlled co-culture in three-dimensional (3D) environments that appropriately mimic *in vivo* tissue architecture is a highly desirable goal in studies of stem cell physiology (e.g. proliferation, matrix production, and tissue repair) and in enhancing the development of novel stem cell-based clinical therapies for a variety of ailments. Current technologies that enable co-culture of two cell types largely rely on 2D culture that does not adequately recreate the native tissue environment or allow separation of the two cell populations for further downstream culture and analytical assays. Therefore, the objective of

this aim was to develop techniques to accomplish photopatterning, cell encapsulation, and 3D co-culture, and selective on-demand separation of different populations of cells post-culture. The rationale for this aim was that successful completion of the proposed experiments would lead to a vastly improved technological platform for studying the effects of soluble factors on cell fate and physiology of multiple cell types simultaneously.

The general goals of this aim were: 1) to design photopatternable polymer systems for cell encapsulation, requiring optimizing chemistry of the materials, processing conditions, as well as the overall design of the encapsulation scheme; 2) to design cytocompatible cell-laden constructs that enable long-term (2-3 wks) co-culture of multiple cell populations; and 3) to design a selective enzyme-degradable system where each population of cells could be easily separated after co-culture for detailed gene expression and phenotypic analyses (see Aims II and III). At the completion of Aim I, we were able to pattern, with high fidelity and resolution, specifically designed co-culture constructs. Furthermore, our process maintained cell viability, was compatible with established microscopy, histology, and other techniques for characterization, and permitted successful release of cell populations from the construct. Such results are important because this technology was further applied in Aims II and III to improve understanding of how 3D co-culture of MSCs, osteoblasts, and adipocytes affects changes in clonogenicity and plasticity of MSCs and their derivatives with time along with differential responses to each other under systemic alterations in glucose concentration.

Hypothesis II: MSCs will contribute to osteoblast and adipocyte populations through lineage allocation and differentiation that are biased by the relative amount of each cell type in the tri-culture construct over weeks of long term culture.

Specific Aim II: Assess gene expression and histological markers of differentiation in MSCs and their derivatives with time in response to differential amounts of osteoblasts and adipocytes in co-culture or tri-culture settings.

Design of optimal MSC-based treatment strategies for osteoporosis and other

diseases of bone remodeling have been hampered by a lack of knowledge of how MSCs interact with resident osteoblasts and adipocytes (either prior to their harvest for *ex vivo* expansion and modification, or after their transplantation into the bone marrow cavity). MSCs must maintain their propensity to regenerate an adequate osteopoietic environment through sufficient and appropriate lineage allocation and differentiation to restore absent osteoblast function. Additionally, this requires continued maintenance of self-renewal and plasticity of MSCs in the face of a dynamic niche that contains osteoblasts and adipocytes supplying regulatory cues that encourage their differentiation. Thus, the objective of this Aim was to determine how co- and tri- culture of MSCs with osteoblasts and/or adipocytes differentially affects gene expression of markers of mesenchymal lineage specification in MSCs, osteoblasts, and adipocytes in response to prolonged co- and tri-culture.

To attain this objective, we used an experimental approach centered on the micropatterned hydrogel layering system developed in Aim I combined with quantitative multivariate statistical analysis methods (principle component analysis and partial least squares discriminant analysis). The rationale for this Aim was that successful completion of the proposed study would contribute important knowledge about effects of soluble signals derived from MSCs, osteoblasts, and adipocytes on each others' level of lineage commitment and differentiation. The acquisition of such knowledge is critical to determining optimal dosage and timing of MSC-based treatments for osteoporosis and other diseases of bone remodeling, as well as the design of carrier materials that modulate the MSC niche to produce the desired differentiation outcomes. At the completion of Aim II, hydrogel constructs demonstrating various amounts of MSC lineage commitment in the absence of complete differentiation were produced depending on the culture configuration. Multivariate analysis of the entire gene expression data set enabled us to distinguish differential responses in each encapsulated cell type to its co- or tri-culture condition over the course of 18 days. Additionally, histological markers of differentiation were uniquely affected in osteoblasts and MSCs by the co- or tri-culture condition applied. Such results are important because the location and extent of changes in osteoblastic or adipocytic gene expression provided key

first information about the effect of the presence of multiple cell types and the role of soluble factors on elements of the MSC niche within the bone marrow and MSC contributions to marrow osteogenesis and adipogenesis. This information may be used to direct future MSC-based approaches to encourage trabecular bone formation and appropriate bone remodeling through improved knowledge about how MSCs and their placement relative to native osteoblasts and adipocytes affect tissue formation from all three cell types. These results could also be extended to create model systems to study the roles of stem and progenitor cells in disease pathophysiology, as studied in Aim III.

Hypothesis III: Each culture environment will produce a unique response by MSCs to glucose perturbation, and in particular that cultures containing adipocytes will produce the most detrimental effects on cell viability and clonogenicity since they produce pro-inflammatory cytokines and oxidative stress in response to hyperglycemia.

Specific Aim III: Assess differential modulation of gene expression, cell viability, and clonogenicity of MSCs with time in response to systemic alterations in glucose under mono-, co-, and tri-culture settings with osteoblasts and adipocytes.

Design of appropriate therapies, whether molecular or cellular in nature, that effectively target a dysregulation system of energy metabolism and bone remodeling have been hampered by a lack of knowledge of how MSCs, osteoblasts, and adipocytes work in concert to absorb and respond to systemic perturbations of glucose. The role of each cell type in cell- and non-cell autonomous responses to normal and pathological fluctuations is difficult to elucidate using traditional *in vitro* models systems. Thus, the objective of this Aim was to determine how mono-, co-, and tri-culture of MSCs, osteoblasts, and/or adipocytes differently affects each others' gene expression and fate (cell viability and MSC clonogenicity) in response to normal and pathological levels of systemically administered glucose.

To attain this objective, we used the same experimental approach centered on the micropatterned hydrogel layering system developed in Aim I and evaluated in Aim II combined with quantitative multivariate statistical analysis methods to correlate treatments (culture type and glucose condition) with gene expression responses, and further correlate these outcomes with functional responses (cell viability and MSC clonogenicity). At the completion of Aim III, MSCs displayed different genotypic and cell fate responses governed predominantly by the neighboring cell types when responding to perturbations in glucose levels, rather than a singular, monotonic response to glucose level regardless of culture type. Such results are important because they conclusively demonstrated that the microenvironment sensed by the MSCs dictates their response and validated this platform as an approach for studying the systems level behavior of multiple cell types in response to physiological and disease states.

1.3 Significance and Scientific Contributions

The dissertation research described herein provides critical insight into the effects of crosstalk between MSCs, osteoblasts, and adipocytes in multiple environments. The use of a modular tri-culture system, in which the biomaterial niche of each cell type may be tightly controlled through the addition of adhesion and degradable biofunctionalities, permits explicit control of cellular behaviors and simultaneously enables dissecting the effects on each cell type through its separability after culture. Developing techniques for lamination of each hydrogel module of cells to form an integrated construct enabled the exchange of soluble signals between each cell type and generated unique responses depending on the composition of the modules. The addition of degradable moieties patterned within specific modules enabled isolation of specific cell populations for further phenotypic studies. This integrated platform provides an essential tool for studying the behavior that emerges from the interacting encapsulated cells and allows for additional perturbation of the tailored microenvironment by exogenously added stimuli

during any point in the culture to elicit different responses. While evaluated herein with MSCs, osteoblasts, and adipocytes, these functions readily facilitate the application of this platform to multicellular co-culture to model a host of different tissues.

This research is innovative because this versatile platform allows for the study of integrative physiological and pathophysiological processes governing the lifelong process of continuous bone remodeling and its interdependence with energy metabolism. Simultaneous co- and tri-culture of MSCs, osteoblasts, and adipocytes has yet to be examined in such a controlled manner in a physiologically representative, 3D model system, despite the suggested interplay between all three cell types in the bone marrow microenvironment and within the context of communicating with multiple other tissues and organs. This work is significant because it elucidates the contributions of diffusible biomolecular cues from neighboring terminally differentiated cells on stem cell fate decisions together with stem cell contributions to terminally differentiated cell function. Additionally, it represents a first attempt to use a controlled 3D environment to understand how soluble factors influence systems-level interactions between multiple cell types such as those present during bone deposition and remodeling in the marrow microenvironment. The development of such precisely-controlled test platforms is of critical importance in furthering basic understanding of how progenitor cells interact with native cells to effect normal physiological processes, disease pathogenesis, and tissue healing. Knowledge derived from both crosstalk aspects described in these studies will inform further studies of MSC niche characteristics. Therefore, in the future, we expect results from these studies to lead to improved rational design of molecular, biomaterial, stem cell and combination regenerative therapies for the prevention and treatment of disorders of skeletal function resulting from dysregulated energy metabolism.

CHAPTER 2

BACKGROUND AND LITERATURE REVIEW

2.1 Overview

This chapter summarizes the literature relevant to the work completed in this dissertation. It begins with a summary of mesenchymal stem cell biology, including their discovery, self-renewal and clonogenicity, differentiation potential, plasticity, and in particular focuses on the reciprocally regulated differentiation pathways of osteogenesis and adipogenesis relevant to the work to be described in later chapters. This is followed by an introduction into recent literature detailing how bone remodeling in vertebrate organisms is inextricably coupled with energy metabolism, including: physiological observations supporting their co-dependence and homeostatic control, clinical consequences of dysregulation within this multi-organ system, knowledge gained on key mechanisms of its control from animal models, and the possible role that mesenchymal stem cells play in these integrated processes. It then delves into literature concerning contemporarily available, physiologically relevant *in vitro* model systems based on three-dimensional hydrogels developed for tissue engineering and regenerative medicine that may be applied towards gaining a deeper understanding of the effects of mono-, co-, and tri-culture of MSCs, osteoblasts, and adipocytes on each others' behavior and response as a system to environmental perturbations. Subsequently, current experimental results from conventional monolayer and 2D co-culture of MSCs, osteoblasts and/or adipocytes are reviewed. Finally, an introduction to systems biological approaches to understanding cell fate decision processes and the current state of their application towards tissue engineering is discussed.

2.2 Mesenchymal Stem Cells and Their Fate

2.2.1 Self-Renewal and Clonogenicity

Through a seminal series of experiments in which bone marrow fragments or bone marrow stromal cells were transplanted into ectopic sites outside of the bone medullary cavity to reconstitute haematopoiesis,[28] Tavassoli and Crosby discovered the formation of an ectopic "ossicle" mimicking and reconstituting the haematopoietic and adventitial architecture of the marrow cavity. In a series of seminal experiments thereafter, Friedenstein *et al*. assigned this osteogenic potential first to non-haematopoietic, adherent stromal cells able to form single cell-derived colonies when grown in culture at low density [29, 30]. This was later followed by the observation that heterotopic transplants of cell strains originating from a single clonogenic cell could generate a variety of skeletal tissues (including bone, fat, cartilage, and fibroblasts) [31, 32]. These experiments proved multipotency of single clonogenic bone marrow stromal cells, and their ability to generate differentiated phenotypes [33-43]. Several contemporary experiments have confirmed that a sub-population of $CD45^-$ $CD146^+$ marrow stromal cells comprise the colony-forming adventitial reticular cells within bone marrow and self-renew *in vivo* through serial transplantation experiments [44-47].

MSCs are of great interest for cell-based therapies because they can be easily isolated and expanded *in vitro* with a high rate of proliferation without phenotypic changes before lineage-specific differentiation [48, 49]. MSCs are endowed with clonogenic capacity when plated at extremely low density (1-2 cells/cm^2) *in vitro* as evidenced by their ability to generate colony-forming unit-fibroblasts (CFU-F) for up to at least 4 passages without spontaneous differentiation and maintenance of normal karyotype and telomerase activity [35, 50-56]. The high proliferation rate of stem cells combined with the ability of these cells to remain in an undifferentiated state can result in a dramatic increase in the expansion of total cells while in culture, making it relatively

easy to produce enough cells to fill large tissue defects for clinical applications [48, 49, 57, 58].

2.2.2 Differentiation Potential and Plasticity

MSCs are endowed with the ability to differentiate into elements of the skeletal system including bone, cartilage, fat, muscle, fibroblasts and stromal cells supportive of a reticular vascular network and haematopoiesis [42, 59]. Through *in vitro* experiments, MSCs have been derived into: osteoblasts, which are responsible for depositing collagen type I remodeling it and mineralizing it to form new bone tissue and regulating energy metabolism in concert with adipocytes (Section 2.3.3); chondrocytes, which synthesize collagen type II and proteoglycans and aggrecan that form cartilaginous tissues; adipocytes, which convert glucose to triglycerides to store it for future metabolic demands and also participate in regulating energy metabolism (Section 2.3.3); fibroblasts, which deposit various forms of extracellular matrix and form the cellular units of connective tissues such as tendons and ligaments; and stromal or perivascular cells that stabilize vascular networks and regulate the haematopoietic stem cell (HSC) niche in bone marrow [42-44, 59]. Cell fate and differentiation of stem cells into these many phenotypes is affected by interactions between both biochemical and mechanical factors (Figure 2.1; [48, 49, 57, 58, 60-73]). Another integral property of MSCs is their *in vitro* plasticity (yet to be observed *in vivo*), characterized by the ability to acquire a phenotype of a more differentiated derivative under a defined set of culture conditions [74], followed by reversion to their original phenotype long after removal of those conditions, and application of a different set to produce another phenotype [39, 56, 75, 76]. A potential mechanism for this plasticity, similar to that present in haematopoietic stem cells (HSCs), is that MSCs express a subset of genes associated with the differentiation pathways to which they commit; differentiation along a given pathway is thus

characterized by increased expression of marker genes associated with this pathway and the decreased expression of genes related to other lineages [39, 77].

2.2.3 Reciprocally Regulated Programs of Osteogenesis and Adipogenesis

The phenomena of differentiation potential and plasticity of MSCs are perhaps most readily discerned from examining the reciprocally regulated differentiation programs of adipogenesis and osteogenesis in cultures of MSCs: both RUNX2 and PPARγ master transcriptional regulators are present in low levels in undifferentiated cells, and differentiation towards one lineage completely suppresses genes associated with the other lineage [10, 18, 78]. Differentiation towards either pathway is regulated by a complex set of paracrine signals, including BMPs, Wnts, PPARγ ligands, corticosteroids, and growth factors [18, 79, 80] – all derived from or regulated by cells in the neighboring niche environment including osteoblasts, adipocytes, HSCs, and endothelial cells [38, 47, 80, 81]. Additionally MSC differentiation into either adipocytes or osteoblasts corresponds to unique intracellular redox profiles [82], and each cell type can further modify their extracellular redox environment [83] to be more oxidizing (adipocytes) or reducing (osteoblasts) – suggesting that differentiation into specific phenotypes is likely also regulated by redox states that are permissive to a specific developmental process. Importantly, the pathogenesis of osteoporosis represents a significant imbalance between these reciprocally regulated differentiation programs, with the production of excess marrow adipose tissue at the expense of osteoblasts that deposit new bone in the face of osteoclast resorption [2, 3, 8, 10, 11, 78, 80, 84-86]. These regulatory mechanisms are summarized in Figure 2.1.

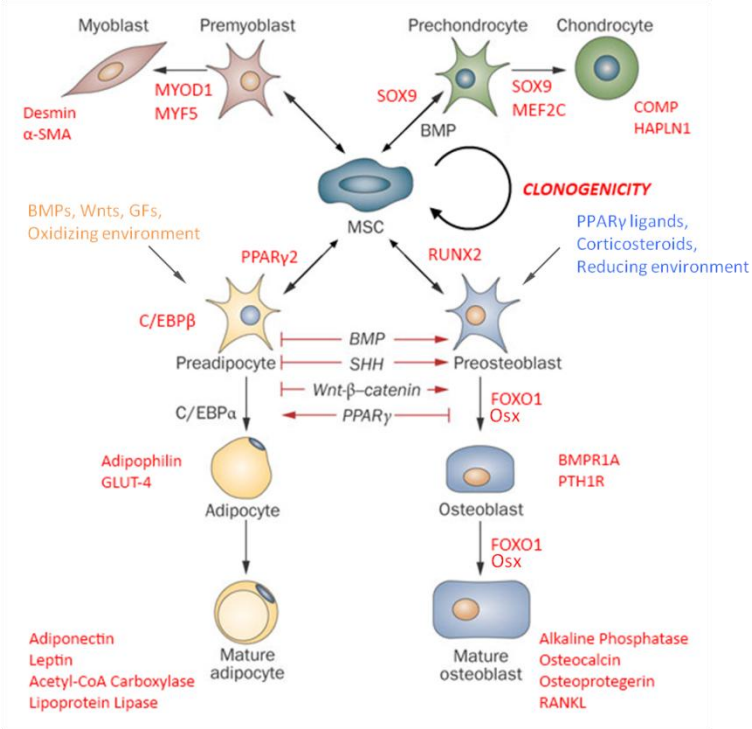

Figure 2.1. A number of regulators control MSC fate. Adapted from [87]with permission.

2.3 Co-Dependence and Homeostatic Control of Bone Remodeling and Energy Metabolism

2.3.1 Physiological Observations

Several physiological observations suggest that bone remodeling and energy metabolism are co-dependent and homeostatically regulated [3, 10, 88, 89]. Bone resorption by osteoclasts (derived from the macrophage lineage of HSCs) and deposition by osteoblasts occur in a balanced manner to maintain bone mass and quality and occur nearly constantly during adulthood [90, 91]. This serves to support the many functions of bone, including: maintaining blood calcium levels, providing mechanical support to soft tissues and points of contact to initiate and constrain muscle movement, supporting haematopoiesis, and protection of several solid organs (*e.g.* brain, spinal cord, heart, lungs). All of these demands correspond with molecular and mechanical sources of

regulatory feedback controls to couple bone deposition with resorption to facilitate homeostatic bone remodeling. Homeostatic failure results in numerous pathologies as described below (Section 2.3.2). This constant remodeling activity constitutes a significant metabolic demand and requires a constant supply of energy [24]. Indeed, marrow fat is non-existent at birth and immediately begins accumulating rapidly during the time of peak bone acquisition [3, 10, 78, 92-94]. Due to the need to promote longitudinal bone growth in children and adolescents and as the result of repeated loading and occasional injury that produces macro- and microdamage (*i.e.* fractures), an enormous energetic cost is associated with the daily destruction of bone by osteoclasts and the *de novo* bone formation to replace what has been resorbed. A purported function of marrow adipocytes is to provide an energy source for these catabolic and anabolic processes [10, 78, 95]. Otherwise, vertebrate mobility cannot be preserved [96] and thereby this function can be considered not as a mere particularity of vertebrate physiology but as a survival function for this branch of evolution. These observations together illustrate the essential need for there to be conserved mechanisms for both co-dependence and co-regulation of energy metabolism and skeletal remodeling in vertebrate organisms.

2.3.2 Clinical Correlates of Energy Metabolism with Skeletal Health

2.3.2.1 Anorexia Nervosa

Abnormities in fat metabolism associated with extreme under- (anorexia nervosa) and over-nutrition (obesity) in animal models and humans enable a global consideration of the relationship between fat and bone [4, 11]. Anorexia nervosa is characterized by self-induced starvation that leads to severe decreases in body fat and muscle mass among other physiological abnormalities such as impairment of insulin-stimulated glucose disposal, failure of nonoxidative glucose metabolism, and increased levels of adiponectin [11, 97, 98]. Together these lead to profound osteopenia and osteoporosis in adolescents

and adults, with some notable differences [97, 99-101]. In adults, observation of decreased markers of osteogenesis coupled with increased markers of resorption have been described, leading to the hypothesis that low osteoblast and high osteoclast activity are responsible for rapid and profound bone loss. By contrast, adolescents show a generalized reduction in bone turnover markers. Bone formation is markedly reduced, whereas bone resorption is increased with a paradoxical increase in marrow fat [102-106]. Weight recovery causes increases in bone formation and decreases in bone resorption [107-109]. In sum, the skeletal components of this disease are directly related to changes in body composition and energy metabolism.

2.3.2.2 Overweight and Obesity

Body weight represents an important risk factor for vertebral and hip fractures since it impacts both bone turnover and bone density [7, 94, 110], yet there is a controversy over whether this is in fact protective or detrimental for skeletal health. Confirming results observed in patients with low body mass index (BMI; e.g. anorexia nervosa, see Section 2.3.2.1 above), a recent meta-analysis clearly indicated that high body mass index is protective against total fractures, osteoporotic fractures and hip fractures and is seen equally in men and women [111]. Those long-standing observations imply that adipose tissue not only insulates the skeleton but may also exert an increased mechanical load to cortical elements of the bone that provides a cue for more bone deposition [112]. This would seem to indicate that overweight and obese individuals are protected from low bone mineral density and bone quality. Additionally, adipose tissue produces leptin (see Section 2.3.3) that may directly stimulate bone formation [26, 27].

However, several cohort studies have indicated that when fat and lean masses are measured with dual-energy X-ray absorptiometry (DXA), fat mass alone was found to be a significant risk factor for hip fractures in adults [113-115] and numerous areas of fracture in children [116]. During ageing, menopause and glucocorticoid therapy, fat

mass is increased or redistributed from subcutaneous to visceral depots at a time when bone mass is declining [7]. In addition, a recent clinical investigation showed an association between metabolic syndrome (*i.e.* visceral obesity, high glucose, high triglycerides, hypertension and low high-density lipoprotein; all linked to insulin resistance) and osteoporotic non-vertebral fractures [117]. Another series of investigations have demonstrated that marrow fat positively correlated with increased visceral fat in obese women and that this is also associated with poor bone quality and osteoporosis [86, 118]. Potential mechanisms for reduction of bone quality (rather than density) by excess fat include adipocytic production of pro-inflammatory cytokines that impair bone formation [119], stimulation of resorption and activation of PPARγ in MSCs by fatty acids (see Section 2.2.3; ref. [7]), and leptin-mediated inhibition of bone formation and activation of resorption via the sympathetic nervous system (see Section 2.3.3; ref. [26, 27, 120]). Together, these results suggest that there is a significant yet complex interaction between obesity and skeletal health.

2.3.2.3 Diabetes Mellitus

Dysregulation of glucose metabolism as a consequence of diabetes mellitus (DM) also has adverse orthopaedic consequences. Both Type I and Type II diabetes mellitus (T1DM and T2DM, respectively) are associated with an increased risk of osteoporotic fractures [121-123]. Bone formation and osteoblast function are impaired with patients with T1DM, while bone mineral density is increased but bone quality is reduced in patients with T2DM. This is coupled with an increased infiltration of fat in the bone marrow cavity [7]. Together these consequences are worsened in patients with poorer glycemic control [124]. Notably, the two types of DM are associated with different insulin phenotypes. Whereas there is a complete absence of insulin in T1DM that is supplemented pharmacologically, T2DM is characterized by insulin resistance. As insulin is a central regulator of bone-fat crosstalk (see Section 2.3.3), this could have profound

implications for the differences in pathological sequelae between Type I and Type II DM. Additionally, pharmacological treatments of T2DM also differentially affect the balance of osteogenesis versus adipogenesis by targeting Runx2 and PPARγ2, respectively [125]. Glitazones are PPARγ2 ligands, which activate adipogenesis in MSCs and suppress osteogenesis by indirectly inhibiting Runx2 expression [125]. Metformin stimulates osteoblastic differentiation of MSCs through transactivation of Runx2. Further, gestational diabetes during pregnancy in expectant mothers results in poor skeletal growth and bone mineral quality in postnatal infants [126-128]. The mechanisms of pathogenesis of osteopenia and osteoporosis secondary to DM are poorly understood as research has focused on a few *in vitro* studies and correlation with serum biomarkers [125]. Elevated levels of glucose induce apoptosis and replicative senescence in MSCs and reduce their colony formation and osteogenic capacity [129-132]. In immortalized osteoblastic cell lines, exposure to high glucose decreases proliferative capacity, mineralization and osteocalcin responses to parathyroid hormone (PTH) and Vitamin D administration, dysregulates collagen I synthesis, and leads to decreased expression of differentiation markers [133-136]. In murine 3T3-L1 adipocytes, high glucose administration leads to decreased insulin sensitivity, triglyceride storage dysregulation, production of reactive oxygen species (ROS) and pro-inflammatory cytokines, and decreased adiponectin secretion [137-139].

2.3.3 Knowledge of Feedback Loops Gained from Mechanistic Studies in Animal Models

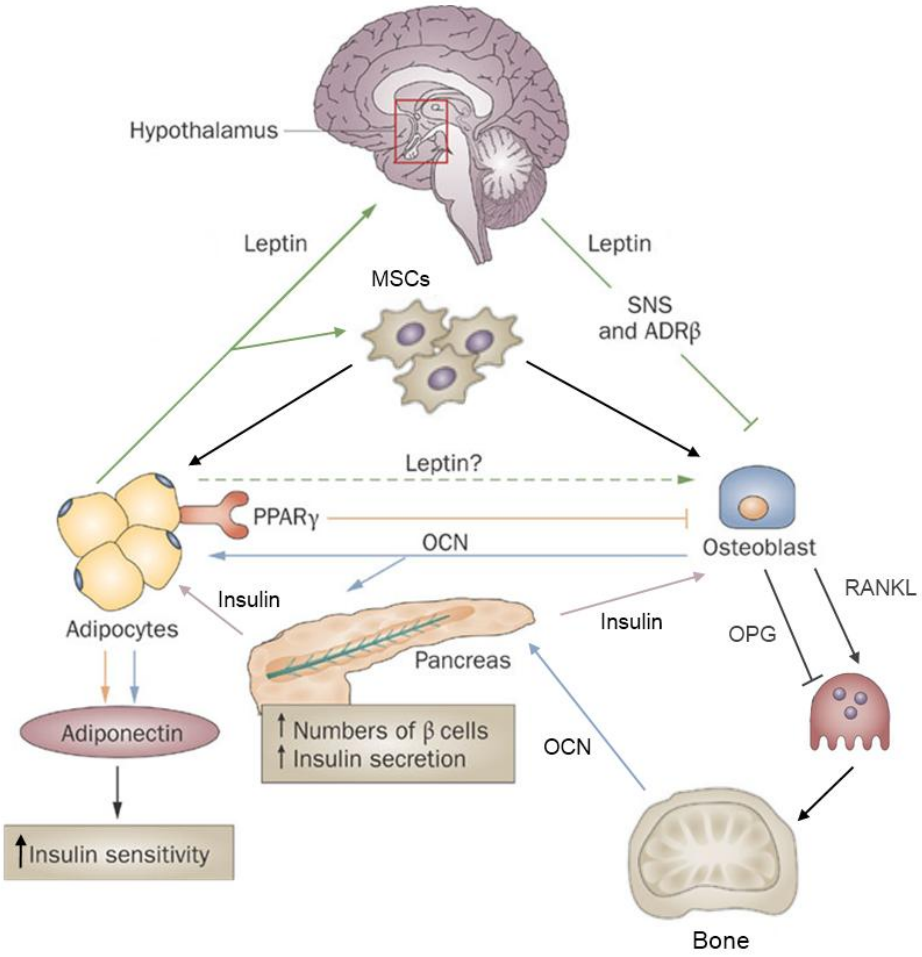

Figure 2.2. Several distinct intercellular signaling networks that link bone and fat. Adapted from [9] with permission.

Elegant experimental studies in mice have confirmed that several homeostatic feedback loops exist between adipocytes and osteoblasts to regulate bone remodeling and energy metabolism. Adipocytes secrete adipokine hormones in addition to their fat storage and release functions [140-143]. Leptin secreted by adipocytes acts on serotonergic neurons in the brainstem, which synapse in the hypothalamus and increase sympathetic output, causing increased catecholamine signaling to β_2 adrenergic receptors on osteoblasts, decreasing their proliferation and stimulating osteoclast-mediated resorption [120, 144, 145]. Leptin, via the same pathway, also reduces bioactivity of

osteoblast-derived osteocalcin (bone γ-carboxyglutamate (gla) protein) via positive regulation of a γ-carboxylase that increases carboxylation of its glutamic acid residues and enhances its binding and retention to bone mineral hydroxyapatite [23]. Bioactive (uncarboxylated) osteocalcin: 1) induces pancreatic β-cell proliferation and insulin secretion; and 2) increases adiponectin secretion by adipocytes, which serves to enhance insulin sensitivity in target cells (adipocytes, myocytes, and hepatocytes) [25, 146]. Insulin signaling, in turn: 1) stimulates osteoblast differentiation and osteocalcin expression [147]; and 2) decreases osteoprotegerin expression in a FOXO1-dependent manner, promoting bone resorption and acidification of bone extracellular matrix (ECM) by osteoclasts that decarboxylates and releases osteocalcin [22]. Notably, dysregulation of one or more of these pathways may manifest clinically as a metabolic disorder (*e.g.* anorexia nervosa, overweight and obesity, and diabetes mellitus; see Section 2.3.2) that secondarily lead to the osteopenia and eventually osteoporosis after chronic illness.

2.3.4 Potential Roles of MSCs

This evidence clearly supports the existence of an interplay that exists between osteoblasts and adipocytes within the bone marrow niche. Critically, evidence that MSCs may play an integral role in this process is beginning to accumulate in the literature [10, 78]. As described in Section 2.2.3, MSCs are a source of both osteoblasts and adipocytes, and the balance of their lineage allocation to either cell type is regulated by a complex network of pleiotropic, interdependent, and antagonistic cues (see Figures 2.1 and 2.2; [2, 7, 8, 10, 11, 18, 78-86]). Osteopenia and osteoporosis, whether primarily induced by age or menopause or secondarily induced by anorexia nervosa, obesity, or diabetes, are accompanied by increased fatty infiltration of bone marrow that suggests an imbalance of this lineage allocation and an altered (perhaps detrimental) microenvironment [10, 78, 86, 95, 106, 118, 148-153]. *In vitro* studies have confirmed that human and murine MSCs express leptin receptor [154-156] and are responsive to leptin, both through enhanced

proliferation and differentiation into the osteoblastic lineage [155, 156], as well as through inhibition of MSC differentiation into adipocytes [154, 156]. Additionally, a population of nestin-expressing MSCs in the bone marrow of mice simultaneously contribute to skeletal formation, provide cues for maintenance of haematopoietic stem cell localization and mobilization, and alter their proliferative and osteoblast differentiation responses to direct neural (sympathetic) and hormonal (G-CSF and PTH) stimulation [47, 157, 158].

2.4 Patterning of Hydrogels and Encapsulated Cells

2.4.1 Hydrogels as Biomaterials for Modeling Microenvironments

Given the plethora of complex questions that arise in stem cell research, increasingly complicated model systems are required to fully capture the biological events that are occurring as these cells interact with their local microenvironment. *In vitro* systems that achieve spatially and temporally controlled interactions between stem and native cells would yield improved understanding of cellular functions that induce healing *in vivo*. To provide relevant test beds for regenerative medicine therapies, such *in vitro* systems should mimic 3D tissue architecture as closely as possible, given that cellular responses can vary substantially from 2D culture [159]. Toward this end, the use of three-dimensional (3D) hydrogel biomaterials as cell carriers has enabled researchers to address many complex questions regarding the role of specific niche components and architecture in regulating the dynamic responses of stem cells to well-defined model microenvironments [160, 161]. Hydrogels are 3D networks composed of chemically or physically crosslinked, hydrophilic, polymer chains that absorb large quantities of water while remaining insoluble in aqueous media [162-166]. Specifically, hydrogels are appealing for biological applications due to their cytocompatibility [167-170], mechanical properties similar to many soft tissues [169, 171], and high water content which allows for the formation of thick constructs (up to 1.5–2 mm) with viable cells

embedded throughout the gel and free diffusion of soluble factors between encapsulated cells [164, 165, 172, 173]. The 3D biomimetic microenvironment provided by patterned hydrogels may allow for the probing of stem cell response to external stimuli in a well-defined and observable manner and is therefore an excellent candidate for building controlled model systems [65, 72, 174-176].

2.4.1.1 Candidate Hydrogel Materials

Hydrogels may be prepared from natural or synthetic polymers using various methods discussed later in this section [177, 178]. Hydrogels can be derived from natural polymers such as collagen, hyaluronic acid (HA), fibrin, alginate, agarose, and chitosan [179]. Many natural polymers, such as collagen, HA, and fibrin, have been used in tissue engineering applications because they are either components of or have macromolecular properties similar to the natural ECM [171, 174, 180-182]. Alternatively, alginate, agarose, and chitosan are hydrophilic, linear polysaccharides derived from marine algae sources or crustaceans [183, 184]. Another naturally derived gel, Matrigel™, is derived from soluble basement membrane extract of mouse tumors [185]. Various natural polymers have specific utilities and properties based on their origin and composition [174, 186], including inherent biodegradability and biologically recognizable moieties that support cellular activities [164, 186].

Synthetic hydrogels are appealing for tissue engineering due to the amount of control scientists have over structure, such as cross-linking density, and tailored properties, such as biodegradation, mechanical strength, and chemical and biological response to stimuli [174, 186]. Synthetic polymers such as poly(ethylene glycol) (PEG) [187] and other PEG-based polymers [188, 189], or poly(vinyl alcohol) can be reproducibly produced with specific molecular weights, block structures, degradable linkages, and cross-linking moieties [190]. These features can be individually modulated to affect gel formation dynamics, cross-linking density, and mechanical and degradation properties of the material. Hydrogels made from synthetic polymers like PEG do not

possess the inherent bioactive properties of gels made from natural polymers. However, they do have well-defined structures and are versatile templates for subsequent modifications that yield tailorable degradability and functionality [164, 174].

2.4.1.2 PEG-Based Hydrogels and Their Functionalization

Poly(ethylene glycol) (PEG) is a non-adhesive synthetic material that is highly resistant to protein adsorption, making it an especially attractive material for allowing freely diffusing cell-derived signals to be transported between encapsulated cells [191-193]. PEG's mechanical and biochemical properties can be easily modified for a variety of tissue engineering applications [194-196]. As such, PEG-based materials provide a template upon which additional bioactive functionality can be specifically tailored into the hydrogel formulation. Functional peptides such as the adhesive peptides glycine-arginine-glycine-aspartic acid-serine (GRGDS) and tyrosine-isoleucine-glycine-serine-arginine (YIGSR) and growth factors including TGF-β, bFGF, and VEGF have been tethered into PEG networks to modulate cell response [197-201]. PEG hydrogels have been extensively investigated for bone, cartilage, vascular, and neural engineering [196, 201-207]. Collectively, these studies have demonstrated the ability of biofunctionalized PEG hydrogels to support viability, spreading, proliferation and ECM deposition by multiple cell types, directed differentiation of stem cells, and more complex functions such as endothelial tubulogenesis, vascular infiltration, and neurite extension.

Biodegradable hydrogels have been favored for biomedical applications since they degrade in clinically relevant time-scales under relatively mild conditions, thus eliminating the need for additional surgeries to recover implanted gels and allowing for progressive replacement of the biomaterial by native or regenerated tissue [165, 186, 208, 209]. They are advantageous for *in vitro* applications because they facilitate cell spreading, proliferation, migration and deposition of extracellular matrix to better mimic native tissue environments [209, 210]. Currently, the fabrication and modeling of

hydrolytically degradable hydrogels [209, 211, 212] are well developed and the synthesis and utilization of synthetic gels incorporating biological moieties for enzymatic degradation are under investigation [209, 213, 214]. While hydrogels made from natural polymers are often enzymatically degraded, synthetic hydrogels containing biological moieties often offer more controlled degradation rates due to their tunable physicochemical properties [164]. Hydrolytically labile components have been added into PEG networks to control degradation [203, 215], and enzymatically degradable peptides have also been incorporated within PEG hydrogels for cell-mediated degradation [216-218]. More recently, novel photodegradable groups have been investigated as a means to degrade PEG networks on demand in the presence of ultraviolet (UV) light [219-221]. These methods have been designed with the ability to elicit a cellular response (*e.g.* migration, spreading, and proliferation) *in vitro* or to eventually fully degrade via hydrolysis or cell-mediated enzymes in an *in vivo* setting to promote regeneration. None have been employed thus far for cell retrieval.

2.4.2 Micropatterning of Hydrogels and Encapsulated Cells

2.4.2.1 Gelation Mechanisms

Several modes of crosslinking PEG-based hydrogels have been developed, including free-radical crosslinking of conjugated acrylate groups (*e.g.* with PEG-diacrylate, PEG-DA), where polymerization occurs through a chain-growth mechanism that involves chain transfer of the radical to a free double bond on another acrylate group [222]. Commonly used radical initiators include the thermodynamically driven combination of ammonium persulfate (APS) and tetramethylethylenediamine (TEMED) redox initiators, as well as the photosensitive Irgacure 2959 (I-2959 or D-2959; [223-226]). Both of these techniques lend unique capabilities for spatially and temporally controlled patterning of hydrogels and the cells encapsulated within them and are accompanied by differences in resolution and fidelity in the geometries produced.

Thermally induced free radical polymerization is particularly advantageous for micromolding applications and producing large constructs since polymerization occurs homogeneously throughout the bulk material. Photo-induced free radical polymerization (photo-polymerization) is uniquely suited to photo- and stereolithographic approaches, offers temporal control of polymerization due to the short half life of light-induced radicals, and produces components that can be assembled post-encapsulation and manipulation. The cytotoxicity of several redox and photointiating systems has been examined and it was determined that redox-initiating system toxicities are dependent, in part, on the pH of the initiator [227] while photoinitiator system toxicities are based upon initiator chemistry and concentration [228, 229]. Additionally, radical concentration and length of cell exposure to radicals and UV light has significant effects on cell viability [229, 230]. Use of these initiation systems in microscale patterning has thus far been limited because of oxygen free radicals that may potentially hinder the cross-linking reaction by quenching activated photoinitiator or terminating polymer free radicals prematurely [231-233].

Alternative step-growth crosslinking mechanisms, including Michael-type addition and "click" chemistry, have been utilized for crosslinking of PEG-based materials, and these techniques can also be used together with chain-growth initiators for sequential or mixed-mode crosslinking reactions to provide orthogonal modes of crosslinking for further spatial control [222, 234-237]. An attractive feature of these cross-linking mechanisms is that they do not require additional components like initiators [238]. Studies utilizing these cross-linking mechanisms verified that the conditions required for chemical cross-linking do not adversely affect cells; however, gelation rates are typically slower compared to radical chain polymerizations, and the addition of catalysts may negate the ability of these systems to maintain cell viability during the encapsulation process [168, 234-237].

2.4.2.2 Patterning Methodologies

Novel micropatterning techniques have been adapted to pattern hydrogel biomaterials with different cells or ligands at the microscale in an effort to probe the basic mechanisms of cell interactions with their surrounding microenvironments. These include extracellular matrix components, physical contacts with neighboring cells, and the presence of soluble paracrine signals.

In photolithography, a photomask containing opaque patterns is placed over a macromer solution containing a photo-initiator and then exposed to UV light to initiate free radical polymerization [173, 239, 240]. Only the hydrogel precursor solution that is exposed to the UV light through the transparent regions of the photomask will crosslink to create hydrogels [73, 241]. Photolithography is versatile since can be used with a variety of multifunctional macromers [173, 242] and can be adapted for utilization in other lithographic techniques such as laser scanning lithography [243, 244] and stop-flow lithography [245, 246] as well as micromolding techniques [247]. A trade-off exists between pattern resolution and the sample thickness (*i.e.* large sample thicknesses sacrifice resolution and result in a loss of feature fidelity) [173, 230, 248].

Laser-scanning lithography (LSL) employs a laser-scanning confocal microscope to pattern photosensitive materials in a static reservoir [243, 249]. This technique facilitates accurate alignment of successive exposures, achieves resolution on the scale of microns, and allows control over laser type, power, and pixel exposure time [244]. However, LSL exposes the sample "pixel-by-pixel", and therefore is a serial technique and generally low throughput. A variation of LSL, known as optofluidic maskless lithography (OFML) uses programmable exposure patterns with spatial light modulators instead of traditional photomasks and the continuous flow of photosensive polymer within microfluidic devices to supply the nonpolymerized material into the photopatternable region [250]. This method also takes advantage of microelectromechanical systems (MEMS)-based high-speed SLMs to dynamically

control the shape of polymerized microparticles and to improve the throughput, which is especially attractive when generating a large number of constructs [250-252]. However, OFML often necessitates complex programs for changing materials on the fly and expensive setup equipment.

Micromolding is another useful technique for forming micropatterned hydrogels that often utilizes a micropatterned master that determines hydrogel shape to mold replicas for repeated fabrication [253-256]. The advantages of the micromolding technique are that it is relatively inexpensive, high-throughput, easy to perform, and the fidelity is well-controlled [254, 255, 257]. The spatial resolution of micromolding technique can be high, but is significantly dependent on the aspect ratio of the structure (width to depth), the cross-linking chemistry of the gel, and the resolution of the technique used to make the master. In general, it is possible to pattern structures with a resolution on the order of a cell. However, the difficult of extracting fabricated gels increases as their size becomes smaller, and a new master has to be fabricated each time a new pattern is designed. Additionally, assembling and laminating molded gels into hierarchical structures to mimic tissues is difficult to do manually and therefore non-trivial [253-257].

2.4.2.3. Applications of Micropatterning Techniques

Several techniques such as surface patterning, micromolding, and dielectrophoresis have been used to pattern structures in gels [62, 258, 259]. Photopatternable polymers [260-267], in combination with patterning techniques for cell encapsulation [268-271], offer a promising potential solution to further understand these mechanisms. Photopatterning techniques have enabled researchers to precisely define ECM density and type, as well as cellular locations, proximity to each other, and cell density [270, 272-276]. Bhatia and colleagues have demonstrated a combined multiphase photo- and electo-patterning technique for precisely patterning different cell types in

isolation or in clusters within hydrogels at 50-500 μm resolution with high cell viability [258, 277], and demonstrated that 3D spatial information encoded by cell density affects chondrocyte variably affects chondrocyte differentiation and matrix production [259], Khetan and Burdick have applied a sequential crosslinking process whereby the presentation of protease-degradable peptides and adhesive ligands with hyaluronic acid hydrogels are spatially controlled in three dimensions to control cell outgrowth from chick aortic arches and dictate MSC fate decisions in mixed differentiation media by controlling cell spreading [64], Stereolithography, an additive process using light-curable photopolymer solution and a computer-guided laser to polymerize components layer-by-layer, has facilitated patterning of multiple layers of cells in three dimensions [249, 278, 279]. A multilayer photolithography scheme, using a mask to spatially control light penetration and photocuring, has been developed by Tsang *et al* to pattern hepatocyte cultures, showing that cells in three-dimensional culture better mimic *in vivo* functions [271]. Another innovative patterning system from Maeda *et al* creates 3D multi-compartmental alginate particles through the use of centrifuge-based micro-droplet formation from a multi-barreled capillary tube [280].

Recently, several approaches have been developed that employ microfluidic devices in combination with these photopatterning techniques to engineer more high-throughput polymerization of microscale, cell-laden hydrogel particles [233, 281-288]. Doyle *et al* have developed stop-flow lithography (SFL) techniques that rely on the projection of a photomask upon a focal plane with a microfluidic channel that is filled with a photopolymerizable polymer solution [285-288]. Features of the photocross-linked particles made using SFL such as size, shape, swelling behavior, and composition can be tailored independently through mask selection, optical exposure intensity, and polymer composition. Furthermore, SFL may take advantage of laminar flow regimes in microfluidic devices to co-flow unique polymer combinations in adjacent streams without mixing and patterning across these streams to fabricate single particles with several

orthogonal chemistries. Stroock *et al* have combined fluid delivery and molding techniques to create pattern microfluidic scaffolds in alginate for uniform delivery of solutes through a bulk scaffold and controlled delivery of solutes to different regions within the bulk hydrogel [289]. This technique was later expanded for patterning co-cultures of endothelial and perivascular cells surrounding a microvascular network within bulk collagen gels that allowed perfusion of whole blood to generate a model of angiogenesis and thrombosis [290]. Günther and colleagues contributed another recent innovation by developing a multilayer microfluidic platform that enables one-step, continuous formation of "mosaic" hydrogels [291]. This device enables a secondary biopolymer with potentially orthogonal chemistries and carrying different molecular, colloidal, or cellular contents to be dynamically incorporated and patterned within a flowing biopolymer sheet prior to crosslinking. This could be used to encode and preserve gradients and precise spatial localization of cells and biomolecules since the alginate base material can be ionically crosslinked as it exits the device. These studies demonstrate that micropatterning techniques applied to photopatternable biomaterials are very attractive ways of fabricating well-defined co-culture systems, and that it is feasible to tailor the chemistry of the gel for a variety of applications. However, to date, precision systems for photopatterning hydrogels have not been developed for long term (~ weeks) co-culture of cells in constructs of tissue-scale thickness (> 1 mm thick, or on the order of > 100 cells thick).

2.5 Co-Cultures to Examine Interactions between MSCs, Osteoblasts, and Adipocytes

2.5.1 Studies with Conditioned Medium

Conditioned medium systems, in which the cell culture medium from one cell type is used to incubate another cell type, have been useful in identifying soluble factors involved in MSC trophic signaling effects on other cell types [292-295]. In particular, in

a study by Maxson and Burg [296], murine MSCs undergoing osteogenic differentiation increased alkaline phosphatase production in response to adipocyte-conditioned medium. Conversely, MSCs undergoing adipogenic differentiation demonstrated increased triglyceride production and enlarged lipid vesicles in response to osteoblast-conditioned medium. Importantly, this study demonstrated that conditioned medium (one-way signaling) from osteoblasts and adipocytes enhanced each others' differentiation, supporting the co-dependence results discussed above (Section 2.3).

2.5.2 Co-Culture of Two Cell Types

To elucidate the effects of two-way crosstalk, several two-dimensional (2D) co-culture systems allow co-culture of two cells types separated by a semi-permeable membrane (e.g. transwell) to allow diffusion of soluble signals between cell populations while preventing direct cell-cell contact. Critically, these systems rely on monolayer culture on separable inserts to enable separation and examination of cell population after the co-culture period, an attribute that is currently lacking in analogous 3D co-culture systems.

Current studies have examined the effects of co-culture of osteoblasts and MSCs in transwell systems [294, 297, 298] or in direct contact with each other [297]. In one study, murine osteoblasts co-cultured with MSCs in a transwell system showed no change in proliferation or gene expression over 3 weeks in dexamethasone-free medium [297]. The co-cultured MSCs, however, demonstrated increased expression of *Runx2*, *Osx, Opn,* and *Ibsp* after 3 weeks and demonstrated significantly enhanced mineralization compared to MSC-only controls. Similarly, human MSCs co-cultured with human osteoblasts (1:2 ratio) in a transwell system exhibited upregulation in *IBSP*, *LEPR, ALPL,* and *BGLAP* after 14 days [294]. Increased secretion of Wnt by osteoblasts was observed with a concomitant increase in β-catenin and TCF/LEF1 levels, and downstream effectors of Wnt in MSCs cultured indirectly with osteoblasts [297, 298]. These results both

indicate that paracrine signals from osteoblasts can induce MSCs into a more osteogenic phenotype by upregulating both early and late bone markers over time.

To date, strikingly few studies have been conducted to examine the effects of co-culture with adipocytes on MSC function [299, 300] and none have examined how MSCs influence adipocytes. This is likely attributable, in part, to the difficulty in culturing plated adipocytes that fail to maintain plate attachment after accumulating significant amounts of intracellular lipid stores. Transwell co-culture of human MSC-derived adipocytes with undifferentiated human MSCs led to increased expression of *PPARG2* and *LEP* with a concomitant decrease in *COL1A2* and no change in *RUNX2* or *ALPL* expression after 48 hours [299]. In the same study [299], MSC-derived osteoblasts demonstrated increased *PPARG2*, *LEP*, and *LPL* expression coupled with increased *ALPL* expression and activity and decreased *BGLAP* expression after 48 h in co-culture with MSC-derived adipocytes. Another study demonstrated decreased proliferation (^{3}[H]-thymidine incorporation) of human osteoblasts but not MSCs in the presence of adipocytes after 20 hours of co-culture [300], with this decrease attributable to ligation of PPARγ with poly-unsaturated fatty acids and concomitant lower mineralization and expression of *ALPL*, *OSX*, *BGLAP*, and *RUNX2* [301-305]. While these studies indicate that soluble factors produced by each cell type affect cell function and differentiation of each other, there is currently no systematic means to examine these effects in all three cell populations simultaneously in 3D culture.

2.6 Approaches Using Systems Biology to Understand Cell Fate and Applications to Tissue Engineering

Systems biology integrates multivariate molecular-level measurement and modeling approaches to seek a deep quantitative understanding of complex biological processes [306]. Methods for high-throughput, multivariate analyses of high-content data currently have yielded systems-level information of complex cellular processes at or

close to a single-cell level. This includes quantifying the abundances and activities of molecular components involved in gene expression, metabolism, and signal transduction [307-309]. Often this collected information is subjected to data-driven modeling of cell signaling and behavioral phenotypes using a wide spectrum of computational modeling approaches, such as differential equation-based physiochemical models [310], principle component analysis (PCA) and partial least-squares regression (PLS/PLSR) [311-315], decision trees [316-318], and Bayesian networks [319, 320]. With respect to resolution and prediction of stem cell differentiation, Platt *et al* compared multi-pathway kinase signatures using PLSR to discover states of the kinase signaling network during stages of osteoblastic differentiation of MSCs [321]. Single cell expression profiling of blastocyst-stage embryonic cells in combination with PCA revealed three molecularly defined cell populations and elucidated their developmental progression as the blastocyst further developed into an embryo [322]. Multi-dimensional scaling has also been used to extract and process cytoskeletal features from imaging data during MSC culture in differentiation medium to forecast osteogenic versus adipogenic lineage commitment within 24 hours, well before histological stains showed evidence of differentiation [63].

Systems-level models of tissues require experimental data of activities of a plethora signaling molecules and responses of multiple cells across a diverse combination of treatments, perturbations, and time points. This is due to the fact that tissue functions are attributed to complex interactions between the numerous components of a cell and interactions between cells in a tissue that form a network, rather than individual molecules [306, 323, 324]. To illustrate the advantages of such systems, Kirouac *et al* cultured non-adherent blood progenitors (haematopoietic stem cells, or HSCs) under defined conditions that were differentially supportive of blood stem cell growth via non-stem cell autonomous mechanisms [325]. Using a combination of high-throughput molecular profiling, database and literature mining, and mechanistic modeling, they demonstrated that specific secreted factor-mediated intercellular communication

networks regulated HSC fate decisions and reconstructed the intracellular signaling network in an attempt to link extracellular signals with intracellular pathway activation. The study of these intercellular networks was facilitated by the ability to isolate cell populations and secreted factors from liquid culture due to the non-adherent nature of HSCs. Further work to elucidate the structure of these networks and perturb them is less prevalent in the literature for adherent stem cells and their progeny due to the inability to isolate individual cell populations from 3D scaffolds typically employed for tissue engineering. This has so far been studied in two-dimensional (2D) cultures of endothelial cells as data regarding their growth, network formation, and signaling are readily amenable to methods used in standard cell culture [326, 327].

2.7 Summary

In conclusion, many technical hurdles remain in optimizing model systems, generating novel analysis techniques, and understanding the biological interplay between MSCs, osteoblasts, and adipocytes and its relevance to homeostatic processes and dysregulation of bone and energy metabolism. Integration of information and tools from each of these scientific areas is key to informing, developing, and interpreting the work contained in this dissertation.

CHAPTER 3

LONG-TERM SPATIALLY DEFINED CO-CULTURE WITHIN THREE-DIMENSIONAL PHOTOPATTERNED HYDROGELS

3.1 Introduction

Stem cells are attractive for a plethora of regenerative medicine applications due to their presence in many tissues of the body and capacity for proliferation and differentiation along multiple lineages [328, 329]. Realizing their full potential for clinical application requires understanding the myriad of molecular mechanisms underlying fate determination, especially those that result from interactions with native tissues, for which a paucity of information currently exists. This knowledge will facilitate integration of stem cells and biomaterials to form a controlled tissue architecture that guides cellular differentiation, extracellular matrix (ECM) production, tissue organization, and optimal integration with the host to restore normal function [323, 330-332]. *In vitro* systems that achieve spatially and temporally controlled interactions between stem and native cells would yield improved understanding of cellular functions that induce healing *in vivo* – particularly in the formation and preservation of complex interfaces that exist between different tissues and implanted biomaterials. Such *in vitro* systems should mimic 3D tissue architecture as closely as possible, given that cellular responses can vary substantially from 2D culture [159], to provide relevant test beds for regenerative medicine therapies. This necessitates thick, tissue-scale biomaterial constructs that are patterned with high fidelity and precision.

---

[1] Portions of this Chapter are adapted from Hammoudi, TM, Lu, H and Temenoff, JS. Long-Term Spatially Defined Coculture within Three-Dimensional Photopatterned Hydrogels. *Tissue Engineering. Part C, Methods* 2010. 16(6), 1621-1628.

Toward this end, hydrogel-based biomaterials offer tunable three-dimensional (3D) environments, hydration that resembles native tissue, and polymer network configurations that mimic mechanical and molecular transport properties of native ECM.[275, 333] Use of hydrogel carriers has consequently enabled researchers to address many complex questions regarding the role of specific niche components and architecture in regulating the dynamic responses of stem cells to well-defined model microenvironments [160, 161, 333]. Of these, synthetic poly(ethylene glycol) (PEG)-based hydrogels are widely utilized for their cytocompatibility, intrinsic resistance to protein adsorption and cell adhesion, and their chemical versatility [334, 335]. Among others, oligo(poly(ethylene glycol) fumarate) (OPF) hydrogels have been explored as cell carriers for promoting structural and functional regeneration of injured orthopaedic tissues [336-339]. Prior work has demonstrated that OPF cross-linked with PEG-diacrylate (PEG-DA) is cytocompatible *in vitro* [339], minimally immunogenic *in vivo* [337], biodegradable via ester hydrolysis [336], and customizable via tethering of bioactive molecules [340] in a manner similar to other PEG-based hydrogels, validating it as a potentially useful biomaterial for tissue engineering applications. Importantly for the prospect of co-culturing multiple diverse cell types, robust and mechanically stable interfaces can be created by laminating several OPF:PEG-DA hydrogels together [341].

Novel micropatterning techniques have been adapted to control the microscale architecture of hydrogels with different cells or ligands. This allows researchers to probe the cell-microenvironment interactions with extracellular matrix components and neighboring cells through physical contacts and soluble paracrine signals. In particular, photopatternable polymers [264], in combination with patterning techniques for cell encapsulation [259, 273, 274, 342], enable precise definitions of ECM density and type, as well as cellular location, proximity, and density. A multilayer photolithography scheme, using a mask to spatially control light penetration and photopolymerization, has been developed to pattern hepatocyte cultures, showing that cells in 3D culture better

mimic *in vivo* functions [343]. Recently, several approaches have been developed that employ microfluidic devices in combination with these photopatterning techniques to engineer more high-throughput polymerization of cell-laden hydrogel microstructures on the order of 100 μm [233, 246, 344]. However, to date, micropatterned hydrogel systems have not been developed for long term (~ weeks) co-culture of cells in constructs of tissue-scale thickness (> 1 mm thick).

In response, we describe in this study a novel, facile photolithographic patterning scheme for generating and assembling thicker (> 1 mm), spatially controlled hydrogel constructs with high fidelity and minimal alteration in standard photo-crosslinking chemistry. Gel size was characterized before and after gels reached equilibrium swelling, and cell-laden gels were successfully laminated together into templated patterns. Following calibration of the system, we spatially patterned primary isolates of tendon/ligament fibroblasts and marrow stromal cells in a single, 1.5-mm thick construct as a co-culture model for interrogating stem cell interactions with injured tendon/ligament tissue. The patterning technique developed in this proof-of-concept study helps maximize diffusion between cells while maintaining spatial segregation and may later be used in combination with other materials to also examine the roles of migration or cell-cell contact in tissue formation. Importantly, these experiments demonstrate maintenance of cell viability for two primary-isolated cell types (bovine marrow stromal cells and tendon/ligament fibroblasts) over culture times relevant for tracking biological phenomena (up to 14 days). Accordingly, this work represents a simple enabling platform at the convergence of biomaterials and micropatterning that facilitates development of *in vitro* biological model systems that may further inform stem-cell based therapies for a variety of clinical applications.

3.2 Materials and Methods

3.2.1 Polymer Synthesis and Characterization

OPF was synthesized as previously described [345]. Briefly, 50 g of poly(ethylene glycol) (PEG; nominal M_n = 10 kDa; Sigma-Aldrich) was dried by azeotropic distillation in toluene (Sigma-Aldrich). The dried PEG was dissolved in 320 mL anhydrous dichloromethane (DCM; Fisher Scientific). Fumaryl chloride (FuCl; distilled before use; Sigma-Aldrich) and triethylamine (TEA; Sigma-Aldrich), in a molar ratio 1:0.9 PEG:FuCl and 2:1 TEA:FuCl, were simultaneously added dropwise to the PEG solution at ~0 °C over 5 h under nitrogen while the reaction was vigorously stirred. After addition of FuCl and TEA, the solution was continuously stirred for 48 h at 25 °C under nitrogen. Upon completion of the reaction, the solvent was removed by evaporation, and the residue was dissolved in 1 L of warm ethyl acetate (Fisher). Then, TEA-HCl salt was removed by filtration. The OPF was re-crystallized twice in ethyl acetate and washed twice in ethyl ether (Fisher). The resulting powder was vacuum dried at <5 mmHg and stored in a sealed container at -20 °C until further use.

PEG-DA was prepared as previously described [278] by combining 0.1 mmol/mL dry PEG (MW 3400 Da; Fluka), 0.4 mmol/mL acryloyl chloride, and 0.2 mmol/mL triethylamine in anhydrous DCM and stirring under nitrogen overnight. The resulting solution was washed with 2 M K_2CO_3 and separated into aqueous and DCM phases to remove HCl. The DCM phase was subsequently dried with anhydrous $MgSO_4$, and PEG-DA was precipitated in diethyl ether, filtered, and dried under vacuum. PEG-DA was stored in a sealed container protected from light at -20 °C until further use.

After synthesis, the OPF and PEG-DA were characterized via gel permeation chromatography (GPC). A GPC system (Prominence LC-20AD, CTO-20AC, SIL-20A, CBM-20A, DUG-20A; Shimadzu) equipped with a refractive index detector (RID-20A; Shimadzu) was used to determine the molecular weights of both the PEG starting

material and the resulting OPF and PEG-DA polymers. The polymer samples were dissolved in chloroform, filtered (0.45 μm filter; Whatman) and injected into a column (50-100,000 Da range; Waters) at a flow rate of 1 mL/min. Molecular weights were determined from elution time based on a calibration curve generated from PEG standards (seven standards ranging in molecular weights from 1,400 – 73,500 Da; Waters). Samples were run in triplicate.

3.2.2 Device Fabrication

Photopatterning experiments were performed in a microfluidic device fabricated from polydimethylsiloxane (PDMS, Dow Corning Sylgard 184; Essex-Brownwell Inc) using micromolding [346]. Devices consisted of a 2 mm-thick rectangular chamber with three inlet and three outlet channels for efficient delivery and removal of macromer solution (Figure 3.1A). Briefly, a poly(urethane) master was fabricated using established techniques [347]. We fabricated PDMS devices by curing the device layer (10:1 base:curing agent ratio) over the master at 70 °C for 2 h, peeling the PDMS off the mold and cutting individual devices to size, and subsequently bonding each to a separate cover glass using oxygen plasma treatment [348]. Medical grade platinum-cured silicone micro tubing (BB518-12, Scientific Commodities) was used for fluidic connections. Holes for fluidic connections were punched to a size determined by the outer diameter of the tubing, and the tubing was connected to the device via type 304 90°-angled stainless steel tubes (21 gauge; Small Parts). Luer lock dispensing needles (21 gauge; McMaster-Carr) were attached to the opposite ends of the tubing for eventual connection to syringes containing macromer solution. A contact-bonded, overlying PDMS enclosure was fabricated using a different poly(urethane) mold to contain a nitrogen atmosphere for the device.

3.2.3 Calibration of Photopatterning Method

Hydrogel constructs were photopatterned from macromer solutions containing OPF and PEG-DA a 50:50 in ratio by weight with 75% initial water content and 0.05% D2959 photoinitiator in phosphate buffered saline (PBS; Invitrogen). A series of photomasks containing polygonal features ranging from 1000 – 3000 μm in size were used to pattern hydrogels. Devices were either equilibrated with an N_2 atmosphere or left in ambient air prior to loading the polymer solution (Figure 3.1). For devices equilibrated with N_2, gas was initially delivered for a minimum of 30 min to the interior of the device via the inlet ports and subsequently delivered within a PDMS enclosure during crosslinking (Figures 3.1B,D). The photomask was aligned and the polymer solution injected and allowed to cross-link under exposure to ~10.5 mW/cm^2 of 365 nm light (as measured before passing through the cover glass and mask; ~7 mW/cm^2 of light passes through the glass and mask layers to reach the polymer solution) for 12 or 20 min (Figure 3.1B). The dimensions of the hydrogels immediately after crosslinking and after reaching equilibrium swelling were measured using a stereomicroscope (MZ16F; Leica) and ImageJ software (version 1.43*n*; NIH).

3.2.4 Cell Harvest and Isolation

Fibroblasts were isolated from the cruciate ligaments and patellar tendons of immature bovine knee joints (Research 87). Briefly, excess tissue was removed and the joint capsule was transferred to a cell culture hood, where the ligaments and tendons were removed in a sterile fashion. The tissue was digested in a solution containing Dulbecco's modified Eagle's medium (DMEM), 5 μg/mL penicillin, 5 μg/mL streptomycin, 10 μg/mL neomycin (PSN; Invitrogen), 10 μl/mL kanamycin (Mediatech), 1 μl/mL gentamicin (Mediatech), 1 μl/mL fungizone (Invitrogen) and 0.4% collagenase II (w/v) (Invitrogen) for 48 h, at which point the solution was filtered through a cell strainer with nylon mesh lining (80 μm pores; Small Parts). The harvested cells were resuspended in

DMEM, counted on a hemocytometer, and cyropreserved in liquid nitrogen in DMEM containing 20% fetal bovine serum (FBS; Hyclone, Logan, UT) and 10% dimethyl sulfoxide (DMSO; Sigma–Aldrich) for storage until use in cell culture experiments.

Bone marrow stromal cells (MSCs) were isolated from the femora and tibiae of immature bovine hindlimbs (Research 87). Briefly, excess tissue was removed and the bones transferred to a cell culture hood, where they were sawed open in a sterile fashion. Bone marrow was removed and mixed with sterile PBS containing 1x Antibiotic/Antimycotic solution (A/A; Mediatech). The suspension was progressively filtered to dissociate or remove insoluble debris and centrifuged at 300 *g* for 15 minutes. The pelleted fraction was collected and red blood cells were lysed with 4% acetic acid. Remaining cells were plated at 1.6×10^6 cells/mL and incubated at 37 °C for 30 min. Non-adherent cells were collected and plated in tissue culture flasks and cultured to confluency in DMEM containing 1 g/L glucose and L-glutamine (Mediatech) and supplemented with 10% FBS and 1% A/A. Cells were subsequently lifted using 0.05% Trypsin/0.53 mM EDTA (Mediatech), resuspended in DMEM containing 20% FBS, 10% DMSO, and 1% A/A, and cryopreserved in liquid nitrogen until further use in cell culture experiments.

3.2.5 Cell Patterning and Co-Culture

Prior to encapsulation, tendon/ligament fibroblasts were thawed and plated at 2×10^6 cells/flask in growth medium containing DMEM, 10% FBS, 1% non-essential amino acids (NEAA; Mediatech), 1% HEPES (Mediatech), 1% A/A, and 50 μg/mL ascorbate (Sigma–Aldrich), with medium changes every 2 days. MSCs were thawed and plated at 1×10^6 cells/flask in growth medium containing DMEM, 10% FBS, 1% A/A, and 1 ng/mL basic fibroblast growth factor (bFGF; Peprotech), with medium changes every 2 days. Cells were grown to near confluency and lifted using 0.05% Trypsin/0.53 mM EDTA at passage 2 for encapsulation experiments. To distinguish the two cell populations during

co-culture experiments, fibroblasts and MSCs were differentially stained with CellTracker Orange CMRA and CellTracker Green CMFDA reagents (Invitrogen), respectively, according to manufacturer's recommendations at one day prior to encapsulation. Briefly, cells were washed twice with sterile PBS and incubated with serum-free medium containing 10 μM CellTracker at 37 °C for 45 minutes. After incubation, medium containing unincorporated fluorophore was rinsed twice with sterile PBS and replaced with normal cell culture medium.

These cells were subsequently patterned into 3×5 arrays of 1.5 mm-squares with alternating cell types using sequential photo-crosslinking steps inside microfluidic devices. Completely assembled devices were sterilized using an autoclave prior to use. Sterilized devices were equilibrated with an N_2 atmosphere for a minimum of 30 minutes prior to loading the polymer solution. Macromer solutions containing OPF and PEG-DA in a 1:1 ratio were dissolved in PBS at 90% initial water content and filter sterilized using 13 mm-diameter syringe filters (0.2 μm pore size; Fisher Scientific). Sterile photoinitiator (0.05% D2959 in PBS) was subsequently mixed into the macromer solution. Cells were resuspended in macromer solution at a concentration of 10×10^6 cells/mL. Prior to loading the device, each solution containing cells was filtered through nylon mesh with 80-μm pores to dissociate or remove any remaining large aggregates of cells. The first suspension containing one cell type was delivered into the device and patterned into 1.5-mm cubic hydrogel blocks using 365 nm UV light for 12 min (Figure 3.3A). The remaining uncross-linked cell solution was washed out of the device using macromer solution containing no cells. A second suspension containing another cell type was delivered into the device and laminated to existing blocks using the same crosslinking parameters through the use of a second photomask. Cells patterned during the first round of crosslinking were protected from a second dose of UV light by overlying dark areas present on the second photomask. Alignment marks were included on the masks and device to allow for registration of laminated gels. Array constructs were extracted from

the PDMS devices using a scalpel and placed in 6-well tissue culture plates with 5 mL of DMEM containing 10% FBS, 1% NEAA, 1% HEPES, 1% A/A, 50 μg/mL ascorbate, and 1 ng/mL bFGF.

3.2.6 Image Analysis of Cell Patterning

Image analysis was performed to reveal interfaces between different cell populations after the gel constructs reached equilibrium swelling (~24 h). Gels were rinsed for 45 minutes in sterile PBS to remove media, and constructs containing stained cells were imaged at 5x and 10x magnification on a laser-scanning confocal microscope (LSM 510/NLO; Zeiss). A total of 15 overlapping images were acquired for each gel throughout its entire thickness (~2000 μm) at 10-μm intervals. Images were analyzed using ImageJ software. The separate slices of each z-series were examined to verify the absence of an overlap between green- and red-stained cell populations. The images were then processed to provide single images demonstrating a non-overlapping interface between adjacent cell populations. To accomplish this, the green and red channels were merged for each image slice in the z-series, and then the entire z-series was projected onto a single plane using a standard deviation-based algorithm. Separate images were then stitched together to provide an overall view of the entire construct.

3.2.7 Cell Viability Assessment

A separate set of studies was conducted to assess the effects of this photopatterning technique on cell viability in OPF/PEG-DA gels over a 14-day period. A series of 3×5 hydrogel arrays were fabricated using same methodology as described above and containing homogeneous populations of either fibroblasts or MSCs. Patterned hydrogel arrays were subsequently cultured for various time periods in culture medium appropriate for the specific cell type as detailed above, with media changes every 2 days.

3.2.7.1 LIVE/DEAD Assay

Hydrogel constructs (n = 2) were analyzed on days 1, 7, and 14 using a LIVE/DEAD assay (Invitrogen) as a qualitative indicator of cell viability. Constructs were rinsed in sterile PBS at 37 °C and subsequently incubated in staining solution (1 µM calcein AM, 1 µM ethidium homodimer-1 in sterile PBS) for 30 minutes at 37 °C. After a second PBS rinse to remove excess dye, stained constructs were imaged with confocal microscopy. For each construct, 4-5 images were collected from different sections of the gel (stack depth = 0 – 800 µm; 10-µm intervals).

3.2.7.2 PicoGreen dsDNA Assay

DNA content was quantitatively assessed as a measure of cell content over time using the Quant-iT PicoGreen dsDNA Assay kit (Invitrogen) per manufacturer's instructions [349]. Hydrogel constructs (n = 4) were collected on days 1, 7, and 14 and rinsed in PBS to remove media. Their wet weights were recorded and the gels were homogenized with a pellet grinder. Samples were mixed with 750 µL of dH_2O were subjected to three cycles of freeze/thawing at -80 °C and ultrasonication at room temperature to promote cell lysis. Fluorescence of each sample was read at 485/525 nm excitation/emission using a plate reader (SpectraMax M2e; Molecular Devices, Sunnyvale, CA) and the amount of DNA per sample was determined using a standard curve using standards from the kit.

3.2.8 Statistical Analysis and Multivariate Modeling

All measurements were compared using ANOVA and Tukey's *post hoc* test ($p \leq 0.05$) performed with Minitab (version 15.1.30.0; Minitab). Linear regression was performed to determine the correlation between mask size and the size of the resulting hydrogel for calibration experiments. All results are reported as mean ± standard deviation.

3.3 Results

3.3.1 Characterization of Patterning Fidelity and Calibration of Gel Size

We show that three-dimensional gels with a variety of shapes could be easily and reproducibly patterned using inexpensive, easily fabricated, disposable microfluidic devices (Figure 3.1A). Feature shapes in the *xy* plane roughly resembled those of the applied photomask for straight edges as well as concave and convex corners and arcs (Figure 3.1C, top view). When cross-linked under ambient conditions, these gels exhibited somewhat sloped side profiles and shallow thicknesses $\leq$ 1 mm despite relatively long crosslinking times (20 min), indicating incomplete polymerization of the hydrogel throughout its entire depth (Figure 3.1C, side view). Alternatively, efforts to pattern hydrogels in devices equilibrated in an atmosphere of N_2 gas (Figure 3.1D) yielded improved results: shape features such as edges and corners were more sharply defined; overall hydrogel thickness was visibly greater, exceeding 1 mm for multiple feature types, and side faces of the gels were noticeably straighter and less sloped for the same crosslinking time of 20 min (Figure 3.1E).

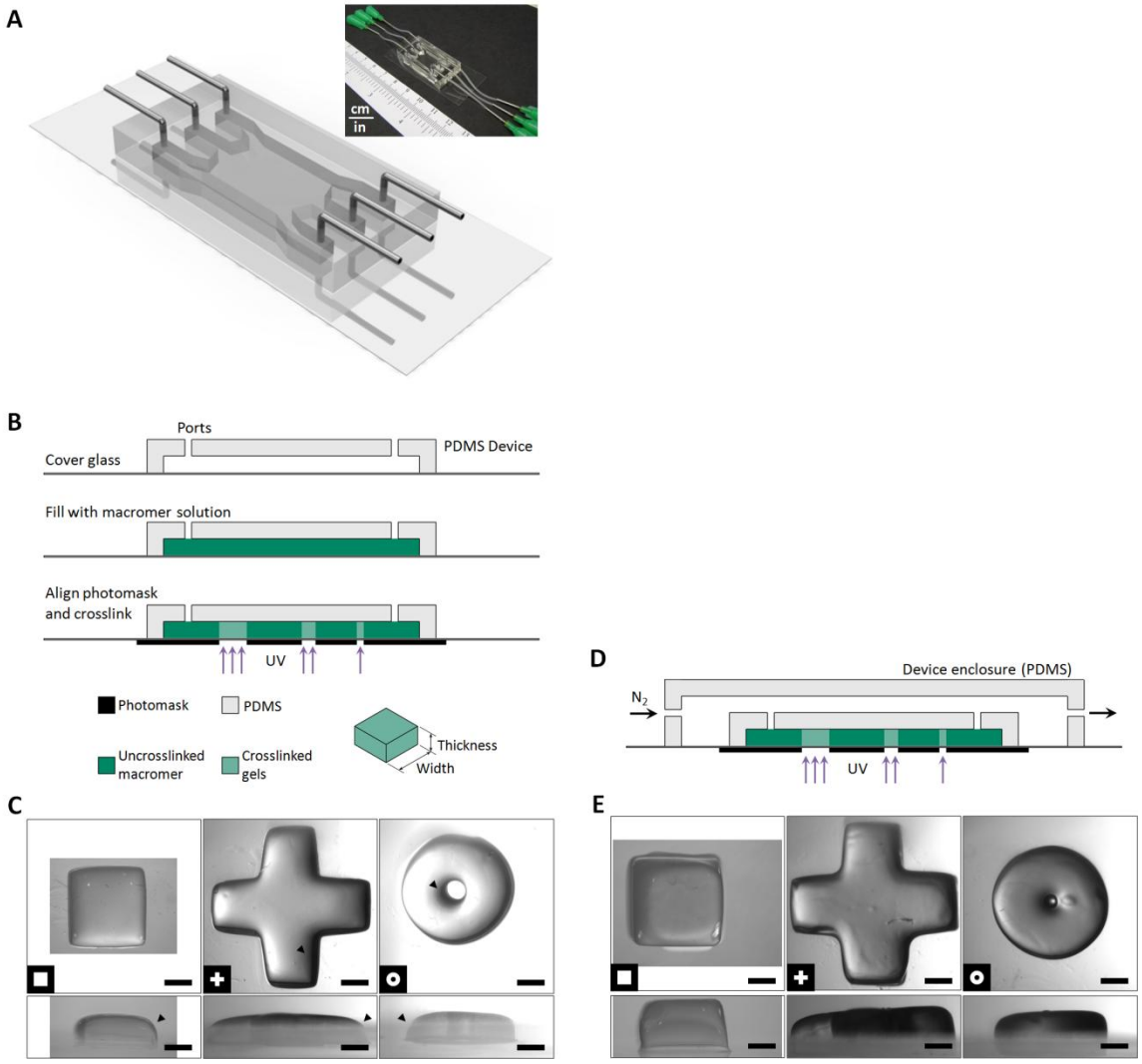

Figure 3.1. OPF hydrogels can be photolithographically patterned into a variety of three-dimensional shapes in a controllable, high fidelity manner at the micron to millimeter scale. (A) 3D rendering of an inexpensive microfluidic device used for hydrogel photopatterning that consists of a replica-molded PDMS chamber with inlet and outlet ports that is plasma-bonded to a cover glass. Inset: photograph of an assembled device. (B) Schematic depicting a technique for simple photolithographic patterning hydrogels within the microfluidic device. Gel precursor solution is injected into the device, and patterning is accomplished by applying a photomask to the glass side of the device followed by crosslinking the exposed gel using a 365-nm UV source. (C) Multiple shapes including straight edges, concave or convex corners, and arcs may be generated with high fidelity. Photomicrographs illustrate top and side views, arrows indicate sloped walls. Insets: photomask applied for each patterned hydrogel. Scale bar = 1 mm. (D) Scheme depicting process of device equilibration in an inert N_2 atmosphere to improve photo-polymerization and patterning fidelity. The microfluidic device is purged with N_2 gas for 30 minutes prior to crosslinking, after which N_2 is delivered to the PDMS enclosure during loading of macromer solution and subsequent crosslinking. (E) Pattern registration,

gel thickness, and side profiles are improved with photopolymerization in a N_2 atmosphere when applying the same photomask. Scale bar = 1000 μm. Figure 3.1 continued.

This photopatterning technique was readily characterized and calibrated by photo-crosslinking hydrogel blocks using masks with square sizes ranging from 0.9 – 3 mm and measuring gel dimensions before and after swelling. Gels cross-linked under N_2 had widths that more closely adhered to the size of features designed into photomask, in sharp contrast to gels cross-linked in ambient air, which were consistently lower than the mask size (Figure 3.2A). For smaller feature sizes (< 2 mm), hydrogels patterned under nitrogen exhibited widths significantly greater than those cross-linked in ambient air, indicating that employing a N_2 environment enables higher fidelity patterning at small feature sizes. Even more pronounced are the significant differences in initial gel thickness observed between gels cross-linked in these two environments. For large features approaching 3 mm in width, gels photo-crosslinked in ambient air barely approached 1 mm in thickness (Figure 3.2B, white bars). Conversely, gel thickness exceeded 1 mm for all mask sizes tested using our nitrogen atmosphere system, surpassing 1.5 mm in thickness for larger gel widths (Figure 3.2B, grey bars). As a consequence of this novel crosslinking environment, a larger aspect ratios (thickness:width) could be achieved: 0.49 – 1.19 under nitrogen vs. 0.33 – 0.51 under ambient conditions. Gel thickness and thus aspect ratio could be further tuned by adjusting crosslinking time, device chamber thickness, or initial polymer concentration (data not shown). Gels patterned in a nitrogen atmosphere exhibited a lower relative increase in thickness upon swelling than ambient air counterparts (Figure 3.2C).

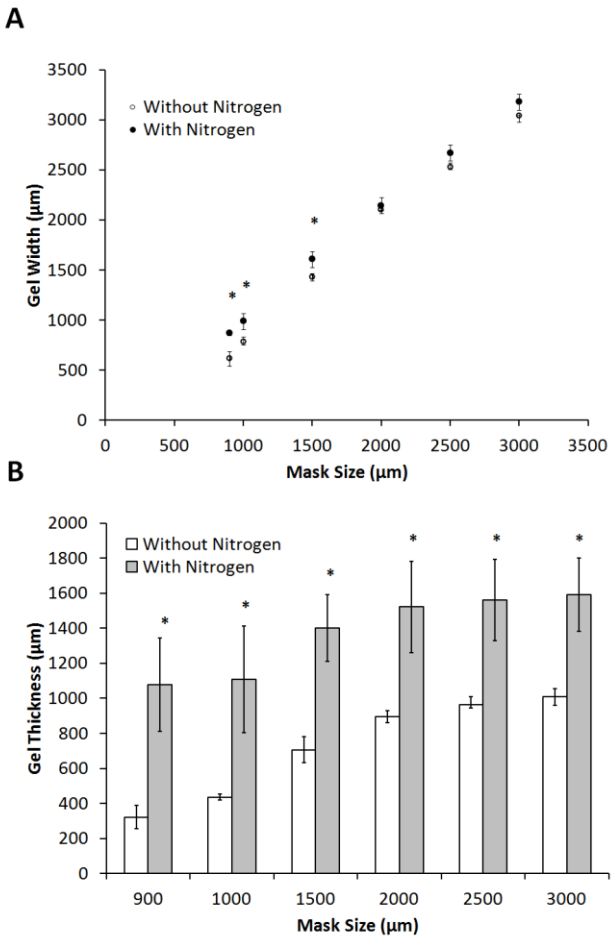

Figure 3.2. Patterning fidelity of OPF hydrogels is enhanced under a nitrogen atmosphere, enabling fabrication of constructs with highly tunable aspect ratios. (A) Performing photopolymerization in a N_2 atmosphere reproducibly generates gel widths closer to the size of the applied photomask, particularly at low mask sizes, allowing facile calibration of this photopatterning method. (B) Gel thickness before swelling significantly increases under a N_2 atmosphere. (C) Gel width and thickness increase proportionally after swelling, though the extent of this increase differs depending on the crosslinking environment, indicating different degrees of crosslinking. [*n* = 3; mean ± s.d. for all experiments. * = significant when compared to same mask size without N_2, $p \leq 0.05$]

3.3.2 Lamination of Multiple Gels Containing Different Cell Types

Monolithic, laminated hydrogel modules containing segregated cell types were generated through serial photopatterning within the same microfluidic device as described in the methods and depicted in Figure 3.3A. Using this procedure facilitated the creation of a templated 3×5 array pattern of adjacent gels that were well-aligned and

remained laminated together after reaching equilibrium swelling within 24 h (Figure 3.3B, left). Differential staining of MSCs and fibroblasts encapsulated in alternating blocks revealed excellent patterning fidelity and segregation of cell populations throughout the entire 2-mm thickness of the gel as demonstrated through confocal microscopy image stacks projected onto a single plane (Figures 3.3B,C). Well-defined, high-fidelity interfaces including corners and straight edges existed between the two encapsulated cell populations, and there was negligible intermixing within the thick gels (Figure 3.3C). The uniformity of this pattern throughout the entire depth of the gel array was verified by longitudinally or transversely sectioning the construct and imaging these cross-sections with confocal microscopy (Figure 3.3D), revealing a consistently straight interface.

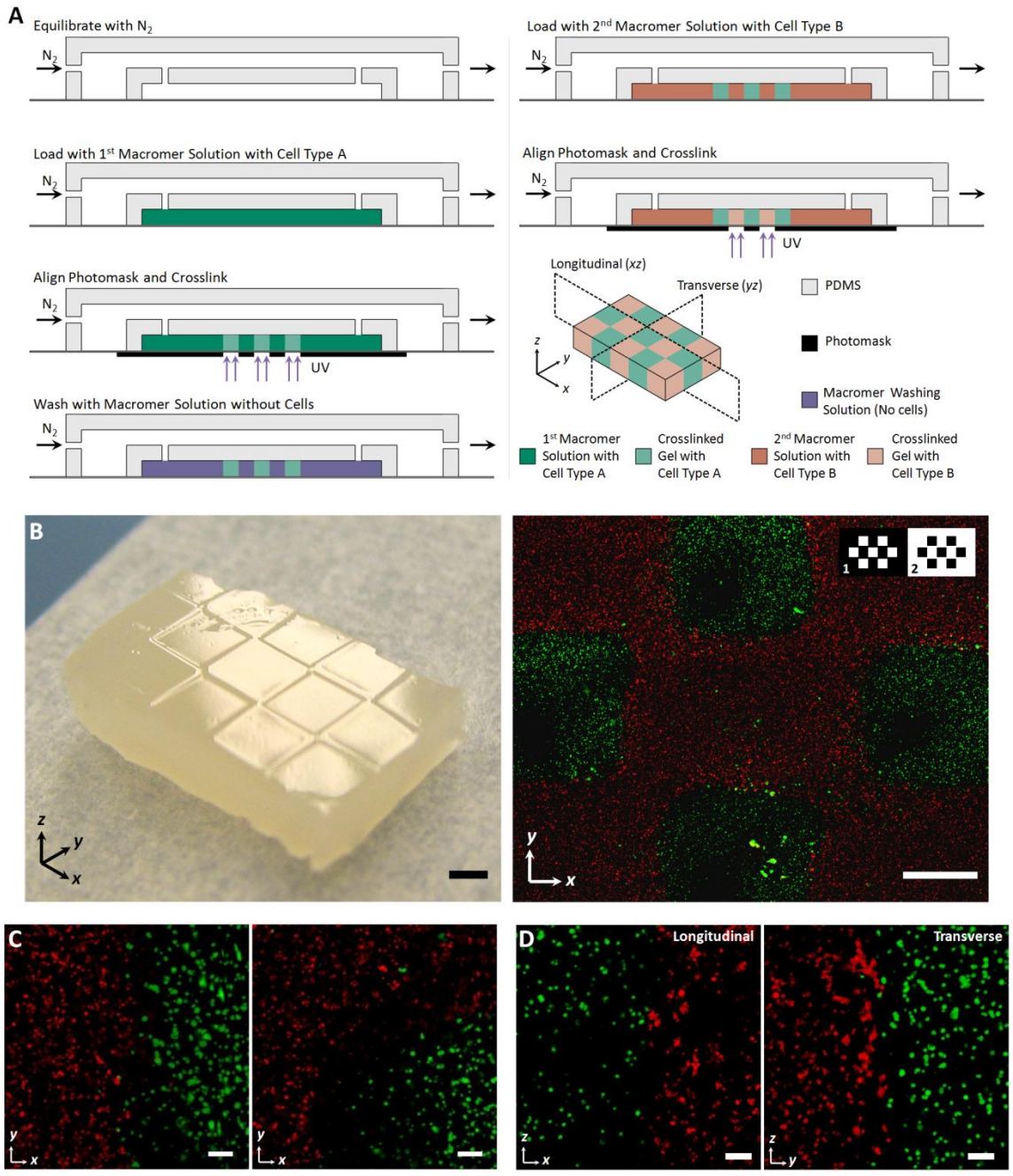

Figure 3.3. Spatially controlled, tissue scale co-culture of multiple cell types can be realized through serial photo-crosslinking and lamination of hydrogels into templated patterns. (A) Schematic illustrating serial photopatterning steps utilized in the fabrication of a hydrogel construct for co-culture of multiple cell types. (B) Left, a photograph of a 3×5 hydrogel array after swelling for 24 h. Right, a stitched, flattened confocal image of a portion of the array containing alternating marrow stromal cell (green) and tendon/ligament fibroblast (red) populations. Each cell type is segregated within well-defined laminated hydrogel modules that remain well-bonded during culture. Inset: photomasks applied during each step. Scale bar =

1000 μm. (C) Flattened confocal image stacks (top view) of straight and cornered interfaces between the two cell populations demonstrate a clear interface between them that is preserved throughout the entire depth of the acquired stack. Scale bar = 100 μm. (D) Confocal images of hydrogel array cross-sections (longitudinal, left and transverse, right) providing further evidence that the interface between the two populations of cells is consistent through the entire gel thickness. Scale bar = 100 μm. Figure 3.3 continued.

3.3.3 Cell Viability during Long-Term Culture

Cell viability was qualitatively and quantitatively assessed for 3×5 hydrogel array constructs containing homogenous cell populations (either MSCs or fibroblasts only) following their extraction from microfluidic devices and culture over two weeks in their respective media. LIVE/DEAD assay of intact gels on days 1, 7, and 14 consistently revealed predominately live cells throughout the entire gel thickness when imaged with confocal microscopy [primary bovine tendon/ligament fibroblasts (Figure 3.4A, left); primary bovine marrow stromal cells (Figure 3.4A, right)]. A separate set of samples was analyzed for DNA content as an indicator of cell number over the two-week culture period (Figure 3.4B). Relative to day 1, gels containing fibroblasts exhibited a small yet significant decrease in DNA content at day 14, while gels with MSCs showed a slight significant decrease at day 7. No difference was observed between MSCs on day 14 versus day 7.

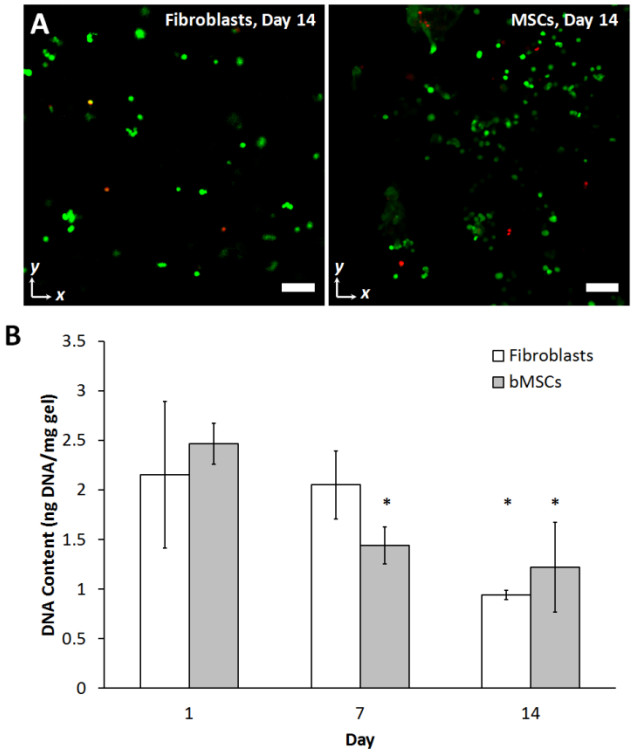

Figure 3.4. Primary tendon/ligament fibroblasts and marrow stromal cells remain viable during long-term culture after photopatterning. (A) Confocal images of encapsulated tendon/ligament fibroblasts (left) and marrow stromal cells (right) within a serially photopatterned 3×5 hydrogel array after 1 and 14 d in culture stained with LIVE/DEAD reveal predominately viable cells at each time point. Scale bar = 100 µm. (B) Assaying for DNA content of these constructs demonstrates a small but statistically significant decrease over the 14-day culture period [* = significantly different from same cell type on day 1, $p \leq 0.05$].

3.4 Discussion

This work presents a novel photolithographic technique for spatially controlling hydrogel network formation that facilitates patterning of multiple cell types into three-dimensional hydrogel constructs of greater than 1 mm thick. Size and shape of hydrogel features within each construct may be reproducibly tuned and controlled through simple alterations in the photomask and implementation of a nitrogen atmosphere during the photo-crosslinking procedure (Figure 3.1). The feature sizes used to calibrate the system (Figure 3.2A) and the resulting gel thicknesses (Figure 3.2B) and aspect ratios demonstrate the versatility of this technique for patterning gels at multiple size scales. We

postulate that the success of this technique in improving patterning fidelity and gel size characteristics derives from limiting the presence of oxygen free radicals that may potentially hinder the polymerization reaction by quenching activated photoinitiator or terminating polymer free radicals prematurely [231-233]. Previously, photopatterning hydrogels under ambient air limited the ability to generate hydrogels with features smaller than 1 mm and with reasonable fidelity (Figures 3.1 and 3.2), possibly due to the presence of oxygen at the PDMS interface into the crosslinking area; a smaller gel also has an increased surface area-to-volume ratio, making it more vulnerable to such surface dependent effects. Using PDMS devices resulted in shape features with significantly more rounded corners that did not adequately correlate with the shape of the photomask and side walls that were dramatically sloped and shallow (Figure 3.1C), but using nitrogen purging improved the fidelity significantly (Figure 3.1E). Furthermore, data demonstrating greater increase in gel thickness during swelling in gels that were cross-linked under ambient air (Figure 3.2C) also points to a lower degree of crosslinking in those samples.

With less oxygen in the system under this novel approach, hydrogels could be consistently photopatterned to thicknesses approaching 2 mm with shape features that accurately reflected the photomask (Figures 3.1 and 3.2). Gel thickness resulting from crosslinking in this environment is thus primarily limited by the concentration and molar absorptivity of the polymer solution, the kinetic efficiency of the free radical initiation and propogation reactions, and the length of the polymer chains and their cross-linkers [350-353]. Previous efforts by other groups have demonstrated enhanced patterning fidelity at the microscale by altering the chemistry of the free radical polymerization through the use of higher concentrations of photoinitiators, the addition of short length cross-linkers, and the use of shorter polymer chains in an effort to induce crosslinking on much shorter timescales for much smaller gels [233, 245, 354]. While each of these potential modifications may result in improved crosslinking and fidelity of hydrogels,

these enhancements may be delivered at the expense of cell viability, especially for culturing primary cell types over long periods of time [350]. Free-radical photoinitiators and short length cross-linkers are cytotoxic at high concentrations [229, 350], and the low network mesh size that results from using low molecular weight polymers may impose harmful physical constraints on encapsulated cells due to their lower water content and a mesh size that may limit diffusion of macromolecules [355-357]. Without altering any of these chemical parameters and instead crosslinking under a nitrogen atmosphere, we simultaneously avoid these potential detriments and potentially reduce the presence of cytotoxic oxygen free-radicals [358].

In addition to patterning of individual gels, this facile photolithographic scheme may be sequentially employed in the generation of multiple laminated, spatially defined hydrogel domains that consistently remain adherent at their interface despite the internal stresses generated while the gels reach equilibrium swelling (Figure 3.3B). This serial crosslinking process may be performed multiple times *in situ* within the same microfluidic device and enables the spatially controlled segregation of multiple cell types within the same laminated hydrogel construct (Figure 3.3A,B). This work demonstrates that this cell patterning occurs with high fidelity and with interfacial uniformity throughout the entire gel thickness. Confocal microscopy consistently demonstrated negligible overlap between two cell populations in different areas and at different depths within the overall hydrogel construct (Figures 3.3B-D). Consequently, these templated hydrogel constructs enable tissue-scale co-culture between two or more cell types in defined spatial locales and orientations.

Additionally, cell viability for two different types of primary cells, tendon/ligament fibroblasts and marrow stromal cells, is largely preserved for at least two weeks of cell culture in the laminated constructs developed in this study (Figure 3.4). This is possible despite the presence of UV light, the use of free-radical polymerization, and the low oxygen concentration present during crosslinking, all of which could have

been potentially harmful to the non-immortalized cell lines used in this study. Slow declines were observed in DNA content over time for both cell types after two weeks in culture (Figure 3.4B), similar to previous observations with cells encapsulated in non-patterned OPF:PEG-DA gels crosslinked in ambient air [359]. This response may be attributable to the specific cell source studied or the seeding density. At each time point evaluated in this study, remaining cells appeared predominately viable (Figure 3.4A); it is conceivable that additional modifications of the hydrogels to provide additional adhesion or degradation sites may be required in future studies to provide a more optimal microenvironment that would enhance cellularity during long-term culture in OPF hydrogels.

3.5 Conclusions

In this study, we focused on design, characterization, and preliminary *in vitro* evaluation of a novel tissue-scale, hydrogel-based scaffold for long-term, three-dimensional co-culture of multiple primary cell types with excellent spatial control. Hydrogels were successfully photopatterned into well-defined shapes at 1-2 mm thicknesses using a modified photolithographic process in simple, inexpensive microfluidic devices equilibrated in a nitrogen atmosphere to enhance crosslinking. Shape fidelity was maintained throughout the entire thickness of the construct, and this system was easily calibrated to allow for the production of hydrogels with tunable sizes and shapes depending on user specifications. Separate hydrogel modules were successfully laminated together with robust, well-defined interfaces, and this process enabled encapsulation and spatially controlled orientation of multiple cell types in monolithic arrays. Cell viability of sensitive primary cell isolates, namely tendon/ligament fibroblasts and marrow stromal cells, was successfully demonstrated for up to two weeks in culture in gel arrays photopatterned using this process. The system developed here establishes a proof of concept for examining MSC-based therapies for

tendon/ligament tissue regenerative medicine strategies. Additionally, this system may be extended to a variety of stem-cell types to inform basic science studies of interactions between multiple cell types in stem-cell mediated healing, as well as to improve design of a wide range of cell-based regenerative medicine therapies.

CHAPTER 4

3D *IN VITRO* TRI-CULTURE PLATFORM TO INVESTIGATE EFFECTS OF CROSSTALK BETWEEN MESENCHYMAL STEM CELLS, OSTEOBLASTS AND ADIPOCYTES

4.1 Introduction

An improved understanding of the multiple and complex molecular mechanisms underlying stem cell fate determination, especially those that result from interactions with native tissues, is an important prerequisite for designing and implementing cytotherapies involving stem cells [176, 323]. As test beds, *in vitro* systems with spatially and temporally controlled stem and native cell interactions can complement, inform, and predict potential outcomes of *in vivo* studies by reducing the complexity of interactions the cells encounter while minimizing cost of multiple animal studies. Results from these studies thereby fuel knowledge of how therapeutically implanted cells might facilitate repair and regeneration [360, 361]. To provide relevant platforms for evaluating regenerative medicine therapies, such *in vitro* systems should mimic niche environments of a 3D tissue as closely as possible by allowing for dynamic cell-cell interactions, given that cellular responses can vary substantially depending on the surrounding microenvironment [61, 159].

---

[2] Portions of this Chapter are adapted from Hammoudi, TM, Rivet, CA, Kemp, ML, Lu, H, and Temenoff, JS. 3D *In Vitro* Tri-Culture Platform to Investigate Effects of Crosstalk between Mesenchymal Stem Cells, Osteoblasts and Adipocytes. *Tissue Engineering A* (2012). Epub Ahead of Print.

Toward this end, use of biomaterials may provide a way to recreate these 3D environments, while allowing the study of complex cellular interactions. This includes the application of methods for high-throughput, multivariate analyses of high-content data (*e.g.* from gene microarrays, suspension arrays, TOF-mass spectrometry, and microscopy images) [62, 63, 312, 322, 327] that yield system-level information of complex cellular processes at or close to a single-cell level. However, innovative strategies that more closely mimic *in vivo* microenvironments need to be further coupled with the sophisticated methods outlined above [306]. Moreover, use of primary human cells (rather than immortalized mammalian cell lines), co-culture systems containing two or more cell types to permit better simulation of interactions within realistic microenvironments, and tissue-scale 3D-culture systems, have the potential to yield further progress toward making regenerative medicine a reality. Therefore, in these studies we employed an extension of novel photopatterning techniques (previously developed in our laboratory [362]) to generate and assemble 3D laminated hydrogel modules of three different primary human cell types (mesenchymal stem cells, osteoblasts, and adipocytes) into millimeter-scale co- and tri-culture constructs.

These cell types reside in close proximity within the same bone marrow niche, motivating their use in this platform as a model of interactions between them. Mesenchymal stem cells (MSCs), which are endowed with the ability to differentiate into many elements of the skeletal system [37], have been used clinically for cytotherapies both for musculoskeletal and other disorders [42]. The MSC differentiation programs of adipogenesis and osteogenesis are reciprocally regulated in cultures of MSCs: both RUNX2 and PPARγ master transcriptional regulators are present in low levels in

undifferentiated cells, and differentiation towards one lineage completely suppresses genes associated with the other lineage [10, 18]. This phenomenon has been exploited in past work to evaluate how cell shape [67], substrate stiffness [60], and the 3D biomaterial network structure [64] differentially regulate MSC fate under defined media conditions. Differentiation towards either pathway is also regulated by a complex set of paracrine signals [10, 18] derived from or regulated by cells in the neighboring bone marrow niche environment including osteoblasts, adipocytes, HSCs, and endothelial cells [10, 47]. Conditioned media and 2D co-culture studies have provided some insight into how one cell type (osteoblasts or adipocytes) affects the function and differentiation of MSCs [296, 299, 363]. However, these experiments only model static, one-way interactions and there is currently no systematic means to examine the effects of multi-directional and dynamic crosstalk over time between *multiple* cell types simultaneously in 3D culture in a way that better mimics interactions that occur *in vivo*.

To address these limitations, we encapsulated primary human MSCs, osteoblasts, and adipocytes into tissue-scale co- and tri-culture constructs, as described above. In particular for this study, we employed poly(ethylene glycol)-based hydrogels that maximized diffusion of soluble factors between cell types, and that were cultured in media without exogenously added differentiation cues. We hypothesized that this would enable us to specifically evaluate effects of soluble paracrine signals derived solely from the encapsulated cells. As a proof-of-principle experiment, we evaluated two co-culture configurations (MSCs flanked by adipocytes or osteoblasts on both sides) and a tri-culture configuration (one module each of osteoblasts, MSCs, and adipocytes; see Figure 4.1). We hypothesized that each culture environment would uniquely affect the differentiation of encapsulated MSCs and functional responses of osteoblasts and adipocytes as a result of continuous paracrine crosstalk and feedback. After 1, 7, and 18

days in culture, whole constructs were either: analyzed using histochemical staining to assess osteogenic or adipogenic differentiation, or sectioned with a scalpel to separate cell populations for qPCR analysis of mRNA expression for genes from several mesenchymal lineages. We further incorporated the relative expression levels of each gene assessed at each time point into a series of multivariate analyses. This provided the means to ascertain the covariance between genes and to determine how the dynamics of these co-variant genes correlate with possible emergent cell phenotypes.

4.2 Materials and Methods

4.2.1 Polymer Synthesis and Characterization

All chemicals were purchased from Sigma-Aldrich unless otherwise noted. Poly(ethylene glycol)-diacrylate (PEG-DA) was prepared as previously described [278] from PEG (M_n = 3,400 Da). The resultant polymer had a molecular weight M_n = 3,676 ± 16 Da with a polydispersity of 1.088 ± 0.015 as determined by gel permeation chromatography (Shimadzu), and the presence of conjugated acrylate groups was verified with ^{1}H-NMR.

To allow presentation of adhesive ligands that promote viability of encapsulated cells, fibronectin-derived GRGDS (PeproTech) and laminin-derived YIGSR (Anaspec) adhesion peptides were conjugated to a 3,400 Da molecular weight Acryl-PEG-succinimidyl valerate spacer (Acryl-PEG-SVA; Laysan Bio) in $NaHCO_3$ buffer (pH 8.5) according to previous protocols [364], dialyzed (1,000 Da MW cutoff), lyophilized, and stored at -20 °C until further use.

4.2.2 Cell Culture and Expansion

All cell culture reagents were obtained from Mediatech unless otherwise specified. Primary human MSCs (hMSCs) were obtained from the laboratory of Dr. Darwin Prockop (Texas A&M Health Sciences Center) and expanded according to

recommended protocols in Minimal Essential Medium-Alpha (αMEM) with 16.5% fetal bovine serum (FBS; Hyclone), 1 g/L glucose, 2 mM L-glutamine, 1% amphotericin B, and 0.1% gentamicin and cultured at 37°C with 5% CO_2 in a humidified incubator [365]. Primary human osteoblasts (hObs; Lonza) were expanded to 7 or 8 population doublings according to the manufacturer's protocol in Dulbecco's Modified Eagle Medium (DMEM) with 10% FBS, 1 g/L glucose, 1% amphotericin B, and 0.1% gentamicin. Primary human subcutaneous pre-adipocytes (Lonza) were expanded to 3-4 population doublings according to the manufacturer's protocol in DMEM with 10% FBS, 4.5 g/L glucose, 2 mM L-glutamine, 1% amphotericin B, and 0.1% gentamicin. Cultures at 80% confluence were differentiated into adipocytes (hAds) for 2 wks in expansion medium with 60 µM indomethacin, 0.5 mM 3-isobutyl-1-methylxanthine (IBMX), 0.5 µM dexamethasone, and 1 µM insulin.

4.2.3 Construct Fabrication and Long-Term 3D Co- and Tri-Culture

Layering devices were fabricated and employed for cell patterning as described in Figure 4.1. Briefly, 1 mm-thick spacers were cut from cured polydimethylsiloxane (PDMS; Sylgard 184; Dow Corning) and contact-bonded on each side to glass slides (Corning). Each spacer contained a cavity for polymer solution/gels as they were loaded and crosslinked. Assembled devices were sterilized by autoclave prior to use for encapsulation.

Hydrogel precursor solutions were formulated with 10% w/w PEG-DA in phosphate-buffered saline (PBS) containing 0.05% w/w D-2959 photoinitiator (Ciba) and 1 mM Acryl-PEG-GRGDS (for hMSCs) or Acryl-PEG-YIGSR (for hAds). Cell suspensions were prepared from near-confluent cultures using 0.05% Trypsin/0.53 mM EDTA and resuspended in their respective gel precursor solutions at a concentration of 15 million cells/mL. These solutions were loaded into layering devices and sequentially photocrosslinked into laminated 1 mm-thick, 1.5 mm-tall hydrogel strips (Figure 4.1).

After each patterning step, residual non-crosslinked material was rinsed out of the device with fresh 10% w/w PEG-DA solution using a syringe.[362] An opaque photomask was used in subsequent steps to prevent any further UV exposure and crosslinking of the existing gels. Single, laminated constructs were extracted from the device and sectioned with a scalpel perpendicular to the long axis of the laminate to yield twenty-one 1.5 mm-wide co- and tri-culture constructs (Figure 4.1).

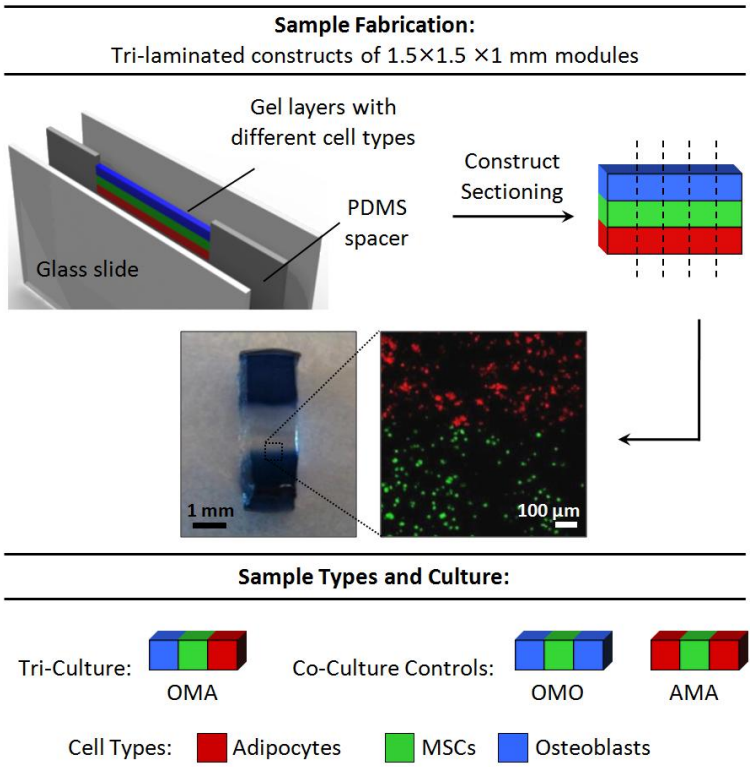

Figure 4.1. Sample fabrication and study design. Fabrication of co- and tri-culture constructs using the techniques outlined in the Methods yield sample sets with well-segregrated cell populations (Photographs: Sample tri-laminated hydrogel construct after reaching equilibrium swelling (left), and confocal image demonstrating hMSCs differentially stained with CellTracker Green (bottom) or Orange (top) segregated at an interface between modules). Three sample types were examined in this study: MSCs in the center module flanked by only one other cell type (co-culture controls) or by both osteoblasts and adipocytes (tri-culture).

Co-culture constructs consisted of hMSCs flanked on both sides by hObs (OMO) or hAds (AMA), while tri-culture constructs consisted of hMSCs flanked on one side by hObs and hAds on the other (OMA). Constructs were placed in separate wells of 6-well

tissue culture plates with 4 mL of co-culture medium [DMEM with 10% FBS, 50 μg/mL L-ascorbate-2-phosphate (Sigma), 1 μM insulin, 1% amphotericin B, and 0.1% gentamicin; replenished every 2 days] designed by our lab to maintain each cell type in culture while eliminating traditional exogenous differentiation cues. Constructs containing only hMSCs in each module were fabricated and cultured in osteogenic or adipogenic differentiation medium for 21 days as a positive control to verify that differentiation was possible in this culture system under a standard set of cues. Osteogenic differentiation medium consisted of αMEM with 10% FBS, 50 μM L-ascorbate-2-phosphate, 20 mM β-glycerophosphate (Sigma), 10 nM dexamethasone, 1% amphotericin B, and 0.1% gentamicin. Adipogenic differentiation medium consisted of αMEM with 10% FBS, 0.5 mM IBMX, 60 μM indomethacin, 1 μM insulin, 0.5 μM dexamethasone, 1% amphotericin B, and 0.1% gentamicin.

4.2.4 mRNA Isolation and qPCR

Hydrogel constructs were rinsed in PBS and blocks containing individual cell populations were separated from each other using a scalpel for gene expression analysis by qPCR after 1, 7, and 18 days in co- or tri-culture. Gel blocks containing the same cell type were pooled from 3 constructs of the same culture condition to provide sufficient copies of mRNA for quantification. These blocks were homogenized in microcentrifuge tubes with pellet grinders, after which mRNA was extracted using a QIAshredder tissue homogenizer and RNeasy kit with DNase I digestion (Qiagen). cDNA was generated using SuperScript III Reverse Transcriptase (Invitrogen) with Oligo$(dT)_{15}$ primers and dNTPs (Promega). Gene expression of each cell type was analyzed for target mesenchymal lineage genes using custom-designed primers (Table 4.1) with quantitative PCR amplification performed on a StepOnePlus^{TM} Real-Time PCR System (Applied Biosystems) in the presence of SYBR Green/ROX master mix (Applied Biosystems). *RPS18* and *ACTB* were both used as endogenous controls for normalization through

geometric averaging [366], and relative expression (n = 4 per culture type and time point) of each target gene was calculated using the formula: $2^{\Delta C_t} = \frac{2^{C_t,\text{ target gene}}}{\sqrt{2^{C_t,RPS18} \cdot 2^{C_t,ACTB}}}$ where C_t represents the cycle threshold for amplification. Endogenous controls were evaluated in each cell type to ensure that their expression levels were not altered across time or culture conditions [367, 368].

Table 4.1 Library of lineage-specific mRNA transcripts for gene expression analysis*

Lineage	*Target Gene*	*NLM Accession Number*	*Primer Set (Forward, Reverse)*
Osteogenic	*RUNX2*	NM_001024630.3	TTTGCACTGGGTCATGTGTT TGGCTGCATTGAAAAGACTG
	OCN	NM_199173.4	GTGCAGAGTCCAGCAAAGGT AGCAGAGCGACACCCTAGAC
Adipogenic	*PPARG2*	NM_015869.4	TCCATGCTGTTATGGGTGAA GGGAGTGGTCTTCCATTACG
	LEP	NM_000230.2	ACCCTGTGCGGATTCTTGTGGCTTTGG GGCTCTGCCTACCCCTCTGCCCT
Chondrogenic	*SOX9*	NM_000346.3	GCGGAGGAAGTCGGTGAAGAACGGGCA TGTGAGCGGGTGATGGGCGGG
Myogenic	*MYOD*	NM_002478.4	GTCGAGCCTAGACTGCCTGT GTATATCGGGTTGGGGTTCG
Endogenous Controls	*RPS18*	NM_022551.2	CGATGGGCGGCGGAAAATAGCCTTGC CAGTGGTCTTGGTGTGCTGGCCTCGG
	ACTB	NM_001101.3	GCAGTCGGTTGGAGCGAGCATCCCC TCCCCTGTGTGGACTTGGGAGAGGAC

* Full gene names: *RUNX2* (runt-related transcription factor 2), *OCN* (osteocalcin), *PPARG2* (peroxisome proliferator-activated receptor γ, isoform 2), *LEP* (leptin), *SOX9* (SRY (sex determining region Y)-box 9), *MYOD* (myogenic differentiation 1), *RPS18* (ribosomal protein 18S), *ACTB* (β-actin).

4.2.5 Histological Analysis for Differentiation

Following co- or tri-culture, whole constructs (n = 1-2 per culture type and time point; same times points as above) were collected for histological staining. Constructs were rinsed in PBS and infiltrated by graded concentrations of sucrose in PBS followed by graded concentrations of optimal cutting temperature compound (OCT; Sakura Finetek) using a technique adapted from the literature (Appendix B, [369]) and individually embedded in OCT, flash-frozen in liquid N_2, and stored at -80 °C until sectioning. Embedded constructs were serially sectioned into 20 µm-thick slices (Microm

HM 560 Cryostat; Thermo Scientific), mounted on Superfrost Plus slides (Fisher), and stored at -80 °C until staining. Adipogenic differentiation was assessed with an Oil Red O stain for triglyceride accumulation in intracellular storage vesicles using standard protocols [365] and visualized with brightfield microscopy. Osteogenic differentiation was examined by assessing *in situ* alkaline phosphatase activity (Vector® Red Alkaline Phosphatase Substrate Kit; Vector Labs). Briefly, unfixed sections were reacted with an alkaline phosphatase substrate in 100 mM Tris buffer (pH 8.5) according to the manufacturer's protocol and counterstained with Hoechst 33258 (0.25 μg/mL in PBS for 5 min; Molecular Probes), and visualized with epifluorescence microscopy under Texas Red and DAPI filters, respectively.

4.2.6 Statistical Analysis and Multivariate Modeling

Gene expression results are depicted as mean ± standard deviation unless otherwise noted. Prior to statistical analysis, all data were transformed with a Box-Cox transformation. Data were analyzed by multi-factor analysis of variance (ANOVA) to identify significant factors (cell type, culture type, day) and factor interactions (cell type*day, culture type*day) for each target gene assayed. Where significance factors and interactions were identified by ANOVA, Tukey's *post hoc* test (significance level $p < 0.05$) was used to determine significant differences between individual sample groups.

Multivariate statistical modeling was performed with the overall goal of extracting combinations of time-variant gene expression markers that were the most informative for distinguishing differences among cell types and co- or tri-culture conditions. All Box-Cox-transformed data were mean-centered and scaled to unit variance prior to analysis as a means of normalization to allow all variables to be considered equally scaled in the principal components or latent variables [312]. For these analyses, the data set (total of 504 data points) was organized into an $N \times K$ matrix X that denotes the measured gene expression levels with time as well as cell type and culture

type. Principal component analysis (PCA) was first performed to discern possible clusters of observations and their qualitative similarities among the global data set in an unbiased fashion. PCA was performed using SIMCA-P$^+$ software (Umetrics) to analyze the X matrix and generated linear combinations of the X-variables (target gene and time; K = 18) that described the sources of maximum variation to cluster them by their contributions to the variance of the entire set of X-observations (cell type and culture type; N = 28). Using the observed clusters, partial least squares discriminant analysis (PLS-DA) was then performed (SIMCA-P$^+$) using an additional $N \times M$ matrix Y that encoded m purported classes of data (*e.g.* cell type or culture type) to find latent variables (linear combinations of the independent X-variables) that served as discriminating features to best separate the N observations into M different purported classes designated by the dependent Y-variables. In summary, PCA was used to observe the overall correlation structure of the gene expression data and understand how it contributed to the largest variance among the observations, while PLS-DA aided in separating tight clusters of observations and revealing the covariant genes that correlated with each class [370, 371].

To optimize the quality of PCA and PLS-DA models, several pruning procedures were performed to remove outlying observations (outside 95% confidence interval) and non-influential variables (weight approximately 0 in both components) and enable statistical significance-testing of the model and the variables used to generate it [370, 372]. The quality of each model was summarized by two non-dimensional statistical parameters: 1) R^2X (for PCA) or R^2Y (for PLS-DA), which quantitatively measure the extent to which the model explains the variation in the data matrices and dictate a *goodness of fit*; and 2) Q^2, which quantitatively measures the extent to which the variation of a future experimental data set may be predicted by the model (*goodness of prediction*) [372]. Both of these parameters are analogous to regression statistics, with a value ranging from 0 (poor) to 1 (perfect) fit or predictive capability. The appropriate

number of principal components or latent variables was determined by cross-validation [370, 372]. The results of this procedure were fed into a jack-knifing analysis [370] to calculate the standard errors of the regression coefficients (weights), which were then converted into 95% confidence intervals via the *t*-distribution to determine which X-variables (genes) of high weight have a statistically significant influence ($p < 0.05$) on each class of observations (Y-variables) in each of the PLS-DA models generated (Figs. 5D and 6D-F).

4.3 Results

4.3.1 Gene Expression Dynamics and Histochemical Staining

We demonstrate that each of the examined mesenchymal lineage genes (Table 1) exhibited expression dynamics in each cell type with time that appeared to vary depending on the co- or tri-culture condition employed (Figures 4.2-4.4). Certain genes were often uniquely variable only within a particular cell type, with MSCs exhibiting time-variant changes in most of the genes examined (Figure 4.4), while adipocytes (Figure 4.2) and osteoblasts (Figure 4.3) exhibited changes in expression among only two or three of the genes evaluated.

4.3.1.1 Adipocytes

Adipocytes co-cultured only with MSCs (AMA configuration) exhibited significant decreases in expression of *RUNX2* (29-fold), *PPARγ2* (15-fold), *OCN* (11-fold), and *LEP* (64-fold) at day 7 (Figure 4.2A). Relative to day 1, *RUNX2* expression at day 18 was still significantly lower (1.5-fold), *OCN* expression was significantly higher (2.1-fold), and *PPARγ2* and *LEP* were unchanged. Adipocytes from tri-culture (OMA) showed a significant decrease in expression of *RUNX2* (3.0-fold), *PPARγ2* (6.8-fold), and *LEP* (22-fold) at day 7 that persisted through day 18. Relative to AMA adipocytes, expression of *RUNX2* was significantly lower at each time point and *OCN* was expressed

in higher quantities at day 18. Compared with the osteoblastic and adipocytic genes, expression of *MYOD* and *SOX9* remained relatively stable in each cell type over time. Over the entire culture period, examination of Oil Red O staining revealed no qualitative differences in triglyceride storage vesicles in adipocytes from either culture condition (Fig 2B).

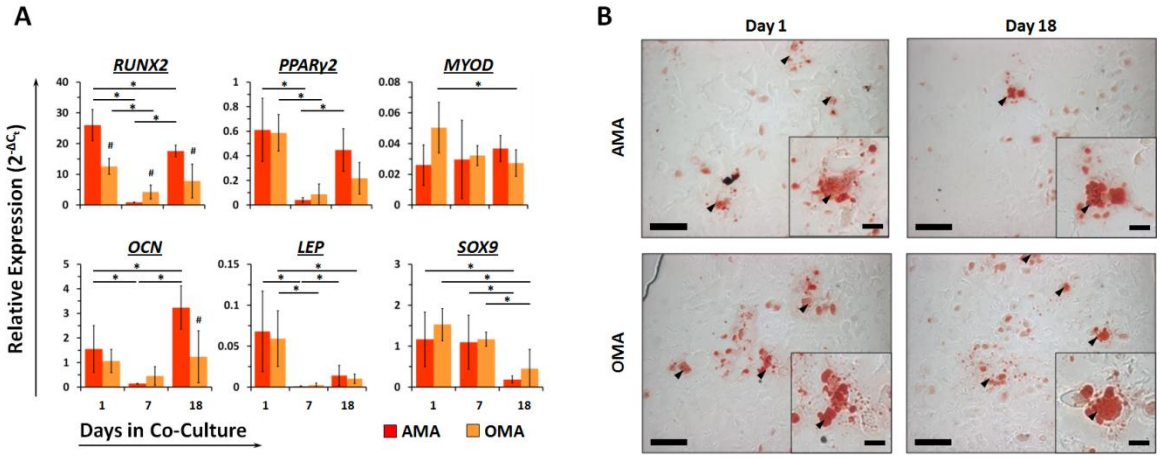

Figure 4.2. Co-culture and tri-culture differentially affect expression dynamics of osteoblastic (*RUNX2* and *Osteocalcin*) and adipocytic (*PPARγ2* and *Leptin*) genes in adipocytes but does not affect triglyceride storage with time. A) Adipocyte expression levels of gene regulators of several mesenchymal lineages relative to *RPS18* and *ACTB* over 18 days in co- and tri-culture. Values scaled × 10^3. * = Significantly different from another day, same culture type; # = Significantly different from another culture type, same day; $p < 0.05$. B) Oil Red O staining of triglyceride storage vesicles (arrows) in adipocytes from AMA and OMA culture conditions over time. (Brightfield microscopy, scale bar = 50 µm; Inset scale bar = 20 µm)

4.3.1.2 Osteoblasts

Osteoblasts co-cultured only with MSCs (OMO) exhibited significant decreases in expression of *RUNX2* (2.0-fold), *OCN* (2.1-fold), and *SOX9* (7.9-fold) at day 7, and *RUNX2* decreased further by day 18 (2.7-fold relative to day 1; Figure 4.3A). Osteoblasts from tri-culture (OMA) also exhibited significant progressive declines in *RUNX2* (1.6- and 3.8-fold at day 7 and day 18, respectively, relative to day 1) and *OCN* (1.5- and 2.8-fold) through day 18. While *RUNX2* and *OCN* expression were higher in OMA than OMO osteoblasts at day 7, both genes exhibited the same expression levels in each

culture setting by day 18. Expression of *SOX9* in OMA osteoblasts, while much lower than OMO osteoblasts on day 1, remained the same by day 7 and significantly decreased (48-fold) by day 18. Alkaline phosphatase activity appeared similar in osteoblasts from both culture conditions on day 1 (Figure 4.3B). This activity persisted longer in osteoblasts from OMO than OMA constructs by day 7. By day 18, no alkaline phosphatase activity could be observed in either of the sample types.

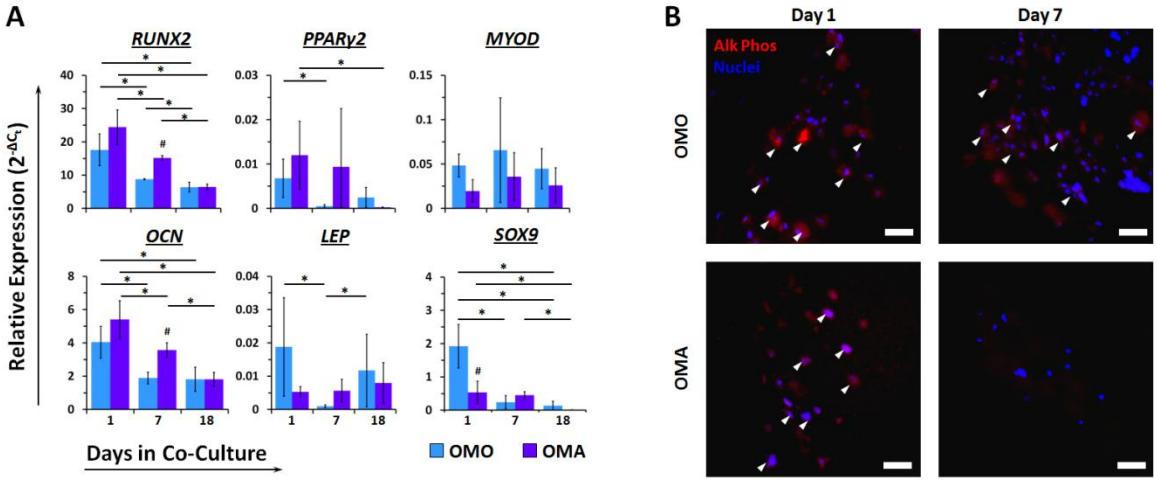

Figure 4.3. Co-culture and tri-culture differentially affect expression dynamics of osteoblastic (*RUNX2* and *Osteocalcin*) and chondrogenic (*SOX9*) genes in osteoblasts, in addition to alkaline phosphatase activity persistence with time. A) Osteoblast expression levels of gene regulators of several mesenchymal lineages relative to *RPS18* and *ACTB* over 18 days in co- and tri-culture. Values scaled × 10^3. * = Significantly different from another day, same culture type; # = Significantly different from another culture type, same day; $p < 0.05$. B) *In situ* alkaline phosphatase substrate conversion in osteoblasts from OMO and OMA culture conditions over time. (Scale bar = 20 µm; Arrows indicate cells with enzyme activity)

4.3.1.3 Mesenchymal Stem Cells (MSCs)

Lineage markers in MSCs exhibited much more diverse and complex expression dynamics dependent on their co- or tri-culture setting (Figure 4.4A). *RUNX2* expression levels persisted through day 7 in MSCs from co-culture settings while declining significantly in tri-cultured MSCs by day 7 (1.6-fold). By day 18, *RUNX2* expression was graded in MSCs depending on the relative amount of osteoblasts present in the co- or tri-culture construct. Conversely, *PPARγ2* expression was dramatically higher in MSCs co-

cultured with adipocytes (AMA) as early as day 1 and persisted throughout the culture period, while OMO MSCs exhibited consistently low levels that did not change. Tri-cultured MSCs (OMA) exhibited a 14-fold reduction in *PPARγ2* expression at day 7, but this was upregulated 6.6-fold relative to day 1 after 18 days to an intermediate level between AMA and OMO MSCs. Expression of *MYOD* increased only in MSCs from OMO and OMA culture conditions by day 7 (3.6- and 4.1-fold, respectively), and was sustained through 18 days in culture. *SOX9* expression was only upregulated in MSCs co-cultured with osteoblasts at day 7 (3.0-fold) before declining to day 1 levels. Genetic markers of terminal differentiation towards osteoblasts (*OCN*) and adipocytes (*LEP*) were not significantly upregulated over time in MSCs from any of the co- or tri-culture conditions tested, and this was reflected in our histological analysis. No triglyceride storage occurred in MSCs from any culture condition over the entire length of the co-culture period (Figure 4.4B). Transiently increased, relatively low alkaline phosphatase activity was observed only in a small number of MSCs from constructs containing osteoblasts (OMO and OMA, day 7) which was absent on day 18 (Figures 4.4C,D). Positive control gels containing only MSCs and cultured in osteogenic or adipogenic medium exhibited visible alkaline phosphatase activity and triglyceride storage, respectively (Figure 4.4D).

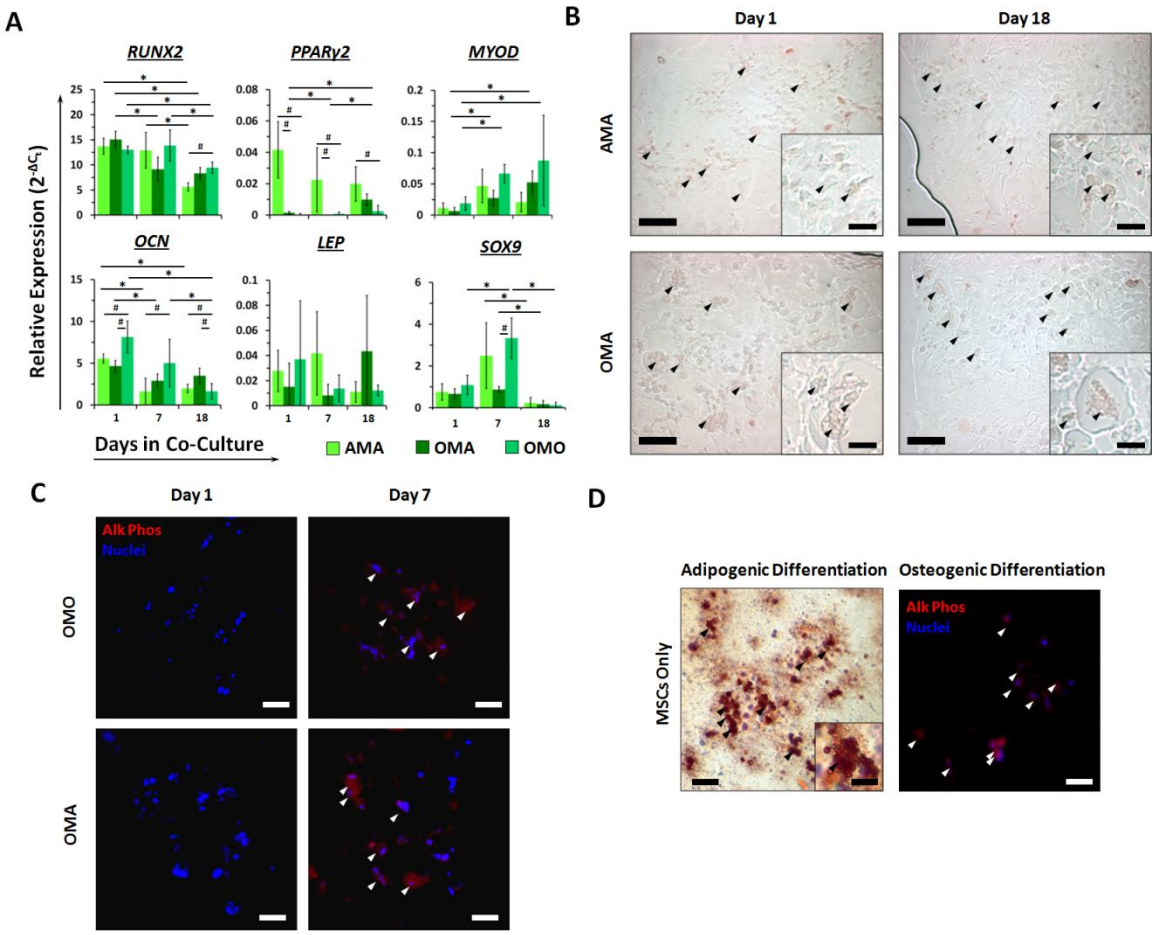

Figure 4.4. Co- and tri-culture differentially affect expression levels and dynamics of several lineage specific transcription factors (but not terminal differentiation markers) in MSCs, while only causing scant and transient alkaline phosphatase expression in MSCs from osteoblast-containing cultures. A) MSC expression levels of gene regulators of several mesenchymal lineages relative to *RPS18* and *ACTB* over 18 days in co- and tri-culture. Values scaled × 10^3. * = Significantly different from another day, same culture type; # = Significantly different from another culture type, same day; $p < 0.05$. B) Absence of Oil Red O staining in MSCs (arrows) from different co- and tri-culture conditions over time. (Brightfield microscopy, scale bar = 50 µm; Inset scale bar = 20 µm) C) *In situ a*lkaline phosphatase substrate conversion in MSCs from different co- and tri-culture conditions over time. (Scale bar = 20 µm; Arrows indicate cells with enzyme activity). D) MSCs exposed to exogenous differentiation cues are able to undergo osteogenesis and adipogenesis after encapsulation in this culture platform (monoculture of MSCs only). Left: Oil Red O staining of triglyceride storage vesicles (arrows) in MSCs cultured in adipogenic medium for 28 days. (Brightfield microscopy, scale bar = 50 µm; Inset scale bar = 20 µm). Right: *In situ a*lkaline phosphatase substrate conversion in MSCs cultured in osteogenic medium for 28 days. (Scale bar = 20 µm).

4.3.2 Multivariate Modeling of Gene Expression Data

Given the seemingly complex gene expression responses among different cell types placed under different co- and tri-culture conditions, we thought that taking a more global view of these factors using multivariate modeling would provide additional information; from this analysis, one could potentially extract and examine clusters of cell types that exhibit similar responses in gene expression to their culture conditions based on covariance of more than one gene. Therefore, we performed principal component analysis (PCA) to reduce the dimensionality of all the summarized gene expression data based on the sources of maximum variance (Figure 4.5A). Plotting samples in the first two principal components (PCs), which captured ~69% of the variability in the data set, indicated that MSCs and osteoblasts cluster apart from adipocytes (first PC; 51.1% of data set variability). The second PC captured an additional 17.8% of the variance in the data and separated MSCs co-cultured with adipocytes (AMA) from osteoblasts and MSCs from other culture conditions (OMO and OMA). Plotting the variable loadings in the first two PCs indicated that each of the genes evaluated was highly influential in the model at one or more time points since each has large weight on one or both PCs (Figure 4.5B; variables with 0 weight were removed during pruning). In distinguishing the different clusters of observations from the score plot, adipocytes from OMA and AMA constructs were most distinguishable by *PPARγ2* expression, MSCs from AMA constructs were most correlated with high *PPARγ2* and *LEP* expression, and osteoblasts and MSCs from OMO and OMA constructs were highly correlated with *RUNX2* and *OCN* expression.

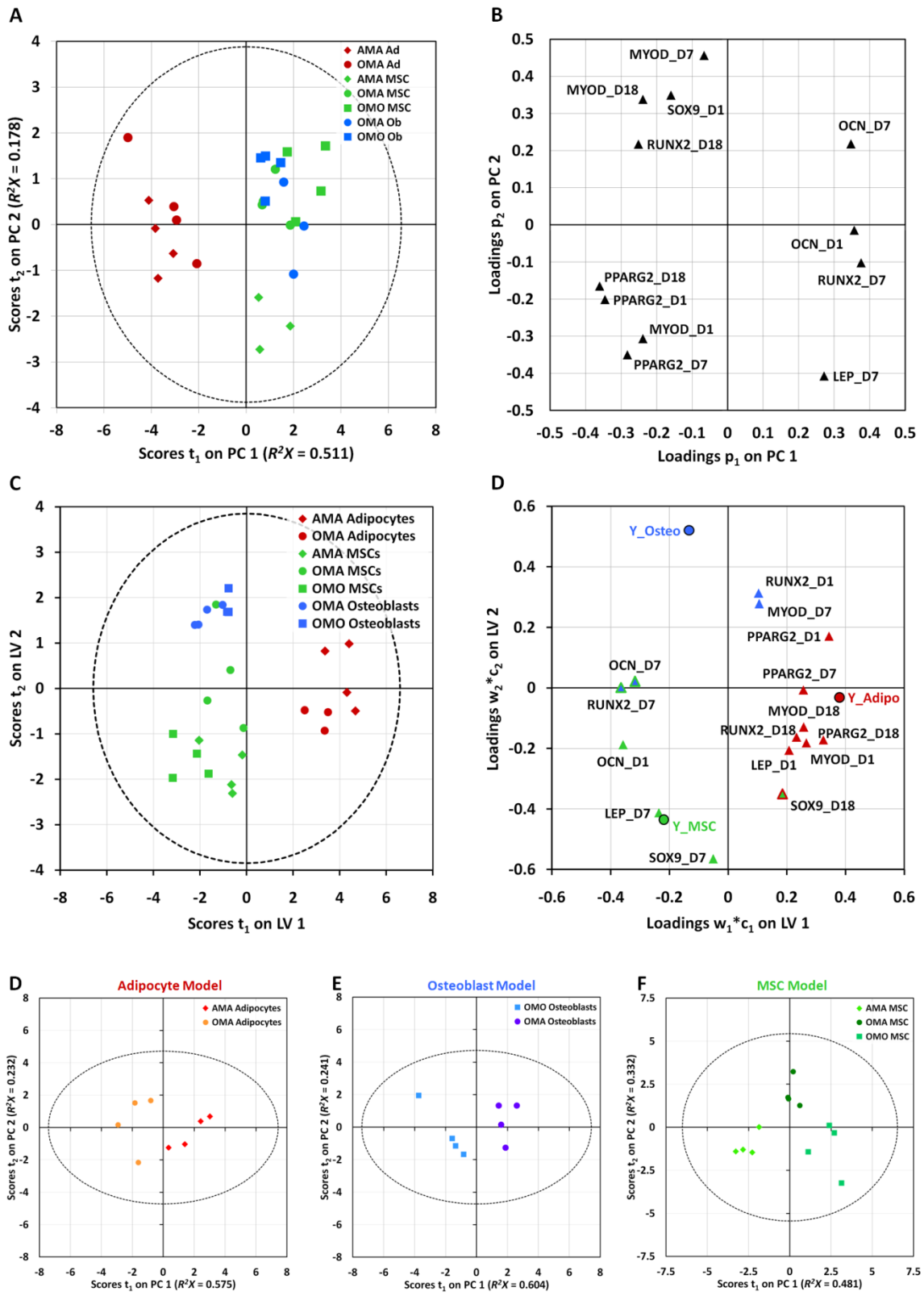

Figure 4.5. Statistical modeling based on covariance of the expression of several mesenchymal lineage genes yields two latent variables that are able to distinguish

MSCs from adipocytes and osteoblasts, respectively, and elucidates the correlation structure of the gene expression at various time points with each cell type present. A) Plot of PCA scores, t_1 and t_2, separating the observations by two principal components (PC) that explain 51.1% and 17.8% of the variance in data, respectively. Dashed line represents the 95% confidence limit of the distribution of scores. B) Plot of PCA loadings, p_1 and p_2, that shows the correlation of the gene expression data with the sources of maximum variance. Model quality parameters: R^2X = 0.689, Q^2 = 0.450. C) Plot of PLS-DA scores, t_1 and t_2, for observations (cell type and culture type) that segregates three distinct cell types by two latent variables (LVs). D) Loading plot depicting the correlation structure of the gene expression data and the corresponding cell types, indicating: 1) the weights, w*, that combine the X-variables (gene expression values at different time points) to form the scores, t; and 2) and the weights, c, of the discriminating Y-variables (corresponding to each cell type). Gene expression values at specific times (X-variables, triangles) that contribute most to the cell type classification (Y-variables, circles) are labeled accordingly with the corresponding color scheme. R^2Y = 0.750, Q^2 = 0.681. D-F) PCA within each cell type demonstrates that more than 80% of the variance between samples is explained by differences between co- and tri-culture. A) Model discriminating between adipocytes from co- and tri-culture. R^2X = 0.807, Q^2 = 0.373. B) Model discriminating between osteoblasts from co- and tri-culture. R^2X = 0.845, Q^2 = 0.400. C) Model discriminating between MSCs from different co- and tri-culture conditions. R^2X = 0.812, Q^2 = 0.547. Figure 4.5 continued.

Several clusters of data by cell type and/or culture type were discernible by the PCA results, though they overlapped to an extent. These findings motivated further supervised analysis to deconvolve this complex data set into a meaningful set of variables that adequately describe the patterns of samples and their gene covariance in the overall data set. We first classified the observations into three groups by cell type and generated a two-latent variable PLS-DA model with quality parameters R^2Y = 0.75 and Q^2 = 0.681. The model distinctly classified the scores with the first latent variable describing the differences of adipocytes from the other cell types present, and the second latent variable describing the differences between MSCs and osteoblasts (Figure 4.5C). Osteoblasts and adipocytes constitute smaller clusters on this score plot, while MSCs constitute a much larger cluster, owing to differences in heterogeneity between the three cell types. With respect to the gene expression dynamics that constitute the latent variables, several genes from different mesenchymal lineages overlap in their contribution to discrimination of

the different cell types. This can be visualized by their proximities to one another on the weight plots in the latent variable space (Figure 4.5D). *PPARγ2* (days 1, 7, and 18), *MYOD* (days 1 and 18), *LEP* (day 1), and *RUNX2* (day 18) significantly correlated with adipocytes; *SOX9* (day 7), *LEP* (day 7), and *OCN* (day 1) significantly correlated with MSCs; and *RUNX2* (day 1) and *MYOD* (day 7) significantly correlated with osteoblasts. In addition, *SOX9* (day 18) is significantly correlated with both MSCs and adipocytes, and *RUNX2* (day 7) and *OCN* (day 7) are significantly correlated with both MSCs and osteoblasts.

Within the larger clusters of cell types in our first PLS-DA model (Figure 4.5C), we noticed that several observations appeared to also cluster by co- or tri-culture setting. After generating several preliminary PCA models, we were able to verify that much of the variation within these clusters (> 80%) could be accounted for in PCs that separated the observations by co- or tri-culture conditions (Figure 4.5D-F). This motivated the development of a separate PLS-DA model for each cell type (Figure 4.6) to further classify the observations by culture condition and determine gene expression variables at specific times that are highly determinative of cells from each condition. A single-latent variable model of adipocytes revealed that expression dynamics of adipocytic (*PPARγ2*), osteoblastic (*RUNX2* and *OCN*), and myogenic (*MYOD*) genes are important for discriminating the cell populations from AMA and OMA culture conditions (Figures 4.6A,D). A single-latent variable model of osteoblasts discriminates OMO and OMA populations largely by their expression dynamics of osteogenic (*RUNX2* and *OCN*) and chondrogenic (*SOX9*) markers (Figures 4.6B,E). Further, a two-latent variable model of MSCs discriminates cell populations from all three culture conditions (Figures 4.6C,F) on the basis of several mesenchymal lineage markers unique to each population. AMA MSCs are most significantly correlated with expression of adipogenic marker *PPARγ2* on days 1 and 7, while OMO MSCs are characterized by osteogenic markers *RUNX2* (day 18) and *OCN* (day 1). Interestingly, we observed that unlike co-cultured MSCs, tri-

cultured MSCs (OMA) correlated strongly with osteogenic (*RUNX2*, day 1; *OCN*, day 18), adipogenic (*LEP*, day 18), and myogenic (*MYOD*, days 7 and 18) markers.

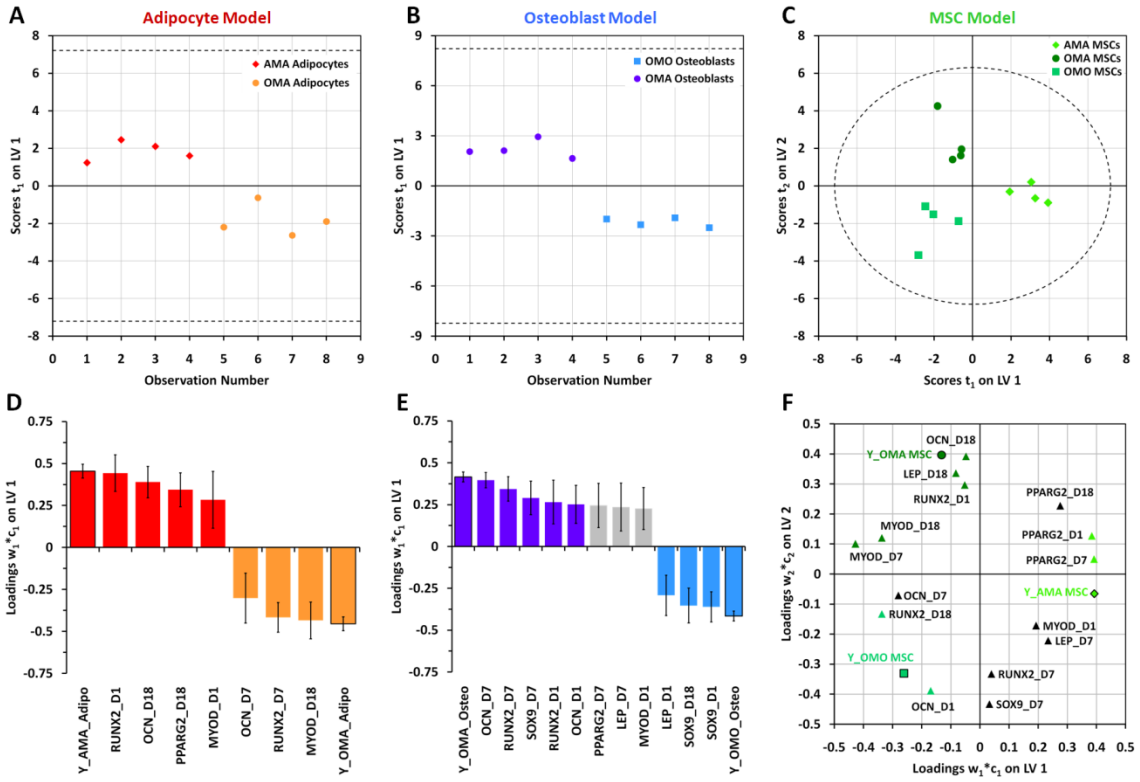

Figure 4.6. PLS-DA models of single cell types can robustly separate cell samples derived from different culture conditions and describe the important gene expression variables that correlate with each response to co- or tri-culture. A,D) Model discriminating between adipocytes from co- and tri-culture. R^2Y = 0.898, Q^2 = 0.820. B,E) Model discriminating between osteoblasts from co- and tri-culture. R^2Y = 0.972, Q^2 = 0.920. C,F) Model discriminating between MSCs from different co- and tri-culture conditions. R^2Y = 0.854, Q^2 = 0.716. A-C) Score plots of clusters of adipocytes (A), osteoblasts (B), and MSCs (C) segregated into distinct groups by one (adipocytes, osteoblasts) or two (MSCs) latent variables. Dashed lines represent the 95% confidence limit of the distribution of scores for the corresponding model. D-F) Loading plots depicting the correlation structure of gene expression data and the corresponding observation sets for each model. Gene expression values at specific times (X-variables) that significantly contribute (p < 0.05) most to the cell type classification (Y-variables) are shaded accordingly with the corresponding color scheme. Bar graphs depict mean ± S.E.M.

4.4 Discussion

This work presents a simple platform for patterning multiple types of cells into tissue-scale 3D hydrogel constructs that are permissive for multi-directional paracrine signal communication and produce distinct responses in each cell type dependent on the co- or tri-culture environment surrounding it. Devices used to generate these platforms (Figure 4.1) are easily constructed from inexpensive, sterilizable, and reusable materials, making them appropriate and readily adaptable for use in any laboratory environment. The size of the PDMS cavity can be readily adapted to contain modules of different sizes and thicknesses with some limitations depending on the materials used (*e.g.* light penetration through the entire thickness, efficiency of the crosslinking reaction) [362]. The modularity of this hydrogel system, enabled by the sequential crosslinking and lamination of these synthetic, chemically tailorable hydrogels, allows for flexibility in the configuration of patterned cells and also provides a means for tailoring the microenvironmental niche of each cell type (*e.g.* biomaterials, material stiffness, biochemical moieties, and cell density) independently [65, 176]. This feature stems from the ability to use a mask for preventing further crosslinking, UV exposure of cells, or other modification of a gel module after each step.

The data acquired from these proof-of-principle experiments suggest that the differential effects of each co- and tri-culture environment on each cell type can result from paracrine signaling that occurs between each cell type in the absence of proliferation, migration, cell spreading, and direct cell-cell contact. Our hydrogel platform is specifically designed to isolate these effects due to its sufficiently small mesh size to prevent cell migration and proliferation while allowing the diffusion of soluble cues from the small molecule to protein scale [373]. While cell spreading is permissive

for and promotes osteogenesis [67], we chose to decouple the effects of cell spreading from soluble signals in these experiments to isolate the effects of signaling crosstalk alone.

Fibronectin- and laminin-derived peptides (RGDS and YIGSR, respectively) were employed here to promote cell viability of encapsulated hMSCs and adipocytes during the culture as this may be adhesion-dependent [198, 374]. During co- and tri-culture, cells are coupled via these peptides to the polymer network of the hydrogel and may additionally deposit extracellular matrix (ECM). Consequently, we cannot definitively rule out the possibility of intercellular communication via mechanical coupling between the cells and the polymer/ECM. However, all of the cells sense the same bulk mechanical properties of the gel modules since they are composed of the same gel material. The encapsulated cells are likely unable to generate large traction forces (due to lack of cell spreading) [67, 375], and mechanical signals would have to propagate over relatively long distances for cells from different modules to communicate. Furthermore, the synthetic polymer matrix of high crosslink density used here cannot be remodeled to aid in mechanical signal propagation (*e.g.* compared with collagen [376], hyaluronic acid [64], ionically crosslinked alginate [60]), and much of the matrix deposition in these synthetic, non-degradable gels likely remains confined to a pericellular location [364]. Together, these considerations support the likelihood that much of the intercellular crosstalk in this system is dominated by soluble paracrine factors.

Traditional mono- and co-culture experiments with MSCs and their differentiated counterparts use exogenous factors to drive and maintain their differentiation and terminal function [365], or employ a mixture of differentiation media as a method for

providing a permissive environment for differentiation while minimizing bias [60, 64]. We formulated our co-culture medium without any exogenous differentiation cues, relying instead on the cells themselves to produce the soluble signals necessary to drive each other's responses. While terminal differentiation was not observed, environment-dependent responses occurred in each cell type. This suggests that the encapsulated cells are both producing and responding to soluble signals during the 18-day culture period evaluated in this study. Although these signals were not directly measured in these experiments, characterizing their roles will be included as a part of future studies with this platform.

As a direct consequence of being able to readily separate each cell type after the co- or tri-culture period by simple gel sectioning, we were able to observe the effects of paracrine crosstalk on each cell type independently at the individual gene level (Figures 4.2-4.4) and more globally through multivariate analysis (Figures 4.5-4.6). While controls containing only one encapsulated cell type were not examined in this study, our analysis does demonstrate gene expression dynamics and potential histological changes that vary with co- and tri-culture conditions and are independent of the effects of time in culture. While these culture-dependent effects could be inferred from close examination of the data on a gene-by-gene basis (Figures 4.2-4.4), we were able to leverage the power of multivariate modeling to examine how distinct our observations were from each other given the covariance that existed across the multiple genes we examined. Our high quality PLS models ($R^2 \geq 0.75$ and $Q^2 \geq 0.68$) [370] confirmed many of the findings present in our preliminary inspection of the data, such that: i) adipocytes could be clearly distinguished from the other cell types, ii) AMA MSCs could be represented as a distinct

cluster from other MSCs, iii) similarities in osteoblasts and MSCs from OMO and OMA samples could be mapped, and iv) a reduced set of genes that dynamically contribute to different emerging phenotypes of each cell type from the different co- and tri-culture conditions could be clearly distinguished.

Our analysis showed that adipocytes in co- and tri-culture differentially expressed the adipogenic genes *PPARγ2* and *LEP* and (surprisingly) osteogenic genes *RUNX2* and *OCN*, though this did not appear to affect their triglyceride storage (Figures 4.2 and 4.6D). The presence of MSCs (with or without adipocytes) affected osteoblastic (*RUNX2* and *OCN*) and chondrogenic (*SOX9*) markers in osteoblasts (Figures 4.3 and 4.6B,E). Interestingly, alkaline phosphatase activity appeared to persist longer in co-cultured than tri-cultured osteoblasts (Figure 4.3B). Taken together, our results suggest that adipocytes and osteoblasts in co- and tri-culture maintain some of their major functions or phenotypic markers. However, there may be subtle and previously unreported differences in the functional capacities of adipocytes and osteoblasts depending on neighboring cell types, based on the differential expression of genes regulating each lineage. Conversely, these findings may suggest that the culture environment (soluble cues, the presence of MSCs, or the hydrogel scaffold) or the pre-culture of primary cells may need further optimization to promote sustained functions associated with terminal differentiation. These potentially novel phenotypes and their determinants, including intercellular signals and potential artifacts of the *in vitro* microenvironment, could be more closely evaluated further in future studies.

The analytical techniques applied here were particularly useful in clearly discerning population-level differences among MSCs from different co- and tri-culture

settings. We selected transcription factors for multiple MSC lineages, since their plasticity and level of lineage commitment are attributable to the simultaneous expression of these markers in their undifferentiated state that are progressively down-regulated as the cells commit [77]. All lineage-specific transcription factors in these cells were affected to some extent by the co- and tri-culture settings. For example, AMA MSCs, the most distinct population of MSCs (Figure 4.5A), were most highly correlated with increased expression levels of *PPARγ2* (Figures 4.4A and 4.6F) and were the only MSCs that failed to exhibit alkaline phosphatase activity during the co-culture period (Figure S2). Conversely, OMO MSCs correlated with higher expression levels of *RUNX2* and *OCN* (Figures 4.4A and 4.6F), clustered with osteoblasts (PCA analysis; Figures 4.5A,B), and appeared to exhibit alkaline phosphatase expression in some cells at day 7 (Figure 4.4B). In contrast, MSCs cultured alone in the same hydrogel formulation, but using standard differentiation media, exhibited marked histological signs of differentiation (Figure S3). This finding suggests that the lack of significant staining in co- or tri-culture for either differentiation marker in MSCs (as well as other cell types) may not be an artifact of the culture system, but rather a sign that the signaling cues from neighboring cell types is not sufficient to induce terminal differentiation. Taken together, this suggests that co-cultured MSCs, while not terminally differentiated, may be biased towards differentiation toward the cell type with which they were co-cultured, in agreement with previously published data from other groups [296, 299, 363]. Tri-cultured (OMA) MSCs, while closely related to osteoblasts and OMO MSCs in their gene expression and apparent alkaline phosphatase expression (Figures 4.4A,B and 4.5A,B), correlated with a broader set of mesenchymal lineage genes, including *MYOD* (Figure 4.6F). This might

suggest a much more heterogeneous population of cells that emerged from tri-culture or a different bias in lineage commitment, each of which merit further study given the paucity of literature describing the combined effects of osteoblast- and adipocyte-derived soluble signals on MSCs. Additionally, this validates the relevance of this tri-culture system for future efforts to re-capitulate the bone marrow niche and to model bone marrow pathologies [10].

4.5 Conclusions

In this study, we develop a simply fabricated, photopatternable 3D culture system that enabled observation of distinct gene expression dynamics resulting from dynamic paracrine interactions between MSCs, osteoblasts, and adipocytes. This may result in distinct phenotypes for both the stem and terminally differentiated cells, representing changes in their lineage plasticity and physiological function, respectively. Importantly, our versatile platform can be applied in the collection of rich data that could not have been elucidated with traditional co-culture systems that examine interactions between only two cell types. These findings suggest that this system provides a powerful platform to study the cell fate and potential healing functions of MSCs and how they are affected by the types of cells surrounding them. Similarly, the system allows assessment of the effects of MSCs on cells from their surrounding niche in mediating normal physiological functions, and tissue repair, and regeneration in orthopaedic and other settings.

CHAPTER 5

MESENCHYMAL STEM CELLS DISPLAY UNIQUE GENETIC AND PHENOTYPIC RESPONSES TO GLUCOSE PERTURBATION UNDER DIFFERENT MONO-, CO-, AND TRI-CULTURE CONDITIONS

5.1 Introduction

Within multicellular organisms, functional interdependencies exist between a myriad of cell types, tissues, and organ systems that serve to regulate homeostatic processes and responses to disease states. Most cellular components exert their functions not just within cells, but across neighboring cell types and distant organs via a multitude of crosstalk mechanisms, including: direct cell-cell contact, soluble autocrine, paracrine, and endocrine signaling molecules, mechanical forces, neuronal signaling, and extracellular matrix interactions [61, 159]. These mechanisms form the components of dense cell-cell, cell-tissue, and cell-organ interaction networks that are rich in the complexity of their response to normal and pathophysiological perturbations [377, 378].

Much of our understanding of these networks is derived from studies of model organisms and *in vitro* studies using model cell lines [379-381], and most of our attention has been focused on molecular-level interactions either within single cells or globally at the organismal level with the advent of "omics" technologies [382-386]. However, owing to heavy reliance on high-throughput techniques and assays of intracellular networks and the inability to reduce the complexity of *in vivo* model systems, knowledge regarding effects of perturbing interacting systems of multiple cells, tissues, organs is significantly lacking. In response, we have developed a biomaterial-based platform with the goal of recreating complex 3D microenvironments and allowing the study of complex

intercellular interactions (detailed in Chapters 3 and 4; [362, 387]). When coupled with multivariate analysis techniques, this novel platform enabled observation of distinct gene expression dynamics resulting from paracrine crosstalk between co- and tri-cultured MSCs, osteoblasts, and adipocytes that may have produced distinct cell phenotypes for both the stem and terminally differentiated cells [387].

More recently, increasing attention has been concentrated on mapping and correlating interaction networks with physiologic and disease phenotypes, operating on the notion that interactions of these networks reflect underlying molecular interactions between different cell types and tissues [388-390]. Under normal homeostatic conditions, MSCs, osteoblasts, and adipocytes have emerged as key co-regulators of bone remodeling and energy metabolism [19, 20]. MSCs in the bone marrow differentiate into populations of adipocytes and osteoblasts, and this lineage-allocation is reciprocally regulated [10, 18]. Mature osteoblasts secrete osteocalcin that decreases fat mass, promotes adiponectin production and insulin sensitivity in adipocytes, and increases numbers of pancreatic β-cells and insulin secretion [21, 25]. Adipocytes secrete leptin that (acting via the hypothalamus and the sympathetic nervous system) decreases osteoblast activity and bone formation, and may also have putative direct anabolic effects on osteoblasts [26, 27]. Additionally, they produce adiponectin in response to osteocalcin and insulin stimulation that leads to increased insulin sensitivity and osteoblast activity [25, 391]. Insulin signaling has also been demonstrated to stimulate osteoblast differentiation, osteocalcin expression and release from bone matrix, and bone resorption (via decreased osteoprotegrin) [392, 393].

Conversely, dysregulation of glucose metabolism as a consequence of diabetes mellitus (DM) has adverse orthopaedic consequences and often leads to secondary osteopenia and osteoporosis. Both Type I and Type II diabetes mellitus (T1DM and T2DM; respectively) are associated with an increased risk of osteoporotic fractures [121-123]. Bone formation and osteoblast function are impaired with patients with T1DM,

while bone mineral density is increased but bone quality is reduced in patients with T2DM. This is coupled with an increased infiltration of fat in the bone marrow cavity [7]. Together, these consequences are worsened in patients with poorer glycemic control and chronic hyperglycemia [124]. Additionally, pharmacological treatments of T2DM that are designed to enhance insulin sensitivity and restore normal glucose homeostasis also differentially affect the balance of osteogenesis versus adipogenesis by targeting *RUNX2* and *PPARγ2*, respectively [125]. Further, gestational diabetes during pregnancy in expectant mothers leads to profound bouts of hyperglycemia and hyperinsulinemia in developing fetuses that leads to large amounts of peripheral fat deposition and hypoxia prenatally and poor skeletal growth and bone mineral quality postnatally [126-128].

A mechanistic understanding of why these sequelae inevitably occur in DM remains poor since research has focused only on a few *in vitro* studies and correlation with serum biomarkers [125]. Multiple cell types and pathways may be involved. With respect to the balance and extent of osteogenesis and adipogenesis, elevated levels of glucose induce apoptosis and replicative senescence in MSCs and reduce their colony formation and osteogenic capacity [129-132]. Exposure of immortalized osteoblast cell lines to high glucose decreases proliferative capacity, mineralization and osteocalcin responses to parathyroid hormone and Vitamin D administration, dysregulates collagen I synthesis, and leads to decreased expression of differentiation markers [133-136]. In murine 3T3-L1 adipocytes, high glucose administration leads to decreased insulin sensitivity, triglyceride storage dysregulation, production of reactive oxygen species (ROS) and pro-inflammatory cytokines, and decreased adiponectin secretion [137-139]. However, these experiments were conducted on single, often non-primary and non-human, cell types; there are currently no systematic means to simultaneously examine these cell types as a multicellular system with multidirectional and dynamic crosstalk. How glucose levels modulate the responses of MSCs, osteoblasts, and adipocytes to each other remain an open question.

To address this knowledge gap and the limitations of current *in vitro* methodologies in tackling these open questions, we encapsulated primary human MSCs (hMSCs), osteoblasts (hObs), and adipocytes (hAds) into tissue-scale mono-, co-, and tri-culture constructs as described previously (Chapter 4 and [387]). In particular for this study, we applied non-degradable PEG-based hydrogels (which facilitate maximum diffusion of soluble cues between cell populations), and we introduced PEG-based hydrogels with a collagenase-sensitive degradable peptide crosslinker [218, 394] that allowed for recovery of cell populations after the culture period for functional assays. To validate the utility of this platform for addressing complex intercellular responses to a systemic perturbation in a normal and pathophysiological state, we evaluated three mono-culture configurations (all hMSCs, hObs, or hAds), two co-culture configurations (hMSCs flanked by hObs or hAds on both sides), and a tri-culture configuration (one module each of hMSCs, hObs, and hAds; see Figure 5.1) coupled with either normoglycemic or hyperglycemic media conditions for 1 week (Figure 5.2). Cell viability of each cell type under each condition was monitored over time, and gene expression, clonogenicity (hMSCs), markers of differentiation (alkaline phosphatase activity, osteogenesis; triglyceride storage, adipogenesis), and secreted factors were determined as measures of cellular response to culture type and glucose condition. We hypothesized that each culture environment would produce a unique response by each cell type to glucose perturbation, and in particular that cultures containing adipocytes would produce the most detrimental outcomes in cell viability and clonogenicity since they produce pro-inflammatory cytokines and oxidative stress in response to hyperglycemia.

5.2 Materials and Methods

5.2.1 Polymer Synthesis and Characterization

All chemicals were purchased from Sigma-Aldrich unless otherwise noted. Poly(ethylene glycol)-diacrylate (PEG-DA) was prepared as previously described [278] from PEG (M_n = 8,000 Da). Briefly, 24 g PEG was dissolved in 25 mL distilled dichloromethane (DCM) to create a 0.12 M solution, then reacted at a 2:1 molar ratio with acryloyl chloride (AcCl; added dropwise) and at a 1:1 molar ratio with triethanolamine (TEA) under nitrogen overnight. Purification was performed by reaction with 2 M K_2CO_3 (Fisher) at a 2:1 K_2CO_3:AcCl molar ratio and separation into aqueous and organic phases. This was followed by drying the solution with anhydrous $MgSO_4$ (Fisher) and precipitating the polymer in ethyl ether (Fisher). This product was filtered, vacuum dried and frozen at -20ºC until further use.

To allow presentation of adhesive ligands that promote viability of encapsulated cells, fibronectin-derived GRGDS (Bachem) and laminin-derived YIGSR (Anaspec) adhesion peptides were separately reacted as previously described [218, 364, 387, 395] in a 1:2 molar ratio with a 3,400 Da MW Acryl-PEG-succinimidyl valerate spacer (Acryl-PEG-SVA; Laysan Bio) in 50 mM $NaHCO_3$ buffer (pH 8.5; Fisher) at room temperature with gentle stirring for 3 h, dialyzed (1,000 Da MW cutoff) for 60 h, lyophilized for 72 h, and stored at -20 °C until further use. Similarly, to create enzymatically-degradable PEG, the unmodified peptide, Gly-Gly-Gly-Leu-Gly-Pro-Ala-Gly-Gly-Lys (GGGLGPAGGK, MW 769.84 Da; Aapptec), was reacted with Acrl-PEG- SVA at a 1:2.2 peptide:Acrl-PEG-SVA molar ratio in 50 mM $NaHCO_3$ buffer at pH 8.5 for 3 h. The resulting solution containing Acrl-PEG-GGGLGPAGGK-PEG-Acrl (enzymatically-degradable PEG) was then purified as described above. Preliminary evaluation of this and other potential enzymatically sensitive peptide candidates are detailed in Appendix A.

5.2.2 Cell Culture and Expansion

All cell culture reagents were obtained from Mediatech unless otherwise specified. Primary human MSCs (hMSCs) were obtained from the laboratory of Dr. Darwin Prockop (Texas A&M Health Sciences Center) and expanded according to recommended protocols in Minimal Essential Medium-Alpha (αMEM) with 16.5% fetal bovine serum (FBS; Hyclone), 1 g/L glucose, 2 mM L-glutamine, 1% amphotericin B, and 0.1% gentamicin and cultured at 37°C with 5% CO_2 in a humidified incubator [365]. Primary human osteoblasts (hObs; Lonza) were expanded to 4 population doublings in OGM Osteoblast Growth Medium (Lonza) containing 10% FBS, ascorbic acid (concentration proprietary), 50 μg/mL gentamicin, and 37 ng/mL amphotericin B. Primary human subcutaneous pre-adipocytes (Lonza) were expanded to 1-2 population doublings according to the manufacturer's protocol in PGM-2 Basal Medium (Lonza) containing 10% FBS, 2 mM L-glutamine, 50 μg/mL gentamicin, and 37 ng/mL amphotericin B. Cultures at 80% confluence were differentiated into adipocytes (hAds) for 9 days in Dulbecco's Modified Eagle Medium (DMEM) with 10% FBS, 1 g/L glucose, 60 μM indomethacin, 0.5 mM 3-isobutyl-1-methylxanthine (IBMX), 0.5 μM dexamethasone, and 45 pM insulin.

5.2.3 Crosslinking Device Design and Construct Fabrication

Layering devices were fabricated and employed for cell patterning as described in Figure 4.1. Briefly, 1 mm-thick spacers were cut from cured polydimethylsiloxane (PDMS, Sylgard 184, 10:1 ratio base to curing agent; Dow Corning) and bonded with O_2 plasma to a 25 × 75 mm glass slide (VWR). This slide was contact bonded with another coated with fluorinated ethylene propylene film (Bytac FEP; U.S. Plastic Corp) to form a cavity for polymer solution/gels as they were loaded and crosslinked. The use of FEP film prevented adhesion of crosslinked gels to glass that could result in ripping following

device disassembly. Devices were sterilized by autoclave prior to assembly and use for encapsulation.

Hydrogel precursor solutions were formulated with 10% w/w 8K PEG-DA (for hObs and hAds) or 10% w/w Acrl-PEG-GGGLGPAGGK-PEG-Acrl enzyme-sensitive polymer (for hMSCs) in phosphate-buffered saline (PBS) containing 0.05% w/w D-2959 photoinitiator (Ciba) and 1 mM Acryl-PEG-GRGDS (for hMSCs and hObs) or Acryl-PEG-YIGSR (for hAds). Cell suspensions were prepared from near-confluent cultures using 0.05% Trypsin/0.53 mM EDTA and resuspended in their respective gel precursor solutions at a concentration of 15 million cells/mL. These solutions were loaded into layering devices and sequentially photocrosslinked (365 nm light, 10.5 mW/cm^2, 12 min) into laminated 1 mm-thick, 1.5 mm-tall hydrogel strips as described in Figure 5.1. After each patterning step, residual non-crosslinked material was rinsed out of the device with fresh 10% w/w PEG-DA solution using a syringe [362]. An opaque photomask was used in subsequent steps to prevent any further UV light exposure and crosslinking of the existing gels. Whole, laminated constructs were extracted from the device and sectioned with a scalpel perpendicular to the long axis of the laminate to yield up to eighteen 1.5 mm-wide mono-, co-, and tri-culture constructs (Figure 5.1).

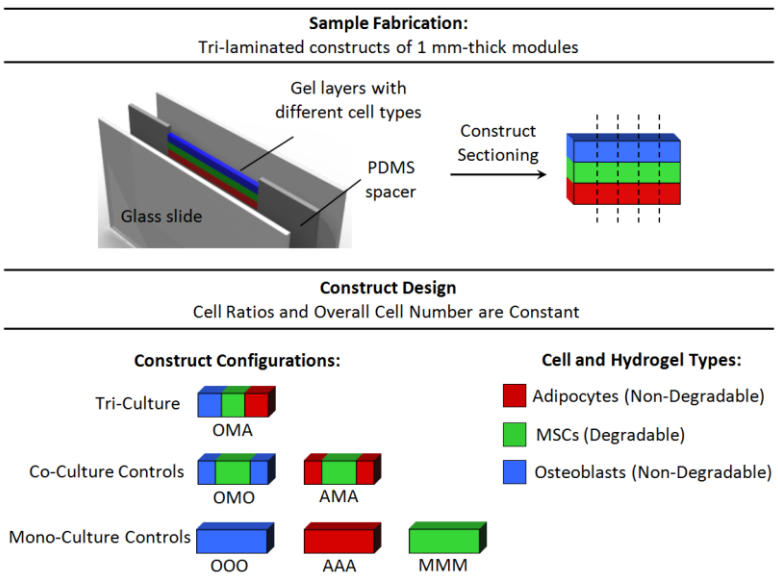

Figure 5.1. Sample Fabrication and Construct Design. Fabrication of mono-, co-, and tri-culture constructs using the techniques outlined in Section 5.2.3 yield sample sets with well-segregated cell populations. Six sample types (overall dimensions 4.5 × 1.5 × 1 mm) were examined in this study: Mono-cultures of hMSCs (MMM), hAds (AAA), and hObs (OOO); Co-cultures of hMSCs in the center module (2.25 × 1.5 × 1 mm) flanked on both sides by only one other cell type (hAds or hObs; 1.125 × 1.5 × 1 mm per module); and Tri-cultures with hMSCs flanked on either side by hObs or hAds (each module is 1.5 × 1.5 × 1 mm).

5.2.4 Construct Culture Conditions

Constructs were placed in separate wells of 12-well tissue culture plates with 2 mL of tri-culture medium for 24 h [DMEM with 10% FBS, 1.0 g/L glucose (5.5 mM; normal fasting serum glucose), 2 mM L-glutamine, 70 µM L-ascorbate (normal serum concentration; Sigma), 45 pM insulin (normal fasting serum insulin; Sigma), 1% amphotericin B, and 0.1% gentamicin. After this period (day 1), which allowed the hydrogel constructs to reach equilibrium swelling, half were replenished with medium containing 1 g/L glucose, and the other half were switched to 4.1 g/L glucose (22.3 mM; hyperglycemic). All constructs were then cultured for a total of 7 days with an additional media change at Day 4 (Figure 5.2). Levels of glucose and insulin were selected for this experiment based on the Homeostasis Model Assessment (HOMA-2). Insulin levels were kept consistent between the two experimental conditions and represent a normal fasting

level of serum insulin. Using HOMA-2, the normal glucose concentration used (1.0 g/L), when coupled with this insulin level, corresponds to 100% insulin sensitivity, 77.4% beta cell activity, and no insulin resistance. The high glucose concentration used (4.1 g/L) corresponds to 20.2% insulin sensitivity (5-fold reduction), 7.7% beta cell activity (10-fold reduction), and a 5-fold increase in insulin resistance.

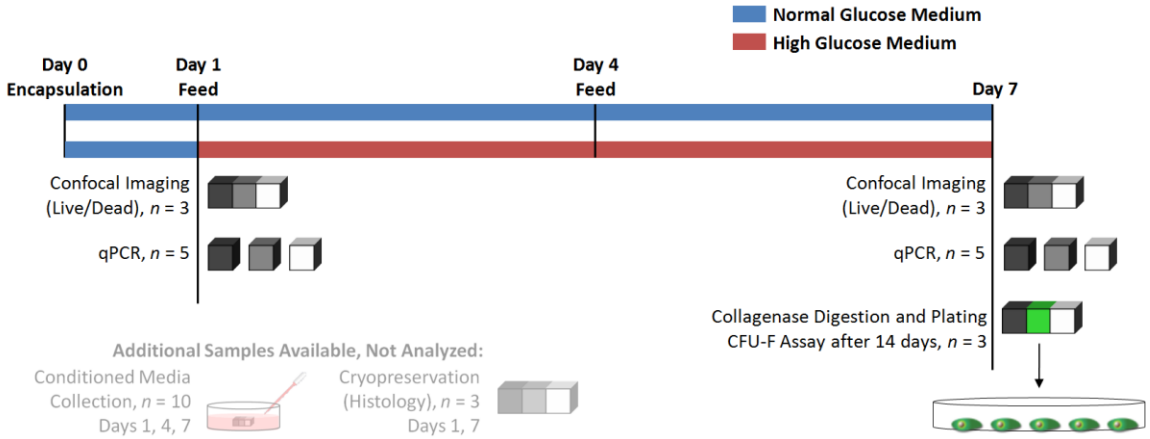

Figure 5.2. Study Design. Mono-, co-, and tri- constructs were cultured in separate wells of a 12-well TCPS plate for up to 7 days. Media changes were performed at 1 and 4 days. After 1 day in culture, half of the constructs were switched to high glucose medium for the remainder of the study. Outcome measures analyzed in this study included cell viability (Live/Dead staining and confocal microscopy, *n* = 3), mRNA expression (qPCR, *n* = 5), and colony formation (CFU-F assay after gel digestion, re-plating, and culture for 14 days, *n* = 3) at the time points depicted.

5.2.5 Cell Viability Assessment and Image Analysis

Hydrogel constructs (n = 3) were analyzed on Days 1 and 7 of mono-, co-, or tri-culture using a LIVE/DEAD assay (Invitrogen) as a qualitative indicator of cell viability (Figure 5.2). The kit uses calcein AM (ex/em: 495/515 nm), which is conjugated by active cytosolic esterases to remain within the cell membrane and label live cells, and ethidium homodimer-1 (EthD-1; ex/em: 495/635 nm), which can only enter permeable nuclear membranes and binds to DNA to indicate dead or dying cells. Constructs were rinsed in sterile PBS at 37 °C for 30 minutes and subsequently incubated in staining solution (1 µM calcein AM, 1 µM ethidium homodimer-1 in sterile PBS with Ca^{2+} and Mg^{2+}) for 45 minutes at 37 °C. After a second PBS rinse for 15 minutes to remove excess

dye, stained constructs were imaged with confocal microscopy (10x objective, LSM 700; Zeiss). For each construct, 1 image stack was collected for each cell type present (dimensions: 693 × 693 μm; stack depth = 0 – 800 μm with 10-μm intervals).

Image stacks were analyzed using ImageJ software (version 1.46a; NIH). Each stack was split into green (calcein) and red (EthD-1) channels. The red channel containing dead cells was then projected onto a single plane using a maximum intensity projection algorithm. A threshold (pixel intensity > 20; scale of 0-255) was then applied to each projection image to convert it to a binary image. Particles greater than 12 μm^2 in size were counted using the built-in Particle Analysis macro and recorded for further statistical analysis.

5.2.6 mRNA Isolation and qPCR

Hydrogel constructs (n = 5) were rinsed in PBS and blocks containing individual cell populations were separated from each other using a scalpel for gene expression analysis by qPCR after 1 and 7 days in mono-, co-, or tri-culture (Figure 5.2). Gel blocks containing the same cell type were pooled from 2 co-culture constructs or 3 tri-culture constructs of the same culture type and glucose condition to provide sufficient and equivalent amounts of mRNA for quantification. These blocks were homogenized in microcentrifuge tubes with pellet grinders (Kontes), after which mRNA was extracted using a QIAshredder tissue homogenizer and RNeasy kit with DNase I digestion (Qiagen). cDNA was generated using SuperScript III Reverse Transcriptase (Invitrogen) with Oligo$(dT)_{15}$ primers and dNTPs (Promega). Gene expression of each cell type was analyzed for several target genes using custom-designed primers (Table 5.1; Invitrogen) with quantitative PCR amplification performed on a StepOnePlus™ Real-Time PCR System (Applied Biosystems) in the presence of SYBR Green/ROX master mix (Applied Biosystems).

To analyze PCR amplification data, the raw fluorescence data was processed using LinRegPCR (v12.11; http://www.hartfaalcentrum.nl) [368]. This software estimates individual well baselines by reconstructing the log-linear portion of the amplification curve, and then calculates individual PCR efficiencies (E) for each reaction. This is followed by computing a mean efficiency ($\overline{E}$) for the amplicon of interest and computes a starting amplicon number (N_0) based on a universally applied cycle threshold (C_t) using the formula $N_0 = N_t / \overline{E}^{C_t}$. Starting amplicon numbers of each target gene were normalized to a geometric mean of the starting amplicon numbers of two housekeeping genes – ribosomal protein-S18 (*RPS18*) and β-actin (*ACTB*) – to obtain relative expression values [366]. Endogenous controls were evaluated in each cell type to ensure that their expression levels were not altered across time or culture conditions [367, 368].

Table 5.1 Custom Primers Used for qPCR Analysis of mRNA Expression*

Gene Family	*Target Gene*	*NLM Accession Number*	*Primer Set (Forward, Reverse)*
Osteogenesis	*RUNX2*	NM_001024630	TTTGCACTGGGTCATGTGTT TGGCTGCATTGAAAAGACTG
	OCN	NM_199173	GTGCAGAGTCCAGCAAAGGT AGCAGAGCGACACCCTAGAC
	OPG	NM_002546	CGGGAAAGAAAGTGGGAGCAGAAG CGTCTTTGAGTGCTTTAGTGCGTG
Adipogenesis	*PPARG2*	NM_015869	TCCATGCTGTTATGGGTGAA GGGAGTGGTCTTCCATTACG
	CEBPB	NM_005194	CGAGTCAGAGCCGCGCAC GCAGGGGGAGACATGCTGGG
	LEP	NM_000230	ACCCTGTGCGGATTCTTGTGGCTTTGG GGCTCTGCCTACCCCTCTGCCCT
	ADIPOQ	NM_001177800	ATCTGGTTGGGGTGGGCTCCTTAC GTTGACTCTCTCTGTGCCTCTGGTT
Glucose-Responsive	*ATF2*	NM_001880	GGTCCTTCCTCTCCCCAACCAGTA CTGTAGTGGATGTGGCTGGCTGT
	JUN	NM_002228	GACAGACACAGCCAGCCAGCCAG GGACACTCCCGAAACACCAGCCC
	FOXO1	NM_002015	GCTACCAATAACCCCAGCCCCAA AATGCCAGGTTGGTCTGTTCGCA
	NFKB1	NM_003998	AGACAAAAACTGGGCTACTCTGGCG TGAGAGGTGGTCTTCACTGGGCT
Endogenous Controls	*RPS18*	NM_022551	CGATGGGCGGCGGAAAATAGCCTTGC CAGTGGTCTTGGTGTGCTGGCCTCGG
	ACTB	NM_001101	GCAGTCGGTTGGAGCGAGCATCCCC TCCCCTGTGTGGACTTGGGAGAGGAC

* Targets were on the basis of corresponding with genes unique to each mesenchymal lineage, or that have

been shown to be responsive to hyperglycemia in previous experiments with MSCs, osteoblasts, or adipocytes (termed 'glucose-responsive' [129-139]).

Table 5.1 Continued.

5.2.7 Gel Digestion, Cell Recovery, and Colony Formation Analysis

After 7 days in mono-, co-, or tri-culture, hydrogel constructs containing hMSCs (n = 3) were each placed in 500 μL of hMSC expansion medium (as described in Section 5.3.2) containing 1,100 U/mL collagenase type II (Gibco), and the degradable hydrogel block (Acrl-PEG-GGGLGPAGGK-PEG-Acrl) was digested for 1 hour on a shaker table to extract the hMSCs (Figure 5.2). Fractions of the media containing the recovered cells (100 μL for MMM, 200 μL for OMO and AMA, and 300 μL for OMA; used to seed an approximately similar number of cells for each construct type at ~ 1-2 cells/cm^2) were immediately plated into 15-cm TCPS dishes (Corning) containing 20 mL of hMSC expansion medium. Media changes were performed 1 day after seeding and every 3 days subsequently. After colonies were allowed to form for 14 days, the dishes were washed with 10 mL of PBS with Ca^{2+} and Mg^{2+}, stained with 3% crystal violet (Sigma) in 100% methanol for 10 min, and rinsed thoroughly with tap water. Stained colonies greater than 2 mm in size were counted [50].

5.2.8 Statistical Analysis and Multivariate Modeling

Gene expression results are depicted as mean ± standard deviation unless otherwise noted. Prior to statistical analysis, all data were transformed with a Box-Cox transformation [396, 397]. Data were analyzed by multi-factor analysis of variance (ANOVA) to identify significant factors (culture type, glucose, day) and factor interactions (culture type*glucose, culture type*day, glucose*day, and culture type*glucose*day) for each target gene assayed. Where significant factors and interactions were identified by ANOVA, Tukey's *post hoc* test (significance level $p < 0.05$) was used to generate pairwise comparisons between means of individual sample groups and determine statistically significant differences.

Multivariate statistical modeling was performed with the overall goal of extracting combinations of time-variant gene expression markers that were the most informative for distinguishing different responses among culture types and glucose conditions. All Box-Cox-transformed data were mean-centered and scaled to unit variance prior to analysis as a means of normalization to allow all variables to be considered equally scaled in the principal components or latent variables [312]. For these analyses, the data set (total of 1600 data points) was organized into an $N \times K$ matrix **X** that denotes the measured gene expression levels with time (variables/responses) as well as culture type and glucose conditions (observations/treatments). Principal component analysis (PCA) was first performed to discern possible clusters of observations and their qualitative similarities among the global data set in an unbiased fashion. PCA was performed using SIMCA software (v13; Umetrics) to analyze the **X** matrix and generated linear combinations of the X-variables (target gene and time; $K = 20$) that described the sources of maximum variation to cluster them by their contributions to the variance of the entire set of X-observations (cell type and culture type; $N = 80$). Using the observed clusters, partial least squares discriminant analysis (PLS-DA) was then performed (SIMCA) using an additional $N \times M$ matrix **Y** that encoded m purported classes of data (*e.g.* culture type or glucose condition) to find latent variables (linear combinations of the independent X-variables) that served as discriminating features to best separate the N observations into M different purported classes designated by the dependent Y-variables. A separate set of models were constructed using partial least squares projections to latent structures (PLS) to ascertain whether functional outcomes (*e.g.* cell viability, colony number) encoded as Y-variables (in lieu of purported classes) correlated significantly with the X-variables. In summary, PCA was used to observe the overall correlation structure of the gene expression data and understand how it contributed to the largest variance among the observations. PLS-DA aided in separating tight clusters of observations and revealing the covariant genes that correlated with each class, and PLS

aided in correlating time variant gene expression data with functional outcomes [370, 371].

To optimize the quality of each model, several pruning procedures were performed to remove outlying observations (outside 95% confidence interval) and non-influential variables (weight approximately 0 in both components) and to enable statistical significance-testing of the model and the variables used to generate it [398, 399]. The quality of each model was summarized by two non-dimensional statistical parameters: 1) R^2X (for PCA) or R^2Y (for PLS-DA and PLS), which quantitatively measure the extent to which the model explains the variation in the data matrices and dictate a *goodness of fit*; and 2) Q^2, which quantitatively measures the extent to which the variation of a future experimental data set may be predicted by the model (*goodness of prediction*) [372]. Both of these parameters are analogous to regression statistics, with a value ranging from 0 (poor) to 1 (perfect) fit or predictive capability. The appropriate number of principal components or latent variables was determined by cross-validation [400]. The results of this procedure were fed into a jack-knifing analysis [401] to calculate the standard errors of the regression coefficients (weights), which were then converted into 95% confidence intervals via the *t*-distribution to determine which X-variables (genes) of high weight have a statistically significant influence ($p < 0.05$) on each class of observations (Y-variables) in each of the PLS-DA and PLS models generated. Further definitions, parameters, and model details are outlined in Appendix C.

5.3 Results

5.3.1 Mesenchymal Stem Cell Viability

Live/Dead cell viability staining demonstrates that hMSCs remained largely viable after the week-long culture period (Figure 5.3A). Considerable amounts of cell spreading occur in co- and tri-cultured hMSCs under both glucose conditions by Day 7. There were no statistically significant differences in the number of dead cells per image

stack in quantified confocal images at Day 1 regardless of culture type (Figure 5.3B). Only hMSCs from AMA and OMO co-cultures exposed to high glucose demonstrated a statistically significant increase in the number of dead cells at Day 7 versus the same culture type and glucose condition on Day 1 (68.8% and 50.5%, respectively).

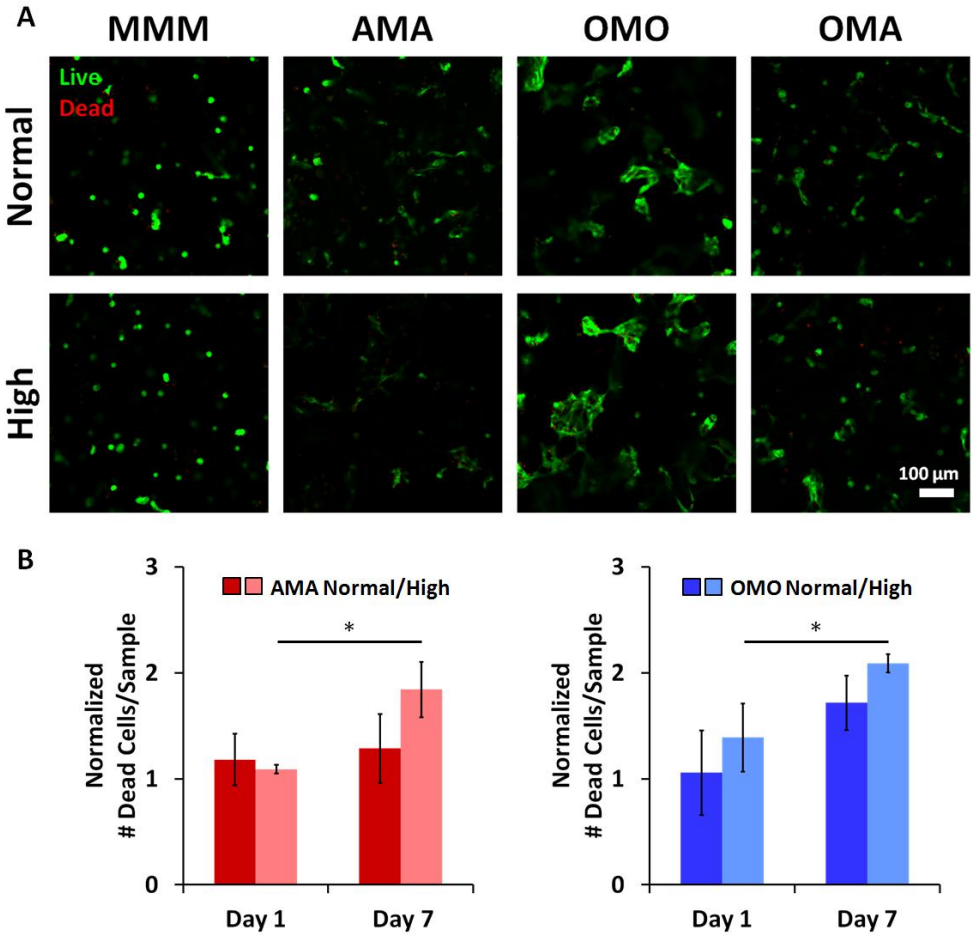

Figure 5.3. Cell Viability of hMSCs in Mono-, Co-, and Tri-Culture under Different Glucose Conditions. A) Representative images of hMSCs stained with Live/Dead reagents taken from confocal laser scanning microscopy image stacks after 7 days. Cells remain largely viable at Day 7 regardless of culture condition. Considerable cell spreading was observed in hMSCs from co- and tri-culture constructs under both glucose conditions. B) Number of dead cells per image stack (*n* = 3 per culture type and glucose condition) remain relatively similar over 7 days in culture, with the exception of hMSCs from AMA and OMO constructs cultured in high glucose medium. (* = Significantly different from same culture type and glucose condition on Day 1; $p < 0.05$)

5.3.2 Gene Expression Dynamics of hMSCs

Many of the genes expressed in hMSCs showed differential expression patterns dependent on the culture type (mono-, co-, or tri-culture), glucose condition (normal or high), and time (Figures 5.4 and 5.5). Genes that varied the most with time include *JUN*, *OCN*, and *RUNX2*, while *FOXO1* appeared to vary more by culture type and *NFKB1* and *ADIPOQ* varied significantly with both culture type and time. Significant factor interaction effects were observed for culture type and day (*FOXO1*, *NFKB1*, *ADIPOQ*, *LEP*, *OCN*, and *RUNX2*), culture type and glucose (*FOXO1*, *NFKB1*, and *RUNX2*), glucose and day *(OCN)*, and all three factors (*JUN*, *NFKB1*, *OCN*, and *RUNX2*). Furthermore, *ATF2*, *CEBPB*, and *OPG* failed to show any statistically significant differences among any of the sample types. Notably, adipocytic master transcriptional regulator *PPARG2* failed to amplify in any samples, and *CEBPB*, *LEP*, and *ADIPOQ* exhibited low expression levels relative to other genes with some notable exceptions (detailed below).

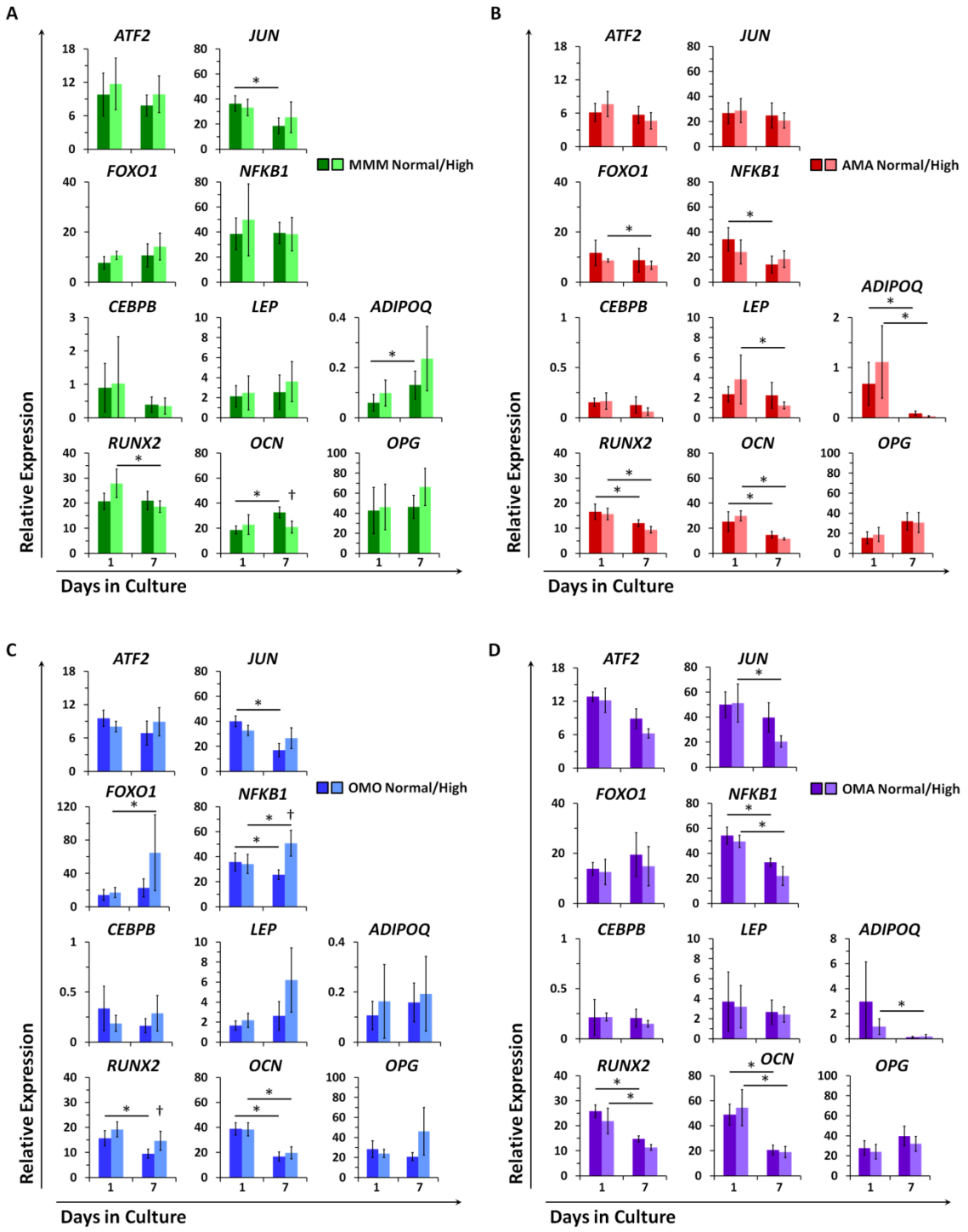

Figure 5.4. Varying glucose content differentially modulates gene expression responses in hMSCs from each culture type. Gene expression relative to *RPS18* and *ACTB* is depicted over time for A) mono-cultured (MMM; green), B,C) co-cultured (AMA, red; OMO, blue; respectively) and D) tri-cultured (OMA; purple) hMSCs exposed to different glucose concentrations (1 g/L, dark shade; 4.1 g/L, light shade). Values scaled × 10^4. * = significantly different than same culture type and glucose concentration on Day 1. † = significantly different from a different glucose

concentration with the same culture type on same day. [Note: The same data is reorganized by glucose condition in Figure 5.5]Figure 5.4 continued.

5.3.2.1 Gene Expression Dynamics with Normal Glucose

hMSCs cultured alone (MMM) under normal glucose conditions (Figure 5.4A; dark green) maintained relatively stable expression of many of the genes evaluated, with only slight changes exhibited in *JUN* (2-fold decrease), *OCN* (1.8-fold increase), and *ADIPOQ* (2.2-fold increase) expression by Day 7.

When co-culturing hMSCs with hAds (AMA) under normal glucose conditions (Figure 5.4B; dark red), decreases in *NFKB1* (2.4-fold), *ADIPOQ* (7.7-fold), and *OCN* (1.7-fold) were observed by Day 7. Compared with MMM hMSCs, *ADIPOQ* expression was 11.4-fold higher on Day 1, but returned to comparable levels by Day 7. *OCN* expression was similar on Day 1, but was 2.2-fold lower by Day 7 (Figure 5.5A). When compared with OMO hMSCs under normal glucose, AMA hMSCs expressed lower levels of *FOXO1* (2.2-fold), *NFKB1* (1.8-fold), and *OCN* (1.5-fold) on Day 7 (Figure 5.5A). *ADIPOQ* expression was 6.4-fold higher than in OMO hMSCs on Day 1 but returned to comparable levels by Day 7. When compared with OMA hMSCs under normal glucose, AMA hMSCs expressed lower levels of *JUN* than on Day 1 (1.9-fold; difference abrogated by Day 7) and consistently lower levels of *NFKB1* (1.5-fold on Day 1, 2.3-fold on Day 7; Figure 5.5A). Expression of *OCN* was 1.9-fold lower than in OMA hMSCs on Day 1 but was similar by Day 7.

hMSCs co-cultured with hObs (OMO) under normal glucose conditions (Figure 5.4C; dark blue) maintained similar levels of gene expression over 7 days, with the exception of decreases in *JUN* (2.4-fold), *NFKB1* (1.4-fold), *RUNX2* (1.6-fold), and *OCN* (2.3-fold). In comparison with MMM hMSCs under normal glucose, *OCN* expression was higher on Day 1 (2.1-fold; 2-fold lower by Day 7), while *RUNX2* was similar on Day 1 but 2.2-fold lower on Day 7 (Figure 5.5A). Gene expression was relatively similar to

OMA hMSCs under normal glucose, with the exception of consistently lower *RUNX2* (1.6-fold on both days) and lower *JUN* (2.3-fold) by Day 7 (Figure 5.5A).

Tri-culturing hMSCs with hObs and hAds (OMA) under normal glucose conditions (Figure 5.4D; dark purple) produced consistent gene expression levels between 1 and 7 days, with the exception of lower levels of *NFKB1* (1.6-fold), *RUNX2* (1.7-fold), and *OCN* (2.4-fold). Compared with MMM hMSCs with normal glucose, *OCN* expression was 2.6-fold higher on Day 1 (changed to 1.6-fold lower by Day 7; Figure 5.5A). *RUNX2* expression was 1.4-fold lower on Day 7, while *JUN* expression was 2.1-fold higher.

5.3.2.2 Gene Expression Dynamics with High Glucose

Culturing hMSCs alone (MMM) under high glucose conditions (Figure 5.4A; light green) did not produce a change in *JUN* expression (as with normal glucose), but did lead to a significant decrease in *RUNX2* (1.5-fold) after 7 days and lower *OCN* expression relative to hMSCs (1.6-fold) under normal glucose at Day 7.

AMA hMSCs cultured with high glucose (Figure 5.4B; light red) showed significant declines in several genes by Day 7 when compared with Day 1 (*FOXO1* – 1.3-fold; *LEP* – 3.1-fold; *ADIPOQ* – 37-fold; *RUNX2* – 1.7-fold; *OCN* – 2.6-fold). When compared with MMM hMSCs under high glucose, gene expression levels were similar on Day 1 with the exception of *ADIPOQ* (11-fold higher; 7.8-fold lower by Day 7; Figure 5.5B). After 7 days, expression levels of several other genes were significantly lower than MMM hMSCs, including *NFKB1* (2.1-fold), *LEP* (3-fold), *RUNX2* (2-fold) and *OCN* (1.8-fold). When compared with OMO hMSCs under high glucose, gene expression levels were similar on Day 1 with the exception of *ADIPOQ* (6.8-fold higher; no difference by Day 7; Figure 5.5B). Expression levels of several genes at Day 7 were significantly lower than OMO hMSCs, including *NFKB1* (2.8-fold), *FOXO1* (9.6-fold), *LEP* (5.1-fold), *RUNX2* (1.6-fold), and *OCN* (1.7-fold). When compared with OMA hMSCs under high glucose, gene expression levels were similar on Day 1 with the exception of *JUN* (1.8-fold lower; no difference at Day 7), *NFKB1* (2.1-fold lower; no difference at Day 7), and *OCN* (1.8-fold lower; 1.6-fold lower at Day 7), and were otherwise similar on Day 7 with the exception of *ADIPOQ* (5.9-fold lower; Figure 5.5B).

hMSCs co-cultured with hObs (OMO) under high glucose conditions (Figure 5.4C; light blue) showed increased levels of *FOXO1* (3.8-fold) and *NFKB1* (1.5-fold; 2-fold higher relative to OMO hMSCs with normal glucose) coupled with decreased *OCN* (1.9-fold) after 7 days. Additionally, *RUNX2* was 1.5-fold higher on Day 7 compared with OMO hMSCs cultured with normal glucose. Compared with MMM hMSCs exposed to high glucose, OMO hMSCs showed 1.7-fold higher *OCN* expression at Day 1, but this

difference did not persist after 7 days (Figure 5.5B). Relative to OMA hMSCs exposed to high glucose, *ADIPOQ* expression on Day 1 was 6-fold lower (similar by Day 7), and *FOXO1* and *NFKB1* were significantly higher (4.4-fold and 2.3-fold, respectively) at Day 7 (Figure 5.5B).

Tri-culturing hMSCs with hObs and hAds (OMA) under high glucose conditions (Figure 5.4D; light purple) produced decreases in *JUN* (2.5-fold), *NFKB1* (2.3-fold), *ADIPOQ* (5.5-fold), *RUNX2* (1.9-fold), and *OCN* (2.9-fold) by Day 7. Relative to MMM hMSCs cultured with high glucose, *ADIPOQ* and *OCN* expression were higher at Day 1 (9.9-fold and 2.4-fold, respectively; levels comparable by Day 7), while *RUNX2* was 1.6-fold lower at Day 7 (Figure 5.5B).

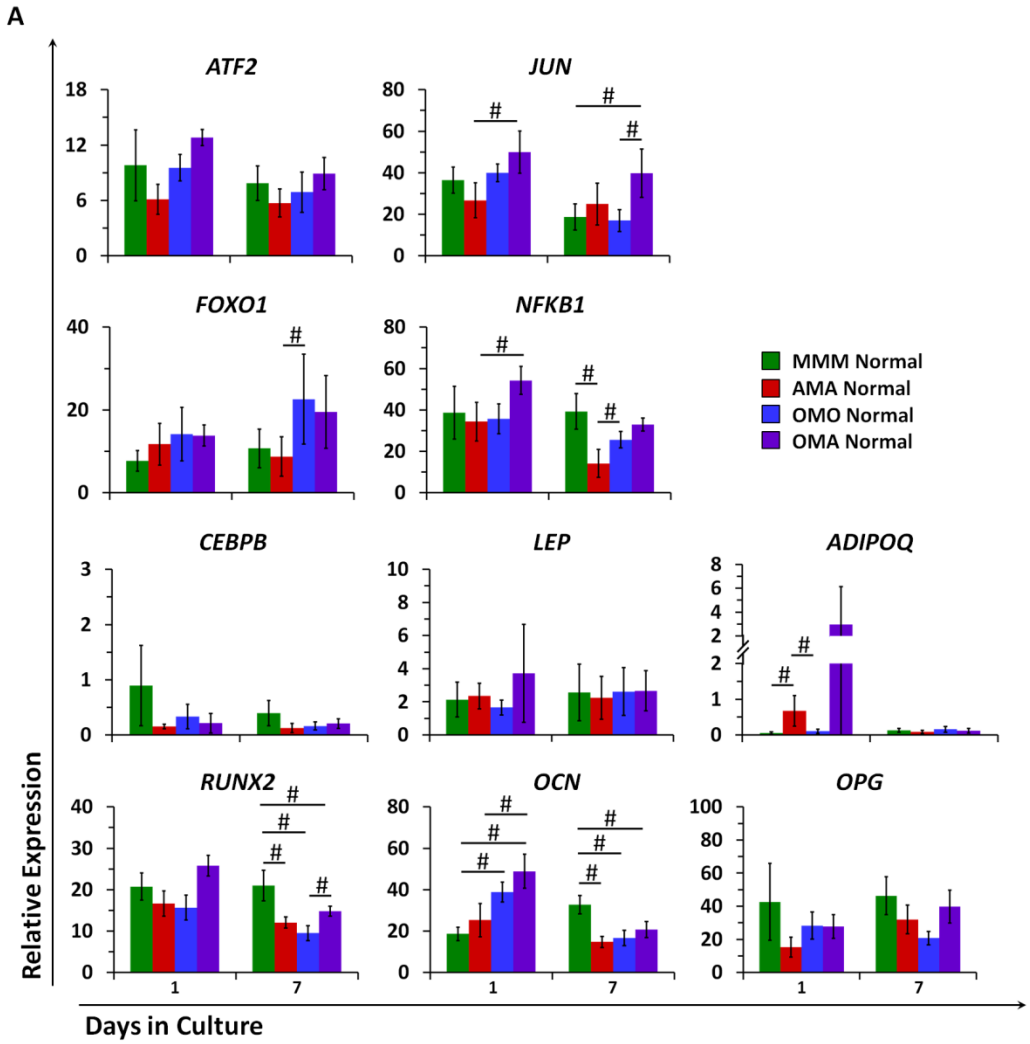

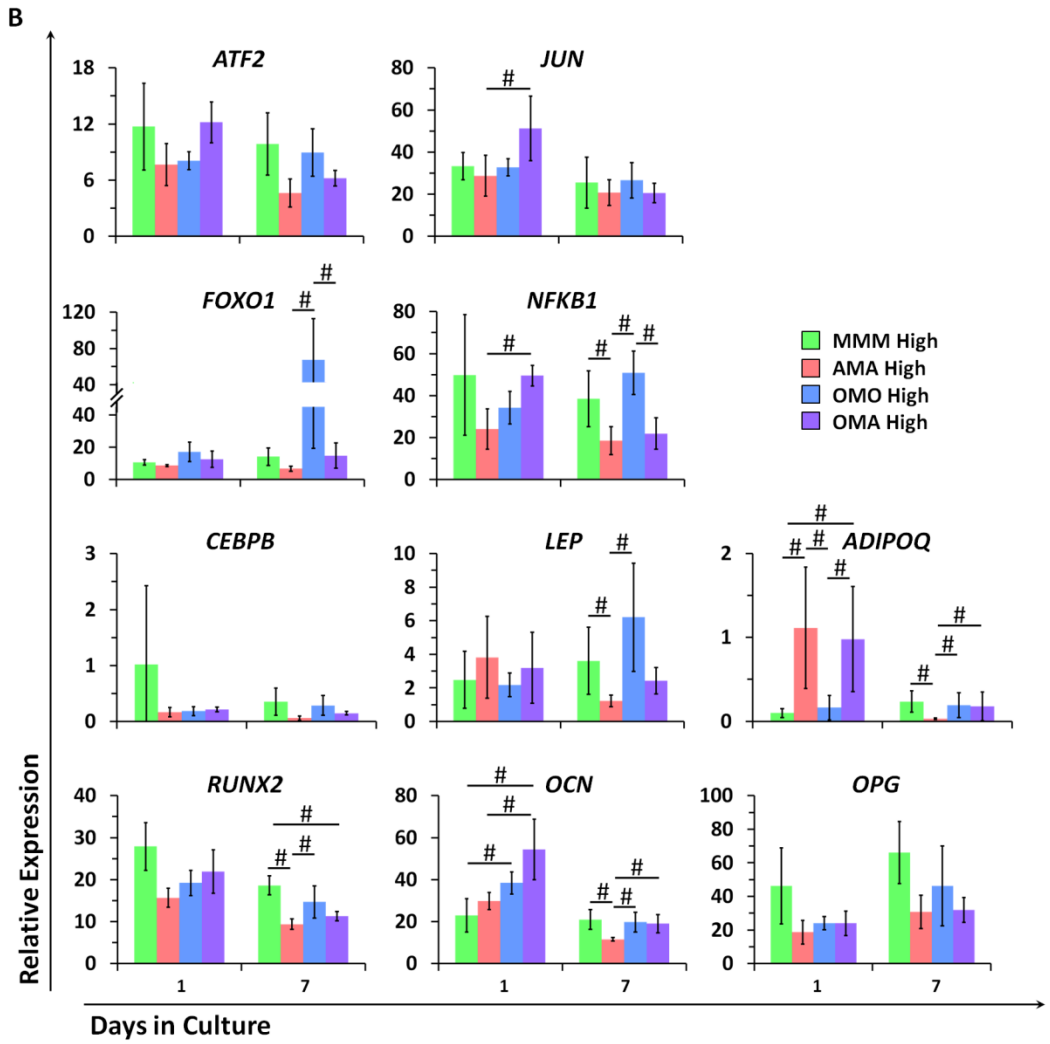

Figure 5.5. Mono-, Co-, and Tri-Culture Differentially Modulate hMSC Gene Expression of Mesenchymal Lineage Markers and Glucose-Responsive Transcription Factors in Response to Varying Glucose Content. Gene expression relative to *RPS18* and *ACTB* is depicted over time for A) MSCs exposed to normal glucose levels (1 g/L), and B) MSCs exposed to elevated glucose (4.1 g/L). # = significantly different from another culture type on the same day with the same glucose concentration. [Note: This figure is a reorganization of Figure 5.4 to allow for comparisons across culture types.]

5.3.3 Colony Formation of hMSCs Recovered from Hydrogels

Encapsulation of hMSC in hydrogel modules composed of Acrl-PEG-GGGLGPAGGK-PEG-Acrl successfully enabled digestion of the hydrogel with collagenase after 7 days of culture. The resulting supernatant contained enough pre-

cultured hMSCs that could be collected and directly plated into TCPS dishes at clonal density. Following 2 weeks of culture in hMSC expansion medium, MSCs from all sample types were still able to form colonies to different degrees (Figure 5.6A; stained with crystal violet). Analysis showed that both culture type and glucose condition influenced hMSC clonogenicity. Significant declines in colony-forming capacity were observed in hMSCs from MMM and OMO samples (33% and 76%, respectively; Figure 5.6B). hMSCs co-cultured with adipocytes retained their colony-forming capacity regardless of glucose condition. A declining trend was observed for tri-cultured (OMA) hMSCs (though not statistically significant), and the high glucose treatment still produced as many colonies as MMM hMSCs under normal glucose.

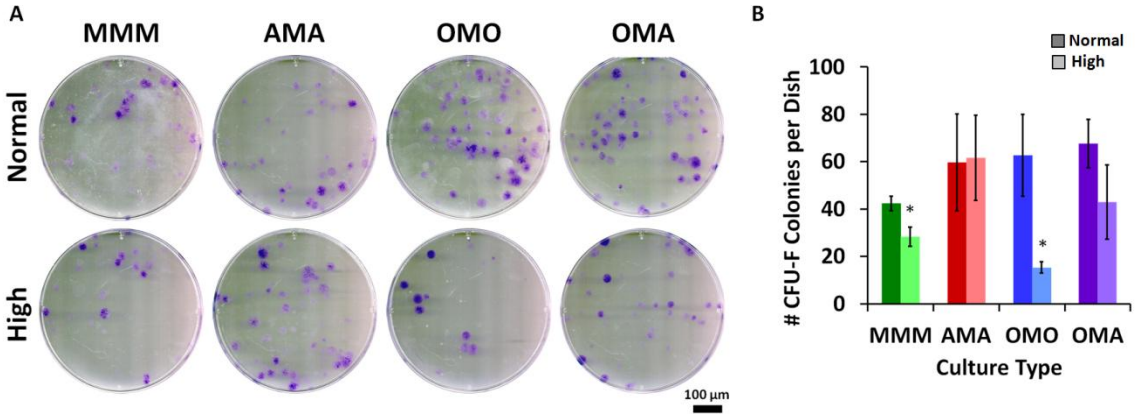

Figure 5.6 Mono-, Co-, and Tri-Culture Interact with Glucose Condition to Alter Clonogenicity of hMSCs. A) Representative photographs of hMSC colonies stained with crystal violet 14 days after construct digestion and cell recovery. Noticeable differences were observed in colony formation among the different culture types and glucose conditions. B) Enumerated colony-forming units > 2 mm in diameter per dish (*n* = 3). MMM and OMO hMSCs cultured under high glucose conditions for 7 days exhibited significant decreases in colony formation. (* = Significantly different from same culture type; $p < 0.05$)

5.3.4 Multivariate Modeling of Gene Expression and Colony Formation Data

5.3.4.1 Modeling of Gene Expression Data with Principle Component Analysis (PCA) to Assess Sources of Maximum Variance

Principle component analysis was performed to further interpret the complex gene expression responses observed (Figures 5.4 and 5.5) by leveraging the covariance of more than one gene and to ascertain their correlation with each other and the different sample groups tested in this experiment. PCA reduced the dimensionality of all the summarized gene expression data based on the sources of maximum variance within the entire data set and optimally produced three principle components (Figure 5.7; first two components depicted). The first principle component (accounting for 42.2% of the variance in the data) appears primarily to distinguish hMSCs co-cultured with adipocytes (AMA) from hMSCs from mono-culture (MMM), while the second principle component (accounting for an additional 20.4% of the variance in the data set) appears to more clearly separate the tri-cultured hMSCs (OMA) from the other sample groups. An overall examination of the scores indicates that much of the variance in the overall gene expression data set arises from differences between culture conditions (Figure 5.7A, different shapes), with a more moderate effect of glucose condition (Figure 5.7A, dark vs. light shades). Plotting the variable loadings in the first two principle components indicated that all of the genes (with the notable exception of *ADIPOQ* and *CEBPB*, the genes with the lowest expression in the entire data set) were highly influential in the model at one or both time points since each has a large weight on one or both principle components (Figure 5.7B; variables with near 0 weight were removed during pruning). In distinguishing the different clusters of observations from the score plot, hMSCs from AMA co-cultures were most distinguishable by being strongly anti-correlated with all of the genes in the model, while MMM hMSCs were strongly correlated with these genes. *OCN* on Day 1 did not have a large weight in the first component. Tri-cultured hMSCs

were strongly correlated with *OCN*, *NFKB1*, *ATF2*, and *RUNX2* (all on Day 1), and strongly anti-correlated with the same variables on Day 7. *OPG* and *LEP* did not have strong weight along the second component.

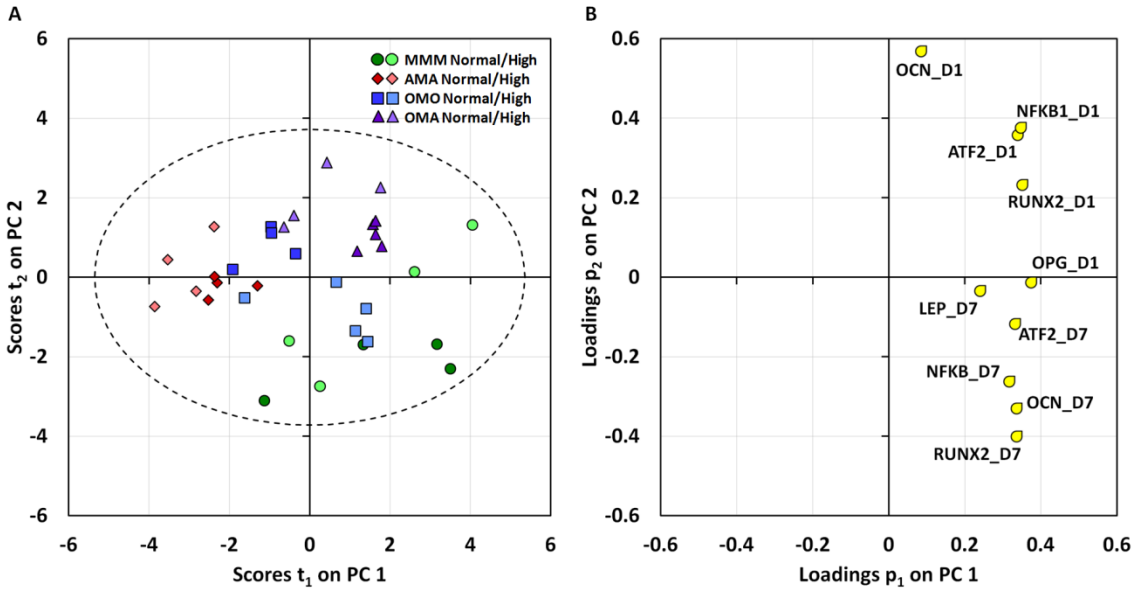

Figure 5.7. Statistical modeling based on maximum variance of the gene expression data set yields three principle components that indicate most of the variance arises from differences in culture type and elucidates the correlation structure of the gene expression at various time points. A) Plot of PCA scores, t_1 and t_2, separating the observations by the first two principal components (PC) that explain 42.2% and 20.4% of the variance in data, respectively. Dashed line represents the 95% confidence limit of the distribution of scores. B) Plot of PCA loadings, p_1 and p_2, that shows the correlation of the gene expression data with the sources of maximum variance. Overall model quality parameters: R^2X = 0.784, Q^2 = 0.403.

5.3.4.2 Multivariate Modeling of Gene Expression Data with PLS Discriminant Analysis (PLS-DA) to Correlate Gene Expression with Culture Type

Several clusters of data by culture type were discernible in the PCA results, though they overlapped to an extent. These findings motivated further supervised analysis to deconvolve this complex data set into a meaningful set of variables that adequately describe the patterns of samples and their gene covariance in the overall data set. The observations first were classified into four groups by culture type and generated a five-latent variable PLS-DA model with quality parameters R^2Y = 0.842 and Q^2 = 0.649, with

the first three being reasonably sufficient to distinguish all four culture types (cumulatively having R^2Y = 0.728 and Q^2 = 0.632). The model distinctly classified the observations with the first latent variable describing the differences between AMA- and MMM-derived hMSCs, the second latent variable delineating the OMA-derived hMSCs, and the third latent variable distinguishing the OMO-derived hMSCs from all the other culture types (Figure 5.8A,C). OMA-derived hMSCs constitute the tightest cluster in all of the first three latent variables, owing to their relative homogeneity between samples compared with the other culture types. With respect to the gene expression dynamics that constitute the latent variables, several genes overlap in their contribution to discrimination of the different culture types. This can be visualized by their proximities to one another on the weight plots in the latent variable space (Figure 5.8B,D). Genes that correlated with MMM hMSCs in one or more latent variables included *OCN* (Day 7), *CEBPB*, *RUNX2*, *NFKB1*, *OPG*, *ADIPOQ*, *ATF2*, and *LEP*. AMA hMSCs were correlated with *LEP*, *RUNX2*, and *ADIPOQ* (all on Day 1). OMA hMSCs were correlated with *OCN*, *FOXO1*, *JUN*, *LEP*, *RUNX2*, and *ADIPOQ* (all on Day 1). OMO hMSCs were correlated with *FOXO1*, *LEP*, and *NFKB1* (all on Day 7).

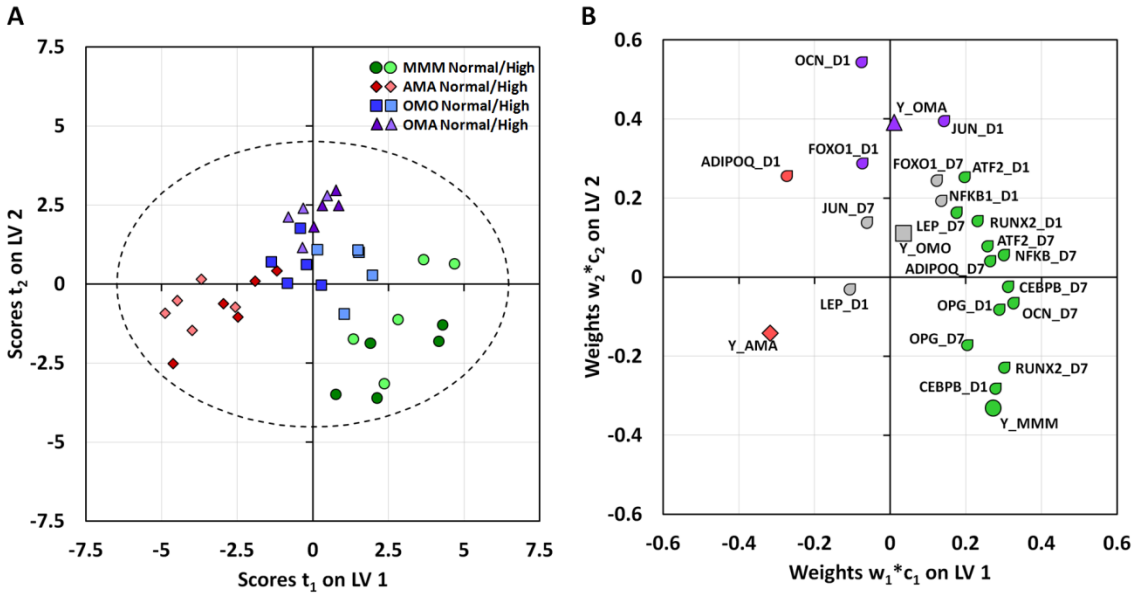

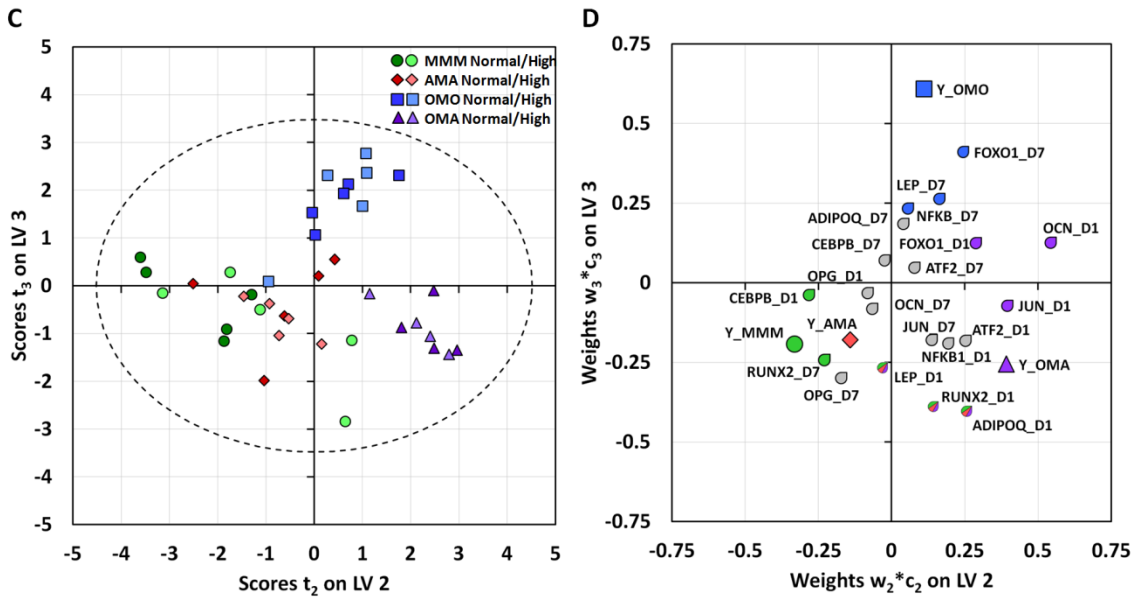

Figure 5.8. Statistical modeling based on covariance of the gene expression data yields three latent variables that distinguish hMSCs from each culture type and elucidates its correlation structure with gene expression at various time points. A,C) Plots of PLS-DA scores, t_1 and t_2 (A) and t_2 and t_3 (C), for observations (culture type and glucose condition) that segregates four distinct culture types by three latent variables (LVs). B,D) Weight plots depicting the correlation structure of the gene expression data and the corresponding culture types, indicating: 1) the weights, w*, that combine the X-variables (gene expression values at different time points) to form the scores, t; and 2) and the weights, c, of the discriminating Y-variables (corresponding to each culture type). Gene expression values at specific times (X-variables) that contribute most to the culture type classification (Y-variables) are shaded accordingly with the corresponding color scheme. R^2Y = 0.842, Q^2 = 0.649.

5.3.4.3 Modeling of Gene Expression Data with PCA to Assess Sources of Maximum Variance within Culture Types

Within the larger clusters of cell types in our first PLS-DA model (Fig. 5.8A,C), several observations appeared to also cluster by glucose condition. The first three latent variables in this model only account for 58.6% of the variance in the X-variables (genes at different time points; R^2X = 0.586), and the addition of two more latent variables account for an additional 11.4 and 12.1% of the variance in the X- and Y-variables, respectively. This observation appeared to indicate that an additional source of variance was present, and it was hypothesized that variance caused by changes in glucose were

masked by larger variances attributable to culture type in the global data set. To test this hypothesis, a set of PCA sub-models that split the data by culture type were constructed to look at the sources of variance within each culture type (Figure 5.9). Using one or more principle components, each model was able to sort the observations by glucose condition within each culture type to varying degrees. Approximately 70% or more of the variance could potentially account for differences in gene expression due to glucose condition within hMSCs from mono- (Figure 5.9A) and co-culture (AMA, Figure 5.9B; OMO, Figure 5.9C) with 50% or greater predictive capability. Variations in glucose appeared to only account for 60% of the variance within the OMA hMSC data set with only 30% predictive capability (Figure 5.9D).

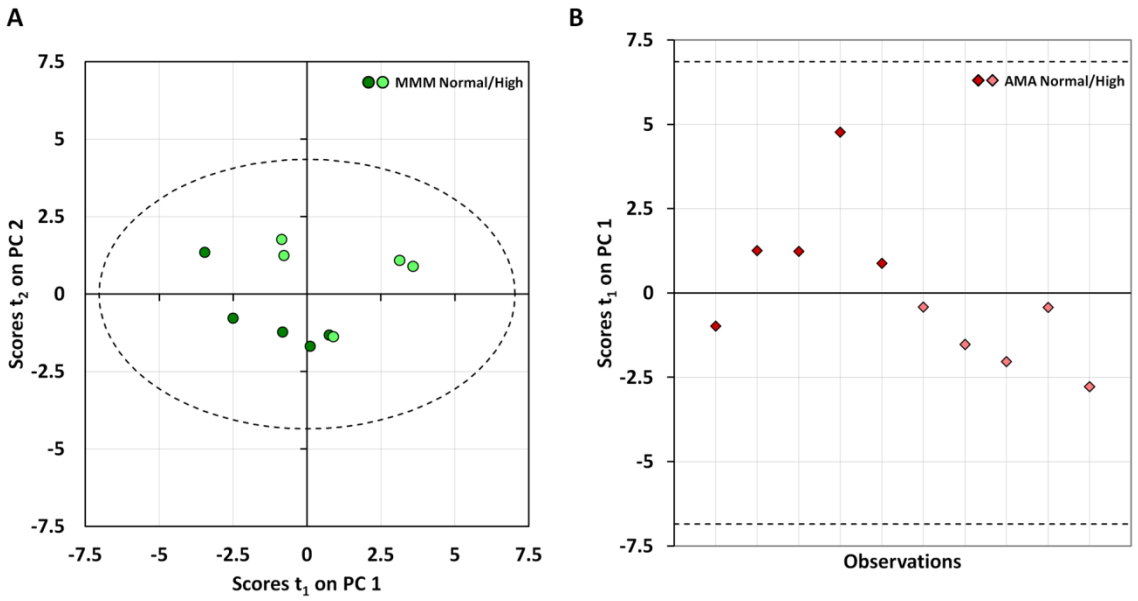

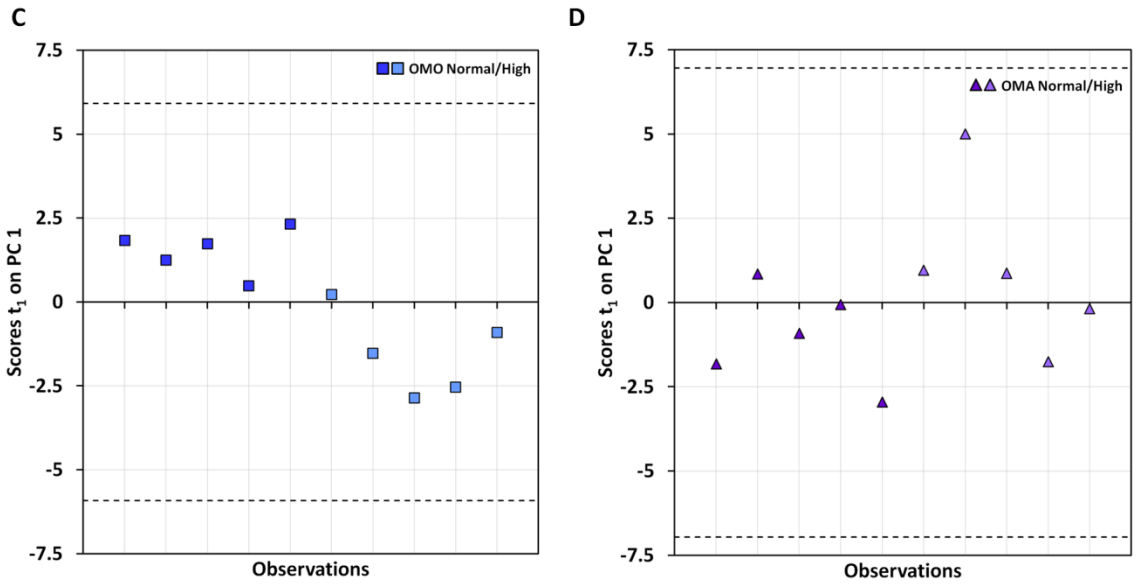

Figure 5.9. PCA within each culture type demonstrates that more than 60% of the variance between samples may be explained by differences from exposure to normal or high glucose. A-D) Score plots for each sub model. A) Model discriminating between MMM hMSCs exposed to normal or high glucose. R^2X = 0.852, Q^2 = 0.564. B) Model discriminating between AMA hMSCs exposed to normal or high glucose. R^2X = 0.669, Q^2 = 0.475. C) Model discriminating between OMO hMSCs exposed to normal or high glucose. R^2X = 0.698, Q^2 = 0.481. D) Model discriminating between OMA hMSCs exposed to normal or high glucose. R^2X = 0.603, Q^2 = 0.3.

5.3.4.4 Modeling of Gene Expression Data with PLS-DA to Correlate Gene Expression with Glucose Condition within Culture Type

After generating several preliminary PCA models, we were able to verify that a reasonable portion of the variation within these clusters (> 60%) could be accounted for in PCs that separated the observations by glucose condition. This motivated the development of a separate PLS-DA model for each culture type to further classify the observations by glucose condition and determine gene expression variables at specific times that are highly determinative of hMSCs from each condition (Figure 5.10). A two-latent variable model for MMM hMSCs revealed that expression dynamics of *RUNX2*, *OCN*, *OPG*, *JUN*, and *NFKB1* were important for discriminating between normal and high glucose conditions (Figure 5.10A,B). A two-latent variable model for AMA hMSCs discriminates normal- from high-glucose samples by expression levels of *NFKB1*, *LEP*,

ADIPOQ, *OCN*, and *RUNX2* (Figure 5.10C,D). A single-latent variable model discriminates OMO hMSCs cultured in the presence of normal or high glucose by expression of *JUN*, *ATF2*, *NFKB1*, *RUNX2*, and *OPG* (Figure 5.10E,F). Finally, a two-latent variable model separates OMA hMSCs from different glucose conditions on the basis of *ATF2*, *JUN*, *NFKB1*, *CEBPB*, *LEP*, *ADIPOQ*, *RUNX2*, and *OPG* expression (Figure 5.10G,H).

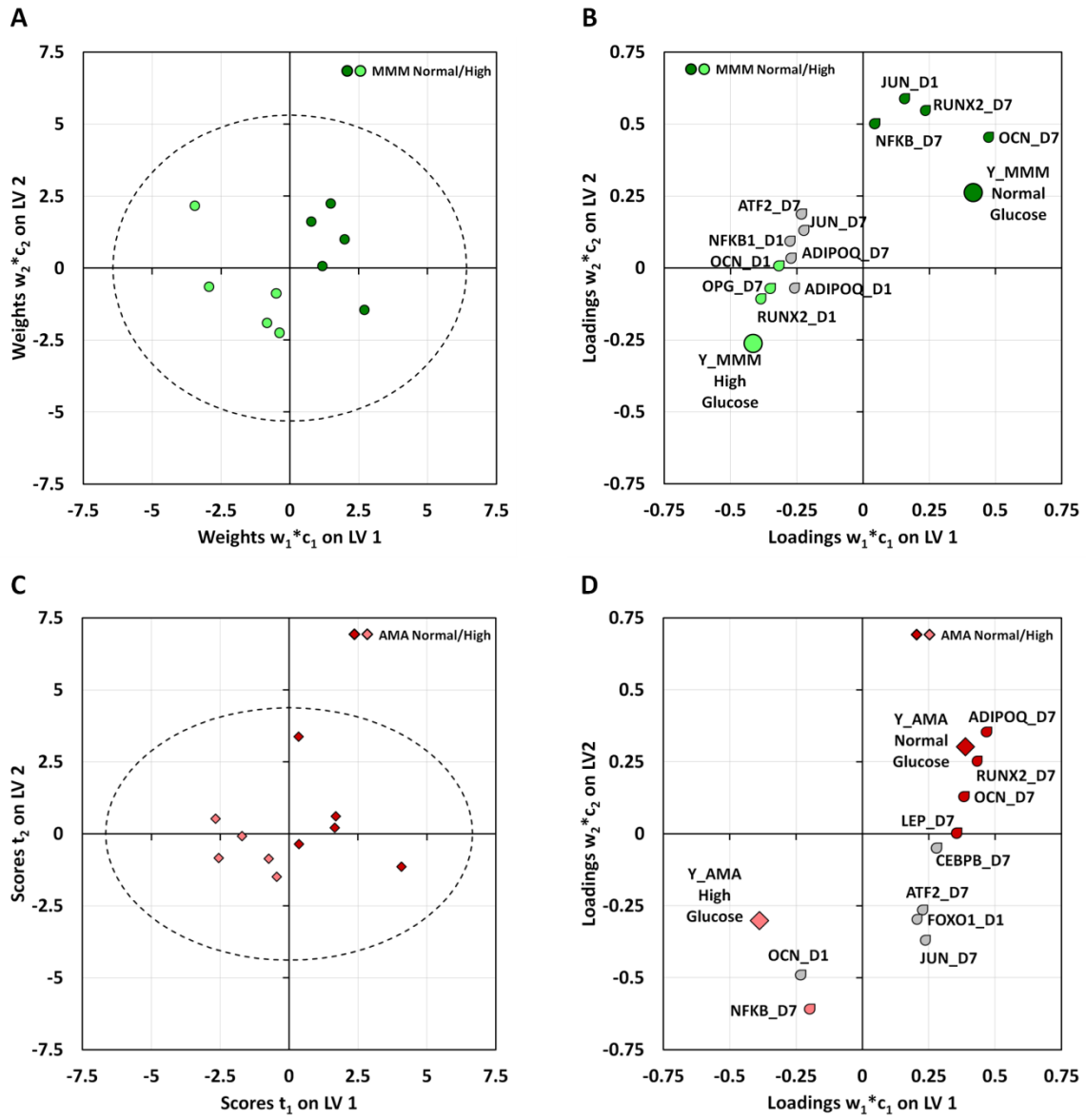

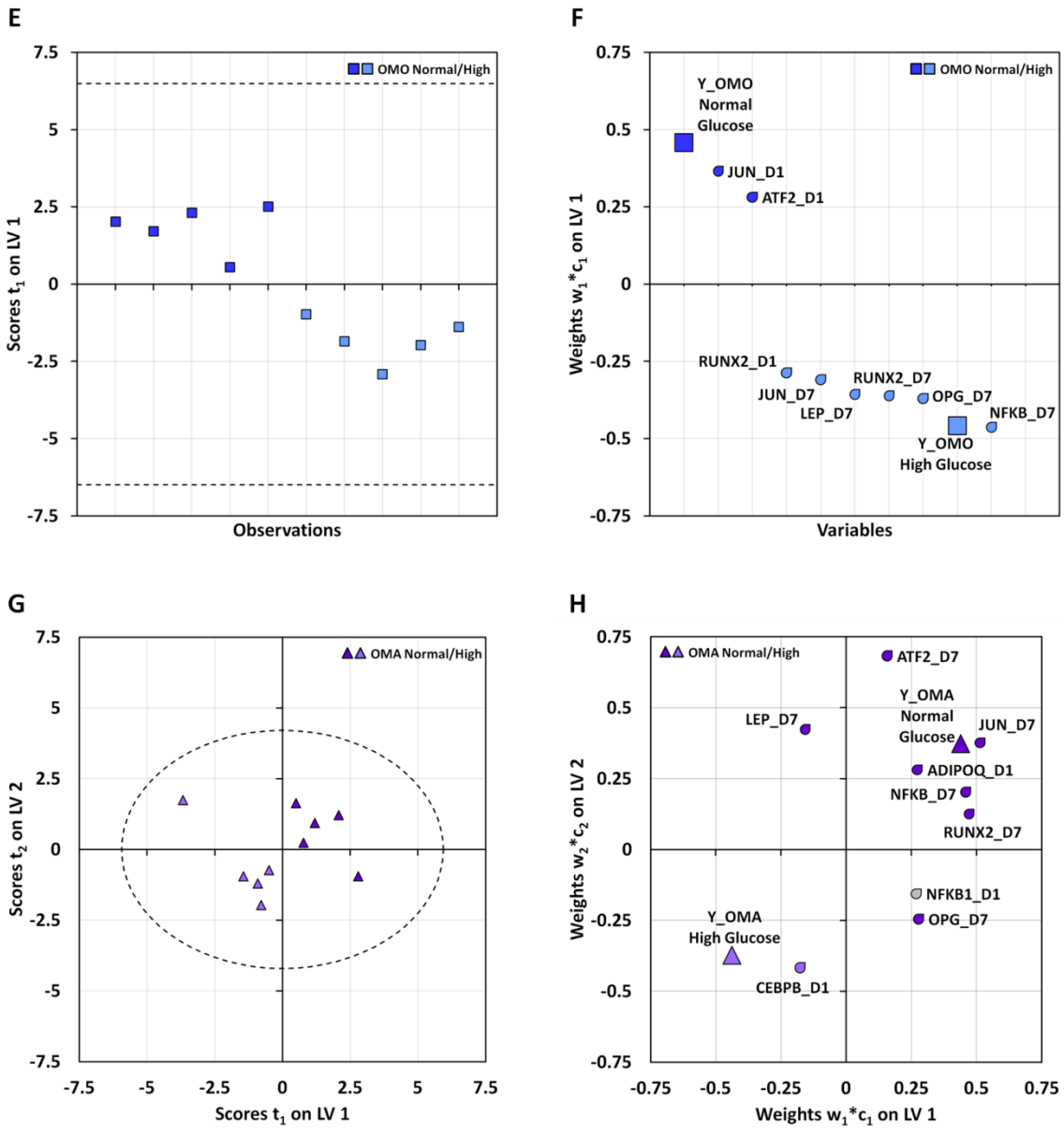

Figure 5.10. PLS-DA models of individual culture types can robustly distinguish hMSC samples cultured under different glucose conditions and describe the important gene expression variables that correlate with response to glucose level. A,B) Model discriminating between MMM hMSCs exposed to normal and high glucose. R^2Y = 0.903, Q^2 = 0.724. C,D) Model discriminating between AMA hMSCs exposed to normal and high glucose. R^2Y = 0.839, Q^2 = 0.593. E,F) Model discriminating between OMO hMSCs exposed to normal and high glucose. R^2Y = 0.881, Q^2 = 0.814. G,H) Model discriminating between OMA hMSCs exposed to normal and high glucose. R^2Y = 0.922, Q^2 = 0.837. A,C,E,G) Score plots of clusters of hMSCs segregated into distinct groups by one or more latent variables. Dashed lines represent the 95% confidence limit of the distribution of scores for each model. B,D,F,H) Weight plots depicting the correlation structure of gene expression data

and the corresponding observation sets for each model. Gene expression values at specific times (X-variables) that significantly contribute ($p < 0.05$) most to the glucose condition classification (Y-variables) are shaded accordingly with the corresponding color scheme. Figure 5.10 continued.

5.3.4.5 Partial Least Squares Projections to Latent Structures (PLS) Modeling to Assess Correlation of Gene Expression with Colony Formation

Given the availability of data quantifying an hMSC functional outcome, namely colony-formation capacity, PLS regression analysis was used to map the variation in CFU-F number (Y-variable) with the corresponding variation in gene expression data (X-variables) from each culture type and glucose condition. A two-latent variable model was generated in which the first latent variable separates MMM and OMO hMSCs exposed to high glucose from all the other samples and encompasses 56.7% of the variation in the gene expression data and 54.2% of the variation in the colony formation data (Figure 5.11A). The second latent variable accounted for an additional 19% of the variation in the gene expression data and 12.7% of the variation in colony formation in separating hMSCs from OMA and AMA cultures. Overall, the observations appear to be clustered by both culture type and glucose condition. Examination of the weight plot (Figure 5.11B) reveals that colony formation is positively correlated with *JUN* expression on Day 1, highly anti-correlated with *FOXO1* on Day 7, and moderately anti-correlated with *ATF*, *NFKB1*, *LEP*, and *OPG* expression on Day 7.

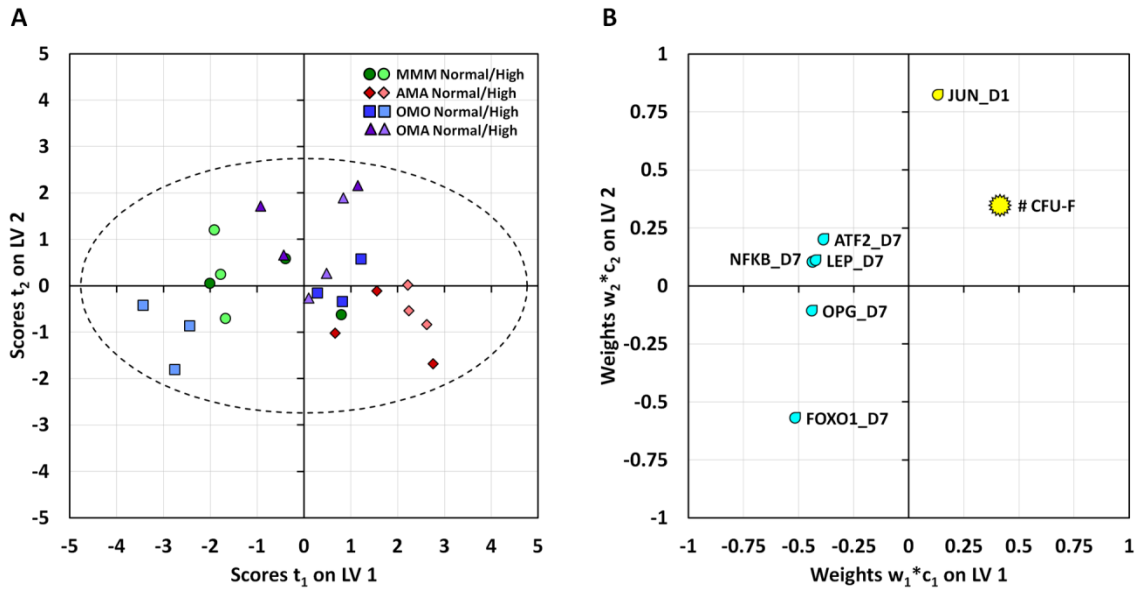

Figure 5.11. Statistical modeling based on covariance of hMSC gene expression data with colony formation yields two latent variables that are able to distinguish hMSCs from different culture types and glucose conditions and elucidates the correlation structure of gene expression and colony formation. A) Plot of PLS scores, t_1 and t_2, for observations (culture type and glucose condition) that segregates high-glucose OMO and MMM hMSCs (1st LV) and OMA and AMA hMSCs (2nd LV). B) Weight plots depicting the correlation structure of gene expression data and colony formation capacity. Gene expression values at specific times (X-variables) that significantly correlate ($p < 0.05$) with colony formation (Y-variable) are shaded yellow, while those that are significantly anti-correlated are shaded cyan. R^2Y = 0.668, Q^2 = 0.569

5.4 Discussion

This work demonstrates that human mesenchymal stem cells have unique genetic and phenotypic responses to glucose perturbations when cultured alone or with one or more differentiated cell types. Using a variety of outcome measures, we were able to discern unique effects of mono-, co-, and tri-culture on cell viability, gene expression, and clonogenicity of hMSCs in the context of systemically delivered normo- and hyperglycemic conditions. Had the changes due to glucose been the overriding influence on these outcomes, the utility of this platform for culturing multiple cell types would be superfluous and culture of a single cell type would suffice for further exploration.

Conversely, if the hMSCs been completely unresponsive to changes in glucose and only to the identity of the neighboring cell types, then their relevance in studying the pathophysiological consequences of hyperglycemia might be diminished. Neither the signaling interactions between the cells themselves nor the global change in glucose concentration provided an overwhelmingly dominant influence over gene expression and functional responses, signifying that this hydrogel tri-culture platform is uniquely suitable for examining both cell-derived and global perturbations to a complex interaction network consisting of multiple cell types in a simplified, highly tunable 3D *in vitro* microenvironment.

5.4.1 Response of hMSCs to Degradable Hydrogel

The modularity of this hydrogel system, enabled by the sequential crosslinking and lamination of these synthetic, chemically tailorable hydrogels, allows for flexibility in the configuration of patterned cells and also provides a means for tailoring the microenvironmental niche of each cell type (*e.g.* biomaterials, material stiffness, biochemical moieties, and cell density) independently [65, 176]. This feature stems from the ability to use a mask for preventing further crosslinking, UV exposure of cells, or other modification of a gel module after each step. As a direct result of this modularity, we were able to encapsulate hMSCs in an enzyme-sensitive PEG derivative that allowed us to retrieve the cells on demand following the conclusion of the 3D culture and evaluate their functional characteristics. This experiment provided a proof-of-principle that our system can incorporate another mode (in addition to manual dissection) of selectively separate cell populations after culture in a specific manner dictated by the sensitivity and specificity of the peptide crosslinker used. Additionally, this represents the first time enzyme-sensitive hydrogels containing encapsulated cells have been used for this purpose.

Fibronectin- and laminin-derived peptides (GRGDS and YIGSR, respectively) were employed here to promote cell viability and normal adhesion-dependent function of encapsulated hMSCs, osteoblasts, and adipocytes during the culture [196, 198, 374]. When coupled with the collagenase-sensitive peptide crosslinker for encapsulation of hMSCs, there existed the possibility of cell-mediated degradation of their surrounding matrix since the peptide is also sensitive to matrix metalloproteinases MMP-1 and MMP-2 [394, 402]. Based on previous literature, the expectation was that over the week-long course of the experiment, the hydrogel network would not degrade quickly enough to induce significant hMSC cell spreading [218], and this was validated prior to the experiment by encapsulating each cell type in separate degradable gels and observing viability and cell spreading over 1 week (Appendix A). MMM hMSCs did not undergo changes in cell spreading over 1 week in culture, regardless of glucose condition (Figure 5.3A); however, co- and tri-cultured hMSCs under normal and high glucose did spread and appear to form some cell-cell contacts. This could be attributed to a high concentration of cells localized near the surface of the gels due to settling of cells; the hydrogel material was not density matched to each cell type and thus cells were not homogeneously distributed within each module.

However, despite the unintended effect of cell settling, hMSCs still responded to glucose in a context-dependent fashion. This suggests that hMSC MMP activity was affected by cues from the differentiated cells, since each cell type alone could not degrade the gels and spread within 1 week (Appendix A). Their spreading and/or coupling may have in turn affected their response to soluble paracrine signals from other cell types or to the glucose condition, since hMSC spreading is permissive for osteogenesis [67] and cell density in culture has been shown to correlate with proliferative capacity [50]. Additionally, more direct cell-cell contacts exist between the hMSCs than the other cell types and thus they are able to generate mechanical forces that may signal to other cells. Encapsulated hObs and hAds, while coupled via adhesion

peptides to the same network, cannot spread, remodel the PEG network, or generate large traction forces, so it remains unclear whether they were able to sense any hMSC-derived mechanical cues [67, 375]. Consequently, we cannot definitively rule out the possibility of intercellular communication via mechanical coupling between the cells and the polymer/cell-secreted extracellular matrix. Given that this PEG-based network readily allows for the diffusion of soluble cues from the small molecule to protein scale [373], it remains likely that much of the intercellular crosstalk between each cell type is largely dominated by soluble paracrine factors. Nevertheless, despite the mode(s) of signaling being unclear, hMSC responses specific to both culture type and glucose condition were still detectable with high confidence (Section 5.3). To maintain the cell-retrieval capability of the system while isolating the effects of soluble signals from other potential modes of communication, the enzyme-sensitive peptide sequence could be optimized in future experiments to enable on-demand degradability using a non-endogenously produced enzyme.

5.4.2 Cellular Responses to Culture Type and Glucose Condition

Much of the variance in the gene expression among the entirety of the samples from this experiment could be attributed more to culture type than glucose condition. Confirmation of this notion is quite difficult if only examining the statistical significance of each factor and their interactions when analyzing each gene separately with ANOVA (Section 5.3.2 and Figures 5.4 and 5.5). Much stronger confirmation of the more dominant influence of culture type was discernible from PCA and PLS-DA of the entire gene expression data set (Figures 5.7 and 5.8). The observations appear to cluster more homogeneously within each culture type rather than by applied glucose condition. Additionally, the principle components (PCA; Figure 5.7) that separate the observations along each axis based almost largely by culture type are determined by the sources of maximum variance in the data by definition. Moreover, the PLS-DA (Figure 5.8)

confirms that the observations are best classified by latent variables that distinguish culture type since those observations have gene expression that co-varies the same way (high R^2Y and Q^2). Additionally, functional outcomes such as cell viability (Figure 5.3) and colony formation (Figure 5.6) were not uniformly affected by glucose condition. While the PLS model (Figure 5.11) was able to discern some correlation of clonogenicity with the gene expression data, many of the variables we measured were pruned from the model and few exhibited strong positive or negative correlation. Together, these results demonstrate that while glucose did affect cell gene and functional responses, it did so only within the context of the existing crosstalk interactions between the cell types present and did not overwhelm their influence on hMSCs. Future experiments would benefit from expanding the repertoire of genes and outcome measures to more fully elucidate underlying mechanisms of the different responses that emerged in each culture system, along with mapping of the network interaction modules that may be differentially activated by each system [377, 403] to these functional outcomes through PLS models that would benefit from more input data.

Evidence exists from the gene expression data that hMSCs sensed and responded to their surrounding environment as soon as the first day in culture (Figures 5.4 and 5.5) when no change had been made yet to the administered glucose concentration. Expression of *JUN* and *NFKB1* were elevated in hMSCs from tri-culture compared with those from AMA co-cultures. Additionally, levels of *ADIPOQ* and *OCN* (generally considered to be secreted by terminally differentiated adipocytes and osteoblasts, respectively; [404, 405]) were quite different among the different culture types. *ADIPOQ* was significantly expressed in higher amounts by hMSCs either co- or tri- cultured with adipocytes than MMM or OMO hMSCs. *OCN* was significantly expressed in higher amount by constructs containing osteoblasts. These results suggest that after one day in culture, hMSCs may have been differentially primed by their surroundings, which could later have affected how each responded to the level of glucose administered during

subsequent feedings. Notably, by the end of the week-long culture, the expression of each gene evaluated in this study responded differently to glucose treatment depending on the mono-, co-, or tri-culture condition.

5.4.2.1 Responses of Mono-Cultured hMSCs

Mono-cultured hMSCs (MMM) constituted one of the largest sources of gene expression variance in all the samples tested (separated by the first component of global PCA; Figure 5.7). When examining their covariance structure with the gene expression data (Figure 5.8), they exhibited strong positive correlations with many of the genes tested with the exception of *JUN*, *FOXO1*, and *OCN*. Exposure to high glucose did not affect their cell viability over time compared with normal glucose (Figure 5.3), but it did significantly reduce their colony formation capacity (Figure 5.6). MMM hMSCs under high glucose also were highly anti-correlated with *JUN* on Day 1 (whereas this gene was highly correlated with MMM hMSCs under normal glucose; Figure 5.10A,B), a variable that positively correlates with colony formation (Figure 5.11). Together, this data may reflect glucose-induced replicative senescence as previously documented in the literature [129-132], which would be consistent with the negative consequences of gestational diabetes for embryonic and neonatal skeletal development [126-128], and for skeletal development in patients with T1DM [121-123]. Follow up staining of histological sections with β-galactosidase (a marker of senescence, [406]) would aid in verifying this hypothesis. Additionally, similar findings were observed in OMO hMSCs but apparently not in AMA hMSCs (Section 5.4.2.2), and comparative gene expression and histological analysis between these cultures would be useful in further elucidating a potential mechanism for this apparent senescence.

5.4.2.2 Responses of hMSCs Co-Cultured with Adipocytes

Examining the culture types overall, hMSCs from AMA co-cultures exhibited the largest variance in gene expression data (largest separation on the first component of

global PCA; Figure 5.7). Interestingly, their gene expression was almost entirely anti-correlated with that of any of the other culture types (Figures 5.7 and 5.8), suggesting that they may be phenotypically the most different from hMSCs from any of the other culture types and that their behavior would be very different. Indeed, when exposed to high glucose, they showed increased numbers of dead cells by Day 7, but once extracted, the viable hMSCs remaining showed the same colony formation capacity as AMA hMSCs under normal glucose conditions (Figure 5.6), leading us to refine our original hypothesis since the effects of AMA co-culture were more nuanced than originally conjectured. This may result from the ability of adipocytes in co-culture that can accommodate and store the extra glucose, which may serve as an acute compensatory mechanism. Despite similar clonogenicity, the gene expression of AMA hMSCs is quite different under normal and high glucose (Figure 5.10C,D); AMA hMSCs exposed to high glucose are highly correlated with *NFKB1*, a potent transcription factor in eliciting production of pro-inflammatory cytokines that could have led to increased cell death [137, 139]; and they are anti-correlated with *ADIPOQ*, *LEP*, and *OCN*, all of which serve to maintain glucose homeostasis [25]. Together, these results suggest there may be phenotypic traits other than cell death and colony formation worth probing in future experiments (e.g. changes in lineage allocation [129, 132], or in ability to modulate inflammation and ROS [137, 139]). Histological evidence of increased triglyceride storage would support the notion that adipocytes provide a buffering capacity to the co-culture system, while analysis of conditioned medium could yield insight into the degree of inflammatory molecules and ROS produced. Should this evidence be lacking, an alternative hypothesis may be that hMSCs have the capacity to moderate negative effects of adipocytes in the face of hyperglycemia by counteracting the oxidative stress and modulating inflammation, both known properties of hMSCs in other regenerative contexts [61, 407-409].

5.4.2.3 Responses of hMSCs Co-Cultured with Osteoblasts

hMSCs co-cultured with osteoblasts (OMO) did not contribute nearly as much variance to the overall gene expression data. Like AMA hMSCs exposed to high glucose, OMO hMSCs were also characterized by reduced cell viability (Figure 5.3). However, this was instead coupled with vastly reduced colony-forming capacity (Figure 5.6), constituting the largest decline compared with its normal glucose counterpart. Since hMSCs and hObs do not have nearly the glucose absorption capacitance of adipocytes, it is possible that the hyperosmotic stress caused by excess extracellular glucose leads to ROS production that upregulates *FOXO1* as a protective mechanism, but can also lead to *NFKB1* expression if it persists for too long [134, 410]. Both of these genes were found to be upregulated in high glucose-exposed OMO hMSCs (Figures 5.4 and 5.5), and strongly correlated with them in PLS-DA models (Figure 5.10E,F). Similarly to high glucose-treated MMM hMSCs, these cells were also negatively correlated with *JUN* on Day 1. Both of these gene correlations are in good agreement with the PLS model, which shows that the same genes co-vary in the same ways with CFU number (Figure 5.11), lending strength to the potential role of these genes in regulating hMSC clonogenicity. The finding that co-culture setting differentially regulates hMSC clonogenicity while having similar effects on cell viability is both striking and unexpected, since dysregulated adipogenesis correlates with poorer skeletal health and inflammatory adipokines are thought to play a significant role in reducing bone quality [7, 9, 11]. However, hMSCs and osteoblasts do not have the glucose absorptive capacity of adipocytes, thus leading to potential hyperosmotic shock as previously described in the literature [133-135]. This lends strength to the hypothesis that the accumulation of excess marrow fat may be a compensatory mechanism to counteract the effects of hyperglycemia, though this may become detrimental in the long term.

5.4.2.4 Responses of Tri-Cultured hMSCs

Tri-cultured hMSCs (OMA) provided a moderate source of variability in the gene expression data set (distinguished by the second principle component in the global PCA; Figure 5.7A). Examination of this culture type with a PCA sub-model (Figures 5.8D) revealed that these observations were tightly clustered and difficult to separate into high and normal glucose conditions, owing to their low intrinsic variability (R^2X = 0.603 and Q^2 = 0.3). When attempting to model this sample set with PLS-DA to try and discriminate between glucose conditions, two latent variables were required when one that distinguished between normal and high glucose conditions would have sufficed, suggesting the presence of variability in the data that could not be accounted for by glucose alone. The scores in this model still placed the observations near the origin, which indicates that the latent variables are separating a tightly clustered data set, again suggesting that the gene expression is not that variable between the two glucose conditions (Figure 5.10G,H). Taken together, this suggests that the variance within this sample group could not be primarily attributed to differences in response to glucose. This provided a striking correlation with their functional outcomes, in which no statistically significant differences were observed in cell viability or colony formation (Figures 5.3 and 5.6). One possible interpretation of these results then is that the data in this sample set is particularly noisy because of multiple confounding processes within the system; however, this appears unlikely as the variance in this sample set when examining gene expression or functional outcomes is no larger than any other culture type. Therefore, this likely indicates that the tri-culture system as a whole is robust to glucose perturbations and maintains a relatively stable state over the 1-week culture period. Conceivably, the compensatory mechanisms of all three cell types lead to stability where those present in the mono- and co-culture settings are insufficient, suggesting that a proper balance and regulation of all three cell types is needed to maintain adequate skeletal health in the context of diabetes. As outlined above, histological and conditioned medium assays and

comparison of these with mono- and co-cultures may yield insights into the degree of compensation and the key players in maintaining a relatively stable state.

5.4.3 Limitations and Future Directions

Further data acquisition and examination is necessary to more fully characterize the system-level responses of the cell types in our platform in response to mono-, co-, and tri-culture in response to glucose perturbations. Insight into the interplay between culture type and glucose condition on the osteoblasts and adipocytes from these mono-, co-, and tri-cultures would provide further evidence to support the hypothesis surrounding the behavioral responses of the hMSCs in this system outlined above. This data would include cell viability quantification of osteoblasts and adipocytes, collecting their gene expression data and expanding the repertoire of genes evaluated, and protein expression of glucose-regulating hormones and remaining glucose content from media samples. Together, these would strengthen our multivariate models to elucidate the correlation structure between all of these outcomes and provide further opportunities to test our hypotheses and generate new ones. Future experimentation to evaluate potential lineage restriction of hMSCs through clonal selection, assays for senescence, and assessment of osteoblast and adipocyte function (*e.g.* ability to mineralize or store and release triglycerides, respectively) would provide even more comprehensive insight into the complex behavior elicited in this study. Quantitative analysis of soluble factors within the conditioned media (*e.g.* residual glucose content, free fatty acids, inflammatory cytokines, growth factors, and hormones), when combined with comparative analysis using our multivariate techniques across culture types and glucose conditions would readily enable discovery of key mediators of the cell fate processes observed. Previous work detailed in Chapter 4 demonstrates that longer term mono-, co-, and tri-cultures are feasible and would enable further elucidation of the consequences of prolonged exposure to hyperglycemia that may align more with clinical observations and previously

generated hypotheses [9-11, 106, 118]. Nonetheless, the preliminary data collected solely from examination of the hMSC outcomes from this study validates this platform for use in examining the complex interplay between bone remodeling and energy metabolism in homeostasis and disease states.

Since the culture systems studied herein respond to a systemic perturbation in a complex, context-dependent way, this motivates further exploration of responses of these systems to the addition of drugs used to treat diabetes, since often these coexist with and modulate hyperglycemia and insulin resistance in clinical settings [125]. Metformin stimulates osteoblast differentiation through the transactivation of Runx2 [411-415]. Glitazones activate PPARγ which might shift precursor cells towards the adipocytic lineage at the cost of osteoblast formation [416-421]. However, as with glucose, these medications may produce counterintuitive and perhaps counterproductive effects when applied to systems of cells such as those studied in these experiments. Additionally, their interactions with fluctuations in glucose levels have yet to be studied in such a controlled environment like the one offered by this platform. Studying these networks and their dynamic responses to these perturbations may reveal new modes of treatment that target networks rather than individual proteins or genes [377, 378, 422-424], as was recently illustrated by Lee *et al* who successfully increased the susceptibility of non-drug-responsive breast cancer tumors to attack by time- and order-dependent drug combinations that progressively rewired cellular signaling networks within the tumor [425].

5.5 Conclusions

In this study, we have leveraged our 3D tri-culture platform developed in Chapter 4 to enable observation context-dependent interactions between hMSCs, osteoblasts, and adipocytes in response to different amounts of systemically administered glucose to mimic poorly controlled diabetes. hMSCs from each culture type displayed distinct gene

expression, viability and colony formation after one week of culture, suggesting that both cell- non-cell autonomous mechanisms drive their responses to high glucose levels. Together, these data suggest a more complex pathophysiology surrounding diabetes than previously hypothesized and that the mechanisms of disease progression are likely a function of more than just the sum of individual cell type-responses to hyperglycemia that have been studied more extensively in the literature. Indeed hMSCs respond in unpredictable ways when in co- and tri-culture, suggesting that clinical correlates such as excess marrow fat may have both positive and negative effects and that the entire marrow microenvironment needs to be studied as a system to fully elucidate the mechanisms underpinning skeletal pathology in this disease. In fact, data from tri-culture suggests that all three cell types are potentially needed to satisfactorily maintain skeletal health by preserving hMSC clonogenicity and preventing cell death. These findings suggest that this biomaterial platform provides a powerful systems biology tool to map and correlate complex stem and native cell-cell interaction networks with physiologic and disease phenotypes. When complemented with differential network analysis and combinations of systemic perturbations with biomolecules and/or drugs, this platform could lead to discovery of new mechanisms of skeletal disease in diabetes and allow advancement of novel treatment strategies that target one or more components of a complex system.

CHAPTER 6

CONCLUSIONS AND FUTURE DIRECTIONS

6.1 Summary

In addition to offering the potential to replace and restore function to injured tissues, tissue engineering provides researchers with the ability to generate improved, highly controlled and tailorable *in vitro* model systems to better understand mechanisms of homeostasis, disease, and healing and regeneration. Model systems that allow assembly of modules of MSCs, osteoblasts, and adipocytes in a number of configurations to engage in signaling crosstalk offer the potential to study integrative physiological aspects and complex interactions in the face of changes in local and systemic microenvironments. Each of these aspects will more readily enable prediction and understanding of cell and tissue behaviors *in vivo* with respect to skeletal remodeling and energy metabolism and facilitate design of novel and integrated molecular and cellular therapies to combat skeletal and metabolic diseases. The overall goal of this dissertation was to examine integrative physiological aspects between multiple cell types that exist within the marrow microenvironment, namely: MSCs, osteoblasts, and adipocytes using a novel *in vitro* model system. Specifically, a method was developed to photolithographically pattern and assemble cell-laden PEG-based hydrogels with high spatial fidelity and tissue-scale thickness for long-term three-dimensional co-culture of multiple cell types [362]. These photopatterning and lamination techniques were then adapted to produce an enabling platform to investigate effects of crosstalk between MSCs, osteoblasts and adipocytes on expression dynamics of mesenchymal lineage genes and histological markers of differentiation [387]. Finally, the same platform was used as a model to examine how the responses of MSCs to systemic perturbations in glucose concentration was affected by mono-, co-, and tri-culture with these same cell types as a model of pathogenesis of skeletal disease in diabetes. Together, these studies provided

valuable insight into unique and differential effects of signaling crosstalk between all three cell types and how this crosstalk may be affected during a pathological state, demonstrating a valuable model system for further study of integrative physiological interactions between mesenchymal lineage cells.

In Chapter 3, fluidic and photolithography techniques were combined under an oxygen-depleted environment to enable photopatterning of hydrogels into well-defined shaped at tissue scale thickness (1-2 mm) [362]. Shape and size of hydrogel spatial features within each construct may be tuned and controlled through simple alterations in the photomask and implementation of an N_2 atmosphere during the crosslinking procedure. This was accomplished without altering concentrations of cytotoxic free radical photoinitiators or altering base polymer structure to increase crosslink density and generating oxygen free radicals, all of which would have been detrimental to cell viability. This photolithographic scheme was sequentially employed in the generation of multiple laminated, spatially defined hydrogel domains that consistently remained adherent at their interfaces and segregated multiple cell types in the same laminated construct. These templated constructs enable tissue-scale co-culture between two or more cell types in defined spatial locales with preserved viability over at least 2 weeks and provided a platform with which to study signaling interactions between these cell types in Chapters 4 and 5.

In Chapter 4, a simplified version of the platform developed in Chapter 3 was employed for co- and tri-culture of MSCs, osteoblasts, and adipocytes to evaluate effects of paracrine signaling on markers of differentiation in each cell type [387]. Each gel module containing a different cell type was specifically designed to prevent cell migration, cell-cell contacts, proliferation, and cell spreading to isolate the effects of paracrine signaling. Gene expression and histological analysis over 18 days in culture demonstrated that each cell type was able to respond to signals from its neighbors in a context specific way. Gene expression indicated that MSCs appeared to exhibit some

levels of lineage commitment in cell types that they were co-cultured with but failed to show definitive histological markers of terminal differentiation when compared with mono-culture positive controls cultured in defined differentiation media for osteogenesis or adipogenesis. Tri-cultured MSCs retained gene expression markers for multiple mesenchymal lineages. Multivariate analysis incorporating the global gene expression data set confirmed that MSCs as a whole remained a distinct population from osteoblasts and adipocytes, but revealed that all three cell types responded in a context-dependent manner to their co- and tri-culture environments since they could be discriminated with specifically defined, statistically meaningful latent variables. Together, these data showed that distinct phenotypes for both the stem and differentiated cells may have developed as a result of intercellular soluble signaling, which may represent changes in their lineage plasticity and physiological function, respectively. Additionally, these results validated the relevance of this platform for further efforts to re-capitulate the bone marrow niche and model related pathologies, as described in Chapter 5.

In Chapter 5, the same platform from Chapter 4 was used to evaluate potential differences in MSC response to normal and pathologically elevated levels of systemically administered glucose that were governed by their mono-, co-, or tri-culture setting over 1 week. This platform was adapted to include an enzymatically degradable hydrogel module for the MSCs to separate and re-plate the cells to assess their residual clonogenicity after these experimental treatments. Several outcome measures, including cell viability, gene expression, and clonogenicity were used to assess the degree to which responses differed between culture types and glucose conditions. Mono-cultured MSCs maintained cell viability under high glucose, but exhibited differences in *RUNX2, OCN,* and *JUN* expression and lower colony-forming capacity, suggesting possible cellular senescence. MSCs co-cultured with osteoblasts exhibited decreases in both cell viability and colony formation under high glucose conditions accompanied with changes in expression of *RUNX2, JUN,* and *NFKB1*. Conversely, while MSCs co-cultured with

adipocytes displayed changes in cell viability and gene expression of *NFKB1*, *ADIPOQ*, *LEP*, and *RUNX2*, their colony forming capacity was maintained and illustrated a striking difference between the two co-culture settings that suggested that adipocytes may be protective of MSC clonogenicity to some degree. Tri-cultured MSCs displayed the most stable cell viability, gene expression and clonogenicity in response to different levels of glucose, illustrating a potential balance of compensatory mechanisms and an overall ability to buffer each others' responses to a perturbation that was more overwhelming in other mono- and co-culture contexts. These experiments demonstrated that MSC response to glucose was context-dependent and governed by cell- and non-cell autonomous mechanisms and validated this platform as a model system for future mechanistic studies and evaluating different treatments for the skeletal and metabolic consequences of diabetes.

Together, the findings presented in this dissertation suggested that intercellular signaling within the niche environment of MSCs and their terminally differentiated progeny plays an important role in priming and governing cellular responses to local and systemic factors and that the modular 3D tri-culture platform developed herein provides a novel and unique *in vitro* modality for investigating homeostatic and pathological crosstalk between each cell type in the construct.

6.2 Conclusions

The research presented in this dissertation advances understanding of the roles of context-dependent cues within the stem cell niche and between niche components and other less proximal cells and tissue compartments. Interactions of the MSCs, osteoblasts, and adipocytes examined herein together demonstrate a physiologically relevant subsystem with a larger role in homeostatic and disease processes. Neighboring cell types in combination with various media conditions over different time scales were shown to

affect the response of each cell type within the 3D laminated hydrogel constructs in different and detectable ways.

A broad overview of the transcriptional and phenotypic data that the following conclusions were drawn from reveals a non-trivial amount of noise in gene expression (Figures 4.2-4.4, and 5.4-5.5), cell viability (Figure 5.3), and clonogenicity (Figure 5.7). Conducting a *post-hoc* power analysis revealed that sample sizes used in these experiments were sufficient to detect near 1.6 to 1.8-fold differences in gene expression and 1.8-fold differences in clonogenicity and 2.5-fold differences in cell viability. This suggests that our data is inherently noisy and there are multiple possible reasons for such variability. Our platform analyzes cell populations as a whole, and sample to sample variation, stochastic variation in gene expression, and spatial heterogeneity within a construct on the length scale of hundreds of cells could all produce variance in collected data [426-430]. Despite this level of noise, the multivariate analysis techniques that we employed in these studies (Chapters 4 and 5) aided in discriminating our different sample groups much more cleanly, particularly with gene expression data since within a single sample, genes tended to co-vary the same way as in other samples from the same group. This allowed us to truly determine whether experimental treatments (culture type and/or glucose condition) caused observable differences in cellular responses. With respect to phenotypic data, sample size likely played a much larger role in our diminished ability to distinguish differences among some sample groups, even when incorporating PLS analysis methods. Nevertheless, these results demonstrate that combining our novel culture platforms with multivariate modeling techniques yields a powerful tool for discriminating context-dependent responses of cells and systems of cells to each other and to systemic perturbations (Section 6.3).

This platform fills a sizeable gap between *in vitro* models culturing one or two cell types in monolayer or transwell format and *in vivo* models composed of numerous interacting cells, tissues, and organ systems. Tissue-scale laminated hydrogel constructs

containing two or more cell types retain a higher degree of complexity than traditional *in vitro* models while simplifying and eliminating confounding factors present in animal models by isolating and allowing the study of specific subsystems. Responses within each of these subsystems (*i.e.* mono-, co-, and tri-culture) are governed by cell-autonomous (observable in mono-culture; Chapter 5) and non-cell-autonomous mechanisms (observable in co- and tri-culture; Chapters 4 and 5) [323, 324, 427, 431, 432]. Gene expression data and multivariate models formulated in each of these chapters demonstrates that a unique intercellular communication network, likely composed of numerous network motifs (*e.g.* feedback and feed-forward loops, uni- and multi-directional signaling), is formed in each setting depending on the cells used. Whether these effects are different from those that would be observed in 2D monolayer models is difficult to discern, particularly with tri-culture, since adipocytes tend to become non-adherent with increasing differentiation and 2D *in vitro* tri-culture models are extraordinarily difficult to prepare and then separate to examine cell-type specific effects [294, 296, 297, 299-304, 363]. Rather the platform developed here is easily fabricated and modified, and in combination with these multivariate analysis techniques, enables the study of complex interactions between multiple cell types in an uncomplicated way.

Gene expression data of transcriptional regulators from Day 1 after encapsulation (Chapter 4, Figures 4.2A, 4.3A, 4.4A; and Chapter 5, Figure 5.4) suggests that these communication networks may be set up over relatively short time scales (hours) compared to the overall length of the experimental culture period. Importantly, these transcriptional regulators are key mediators of differentiation (Chapter 4) and cellular metabolism (Chapter 5), and that they are so quickly modulated shows that key cellular processes are already potentially undergoing significant changes. Additionally, the genes selected for analysis in both these series of experiments represent a tiny fraction of the entire transcriptome. That detectable changes were observed in such a small sampling of potential transcripts suggests that other cellular transcriptional pathways and functional

modules may have been activated or repressed according to the cellular context of these cultures (Section 6.3).

Over 18 days in culture, MSCs in co-culture and tri-culture with osteoblasts or adipocytes (Chapter 4) displayed graded expression of master transcriptional regulators of osteo- and adipogenesis (*RUNX2* and *PPARG2*, respectively; Figure 4.4) correlating with which neighboring cells were present in the co- or tri-culture [387]. As expected, this behavior was not observable over a week-long timescale examined in Chapter 5 (Figures 5.4 and 5.5); rather cells never expressed *PPARG2* (Section 5.3.2) and did not exhibit the same patterns in *RUNX2* expression over the week in culture (Figures 5.4 and 5.5). Prior work in the literature has suggested that MSCs are primed toward and even differentiate into the lineages that they are cultured with over a 2-3 week time span, providing conflicting results [294, 297, 299, 300, 303, 363]. These can be reconciled on closer examination of the previous literature, which performed these co-cultures in the presence of media formulations that induce differentiation. A better interpretation of those prior experimental results would be that co-culture enhanced or permitted faster differentiation toward osteoblastic or adipocytic lineages than when cultured alone, which is much more in line with what was observed in Chapter 4 (Figures 4.4 and 4.6).

While more permanent changes in clonogenic phenotype were observed in the MSCs examined in Chapter 5, data from Chapter 4 suggest that this may not be at the expense of plasticity in lineage allocation of MSCs, or even their differentiated progeny. Evidence of any lineage commitment in MSCs was scant by Day 7 in co- and tri-cultures from Chapter 4 (Figure 4.4), with the possible exception of *PPARG2* expression in AMA co-cultures (though this never materialized in terms of enhanced triglyceride storage). Even alkaline phosphatase activity was transiently upregulated at Day 7 (Figure 4.4C) and disappeared by Day 18. Meanwhile adipocytes from co- and tri-culture dynamically expressed levels of osteogenic markers *RUNX2* and *OCN* (Figure 4.2), and osteoblasts displayed altered levels of adipogenic marker *PPARG2* and chondrogenic marker *SOX9*

that suggested these mesenchymal cells may be exhibiting context-dependent plasticity in their level of differentiation. Interestingly, MSCs from different culture settings expressed measureable levels of *OCN*, *LEP*, *ADIPOQ*, and *OPG* transcripts (Figures 4.4 and 5.4-5.5), which have been traditionally associated with hormones that are produced by their terminally differentiated progeny. These expression levels were comparably lower than levels expressed by osteoblasts and adipocytes evaluated in Chapter 4, and need to be further evaluated in Chapter 5.

Evidence from Chapter 5 demonstrates that system components (*i.e.* the cells types within each construct), when properly configured as in the tri-culture setup, can produce a network that is robust (stable) to a systemic perturbation where other configurations (mono- and co-cultures) are not [323, 324, 433-437]. An alternative network property to consider is adaptability (flexibility), which was displayed by cultures containing adipocytes [438-440]. While MSCs from these cultures differed under high glucose (Figures 5.9 and 5.10), clonogenicity was preserved (Figure 5.6) suggesting that the presence of adipocytes in culture confers the property of adaptability to the network that was formed during the week long culture period. To some degree however, this network did exhibit a degree of fragility (vulnerability) since MSC death increased under conditions of high glucose [434, 435, 441, 442]. This network fragility was much more pronounced when MSCs were cultured alone or with osteoblasts, since colony formation was significantly affected in both settings and this was coupled with increased cell death in co-culture. The finding that adipocytes and osteoblasts provide different degrees of network fragility and adaptability while together conferring robustness is a unique one that could only have been elucidated when examining systems of these cells as was performed in the studies in Chapter 5. Each of the network properties represents an important consideration and should continue to be scrutinized when considering systems of interacting cells and tissues in the design of implantable tissues or combination therapies targeted for regenerative medicine [377, 378, 442-444] (see also Section 6.3).

These systemic properties are in turn able to confer relatively stable properties on each of their cellular components. In Chapter 5, after a week-long period in mono-, co-, or tri-culture under conditions of normal or high glucose, MSCs were extracted from their hydrogel modules using enzymatic digestion (analogous to trypsinization or removal of a transwell insert) and re-plated at clonal density to evaluate their ability to generate colony forming units. During this time, they were no longer exposed to the same cellular or media context that existed over the week of encapsulation and instead were switched to media optimized for colony formation for a full two weeks (Section 5.2.7). Staining of colony formation after this culture period revealed different amounts of colony formation depending on the culture type and glucose treatment (Figure 5.6). This provides a proof-of principle demonstration of how degradable modules that allow retrieval of cell populations can be leveraged to provide further phenotypic data that could not be obtained while the cells were still encapsulated. Furthermore, these results demonstrated that the intercellular communication networks imparted phenotypic characteristics on the MSCs encapsulated within them that may last long after a stimulus is removed [426, 445-449]. Translated to an *in vivo* context, this lends insight into how pathological insults, both acute and chronic, can transform stem cell niches (*e.g.* in the bone marrow) and the stem cells themselves in a permanent fashion to affect their ability to self-renew, participate in normal homeostatic remodeling of tissues, and respond in the face of physiological insults [73, 426, 439, 450, 451].

Both iterations of the 3D co- and tri-culture platforms (flow-driven delivery and photolithography in Chapter 3, and layer-by-layer deposition in Chapters 4 and 5) importantly are designed to build laminated constructs in a modular fashion due to the sequential crosslinking steps during fabrication. This key feature means that each gel module containing a different cell type can be tuned to have no biofunctionality, (Chapter 3), or to include adhesive ligands (Chapters 4 and 5), and/or degradable moieties (Chapter 5). Consequently, different cellular behaviors were permitted in Chapters 4

(adhesion) and 5 (adhesion, spreading, cell-cell contacts, and potentially proliferation). Results from Chapter 4 detected differential responses to co- or tri-culture in the absence of cell spreading, which conclusively showed that cells were able to respond to soluble cues derived from other cells (Figure 4.6). In contrast, context-dependent effects were detected in Chapter 5 (Figures 5.6–5.8) while allowing MSCs to spread and form contacts due to their high density (Figure 5.3). Whether these effects differ substantially from those that would have occurred without spreading cannot be deconvolved from the data collected, though it is possible that allowing spreading did modulate behavior. Since these cells are often spread within the marrow microenvironment, which model system is more appropriate for study is an open question. To properly deconvolve soluble and other types of signals, the degradable sequence would need to be redesigned to be sensitive only to a non-endogenous enzyme.

The laminated hydrogel co- and tri-culture platforms presented in this dissertation therefore provide highly controlled and tunable systems to study a variety of signals within stem cell microenvironments. These platforms were shown to facilitate intercellular communication within constructs of tissue scale, produce unique culture type-specific responses in stem and terminally differentiated cells encapsulated within them, and respond in context-dependent ways to systemic perturbations that mimicked the pathological environment observed in diabetes. Therefore, this platform constitutes a valuable tool to investigate a diverse array of signaling cues in directing stem cell differentiation and interaction with terminally differentiated cells to mimic tissue microenvironments observed *in vivo*, and additional material and biological functionalities can be engineered into this unique biomaterial system to modulate this environment in probing behavior of complex biological systems and leveraging those behaviors to designing novel treatments for disease.

6.3 Future Directions

The findings presented in this dissertation provide significant insights into the interactions between MSCs, osteoblasts, and adipocytes, the effects of those interactions on potential cell phenotypes, and the formation of intercellular communication networks that respond in a context-dependent way to glucose perturbations. All of these findings were made possible through the design of a modular, laminated, tissue-scale tri-culture platform that permitted intercellular signaling events to occur over days to weeks in culture to effect changes in each cell type. Future work can utilize the insights gained from this dissertation as a foundation for studies that apply and further refine this model platform for elucidating modes of interaction, mechanisms underlying multicellular behavior, and methods of perturbing the complex networks that emerge from these interactions to better understand how bone and energy metabolism are linked in healthy and disease states and to design targeted treatments.

Future cell- and molecular-based therapies designed to treat diseases of bone remodeling must effectively integrate into a stable, homeostatically controlled marrow microenvironment that supports continued bone remodeling through internal and external regulation by both neural and hormonal cues. Both undifferentiated and differentiated MSCs, as well as the osteoblasts and adipocytes that they interact with, must: 1) appropriately regulate each others' functions through the secretion of peripherally acting hormones, and 2) simultaneously retain their functional susceptibility to external regulatory feedback through hormonal and neural mechanisms. MSCs must be able to supply sufficient and appropriate numbers of osteoblasts to deposit mineralized matrix and adipocytes needed to support this energy intensive process. How co- and tri-culture of MSCs with osteoblasts and/or adipocytes affects production of bone deposition- and resorption-promoting factors and energy storage- and release-promoting factors from each cell type and the susceptibility of each cell type to neural and hormonal regulation

with time is an open question that needs to be addressed to provide fully integrative and restorative therapeutic options.

To accomplish this, secretome analysis may be performed on conditioned media samples from several culture configurations to enable performance of differential network analysis [325, 403] and discovery of soluble mediators that affect MSC, osteoblast, and adipocyte phenotypes and responses in the context of healthy, pathological, and therapeutic microenvironments imparted by biomaterials and media supplements. This system would readily enable this analysis, which has previously only been possible with non-adherent cells [325] since it is often difficult to separate adherent cells from each other or extract them from 3D biomaterials. Additionally, our ability to cryosection hydrogels as if they were tissues (Appendix B) would readily enable us to stain for reporters of signaling gradients as well as expression of paracrine, neural, and hormonal receptors that would provide insight into susceptibility to both intra-systemic and external regulation and responsiveness. Furthermore, leveraging the ability of the platform to separate and isolate specific cell populations would offer the benefit of enabling further study of functional responses (*e.g.* mineralization, triglyceride storage) to stimulation with a plethora of neural and endocrine mediators implicated in regulating this subsystem *in vivo* [22, 88, 89, 147].

The hypothesis that lineage allocation and clonogenicity of MSCs are affected by pathological states such as anorexia, obesity, diabetes, and osteoporosis remains one based on correlation of biomarkers, imaging, and histological findings with clinical findings [7-11, 18, 78, 80, 84, 86]. Through limited gene expression analysis, we have demonstrated that MSC lineage priming and allocation may be affected in a context-dependent way [387]. Further studies combining our cell retrieval techniques with clonal selection and differentiation assays [35, 428, 452] would aid in revealing the extent to which MSC heterogeneity, lineage commitment, differentiation, and plasticity are modulated as a result of exposure to one or more terminally differentiated cell types in

the absence of exogenous differentiation cues [426]. Because this system may be used to model developmental, homeostatic, and disease microenvironments, we can in turn observe how each of these properties is potentially modulated in the face of local (intercellular) and systemic (exogenously administered) microenvironmental cues. Using the same analysis techniques outlined above, we can additionally perform mechanistic studies that can be further tested in animal models [453, 454].

The different culture systems examined in this dissertation confer the ability to study mechanisms of stability imparted by crosstalk interactions between each of the cellular components in a controlled way, another property that emerges from the modularity of this platform [323, 324]. For example, one can test the degree to which adipocytes are able to provide compensatory responses to increased levels of glucose before detrimental processes such as inflammatory adipokine and oxidative stress begin to impose a negative stress on the entire subsystem. Additionally, the degree to which MSCs are able to respond to perturbations and dysfunction in neighboring osteoblastic and adipocytic populations by regulating their lineage allocation before they themselves become overwhelmed by the detrimental effects of high glucose, *e.g.*, would provide important knowledge regarding how MSCs respond to their microenvironments. There is currently a paucity of techniques other than comparative gene expression analysis to discern the source of soluble signals in co- and tri-culture settings. Were such techniques to come to fruition, these data demonstrate that examining the roles of MSCs in participating in hormonal crosstalk between bone and energy metabolism may be worthwhile. Further phenotypic information from clonal selection and differentiation studies in MSCs, mineralization capabilities in osteoblasts, and triglyceride storage in adipocytes gained from utilizing our degradable hydrogel modules would lend insight to the degree of differentiation plasticity in each of these cell types [10, 18, 455-457].

To ensure that the model system developed herein is truly representative of *in vivo* cellular behavior and interactions, further refinement of the hydrogel biomaterials

used that compose each module of cells will need to be performed. As discussed in Section 6.2, the modularity of this system enables us to tune the microenvironment in a manner specific for each cell type – a function that derives both from the patternability of the system as well as the orthogonal chemistries that may be used to independently incorporate numerous factors [458-460]. The functionalities are not just limited to adhesiveness and cell-mediated degradation, but also tethering of ECM molecules that can provide substrates for migration and cellular remodeling [195, 265, 460-464], add mechanical stiffness [465] or that tune the spatial range of soluble signals by providing added charge density, as is observed *in vivo* with heparan sulfate proteoglycans [466], other glycosaminoglycans [467-470], and in previous work from our laboratory [445, 471]. Additionally, bioactive factors such as drugs, growth factors, cytokines, and hormones may be tethered to the polymer network, released in a controlled fashion from embedded particles that act as sources, sequestered by particles that act as sinks, or may interact with embedded ECM to potentiate or suppress bioactivity [164, 174, 235, 468, 470, 471]. The specific factors, their combinations, and dosages may be specifically incorporated and continuously refined based on knowledge gained from *in vivo* models to further refine and better mimic the true microenvironment for each cell type. In these ways, this model platform can be made to tailor a specific niche for each encapsulated cell type that represents its normal *in vivo* environment, a pathological one, or even an environment that is specifically designed to tune cell responsiveness to signals from other cell types or systemically administered to the culture [65, 176, 472].

Taking advantage of photolithography developed as part of this dissertation as well as other micropatterning techniques would enable patterning of many of the molecular features described above [65, 176]. Additionally, the patterning techniques adapted to patterning hydrogels in this dissertation are also scalable with aspect ratio, and could be used to generate larger constructs with incorporated channels to overcome transport limitations and modulate signal transport, as the bone marrow niche consists of

an intricate and complex reticular network of blood vessels [289, 290]. This would additionally allow incorporation of endothelial cells and microvasculature, which constitute another physiologically relevant component of the niche for MSCs and their progeny within the marrow. Conversely, the platform could be scaled down to generate microscale constructs containing single cell types that could be encapsulated within a larger bulk. This would bring different cell types in closer proximity while still retaining the ability to isolate and separate them after degrading the bulk gel, since these cells are not often physiologically separated a large rectangular blocks like the proof-of-principle constructs evaluated in this dissertation. Combination of microfluidic sheet or droplet fabrication techniques in combination with step-growth or ionic crosslinking mechanisms to avoid free-radical toxicity could enable higher throughput fabrication of multicellular micro-tissue models (*e.g.* Janus particles) [280, 291]. This would enable greater experimental throughput with the ability to generate more samples for analysis. Scaling the platform down would also allow for the creation of much more complex geometries, such as concentric spheres that would readily enable the study of cell-generated morphogen gradients due to transport constraints imposed by the geometry. Smaller constructs would necessitate a modified set of analysis techniques with the added benefits of providing richer, high content data in a high-throughput manner [62, 63, 312, 322, 327]. Examples might include digital PCR for gene expression [322] and suspension arrays for assay of proteins [473, 474], and such constructs would be more amenable to techniques such as image cytometry that provide high content imaging data from multiple samples at once [63, 327]. The merging of these novel techniques would more readily yield a compendium of data that would permit detailed inquiry into the behavior of complex systems of cells.

These adaptations or additions to this platform would aid in isolating and characterizing potential sources of noise in the data. The degradable modules designed in this dissertation allow recovery of cells, and when coupled with single cell analysis

techniques such as digital PCR or limiting dilution and clonal selection would allow us to quantify the population level noise. Alternatively, with broader knowledge of which transcription factors were highly variable within a group of samples and different across culture types, immunohistochemical staining could be performed on histological sections of whole constructs to examine if signaling gradient-induced spatial heterogeneities were formed. Further studies assaying a larger repertoire of genes and phenotypic outcomes would strengthen our multivariate models (PCA, PLS-DA, and PLS) by revealing a more detailed and stronger correlation between the phenotypic states acquired by each cell type as they are exposed to other cells in this model microenvironment and less noisy gene transcripts that more accurately distinguish differences between cell types and cultures [306, 309, 311-315, 325, 475]. Furthermore, this would lend insight into how each subsystem studied is primed towards detecting a response to one or more systemic perturbations, such as altered glucose or other soluble factors.

In addition to adding and modulating niche components within each module of the assembled hydrogel construct detailed in this dissertation, we successfully demonstrated that the entire system could be perturbed by and exhibit unique responses to exogenous stimuli added to the media. However, the hyperglycemia that is representative of poorly controlled diabetes mellitus is but one of many systemic perturbations that could be imposed to mimic a pathological state. Over time these cells, within and outside the marrow microenvironment, are exposed to advanced glycation products, reactive oxygen species, changes in extracellular redox potential, hyperlipidemia, inflammatory cytokines, hypoxia, and a whole host of other chemical and biomolecular insults representative of a wide range of metabolic, immune, oncologic, and other diseases [476]. This platform is amenable to exposure to any one or a combination of these perturbations to examine changes in cell fate and function that mediate or result from a number of disease states, which would in turn make this a novel *in vitro* model

system within which to evaluate treatments and predict therapeutic efficacy prior to testing in expensive and much more complex animal models.

By introducing these capabilities and demonstrating their feasibility, the advancements in 3D co-culture detailed in this dissertation may also be used to induce specific cellular states and prime them in defined, controllable ways for further *in vitro* or *in vivo* experimentation or eventually for delivery as an optimized therapeutic product to a patient. Further refinement of the degradable modules to include moieties that are not amenable to cell-mediated degradation would allow on-demand isolation of cells exhibiting a specific stable state. Alternatively, modules of cells can be disassembled using interfaces made from degradable hydrogels and then reassembled into new configurations [477]; or they may be primed in isolated modules under specific conditions prior to assembly. In this fashion, analogous pieces of a LEGO® set, modules could be primed to different stages and assembled in different configurations to yield new emergent complex system-level behaviors [434, 435, 478, 479]. Additionally, these modules could be combined with modules of cells acquired *ex vivo* from animal models of disease states. Together, these prospective advancements would offer temporal control of cell state transitions and process optimization for biological characterization and therapeutic development and evaluation [323, 324].

Future work can expand on the various principles presented in this dissertation to develop precisely controlled, highly tunable, complex, physiologically representative microenvironments with modules of multiple cell types and enable study of their emergent behavior in the presence and absence of systemic perturbations. Additionally, while this dissertation was focused on interactions of MSCs, osteoblasts, and adipocytes with respect to their reciprocally regulated differentiation programs and in the context of their interactions in regulating bone and energy metabolism, the technology developed within is readily extensible to creating models of other cell-cell interactions and subsystems, including but not limited to other solid organs, the immune system, neuronal

interfaces, and tumors. The research presented in this dissertation demonstrated the need and utility for more advanced co-culture systems of multiple cell types, and provided valuable insights into the contributions of MSCs, osteoblasts, and adipocytes to intrinsically regulating each others' fate, function, and coordinated responses in the face of systemic perturbations. Furthermore, these findings improve understanding of the role of intercellular communication networks and the cellular composition of the stem cell microenvironment that may be applied toward future regenerative medicine therapies.

APPENDIX A

DESIGN AND SCREENING OF CONJUGATED POLYMERS FOR HYDROGEL DEGRADABILITY, CYTOCOMPATIBILITY, AND CELL SPREADING

A1. Introduction

Poly(ethylene glycol) (PEG) is a non-adhesive synthetic material that is highly resistant to protein adsorption, making it an especially attractive material for allowing freely diffusing cell-derived signals to be transported between encapsulated cells [191-193]. PEG's mechanical and biochemical properties can be easily modified for a variety of tissue engineering applications [194-196]. As such, PEG-based materials provide a template upon which additional bioactive functionality can be specifically tailored into the hydrogel formulation. Functional peptides such as the adhesive peptides glycine-arginine-glycine-aspartic acid-serine (GRGDS) and tyrosine-isoleucine-glycine-serine-arginine (YIGSR) and growth factors including TGF-β, bFGF, and VEGF have been tethered into PEG networks to modulate cell response [197-201]. PEG hydrogels have been extensively investigated for bone, cartilage, vascular, and neural engineering [196, 201-207]. Collectively, these studies have demonstrated the ability of biofunctionalized PEG hydrogels to support viability, spreading, proliferation and ECM deposition by multiple cell types, directed differentiation of stem cells, and more complex functions such as endothelial tubulogenesis, vascular infiltration, and neurite extension.

Biodegradable hydrogels have been favored for biomedical applications since they degrade in clinically relevant time-scales under relatively mild conditions, thus eliminating the need for additional surgeries to recover implanted gels and allowing for progressive replacement of the biomaterial by native or regenerated tissue [165, 186, 208, 209]. They are advantageous for *in vitro* applications because they facilitate cell

spreading, proliferation, migration and deposition of extracellular matrix to better mimic native tissue environments [209, 210]. Currently, the fabrication and modeling of hydrolytically degradable hydrogels [209, 211, 212] are well developed and the synthesis and utilization of synthetic gels incorporating biological moieties for enzymatic degradation are under investigation [209, 213, 214]. While hydrogels made from natural polymers are often enzymatically degraded, synthetic hydrogels containing biological moieties often offer more controlled degradation rates due to their tunable physicochemical properties [164]. Hydrolytically labile components have been added into PEG networks to control degradation [203, 215], and enzymatically degradable peptides have also been incorporated within PEG hydrogels for cell-mediated degradation [216-218]. More recently, novel photodegradable groups have been investigated as a means to degrade PEG networks on demand in the presence of ultraviolet (UV) light [219-221]. These methods have been designed with the ability to elicit a cellular response (*e.g.* migration, spreading, and proliferation) *in vitro* or to eventually fully degrade via hydrolysis or cell-mediated enzymes in an *in vivo* setting to promote regeneration. None have been employed thus far for cell retrieval.

To address the need for enabling cell retrieval from bulk hydrogels in our tri-culture platform in Chapter 5, we screened the literature for peptide and enzyme combinations that allowed for specific enzyme-substrate reactions to occur and avoid the potential for exogenously added enzymes to degrade any ECM components or cell surface proteins or to diminish cell viability. We then synthesized PEG-peptide-PEG conjugates using standard NHS chemistry (see Section 5.2.1) and evaluated the time to achieve bulk degradation. Additionally, alginate gels derived from non-endogenous polysaccharides were evaluated [60, 178, 184, 280, 289, 480-482]. Hydrogel formulations that achieved bulk degradation in 2 hours or less were then used to encapsulate hMSCs, osteoblasts, and adipocytes to screen for any detrimental effects on cell viability and whether cells were able to locally degrade the hydrogel network.

A2. Materials and Methods

A2.1 Selection of Candidate Peptides

Candidate peptides were collected initially from the literature reviewing currently available fusion tags for recombinant protein purification [483-487], since these enzyme-peptide combinations are known for their highly specific cleavage while leaving recombinant proteins intact. Data detailing enzyme characteristics and known substrate cleavage events was collected from MEROPS (http://merops.sanger.ac.uk/), a database of peptidases compiled and curated from the literature. UniProt identification numbers of proteins containing the purported cleavage substrate used in the fusion tag were then collected and stored. This information was then imported into SitePrediction (http://www.dmbr.ugent.be/prx/bioit2-public/SitePrediction/index.php), an online tool for identifying potential cleavage sites within a protein. SitePrediction then cross-referenced these proteins with known substrate cleavage sites of extracellular enzymes (*e.g.* matrix metalloproteinases (MMPs) and cathepsins) to assess the likelihood that these cell-secreted enzymes could degrade the peptide of interest based on MEROPS data for each cell-secreted enzyme.

Substrates that demonstrated a low likelihood of cleavage by the cell-secreted enzymes were then assessed for their molecular properties to determine if they were amenable to PEG-conjugation with NHS chemistry [218, 364, 387, 395]. These criteria are summarized below in Table A1. Additionally, peptides were selected that would demonstrate neutral charge at pH 7 to prevent limitation of charged molecule transport through the bulk gel.

Table A1. Peptide Criteria for Successful Conjugation and Gelation Using Free-Radical Polymerization

Peptide isoelectric point less than 8.5
[Ensures that all amines are de-protonated to enable efficient conjugation with NHS]

No primary amines except at N-terminus and at terminal lysine
[Ensures site-specific conjugation of Acrl-PEG-SVA]

Percentage of hydrophobic residues < 30%, and hydrophilic and polar residues > 30%
[Ensures solubility of peptide during conjugation reaction]

Number of aromatic residues less than 2, and no tryptophan residues
[Ensures that free-radical crosslinking reaction is not quenched by peptide]

A2.2 Polymer Synthesis and Characterization

To allow presentation of adhesive ligands that promote viability of encapsulated cells, fibronectin-derived GRGDS (Bachem) and laminin-derived YIGSR (Anaspec) adhesion peptides were separately reacted as previously described [218, 364, 387, 395] in a 1:2 molar ratio with a 3,400 Da MW Acryl-PEG-succinimidyl valerate spacer (Acryl-PEG-SVA; Laysan Bio) in 50 mM $NaHCO_3$ buffer (pH 8.5; Fisher) at room temperature with gentle stirring for 3 h, dialyzed (1,000 Da MW cutoff) for 60 h, lyophilized for 72 h, and stored at -20 °C until further use.

Similarly, to create enzymatically-degradable PEG, the unmodified peptides selected from our screen (Table A2), were reacted with Acrl-PEG- SVA at a 1:2.2 peptide:Acrl-PEG-SVA molar ratio in 50 mM $NaHCO_3$ buffer at pH 8.5 for 3 h. The resulting solution containing Acrl-PEG-Peptide-PEG-Acrl (enzymatically-degradable PEG) was then purified as described above.

Alginate was conjugated with double bonds as previously described [481, 482]. Briefly, low molecular weight sodium alginate (2 g; Pronova UP VLVG, Novamatrix) was dissolved in a buffer solution (1% w/v, pH 6.5) of 50 mm 2-morpholinoethanesulfonic acid (MES, Sigma) containing 0.5 M NaCl. N-hydroxysuccinimide (NHS, 0.53 g) and 1-ethyl-3-(3-dimethylaminopropyl)-carbodiimide hydrochloride (EDC, 1.75 g) (molar ratio of NHS:EDC = 1:2) were added to the mixture

to activate the carboxylic acid groups of the alginate. After 5 min, 3-aminopropylmethacrylamide (APMAm) (molar ratio of NHS:EDC:APMAm = 1:2:1) was added to the product and the reaction was maintained at room temperature for 24 h. The mixture was precipitated with the addition of excess of acetone, dried under reduced pressure, and rehydrated to a 1% w/v solution in ultrapure deionized water (diH2O) for further purification. The methacrylated alginate was purified by dialysis against diH2O (MWCO 3500; Spectrum Laboratories) for 3 days, filtered (0.22 μm filter), and lyophilized.

Table A2. Summary of Peptides Chosen for Conjugation

Peptides:	**GGENLYFQSGGK**	**GGIEGRIVEGGK**	**GGGLGPAGGK***
UniProt ID	P04517	P00735	P02452
Enzyme	Tobacco Etch Virus Protease	Factor Xa	Collagenase, MMPs
No. of Amino Acids	12	12	10
Molecular Weight	1256.33	1171.31	769.85
Isoelectric Point (pI)	6.34	6.51	9.69
Charge at pH 7.4	0	0	+1
Charge at pH 8.5	-0.5	-0.5	+0.75
% Hydrophobic	25	25	30
% Hydrophilic	17	33	10
% Polar, Uncharged	25	0	0
Aromatic Residues	0	0	0

***** This peptide sequence was included on the basis of previous work that demonstrated successful conjugation, relatively slow cleavage over 7 days in culture (the length of the experimental period in Chapter 5), and amenability to cell retrieval in our lab [218, 364, 387, 395, 488]. This was not evaluated at part of the screen outlined in A2.1. Also note that once conjugated, the charge of this peptide at pH 7.4 is neutral since both the N-terminal and lysyl amines are conjugated.

A2.3 Assessment of Bulk Gel Degradability

Gel samples were formed as described in Section 5.2.3, with the following exceptions: TEV- and Factor Xa-sensitive gels consisted of 7.5 w/w% polymer; alginate gels consisted of 2.5% w/w polymer; collagenase-sensitive gels were crosslinked for 12

minutes, while all other gels were crosslinked for 10 minutes. After allowing the gels to reach equilibrium swelling overnight in PBS, gels were placed in 500 μL of buffer containing their respective enzymes and incubated at 37 °C on a shaker table until the hydrogel was no longer visible. Collagenase-sensitive gels were degraded in hMSC expansion medium (as described in Section 5.3.2) containing 1,100 U/mL collagenase type II (Gibco). TEV protease-sensitive gels were degraded in 20 mM Tris-HCl with 200 mM NaCl, 5 mM citrate, 3 mM reduced glutathione, 0.3 mM oxidized glutathione and containing 15 Units of TEV-protease (ProTEV; Promega). Factor Xa-sensitive gels were degraded in serum-free αMEM. Alginate gels were degraded in PBS containing 10 Units/mL of alginate lyase (Sigma).

A2.4 Cell Culture and Expansion

All cell culture reagents were obtained from Mediatech unless otherwise specified. Primary human MSCs (hMSCs) were obtained from the laboratory of Dr. Darwin Prockop (Texas A&M Health Sciences Center) and expanded according to recommended protocols in Minimal Essential Medium-Alpha (αMEM) with 16.5% fetal bovine serum (FBS; Hyclone), 1 g/L glucose, 2 mM L-glutamine, 1% amphotericin B, and 0.1% gentamicin and cultured at 37°C with 5% CO_2 in a humidified incubator [365]. Primary human osteoblasts (hObs; Lonza) were expanded to 4 population doublings in OGM Osteoblast Growth Medium (Lonza) containing 10% FBS, ascorbic acid (concentration proprietary), 50 μg/mL gentamicin, and 37 ng/mL amphotericin B. Primary human subcutaneous pre-adipocytes (Lonza) were expanded to 1-2 population doublings according to the manufacturer's protocol in PGM-2 Basal Medium (Lonza) containing 10% FBS, 2 mM L-glutamine, 50 μg/mL gentamicin, and 37 ng/mL amphotericin B. Cultures at 80% confluence were differentiated into adipocytes (hAds) for 9 days in Dulbecco's Modified Eagle Medium (DMEM) with 10% FBS, 4.5 g/L

glucose, 60 μM indomethacin, 0.5 mM 3-isobutyl-1-methylxanthine (IBMX), 0.5 μM dexamethasone, and 1 μM insulin.

A2.5 Crosslinking Device Design and Construct Fabrication

Layering devices were fabricated and employed for cell patterning as described in Figure 4.1. Briefly, 1 mm-thick spacers were cut from cured polydimethylsiloxane (PDMS, Sylgard 184, 10:1 ratio base to curing agent; Dow Corning) and bonded with O_2 plasma to a 25 × 75 mm glass slide (VWR). This slide was contact bonded with another coated with fluorinated ethylene propylene film (Bytac FEP; U.S. Plastic Corp) to form a cavity for polymer solution/gels as they were loaded and crosslinked. The use of FEP film prevented adhesion of crosslinked gels to glass that could result in ripping following device disassembly. Devices were sterilized by autoclave prior to assembly and use for encapsulation.

Hydrogel precursor solutions were formulated as described in Section 5.2.3 with 1 mM Acryl-PEG-GRGDS (for hMSCs and hObs) or Acryl-PEG-YIGSR (for hAds). Cell suspensions were prepared from near-confluent cultures using 0.05% Trypsin/0.53 mM EDTA and resuspended in their respective gel precursor solutions at a concentration of 10 million cells/mL. These solutions were loaded into layering devices and photocrosslinked (as described in Section A2.3) into 1 mm-thick, 4.5 mm-tall hydrogel constructs as described in Figure 5.1 (mono-culture). Whole constructs were extracted from the device and sectioned with a scalpel to yield up to twelve 1.5 mm-wide mono-culture constructs (Figure 5.1).

A2.6 Construct Culture Conditions

Constructs were placed in separate wells of 12-well tissue culture plates with 2 mL of tri-culture medium for 24 h [DMEM with 10% FBS, 1.0 g/L glucose (5.5 mM; normal fasting serum glucose), 2 mM L-glutamine, 50 μg/mL L-ascorbate-2-phosphate

(Sigma), 1 μM insulin (Sigma), 1% amphotericin B, and 0.1% gentamicin. All constructs were then cultured for a total of 7 days with media changea at Days 1 and 4.

A2.7 Cell Viability Assessment and Image Analysis

Hydrogel constructs (n = 3) were analyzed on Days 1 and 7 using a LIVE/DEAD assay (Invitrogen) as a qualitative indicator of cell viability. The kit uses calcein AM (ex/em: 495/515 nm), which is conjugated by active cytosolic esterases to remain within the cell membrane and label live cells, and ethidium homodimer-1 (EthD-1; ex/em: 495/635 nm), which can only enter permeable nuclear membranes and binds to DNA to indicate dead or dying cells. Constructs were rinsed in sterile PBS at 37 °C for 30 minutes and subsequently incubated in staining solution (1 μM calcein AM, 1 μM ethidium homodimer-1 in sterile PBS with Ca^{2+} and Mg^{2+}) for 45 minutes at 37 °C. After a second PBS rinse for 15 minutes to remove excess dye, stained constructs were imaged with confocal microscopy (10x objective, LSM 700; Zeiss). For each construct, 1 image stack was collected for each cell type present (dimensions: 693 × 693 μm; stack depth = 0 – 800 μm with 10-μm intervals). Each image stack was qualitatively assessed for cell viability and the degree of cell spreading visualized by cytoplasmic calcein staining.

A3. Results and Discussion

A3.1 Bulk Hydrogel Degradation

As expected from previous work, collagenase-sensitive gels completely degraded within 1 hour. Alginate gels completely degraded within 10 minutes, likely because the base polymer contains multiple cleavage sites and due to the high efficiency of the alginate lyase. Factor Xa gels completely degraded within 2 hours. TEV-protease sensitive gels degraded within 36-48 hours. Both of these enzyme sensitive gels were highly crosslinked and required lowering the initial polymer content from the typical 10% w/w described throughout this dissertation to 7.5 % w/w. This could be attributable to a

much more efficient conjugation of these gels since both starting peptides are fully de-protonated in the conjugation reaction conditions. Further optimization of both gels would likely entail lengthening the peptide chains with additional endogenous amino acids (within the limits of the above described criteria in Section A2.1) to enhance enzyme substrate binding and reaction or with additional glycine spacers to prevent steric hindrance of enzyme transport throughout the hydrogel bulk and accessibility of the target peptide to the enzyme. Additionally enzyme buffer formulations may need to be further optimized to ensure that enzyme activity is maximized and prolonged. On the basis of these results, all gels except the TEV-protease sensitive gels were further evaluated for cytocompatibility and cell spreading in subsequent experiments.

A3.2 Cell Viability and Cell Spreading

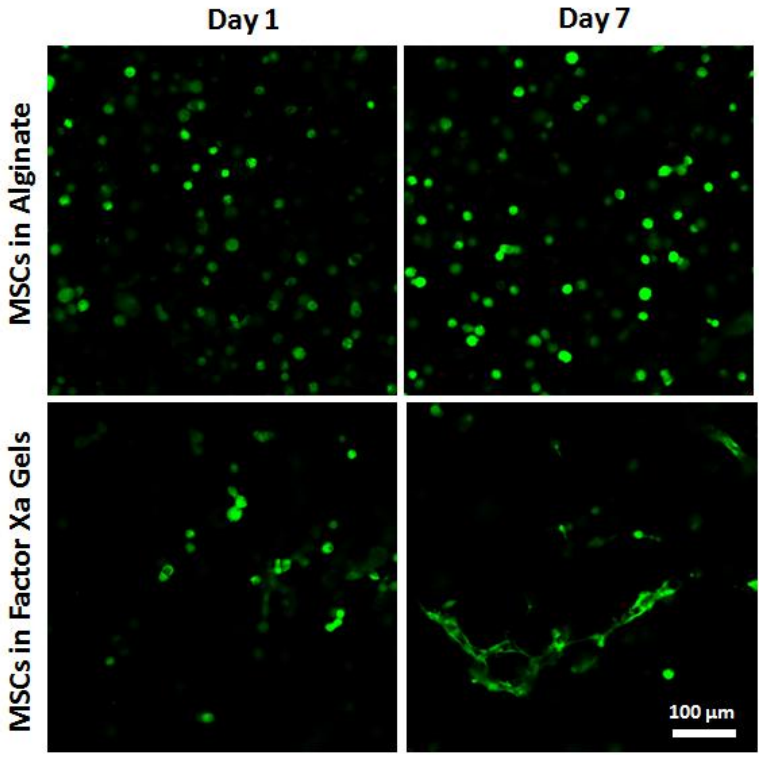

Figure A1. Alginate and Factor Xa-sensitive gels are cytocompatible but demonstrate differences in MSC cell spreading over 7 days in culture.

Alginate gels demonstrate gels demonstrate high cell viability after 1 week in culture and a complete absence of cell spreading. This is readily attributable to the inability of MSCs to produce alginate lyase that can cleave the polysaccharide matrix. Factor Xa gels demonstrated comparable cytocompatibility. However, MSCs exhibited significant cell spreading after 7 days in culture, suggesting that the peptide crosslinker used in these gels is sensitive to an enzyme that is endogenously produced by MSCs and which remains to be identified.

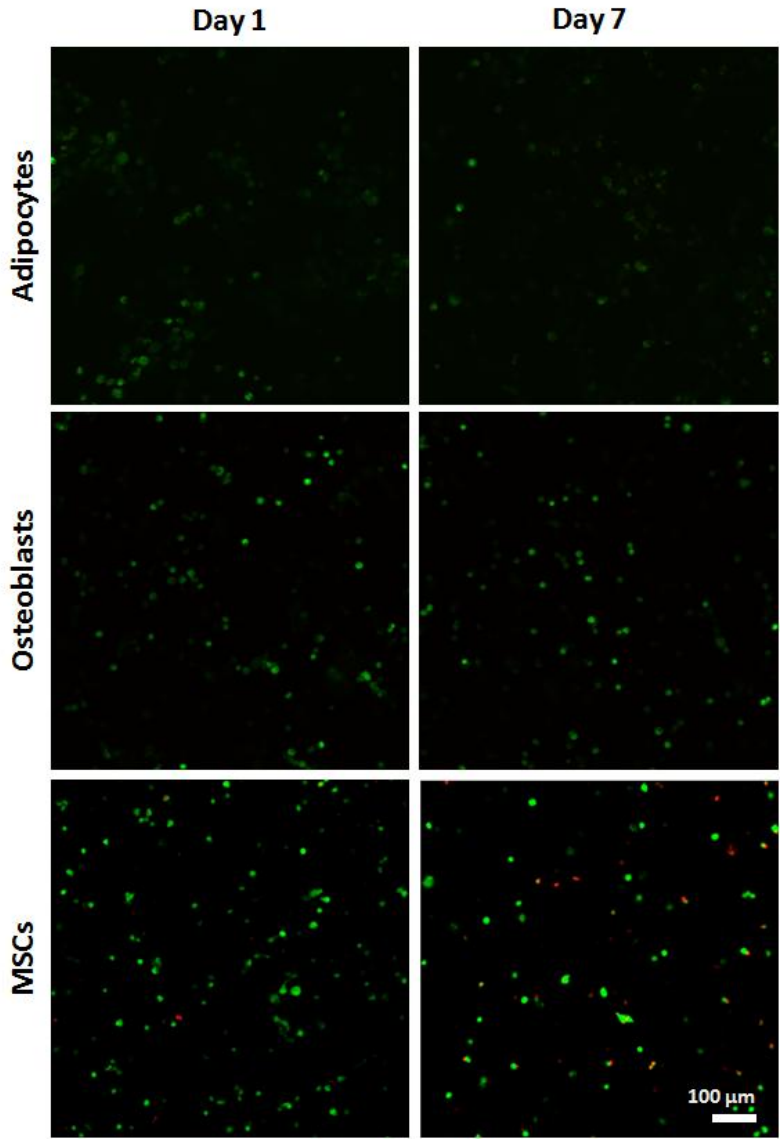

Figure A2. Mono-cultured adipocytes, osteoblasts, and MSCs demonstrate adequate cell viability when encapsulated in collagenase-sensitive gels and no observable cell spreading after 7 days in culture.

In contrast to Factor Xa-sensitive gels, all three cell types are unable to cleave the hydrogel network over the first 7 days in culture. This suggests that while each cell type may produces enzymes that have the ability to cleave the network their activity over the first 7 days in culture negligibly affects cell spreading within these constructs under mono-culture conditions.

A4. Conclusions

Each of the hydrogel materials evaluated in this series of experiments represents a tunable system that offers unique capabilities when used as modular materials within our tri-culture platform (see Chapter 6). Alginate and TEV protease-sensitive gels are not sensitive to degradation by endogenously produced enzymes, while Factor Xa- and collagenase-sensitive gels do exhibit this property with different time scales. Each of the proteolytically sensitive hydrogels has a neutral charge density due to the lack of charged amino acid residues in their respective peptide sequences, while alginate gels contain a carboxyl moiety on each disaccharide unit along the polymer chain. This charge may interact with positively charged growth factors [445, 466-471], thus limiting transport of these molecules between cell types over the length scales of our tri-culture platform. On the basis of these findings and conclusions, we selected the collagenase-sensitive hydrogels for further use in Chapter 5.

APPENDIX B

ADAPTED METHOD FOR CRYOPRESERVATION AND CRYOSECTIONING OF HYDROGELS

Purpose:

To effectively cryopreserve poly(ethylene glycol)-based hydrogels and improve sectioning and mounting using a Microm HM-560 cryomicrotome. This protocol is intended to prevent ice crystal formation in samples with high water content, enhance penetration of embedding medium in the gel sample, and increase the quality of sections by altering the embedding medium composition to match the mechanical properties and refreezing rate of the modified sample. Technique for cryosectioning, including knife and sample temperature, orientation of sample, use of the roll-up preventing glass plate and sample transfer to slides is also described. Please see the following references for further exploration [369, 489-493].

Materials:

Reagents:

- Sucrose (crystalline, VWR: EM-SX1075-3)
- Phosphate-buffered saline (use PBS with Ca^{2+} and Mg^{2+} to preserve cell morphology)
- Sakura Finetek O.C.T. (Optimal Cutting Temperature) Compound 4583
- Liquid nitrogen (alternatively isopentane in liquid nitrogen or dry ice in acetone may be used)

Materials:

- Conical tubes or bottles (solution storage)
- Spatula and/or forceps (for manipulating gels)
- Cryomolds of desired size
- 12-well plates

Equipment:

- Vacuum capable of -20 in Hg pressure

Methods:

Processing: Cryoprotection with sucrose and infiltration with OCT compound

1. Make up a solution of 50% (w/v) sucrose in PBS by dissolving 50 g per 100 mL. Using this concentrated solution, make up the following working solutions:
    a. 5% sucrose in PBS
    b. 20% sucrose in PBS
    c. 20% sucrose : OCT (4:1 ratio by volume)
    d. 20% sucrose : OCT (3:1 ratio by volume)
    e. 20% sucrose : OCT (2:1 ratio by volume)
    f. 20% sucrose : OCT (1:1 ratio by volume)
    g. 20% sucrose : OCT (1:2 ratio by volume)

    Note: For solutions of sucrose in PBS, long term storage is improved with sterile filtration of the sucrose stock solution. For solutions containing sucrose mixed with OCT, these must be prepared with *vigorous* shaking to ensure complete mixing of sucrose solution with OCT. This will result in the formation of air bubbles within the solution that may be removed by placing the solution under vacuum or allowing the solution to sit capped at room temperature overnight.

2. Sucrose serves as a cryoprotectant by allowing vitrification (freezing of water without the formation of ice crystals). OCT acts as a space filler that allows the sample and surrounding embedding medium to refreeze at similar rates after sectioning with a cryotome blade. Gradual infiltration of each of these substances is needed since highly concentrated solutions are substantially more viscous than the fluid in the interior of the hydrogel. The presence of a vacuum environment

aids in penetration of the embedding medium. To achieve optimal sucrose and OCT infiltration, the following steps are recommended:

a. Begin by placing the gel in 1-2 mL of 5% sucrose and vacuum infiltrate (20 in Hg) for 0.5 hour
b. Place the sample in 1-2 mL of 10% sucrose infiltrate for 30 min.
c. Place the sample in 1-2 mL of 15% sucrose infiltrate for 30 min.
d. Place the sample in 1-2 mL of 20% sucrose infiltrate for 30 min.
e. Move gel to 4:1 sucrose:OCT solution, vacuum infiltrate for 1 hour.
f. Move gel to 3:1 sucrose:OCT solution, vacuum infiltrate for 1 hour.
g. Move gel to 2:1 sucrose:OCT solution, vacuum infiltrate for 1 hour.
h. Move gel to 1:1 sucrose:OCT solution, vacuum infiltrate for 1 hour.
i. Move gel to 1:2 sucrose:OCT solution, vacuum infiltrate overnight (or minimum 4 hours).
j. Optional: Use 1:2 sucrose:OCT solution for 1 hour, followed by OCT overnight (or minimum 4 hours). This is likely more useful for gels of higher stiffness (e.g. somewhat mineralized or with higher crosslink density).

Note: The times denoted above are minimum times for each step. Longer infiltration times are not necessarily detrimental, and may be used depending on the time available to the sample preparer.

Embedding and Cryopreservation

3. Label the peel-away cryomold with the sample information, and make sure to label the orientation and approximate location of the sample to be embedded.
4. Place a layer of 1:2 sucrose:OCT solution in bottom of cryomold to the approximate height desired for the hydrogel sample.

5. Place the hydrogel sample on top of the unfrozen layer, making sure it is parallel with the eventual cutting surface. Cover in 1:2 sucrose:OCT solution to desired block thickness and re-orient sample if necessary.
6. Flash freeze the entire sample by submerging ¾ of the cryomold into the liquid nitrogen. Using liquid nitrogen in addition to sucrose minimizes the size of ice crystals that may form during the freezing process that could damage the sample. The sample will freeze from the outside toward the center. Care should be taken not to completely freeze the sample because it is likely to crack. Only submerge in liquid nitrogen until ¼ of the top layer of embedding medium remains unfrozen, and then place the sample in a -80°C freezer to complete freezing. Note: If a loud popping sound is heard, the sample is likely cracked and will need to be thawed and refrozen. Cracked blocks will not remain fixed on the sample holder in the cryostat, and there is a risk of cracking the specimen as well. Alternatively, isopentane in liquid nitrogen or ethanol/acetone on dry ice may be used to help avoid cracking.
7. Samples may be stored at -80°C until ready to be sectioned.

Cryosectioning

8. Set the ambient/sample temperature in the cryostat to -23 to -25°C. Insert a cryotomy blade into the blade holder, and set the knife temperature to -23 to -25°C. (The sample and knife temperatures should match). Allow 10-15 minutes for the blade to cool down to this temperature.
9. Extract embedded sample from the peel-away cryomold and fix to sample holder with a moderate amount of OCT compound. Allow the OCT to freeze, bonding the sample to the sample holder, and then mount and secure the sample holder in the specimen block. Orient the sample so that its cross section is parallel to the

blade, and so that it is diamond shaped. Having a diamond-shaped cross section minimizes roll-up during sectioning.

10. Trim the sample block at 50-µm intervals until the hydrogel sample becomes barely visible, then switch to 20 µm fine setting to acquire sections. It's best to leave a small portion of the section hanging on the sample block to keep the section in place while trying to mount onto slides. NOTE: When sectioning, be sure that there is no frost or residual OCT on the blade, roll-up preventing glass plate, or stainless steel plate by brushing away. Residual material in any of these locations will wrinkle, roll up, or damage the sample as it comes off the blade. Gently use a cotton swab to unroll the sample if necessary.
11. Mount each section onto a frosted slide (Superfrost + slides or similar are best), making sure to mount on the sides that are frosted and labeled with a plus sign. Hydrogel samples stick best to these slides during staining.

FINAL NOTE: With this procedure, serial sections ≥ 20 µm may be acquired with relative ease. Thinner sections still detach from the OCT and fold up. Suggested modifications to achieve thinner sections would include deriving a custom formulation for an embedding medium and sectioning with a much colder knife and larger temperature differential between the knife and sample (see Cocco et al and Ferri et al references for guidance).

APPENDIX C

GUIDE TO MULTIVARIATE MODELING

Purpose: To provide an introduction to the modeling techniques outlined in this dissertation. For further reference, please see [370, 371, 494].

Introduction: Why use multivariate modeling?

- Works well for modeling soft biological data; multiple types of data can be used (gene/protein expression, image quantification, mechanical/material properties, functional outcomes from *in vitro* or *in vivo* studies, etc).
- Since observations are considered in a multivariate way, noise in the data is much more easily accounted for by a within each model
- Works for both explorative (hypothesis-generating) and confirmative (hypothesis-testing) analysis
- Reveals dominant structures in one data table **X**
- Reveals the relevant structures within and between two data tables **X** and **Y**
- Predicts one set of variables **Y** from another set of variables **X**, even in new samples
- Handles cases with far more X-variables than samples, in contrast to many traditional methods
- Allows collinear redundancies in the input data and actively utilize these in the modeling
- Allows errors in both **X** and **Y**
- Allows different error levels in different input variables in **X** and in **Y**
- Handles a few missing data points in a simple and robust way
- Provides compact graphical overviews and statistical details, as chosen by the user
- Gives automatic warnings for outliers and gross mistakes
- Gives understandable statistical assessment of the validity of the model: predictive ability and model parameter stability

- Is compatible with contemporary statistics, but incorporates experiences from other fields
- Works for classification and discrimination issues
- Can address experiment-to-experiment variation and be used for quality assessment
- Is available in several commercial program packages with documentation and support

Principle Component Analysis (PCA):

- *Utility*
    - Extracts and displays systematic variation in data matrix **X** with *N* observations (rows) and *K* variables (columns)
    - Represent a multivariate data table as a low dimensional plane such that an *overview* is obtained. May reveal groups of observations, trends, and outliers.
    - Uncovers relationships between observations and variables, and between variables themselves
- *Under the hood*
    - Statistically, PCA finds *orthogonal* lines, planes, and hyperplanes in K-dimensional space that approximate the data in the least squares sense.
    - PCA is governed by maximum *variance* least squares projection of **X**; in other words information is depicted according to the sources of most variance in the data and can reveal the observations/factors that contribute to that maximum variance. Each principle component includes a non-overlapping amount of variance in the sample set, with the first component describing the most variance, the second describing the next most, and so on. A data set can be completely described if the number of components matches the number of variables (i.e. 100% fit), but those are not the "best" models (see below).
    - ***Overall model*: $\mathbf{X} = \mathbf{1} \cdot \bar{\mathbf{x}}' + \mathbf{T} \cdot \mathbf{P}' + \mathbf{E}$**
        - $\bar{\mathbf{x}}$ = vector mean of all X-variables
        - **T** = matrix of scores for **X** (values of observations on principle component axes)
        - **P** = matrix of loadings for **X** (weights assigned to variables)
        - **E** = matrix of residuals for **X**

- Performs cross-validation and jack-knifing to assess model quality and optimize number of principle components

- *Entering data into the model (pre-processing)*
  - Trim (remove) or Winsorize (re-scale) non-sensical data or egregious outliers (Note: if possible, leave as many perceived outlying data points in as possible and allow the model to prune these out later. An outlier from univariate analyses such as ANOVA is not necessarily an outlier in multivariate analysis where you are analyzing all variables for a given observation.)
  - Perform necessary transformations of data to achieve normality (e.g. Box-Cox, log, etc.)
  - Data need to be scaled to unit variance (i.e. $\sigma^2 = 1$) so that all variables are equally important in the resulting model
  - Data need to be mean centered (i.e. $\bar{x} = 1$) so that all variables are centered on the origin in the resulting model space and do not skew the model

- *Outputs and diagnostics* (^{P} denotes that this parameter can be used to "prune" the model)
  - **R^2X**: explained variation of the model determined for **X**; indicates overall fit, ideal is > 0.7
  - **Q^2**: predictive capacity of the model determined for **X**; indicates ability of model to account for future observations, ideal is > 0.5
  - **Cross-validation**: model optimization to achieve a number of principle components to maximize R^2X and Q^2. Groups of observations are eliminated and the model is re-fit to examine the sensitivity of the scores and loadings.
  - **Jack-knifing**: results from cross-validation are used to evaluate variable sensitivity in the model and calculate the standard errors of the regression coefficients (weights), which can then be converted to 95% confidence intervals (via *t*-distribution) to determine which X-variables have statistically significant influence ($p < 0.05$) in one or more principle components.
  - **Score plot** (t_1 vs. t_2, etc.): t_a represents each principle component *a* found in the model; observations are projected onto these principle components.
  - **Loading plot** (p_1 vs. p_2, etc.): p_a represent the weight assigned to each variable contained in **X** for each principle component *a*; variables are projected onto these plots
  - **^{P} Hotelling's T^2**: multivariate generalization of Student's *t*-test; provides check for *observations* adhering to multivariate normality) => indicates

STRONG outliers, used in conjunction with score plot (default = 95% confidence)

- **^{P} Distance to model in X-space (DModX):** Examination of residuals (matrix **E**); MODERATE outlying observations have **DModX** values > D_{crit} (critical distance, determine by number of observations)
- **^{P} R^2VX and Q^2VX**: explained variation of a X-variable; allows ability to look at extent to which each variable is accounted for by the model

- *Interpretation:*
  - Does the model fit the data well? If not, then no interpretation of the score and loading plots can be performed. *No exceptions!*
  - Do the observation scores cluster according to known independent variables?
  - How do the loadings correlate with the observations? The loading plot can essentially be overlayed with the score plot to assess this.
  - Which observations contribute to the maximum variance (i.e. high score on one or more components, or furthest from the center of the model)?
  - Which variables contribute to the maximum variance (i.e. high loading on one or more components, or furthest from the center of the model)?
  - Are there outlying observations in the data (Hotelling's T2 and/or DModX)?
  - Which observations and variables are statistically significant in one or more components (use results from cross-validation and jack-knifing to generate confidence intervals)?

Partial Least Squares Projections to Latent Structures (PLS):

- *Utility*
  - Used to connect information in two blocks of variables, **X** and **Y**, to each other; effectively multivariate linear regression to elucidate how **X** determines **Y**
  - Precision improves with increasing number of *relevant* X-variables
- *Under the hood*
  - Same pre-processing methods as with PCA

- Maximum *covariance* model of relationship between **X** and **Y**. This constitutes the main difference between PLS and PCA. The observations are modeled based on how **Y** maximally *covaries* with **X**, rather than how they are distributed by the maximum variance in **X**. If **Y** is the source of the maximum variance in **X** (i.e. describes the variance in **X** 100%), then the PLS and PCA scores and loadings will be exactly the same.
- ***Overall Model*:** $\mathbf{X} = \mathbf{1} \cdot \bar{\mathbf{x}}' + \mathbf{T} \cdot \mathbf{P}' + \mathbf{E}$; $\mathbf{Y} = \mathbf{1} \cdot \bar{\mathbf{y}}' + \mathbf{U} \cdot \mathbf{C}' + \mathbf{F} = \mathbf{1} \cdot \bar{\mathbf{y}}' + \mathbf{X} \cdot \mathbf{W}^{*}\mathbf{C} + \mathbf{F}$
  - $\bar{\mathbf{y}}$ = vector mean of all observations
  - **U** = matrix of scores for **Y** (values of observations on principle component axes)
  - **C** = matrix of weights for **Y**
  - **F** = matrix of residuals for **Y**
  - $\mathbf{W}^{*}\mathbf{C}$ = PLS weights
- Performs cross-validation and jack-knifing to assess model quality and optimize number of principle components

- *Entering data into the model (pre-processing)*
  - Same as for PCA; also perform for individual Y-variables

- *Outputs and diagnostics*
  - $\mathbf{R^2X}$: explained variation of the model determined for **X**; indicates overall fit, ideal is > 0.7
  - $\mathbf{R^2Y}$: explained variation of the model determined for **Y**; indicates overall fit, ideal is > 0.7
  - $\mathbf{Q^2}$: predictive capacity of the model determined for **Y**; indicates ability of model to account for future observations, ideal is > 0.5
  - **Cross-validation**: model optimization to achieve a number of principle components to maximize R^2X, R^2Y, and Q^2. Groups of observations are eliminated and the model is re-fit to examine the sensitivity of the scores and loadings.
  - **Jack-knifing**: results from cross-validation are used to evaluate variable sensitivity in the model and calculate the standard errors of the regression coefficients (weights), which can then be converted to 95% confidence

intervals (via *t*-distribution) to determine which X-variables have statistically significant influence ($p < 0.05$) on Y-variables in the model.

- **Score plot for X** (t_1 vs. t_2, etc.): t_a represents each principle component *a* found in the model for the X-variables; observations are projected onto these principle components.

- **Score plot for Y** (u_1 vs. u_2, etc.): u_a represents each principle component *a* found in the model for the Y-variables; observations are projected onto these principle components.

- **Regression plot of scores:** (u_1 vs. t_1, etc.): shows the regression of the Y-scores u with respect to the X-scores t; akin to linear regression to see how the principle components in Y are explained by the principle components in X

- **Weight plot:** combined plot of weights for X- and Y-variables (similar to loading plot for PCA); gives information on what **X** yields **Y** or how to "set" **X** to get a desired **Y** (i.e. correlation structure)

- **PLS regression coefficients (CoeffCS)**: column plot for each Y-variable vs. X-variables of w^*c; *one vector* of concise model information per response Y (correlation structure is lost); useful when a model contains multiple Y-variables

- **[P] Hotelling's T^2**: multivariate generalization of Student's *t*-test; provides check for *observations* adhering to multivariate normality) => indicates STRONG outliers, used in conjunction with score plot (default = 95% confidence)

- **[P] Distance to model in X-space (DModX) and in Y-space (DModY):** Examination of residuals (matrices **E** and **F**); MODERATE outlying observations have **DModX** values > D_{crit} (critical distance, determine by number of observations); no D_{crit} for DModY

- **[P] Variable influence on projection (VIP):** weighted sum of squares of PLS weights, w^*, that summarizes importance of each X-variable in the model

- **R^2VY and Q^2VY**: explained variation of a Y-variable; allows ability to look at extent to which each Y-variable is accounted for by the model

- *Interpretation:*

  - Does the model fit the data well? If not, then no interpretation of the score and loading plots can be performed. *No exceptions!*

  - Ask same questions as PCA, and also…

- How well do the Y-principle components regress onto the X-principle components? (Use u vs. t plots. This will help you determine what the principle components actually separate, or what their 'meaning' might be.)

- Which X-variables most significantly determine the Y-variables (use regression coefficients or w*c weights with results from cross-validation and jack-knifing)?

Classification and Discrimination of Clusters of Observations:

- **Partial Least Squares Discriminant Analysis (PLS-DA):**
  - *Utility*
    - Necessary vs. PCA because not always the case that maximum variation directions coincide with the maximum separation directions among the classes
    - May be that other directions are more pertinent for discriminating among classes of observations
    - Works best with 2-5 classes of observations. May have to split into separate sub-models if more classes exist in the data.
    - When some classes are not "tight" (e.g. because of lack of homogeneity and similarity), discriminant analysis fails and must use SIMCA
  - *Under the hood*
    - Accomplishes a rotation of the projection to give latent variables that focus on class separation ("discrimination")
    - Encodes a class identity using a data matrix of "dummy" Y-variables that describes the class membership of each observation of a training set with a discrete numerical value (0 or 1)
    - Otherwise, same as PLS
  - *Diagnostics*: same as PLS
  - *Interpretation*: same as PLS
- **Soft Independent Modeling of Class Analogy (SIMCA, or PCA-Class):**
- *Utility*

- Approximates data observed on a class of similar observations, often with fewer components
- Overview of training data set with PCA gives indications of class separation, trends, and outliers
- Data should be selected such that each class of observations contains "homogeneous" data material

- *Under the hood*
  - Effectively running a local PCA of each class; useful for identifying new observations

- *Diagnostics:* very similar to PCA, and may also include:
  - **DModX** using training and prediction sets (generates classification and misclassification lists)

Cooman's plot: DModX's for two classes are plotted against each other in a scatter plot that includes critical distance for both; used in conjunction with prediction set to identify new classes

REFERENCES

[1] Lin, J.T., and Lane, J.M. Osteoporosis. *Clinical Orthopaedics and Related Research*. (2004); **425**(425):126-34.

[2] Rodriguez, J.P., Astudillo, P., Rios, S., and Pino, A.M. Involvement of Adipogenic Potential of Human Bone Marrow Mesenchymal Stem Cells (Mscs) in Osteoporosis. *Current Stem Cell Research & Therapy*. (2008); **3**(3):208-18.

[3] Rosen, C.J., and Bouxsein, M.L. Mechanisms of Disease: Is Osteoporosis the Obesity of Bone? *Nature Clinical Practice Rheumatology*. (2006); **2**(1):35-43.

[4] Bone Health and Osteoporosis: A Report of the Surgeon General. In: Services, U.D.o.H.a.H., editor. Rockville, MD: US Department of Health and Human Services; 2004.

[5] Burge, R., Dawson-Hughes, B., Solomon, D.H., Wong, J.B., King, A., and Tosteson, A. Incidence and Economic Burden of Osteoporosis-Related Fractures in the United States, 2005-2025. *J Bone Miner Res*. (2007); **22**(3):465-75.

[6] Harvey, N., Dennison, E., and Cooper, C. Osteoporosis: Impact on Health and Economics. *Nat Rev Rheumatol*. (2010); **6**(2):99-105.

[7] Rosen, C.J., and Bouxsein, M.L. Mechanisms of Disease: Is Osteoporosis the Obesity of Bone? *Nat Clin Pract Rheumatol*. (2006); **2**(1):35-43.

[8] de Paula, F.J.A., Horowitz, M.C., and Rosen, C.J. Novel Insights into the Relationship between Diabetes and Osteoporosis. *Diabetes/metabolism research and reviews*. (2010); **26**(8):622-30.

[9] Kawai, M., Devlin, M.J., and Rosen, C.J. Fat Targets for Skeletal Health. *Nat Rev Rheumatol*. (2009); **5**(7):365-72.

[10] Rosen, C.J., Ackert-Bicknell, C., Rodriguez, J.P., and Pino, A.M. Marrow Fat and the Bone Microenvironment: Developmental, Functional, and Pathological Implications. *Critical Reviews in Eukaryotic Gene Expression*. (2009); **19**(2):109-24.

[11] Rosen, C.J., and Klibanski, A. Bone, Fat, and Body Composition: Evolving Concepts in the Pathogenesis of Osteoporosis. *The American journal of medicine*. (2009); **122**(5):409-14.

[12] Simon, J., Schmidt, U., and Pilling, S. The Health Service Use and Cost of Eating Disorders. *Psychol Med*. (2005); **35**(11):1543-51.

[13] Levine, M.P., and Smolak, L. *The Prevention of Eating Problems and Eating Disorders: Theory, Research, and Practice*. Mahwah, NJ: Lawrence Earlbaum Associates, Inc.; 2006.

[14] Ryan, J.G. Cost and Policy Implications from the Increasing Prevalence of Obesity and Diabetes Mellitus. *Gend Med*. (2009); **6 Suppl 1**:86-108.

[15] Ryder, S.W. Innovation and Improvement in the Treatment of Obesity and Diabetes. *Clin Pharmacol Ther*. (2007); **81**(5):615-9.

[16] Hossain, P., Kawar, B., and El Nahas, M. Obesity and Diabetes in the Developing World--a Growing Challenge. *N Engl J Med*. (2007); **356**(3):213-5.

[17] Yach, D., Stuckler, D., and Brownell, K.D. Epidemiologic and Economic Consequences of the Global Epidemics of Obesity and Diabetes. *Nat Med*. (2006); **12**(1):62-6.

[18] Muruganandan, S., Roman, A.A., and Sinal, C.J. Adipocyte Differentiation of Bone Marrow-Derived Mesenchymal Stem Cells: Cross Talk with the Osteoblastogenic Program. *Cellular and Molecular Life Sciences*. (2009); **66**(2):236-53.

[19] Confavreux, C.B., Levine, R.L., and Karsenty, G. A Paradigm of Integrative Physiology, the Crosstalk between Bone and Energy Metabolisms. *Mol Cell Endocrinol*. (2009); **310**(1-2):21-9.

[20] Wei, J., and Ducy, P. Co-Dependence of Bone and Energy Metabolisms. *Arch Biochem Biophys*. (2010); **503**(1):35-40.

[21] Ferron, M., Hinoi, E., Karsenty, G., and Ducy, P. Osteocalcin Differentially Regulates Beta Cell and Adipocyte Gene Expression and Affects the Development of Metabolic Diseases in Wild-Type Mice. *Proc Natl Acad Sci U S A*. (2008); **105**(13):5266-70.

[22] Ferron, M., Wei, J., Yoshizawa, T., Andrea, DePinho, R.a., Teti, A., Ducy, P., and Karsenty, G. Insulin Signaling in Osteoblasts Integrates Bone Remodeling and Energy Metabolism. *Cell*. (2010); **142**(2):296-308.

[23] Hinoi, E., Gao, N., Jung, D.Y., Yadav, V., Yoshizawa, T., Myers, M.G., Chua, S.C., Kim, J.K., Kaestner, K.H., and Karsenty, G. The Sympathetic Tone Mediates Leptin's Inhibition of Insulin Secretion by Modulating Osteocalcin Bioactivity. *The Journal of Cell Biology*. (2008); **183**(7):1235-42.

[24] Karsenty, G., and Oury, F. The Central Regulation of Bone Mass, the First Link between Bone Remodeling and Energy Metabolism. *The Journal of Clinical Endocrinology and Metabolism*. (2010); **95**(11):4795-801.

[25] Lee, N.K., Sowa, H., Hinoi, E., Ferron, M., Ahn, J.D., Confavreux, C., Dacquin, R., Mee, P.J., McKee, M.D., Jung, D.Y., Zhang, Z., Kim, J.K., Mauvais-Jarvis, F.,

Ducy, P., and Karsenty, G. Endocrine Regulation of Energy Metabolism by the Skeleton. *Cell*. (2007); **130**(3):456-69.

[26] Shi, Y., Yadav, V.K., Suda, N., Liu, X.S., Guo, X.E., Myers, M.G., Jr., and Karsenty, G. Dissociation of the Neuronal Regulation of Bone Mass and Energy Metabolism by Leptin in Vivo. *Proc Natl Acad Sci U S A*. (2008); **105**(51):20529-33.

[27] Takeda, S., Elefteriou, F., Levasseur, R., Liu, X., Zhao, L., Parker, K.L., Armstrong, D., Ducy, P., and Karsenty, G. Leptin Regulates Bone Formation Via the Sympathetic Nervous System. *Cell*. (2002); **111**(3):305-17.

[28] Tavassoli, M., and Crosby, W.H. Transplantation of Marrow to Extramedullary Sites. *Science*. (1968); **161**(3836):54-56.

[29] Friedenstein, A.J. Stromal Mechanisms of Bone Marrow: Cloning in Vitro and Retransplantation in Vivo. *Haematol Blood Transfus*. (1980); **25**:19-29.

[30] Friedenstein, A.J., Chailakhyan, R.K., Latsinik, N.V., Panasyuk, A.F., and Keiliss-Borok, I.V. Stromal Cells Responsible for Transferring the Microenvironment of the Hemopoietic Tissues. Cloning in Vitro and Retransplantation in Vivo. *Transplantation*. (1974); **17**(4):331-40.

[31] Friedenstein, A.J. Osteogenic Stem Cells in Bone Marrow. In: Heersche, J.N.M.,Kanis, J.A., editors. *Bone and Mineral Research*. Amsterdam: Elsevier; 1990. p. 243-72.

[32] Owen, M., and Friedenstein, A.J. Stromal Stem Cells: Marrow-Derived Osteogenic Precursors. *Ciba Found Symp*. (1988); **136**:42-60.

[33] Bianco, P., Riminucci, M., Gronthos, S., and Robey, P.G. Bone Marrow Stromal Stem Cells: Nature, Biology, and Potential Applications. *Stem Cells*. (2001); **19**(3):180-92.

[34] Mendez-Ferrer, S., Michurina, T.V., Ferraro, F., Mazloom, A.R., Macarthur, B.D., Lira, S.A., Scadden, D.T., Ma'ayan, A., Enikolopov, G.N., and Frenette, P.S. Mesenchymal and Haematopoietic Stem Cells Form a Unique Bone Marrow Niche. *Nature*. (2010); **466**(7308):829-34.

[35] Pittenger, M.F. Multilineage Potential of Adult Human Mesenchymal Stem Cells. *Science*. (1999); **284**(5411):143-47.

[36] Baksh, D., Song, L., and Tuan, R.S. Adult Mesenchymal Stem Cells: Characterization, Differentiation, and Application in Cell and Gene Therapy. *Journal of Cellular and Molecular Medicine*. (2004); **8**(3):301-16.

[37] Kolf, C.M., Cho, E., and Tuan, R.S. Mesenchymal Stromal Cells. Biology of Adult Mesenchymal Stem Cells: Regulation of Niche, Self-Renewal and Differentiation. *Arthritis Research & Therapy*. (2007); **9**(1):204-04.

[38] Kuhn, N.Z., and Tuan, R.S. Regulation of Stemness and Stem Cell Niche of Mesenchymal Stem Cells: Implications in Tumorigenesis and Metastasis. *Journal of Cellular Physiology*. (2010); **222**(2):268-77.

[39] Song, L., Webb, N.E., Song, Y., and Tuan, R.S. Identification and Functional Analysis of Candidate Genes Regulating Mesenchymal Stem Cell Self-Renewal and Multipotency. *Stem Cells*. (2006); **24**(7):1707-18.

[40] Horwitz, E.M., Dominici, M., Mueller, I., Slaper-Cortenbach, I., Marini, F.C., Deans, R.J., Krause, D.S., and Keating, A. Clarification of the Nomenclature for Msc: The International Society for Cellular Therapy Position Statement. *Cytotherapy*. (2005); **7**(5):393-5.

[41] Bianco, P., and Robey, P.G. Diseases of Bone and the Stromal Cell Lineage. *Journal of Bone and Mineral Research*. (1999); **14**(3):336-41.

[42] Bianco, P., Robey, P.G., Saggio, I., and Riminucci, M. "Mesenchymal" Stem Cells in Human Bone Marrow (Skeletal Stem Cells): A Critical Discussion of Their Nature, Identity, and Significance in Incurable Skeletal Disease. *Human Gene Therapy*. (2010); **21**(9):1057-66.

[43] Bianco, P., Robey, P.G., and Simmons, P.J. Mesenchymal Stem Cells: Revisiting History, Concepts, and Assays. *Cell Stem Cell*. (2008); **2**(4):313-9.

[44] Sacchetti, B., Funari, A., Michienzi, S., Silvia, Piersanti, S., Saggio, I., Tagliafico, E., Ferrari, S., Robey, P.G., Riminucci, M., and Bianco, P. Self-Renewing Osteoprogenitors in Bone Marrow Sinusoids Can Organize a Hematopoietic Microenvironment. *Cell*. (2007); **131**(2):324-36.

[45] Crisan, M., Yap, S., Casteilla, L., Chen, C.W., Corselli, M., Park, T.S., Andriolo, G., Sun, B., Zheng, B., Zhang, L., Norotte, C., Teng, P.N., Traas, J., Schugar, R., Deasy, B.M., Badylak, S., Buhring, H.J., Giacobino, J.P., Lazzari, L., Huard, J., and Peault, B. A Perivascular Origin for Mesenchymal Stem Cells in Multiple Human Organs. *Cell Stem Cell*. (2008); **3**(3):301-13.

[46] Chan, C.K., Chen, C.C., Luppen, C.A., Kim, J.B., DeBoer, A.T., Wei, K., Helms, J.A., Kuo, C.J., Kraft, D.L., and Weissman, I.L. Endochondral Ossification Is Required for Haematopoietic Stem-Cell Niche Formation. *Nature*. (2009); **457**(7228):490-4.

[47] Méndez-Ferrer, S., Michurina, T.V., Ferraro, F., Mazloom, A.R., MacArthur, B.D., Lira, S.A., Scadden, D.T., Ma'ayan, A., Enikolopov, G.N., and Frenette, P.S. Mesenchymal and Haematopoietic Stem Cells Form a Unique Bone Marrow Niche. *Nature*. (2010); **466**(7308):829-34.

[48] Chen, F.H., Rousche, K.T., and Tuan, R.S. Technology Insight: Adult Stem Cells in Cartilage Regeneration and Tissue Engineering. *Nat Clinical Pract Rheumatol*. (2006); **2**(7):373-82.

[49] Kolf, C.M., Cho, E., and Tuan, R.S. Mesenchymal Stromal Cells. Biology of Adult Mesenchymal Stem Cells: Regulation of Niche, Self-Renewal and Differentiation. *Arthritis Research & Therapy*. (2007); **9**(1):204-13.

[50] Colter, D.C., Class, R., DiGirolamo, C.M., and Prockop, D.J. Rapid Expansion of Recycling Stem Cells in Cultures of Plastic-Adherent Cells from Human Bone Marrow. *Proceedings of the National Academy of Sciences of the United States of America*. (2000); **97**(7):3213-8.

[51] Tsutsumi, S., Shimazu, A., Miyazaki, K., Pan, H., Koike, C., Yoshida, E., Takagishi, K., and Kato, Y. Retention of Multilineage Differentiation Potential of Mesenchymal Cells During Proliferation in Response to Fgf. *Biochemical and Biophysical Research Communications*. (2001); **288**(2):413-19.

[52] Bruder, S.P., Jaiswal, N., and Haynesworth, S.E. Growth Kinetics, Self-Renewal, and the Osteogenic Potential of Purified Human Mesenchymal Stem Cells During Extensive Subcultivation and Following Cryopreservation. *Journal of Cellular Biochemistry*. (1997); **64**(2):278-94.

[53] Colter, D.C., Sekiya, I., and Prockop, D.J. Identification of a Subpopulation of Rapidly Self-Renewing and Multipotential Adult Stem Cells in Colonies of Human Marrow Stromal Cells. *Proceedings of the National Academy of Sciences of the United States of America*. (2001); **98**(14):7841-5.

[54] Larson, B.L., Ylöstalo, J., and Prockop, D.J. Human Multipotent Stromal Cells Undergo Sharp Transition from Division to Development in Culture. *Stem Cells*. (2008); **26**(1):193-201.

[55] Sekiya, I., Larson, B.L., Smith, J.R., Pochampally, R., Cui, J.-G., and Prockop, D.J. Expansion of Human Adult Stem Cells from Bone Marrow Stroma: Conditions That Maximize the Yields of Early Progenitors and Evaluate Their Quality. *Stem Cells*. (2002); **20**(6):530-41.

[56] Ylöstalo, J., Bazhanov, N., and Prockop, D.J. Reversible Commitment to Differentiation by Human Multipotent Stromal Cells in Single-Cell-Derived Colonies. *Experimental Hematology*. (2008); **36**(10):1390-402.

[57] Baksh, D., Song, L., and Tuan, R.S. Adult Mesenchymal Stem Cells: Characterization, Differentiation, and Application in Cell and Gene Therapy. *Journal of Cellular and Molecular Medicine*. (2004); **8**(3):301-16.

[58] Tuan, R.S., Boland, G., and Tuli, R. Adult Mesenchymal Stem Cells and Cell-Based Tissue Engineering. *Arthritis Research & Therapy*. (2003); **5**(1):32-45.

[59] Bianco, P. Back to the Future: Moving Beyond "Mesenchymal Stem Cells". *J Cell Biochem*. (2011); **112**(7):1713-21.

[60] Huebsch, N., Arany, P.R., Mao, A.S., Shvartsman, D., Ali, O.a., Bencherif, S.a., Rivera-Feliciano, J., and Mooney, D.J. Harnessing Traction-Mediated Manipulation of the Cell/Matrix Interface to Control Stem-Cell Fate. *Nat Materials*. (2010); **9**(5):1-9.

[61] Baraniak, P.R., and McDevitt, T.C. Stem Cell Paracrine Actions and Tissue Regeneration. *Regen Med*. (2010); **5**(1):121-43.

[62] Flaim, C.J., Chien, S., and Bhatia, S.N. An Extracellular Matrix Microarray for Probing Cellular Differentiation. *Nature Methods*. (2005); **2**(2):119-25.

[63] Treiser, M.D., Yang, E.H., Gordonov, S., Cohen, D.M., Androulakis, I.P., Kohn, J., Chen, C.S., and Moghe, P.V. Cytoskeleton-Based Forecasting of Stem Cell Lineage Fates. *Proc Natl Acad Sci USA*. (2010); **107**(2):610-5.

[64] Khetan, S., and Burdick, J.A. Patterning Network Structure to Spatially Control Cellular Remodeling and Stem Cell Fate within 3-Dimensional Hydrogels. *Biomaterials*. (2010); **31**(32):8228-34.

[65] Lutolf, M.P., Gilbert, P.M., and Blau, H.M. Designing Materials to Direct Stem-Cell Fate. *Nature*. (2009); **462**(7272):433-41.

[66] Lee, I.-C., Wang, J.-H., Lee, Y.-T., and Young, T.-H. The Differentiation of Mesenchymal Stem Cells by Mechanical Stress or/and Co-Culture System. *Biochemical and Biophysical Research Communications*. (2007); **352**(1):147-52.

[67] McBeath, R., Pirone, D.M., Nelson, C.M., Bhadriraju, K., and Chen, C.S. Cell Shape, Cytoskeletal Tension, and Rhoa Regulate Stem Cell Lineage Commitment. *Dev Cell*. (2004); **6**(4):483-95.

[68] Altman, G.H., Horan, R.L., Martin, I., Farhadi, J., Stark, P.R.H., Volloch, V., Richmond, J.C., Vunjak-Novakovic, G., and Kaplan, D.L. Cell Differentiation by Mechanical Stress. *Fed Am Soc Exp Biol J*. (2002); **16**(2):270-72.

[69] Engler, A.J., Sen, S., Sweeney, H.L., and Discher, D.E. Matrix Elasticity Directs Stem Cell Lineage Specification. *Cell*. (2006); **126**(4):677-89.

[70] Patwari, P., and Lee, R.T. Mechanical Control of Tissue Morphogenesis. *Circ Res*. (2008); **103**(3):234-43.

[71] Discher, D., Dong, C., Fredberg, J.J., Guilak, F., Ingber, D., Janmey, P., Kamm, R.D., Schmid-Schönbein, G.W., and Weinbaum, S. Biomechanics: Cell Research and Applications for the Next Decade. *Ann of Biomed Eng*. (2009); **37**(5):847-59.

[72] Chai, C., and Leong, K.W. Biomaterials Approach to Expand and Direct Differentiation of Stem Cells. *Molecular Therapy*. (2007); **15**(3):467-80.

[73] Morrison, S.J., and Spradling, A.C. Stem Cells and Niches: Mechanisms That Promote Stem Cell Maintenance Throughout Life. *Cell*. (2008); **132**(4):598-611.

[74] Vater, C., Kasten, P., and Stiehler, M. Culture Media for the Differentiation of Mesenchymal Stromal Cells. *Acta Biomaterialia*. (2010).

[75] Phinney, D.G., and Prockop, D.J. Concise Review: Mesenchymal Stem/Multipotent Stromal Cells: The State of Transdifferentiation and Modes of Tissue Repair--Current Views. *Stem Cells*. (2007); **25**(11):2896-902.

[76] Schilling, T., Küffner, R., Klein-Hitpass, L., Zimmer, R., Jakob, F., and Schütze, N. Microarray Analyses of Transdifferentiated Mesenchymal Stem Cells. *Journal of Cellular Biochemistry*. (2008); **103**(2):413-33.

[77] Delorme, B., Ringe, J., Pontikoglou, C., Gaillard, J., Langonné, A., Sensebé, L., Noël, D., Jorgensen, C., Häupl, T., and Charbord, P. Specific Lineage-Priming of Bone Marrow Mesenchymal Stem Cells Provides the Molecular Framework for Their Plasticity. *Stem Cells*. (2009); **27**(5):1142-51.

[78] Kawai, M., and Rosen, C.J. Marrow Fat and Bone: New Insights from Mice and Humans. *Clinical Reviews in Bone and Mineral Metabolism*. (2009); **7**(3):216-23.

[79] Gimble, J.M. The Function of Adipocytes in the Bone Marrow Stroma. *The New Biologist*. (1990); **2**(4):304-12.

[80] Gimble, J.M., Zvonic, S., Floyd, Z.E., Kassem, M., and Nuttall, M.E. Playing with Bone and Fat. *Journal of Cellular Biochemistry*. (2006); **98**(2):251-66.

[81] Yin, T., and Li, L. The Stem Cell Niches in Bone. *The Journal of clinical investigation*. (2006); **116**(5):1195-201.

[82] Imhoff, B.R., and Hansen, J.M. Differential Redox Potential Profiles During Adipogenesis and Osteogenesis. *Cellular & Molecular Biology Letters*. (2011); **16**(1):149-61.

[83] Imhoff, B.R., and Hansen, J.M. Extracellular Redox Environments Regulate Adipocyte Differentiation. *Differentiation*. (2010); **80**(1):31-9.

[84] Nuttall, M.E., and Gimble, J.M. Controlling the Balance between Osteoblastogenesis and Adipogenesis and the Consequent Therapeutic Implications. *Current Opinion in Pharmacology*. (2004); **4**(3):290-4.

[85] Jethva, R., Otsuru, S., Dominici, M., and Horwitz, E.M. Cell Therapy for Disorders of Bone. *Cytotherapy*. (2009); **11**(1):3-17.

[86] Duque, G. Bone and Fat Connection in Aging Bone. *Current opinion in rheumatology*. (2008); **20**(4):429-29.

[87] Takada, I., Kouzmenko, A.P., and Kato, S. Wnt and Ppargamma Signaling in Osteoblastogenesis and Adipogenesis. *Nat Rev Rheumatol*. (2009); **5**(8):442-7.

[88] Confavreux, C.B., Levine, R.L., and Karsenty, G. A Paradigm of Integrative Physiology, the Crosstalk between Bone and Energy Metabolisms. *Molecular and Cellular Endocrinology*. (2009); **310**(1-2):21-9.

[89] Wei, J., and Ducy, P. Co-Dependence of Bone and Energy Metabolisms. *Archives of Biochemistry and Biophysics*. (2010); **503**(1):35-40.

[90] Harada, S.-i., and Rodan, G.a. Control of Osteoblast Function and Regulation of Bone Mass. *Nature*. (2003); **423**(6937):349-55.

[91] Teitelbaum, S.L. Bone Resorption by Osteoclasts. *Science*. (2000); **289**(5484):1504-08.

[92] Botolin, S., Faugere, M.-C., Malluche, H., Orth, M., Meyer, R., and McCabe, L.R. Increased Bone Adiposity and Peroxisomal Proliferator-Activated Receptor-Gamma2 Expression in Type I Diabetic Mice. *Endocrinology*. (2005); **146**(8):3622-31.

[93] Kuk, J.L., Saunders, T.J., Davidson, L.E., and Ross, R. Age-Related Changes in Total and Regional Fat Distribution. *Ageing Research Reviews*. (2009); **8**(4):339-48.

[94] Reid, I.R. Fat and Bone. *Archives of Biochemistry and Biophysics*. (2010); **503**(1):20-7.

[95] Lecka-Czernik, B. Marrow Fat Metabolism Is Linked to the Systemic Energy Metabolism. *Bone*. (2012); **50**(2):534-9.

[96] Seeman, E., and Delmas, P.D. Bone Quality--the Material and Structural Basis of Bone Strength and Fragility. *The New England Journal of Medicine*. (2006); **354**(21):2250-61.

[97] Lawson, E.A., and Klibanski, A. Endocrine Abnormalities in Anorexia Nervosa. *Nat Clin Pract Endocrinol Metab*. (2008); **4**(7):407-14.

[98] Pannacciulli, N., Vettor, R., Milan, G., Granzotto, M., Catucci, A., Federspil, G., De Giacomo, P., Giorgino, R., and De Pergola, G. Anorexia Nervosa Is Characterized by Increased Adiponectin Plasma Levels and Reduced Nonoxidative Glucose Metabolism. *J Clin Endocrinol Metab*. (2003); **88**(4):1748-52.

[99] Vestergaard, P., Emborg, C., Stoving, R.K., Hagen, C., Mosekilde, L., and Brixen, K. Fractures in Patients with Anorexia Nervosa, Bulimia Nervosa, and Other

Eating Disorders--a Nationwide Register Study. *Int J Eat Disord*. (2002); **32**(3):301-8.

[100] Heer, M., Mika, C., Grzella, I., Heussen, N., and Herpertz-Dahlmann, B. Bone Turnover During Inpatient Nutritional Therapy and Outpatient Follow-up in Patients with Anorexia Nervosa Compared with That in Healthy Control Subjects. *Am J Clin Nutr*. (2004); **80**(3):774-81.

[101] Grinspoon, S., Thomas, E., Pitts, S., Gross, E., Mickley, D., Miller, K., Herzog, D., and Klibanski, A. Prevalence and Predictive Factors for Regional Osteopenia in Women with Anorexia Nervosa. *Ann Intern Med*. (2000); **133**(10):790-4.

[102] Ecklund, K., Vajapeyam, S., Feldman, H.A., Buzney, C.D., Mulkern, R.V., Kleinman, P.K., Rosen, C.J., and Gordon, C.M. Bone Marrow Changes in Adolescent Girls with Anorexia Nervosa. *J Bone Miner Res*. (2010); **25**(2):298-304.

[103] Abella, E., Feliu, E., Granada, I., Milla, F., Oriol, A., Ribera, J.M., Sanchez-Planell, L., Berga, L.I., Reverter, J.C., and Rozman, C. Bone Marrow Changes in Anorexia Nervosa Are Correlated with the Amount of Weight Loss and Not with Other Clinical Findings. *Am J Clin Pathol*. (2002); **118**(4):582-8.

[104] Devlin, M.J., Cloutier, A.M., Thomas, N.A., Panus, D.A., Lotinun, S., Pinz, I., Baron, R., Rosen, C.J., and Bouxsein, M.L. Caloric Restriction Leads to High Marrow Adiposity and Low Bone Mass in Growing Mice. *J Bone Miner Res*. (2010); **25**(9):2078-88.

[105] Fazeli, P.K., Bredella, M.A., Misra, M., Meenaghan, E., Rosen, C.J., Clemmons, D.R., Breggia, A., Miller, K.K., and Klibanski, A. Preadipocyte Factor-1 Is Associated with Marrow Adiposity and Bone Mineral Density in Women with Anorexia Nervosa. *J Clin Endocrinol Metab*. (2010); **95**(1):407-13.

[106] Bredella, M.A., Fazeli, P.K., Miller, K.K., Misra, M., Torriani, M., Thomas, B.J., Ghomi, R.H., Rosen, C.J., and Klibanski, A. Increased Bone Marrow Fat in Anorexia Nervosa. *J Clin Endocrinol Metab*. (2009); **94**(6):2129-36.

[107] Bachrach, L.K., Katzman, D.K., Litt, I.F., Guido, D., and Marcus, R. Recovery from Osteopenia in Adolescent Girls with Anorexia Nervosa. *J Clin Endocrinol Metab*. (1991); **72**(3):602-6.

[108] Miller, K.K., Lee, E.E., Lawson, E.A., Misra, M., Minihan, J., Grinspoon, S.K., Gleysteen, S., Mickley, D., Herzog, D., and Klibanski, A. Determinants of Skeletal Loss and Recovery in Anorexia Nervosa. *J Clin Endocrinol Metab*. (2006); **91**(8):2931-7.

[109] Dominguez, J., Goodman, L., Sen Gupta, S., Mayer, L., Etu, S.F., Walsh, B.T., Wang, J., Pierson, R., and Warren, M.P. Treatment of Anorexia Nervosa Is Associated with Increases in Bone Mineral Density, and Recovery Is a Biphasic

Process Involving Both Nutrition and Return of Menses. *Am J Clin Nutr*. (2007); **86**(1):92-9.

[110] Reid, I.R. Relationships between Fat and Bone. *Osteoporos Int*. (2008); **19**(5):595-606.

[111] De Laet, C., Kanis, J.A., Oden, A., Johanson, H., Johnell, O., Delmas, P., Eisman, J.A., Kroger, H., Fujiwara, S., Garnero, P., McCloskey, E.V., Mellstrom, D., Melton, L.J., 3rd, Meunier, P.J., Pols, H.A., Reeve, J., Silman, A., and Tenenhouse, A. Body Mass Index as a Predictor of Fracture Risk: A Meta-Analysis. *Osteoporos Int*. (2005); **16**(11):1330-8.

[112] Patsch, J.M., Kiefer, F.W., Varga, P., Pail, P., Rauner, M., Stupphann, D., Resch, H., Moser, D., Zysset, P.K., Stulnig, T.M., and Pietschmann, P. Increased Bone Resorption and Impaired Bone Microarchitecture in Short-Term and Extended High-Fat Diet-Induced Obesity. *Metabolism*. (2011); **60**(2):243-9.

[113] Lau, E.M., Chan, Y.H., Chan, M., Woo, J., Griffith, J., Chan, H.H., and Leung, P.C. Vertebral Deformity in Chinese Men: Prevalence, Risk Factors, Bone Mineral Density, and Body Composition Measurements. *Calcif Tissue Int*. (2000); **66**(1):47-52.

[114] Premaor, M.O., Pilbrow, L., Tonkin, C., Parker, R.A., and Compston, J. Obesity and Fractures in Postmenopausal Women. *J Bone Miner Res*. (2010); **25**(2):292-7.

[115] Schott, A.M., Cormier, C., Hans, D., Favier, F., Hausherr, E., Dargent-Molina, P., Delmas, P.D., Ribot, C., Sebert, J.L., Breart, G., and Meunier, P.J. How Hip and Whole-Body Bone Mineral Density Predict Hip Fracture in Elderly Women: The Epidos Prospective Study. *Osteoporos Int*. (1998); **8**(3):247-54.

[116] Goulding, A., Grant, A.M., and Williams, S.M. Bone and Body Composition of Children and Adolescents with Repeated Forearm Fractures. *J Bone Miner Res*. (2005); **20**(12):2090-6.

[117] von Muhlen, D., Safii, S., Jassal, S.K., Svartberg, J., and Barrett-Connor, E. Associations between the Metabolic Syndrome and Bone Health in Older Men and Women: The Rancho Bernardo Study. *Osteoporos Int*. (2007); **18**(10):1337-44.

[118] Bredella, M.A., Torriani, M., Ghomi, R.H., Thomas, B.J., Brick, D.J., Gerweck, A.V., Rosen, C.J., Klibanski, A., and Miller, K.K. Vertebral Bone Marrow Fat Is Positively Associated with Visceral Fat and Inversely Associated with Igf-1 in Obese Women. *Obesity (Silver Spring)*. (2011); **19**(1):49-53.

[119] Weisberg, S.P., McCann, D., Desai, M., Rosenbaum, M., Leibel, R.L., and Ferrante, A.W., Jr. Obesity Is Associated with Macrophage Accumulation in Adipose Tissue. *J Clin Invest*. (2003); **112**(12):1796-808.

[120] Yadav, V.K., Oury, F., Suda, N., Liu, Z.-W., Gao, X.-B., Confavreux, C., Klemenhagen, K.C., Tanaka, K.F., Gingrich, J.a., Guo, X.E., Tecott, L.H., Mann, J.J., Hen, R., Horvath, T.L., and Karsenty, G. A Serotonin-Dependent Mechanism Explains the Leptin Regulation of Bone Mass, Appetite, and Energy Expenditure. *Cell*. (2009); **138**(5):976-89.

[121] Merlotti, D., Gennari, L., Dotta, F., Lauro, D., and Nuti, R. Mechanisms of Impaired Bone Strength in Type 1 and 2 Diabetes. *Nutr Metab Cardiovasc Dis*. (2010); **20**(9):683-90.

[122] Strotmeyer, E.S., and Cauley, J.A. Diabetes Mellitus, Bone Mineral Density, and Fracture Risk. *Curr Opin Endocrinol Diabetes Obes*. (2007); **14**(6):429-35.

[123] Janghorbani, M., Van Dam, R.M., Willett, W.C., and Hu, F.B. Systematic Review of Type 1 and Type 2 Diabetes Mellitus and Risk of Fracture. *Am J Epidemiol*. (2007); **166**(5):495-505.

[124] Strotmeyer, E.S., Cauley, J.A., Schwartz, A.V., Nevitt, M.C., Resnick, H.E., Bauer, D.C., Tylavsky, F.A., de Rekeneire, N., Harris, T.B., and Newman, A.B. Nontraumatic Fracture Risk with Diabetes Mellitus and Impaired Fasting Glucose in Older White and Black Adults: The Health, Aging, and Body Composition Study. *Arch Intern Med*. (2005); **165**(14):1612-7.

[125] Hamann, C., Kirschner, S., Gunther, K.P., and Hofbauer, L.C. Bone, Sweet Bone--Osteoporotic Fractures in Diabetes Mellitus. *Nat Rev Endocrinol*. (2012); **8**(5):297-305.

[126] Zhao, J., and Weiler, H.A. Long-Term Effects of Gestational Diabetes on Offspring Health Are More Pronounced in Skeletal Growth Than Body Composition and Glucose Tolerance. *Br J Nutr*. (2010); **104**(11):1641-9.

[127] Mimouni, F., Steichen, J.J., Tsang, R.C., Hertzberg, V., and Miodovnik, M. Decreased Bone Mineral Content in Infants of Diabetic Mothers. *Am J Perinatol*. (1988); **5**(4):339-43.

[128] Tsang, R.C., Kleinman, L.I., Sutherland, J.M., and Light, I.J. Hypocalcemia in Infants of Diabetic Mothers. Studies in Calcium, Phosphorus, and Magnesium Metabolism and Parathormone Responsiveness. *J Pediatr*. (1972); **80**(3):384-95.

[129] Cramer, C., Freisinger, E., Jones, R.K., Slakey, D.P., Dupin, C.L., Newsome, E.R., Alt, E.U., and Izadpanah, R. Persistent High Glucose Concentrations Alter the Regenerative Potential of Mesenchymal Stem Cells. *Stem Cells Dev*. (2010); **19**(12):1875-84.

[130] Stolzing, A., Coleman, N., and Scutt, A. Glucose-Induced Replicative Senescence in Mesenchymal Stem Cells. *Rejuvenation Res*. (2006); **9**(1):31-5.

[131] Li, Y.M., Schilling, T., Benisch, P., Zeck, S., Meissner-Weigl, J., Schneider, D., Limbert, C., Seufert, J., Kassem, M., Schutze, N., Jakob, F., and Ebert, R. Effects of High Glucose on Mesenchymal Stem Cell Proliferation and Differentiation. *Biochem Biophys Res Commun*. (2007); **363**(1):209-15.

[132] Gopalakrishnan, V., Vignesh, R.C., Arunakaran, J., Aruldhas, M.M., and Srinivasan, N. Effects of Glucose and Its Modulation by Insulin and Estradiol on Bmsc Differentiation into Osteoblastic Lineages. *Biochem Cell Biol*. (2006); **84**(1):93-101.

[133] Garcia-Hernandez, A., Arzate, H., Gil-Chavarria, I., Rojo, R., and Moreno-Fierros, L. High Glucose Concentrations Alter the Biomineralization Process in Human Osteoblastic Cells. *Bone*. (2012); **50**(1):276-88.

[134] Botolin, S., and McCabe, L.R. Chronic Hyperglycemia Modulates Osteoblast Gene Expression through Osmotic and Non-Osmotic Pathways. *J Cell Biochem*. (2006); **99**(2):411-24.

[135] Zayzafoon, M., Stell, C., Irwin, R., and McCabe, L.R. Extracellular Glucose Influences Osteoblast Differentiation and C-Jun Expression. *J Cell Biochem*. (2000); **79**(2):301-10.

[136] Inaba, M., Nishizawa, Y., Shioi, A., and Morii, H. Importance of Sustained High Glucose Condition in the Development of Diabetic Osteopenia: Possible Involvement of the Polyol Pathway. *Osteoporos Int*. (1997); **7 Suppl 3**:S209-12.

[137] Sun, J., Xu, Y., Dai, Z., and Sun, Y. Intermittent High Glucose Stimulate Mcp-L, Il-18, and Pai-1, but Inhibit Adiponectin Expression and Secretion in Adipocytes Dependent of Ros. *Cell Biochem Biophys*. (2009); **55**(3):173-80.

[138] Gagnon, A., and Sorisky, A. The Effect of Glucose Concentration on Insulin-Induced 3t3-L1 Adipose Cell Differentiation. *Obes Res*. (1998); **6**(2):157-63.

[139] Lin, Y., Berg, A.H., Iyengar, P., Lam, T.K., Giacca, A., Combs, T.P., Rajala, M.W., Du, X., Rollman, B., Li, W., Hawkins, M., Barzilai, N., Rhodes, C.J., Fantus, I.G., Brownlee, M., and Scherer, P.E. The Hyperglycemia-Induced Inflammatory Response in Adipocytes: The Role of Reactive Oxygen Species. *J Biol Chem*. (2005); **280**(6):4617-26.

[140] Chaldakov, G.N., Stankulov, I.S., Hristova, M., and Ghenev, P.I. Adipobiology of Disease: Adipokines and Adipokine-Targeted Pharmacology. *Current Pharmaceutical Design*. (2003); **9**(12):1023-31.

[141] Fain, J.N., Madan, A.K., Hiler, M.L., Cheema, P., and Bahouth, S.W. Comparison of the Release of Adipokines by Adipose Tissue, Adipose Tissue Matrix, and Adipocytes from Visceral and Subcutaneous Abdominal Adipose Tissues of Obese Humans. *Endocrinology*. (2004); **145**(5):2273-82.

[142] Fantuzzi, G. Adipose Tissue, Adipokines, and Inflammation. *The Journal of Allergy and Clinical Immunology*. (2005); **115**(5):911-9; quiz 20.

[143] Guerre-Millo, M. Adipose Tissue and Adipokines: For Better or Worse. *Diabetes & Metabolism*. (2004); **30**(1):13-9.

[144] Shi, Y., Yadav, V.K., Suda, N., Liu, X.S., Guo, X.E., Myers, M.G., and Karsenty, G. Dissociation of the Neuronal Regulation of Bone Mass and Energy Metabolism by Leptin in Vivo. *Proceedings of the National Academy of Sciences of the United States of America*. (2008); **105**(51):20529-33.

[145] Takeda, S., Elefteriou, F., Levasseur, R., Liu, X., Zhao, L., Parker, K.L., Armstrong, D., Ducy, P., and Karsenty, G. Leptin Regulates Bone Formation Via the Sympathetic Nervous System. *Cell*. (2002); **111**(3):305-17.

[146] Ferron, M., Hinoi, E., Karsenty, G., and Ducy, P. Osteocalcin Differentially Regulates Beta Cell and Adipocyte Gene Expression and Affects the Development of Metabolic Diseases in Wild-Type Mice. *Proceedings of the National Academy of Sciences of the United States of America*. (2008); **105**(13):5266-70.

[147] Fulzele, K., Riddle, R.C., DiGirolamo, D.J., Cao, X., Wan, C., Chen, D., Faugere, M.-C., Aja, S., Hussain, M.a., and Brüning, J.C. Insulin Receptor Signaling in Osteoblasts Regulates Postnatal Bone Acquisition and Body Composition. *Cell*. (2010); **142**(2):309-19.

[148] Di Iorgi, N., Rosol, M., Mittelman, S.D., and Gilsanz, V. Reciprocal Relation between Marrow Adiposity and the Amount of Bone in the Axial and Appendicular Skeleton of Young Adults. *J Clin Endocrinol Metab*. (2008); **93**(6):2281-6.

[149] Krings, A., Rahman, S., Huang, S., Lu, Y., Czernik, P.J., and Lecka-Czernik, B. Bone Marrow Fat Has Brown Adipose Tissue Characteristics, Which Are Attenuated with Aging and Diabetes. *Bone*. (2012); **50**(2):546-52.

[150] Griffith, J.F., Yeung, D.K., Antonio, G.E., Lee, F.K., Hong, A.W., Wong, S.Y., Lau, E.M., and Leung, P.C. Vertebral Bone Mineral Density, Marrow Perfusion, and Fat Content in Healthy Men and Men with Osteoporosis: Dynamic Contrast-Enhanced Mr Imaging and Mr Spectroscopy. *Radiology*. (2005); **236**(3):945-51.

[151] Wren, T.A., Chung, S.A., Dorey, F.J., Bluml, S., Adams, G.B., and Gilsanz, V. Bone Marrow Fat Is Inversely Related to Cortical Bone in Young and Old Subjects. *J Clin Endocrinol Metab*. (2011); **96**(3):782-6.

[152] Gokalp, G., Mutlu, F.S., Yazici, Z., and Yildirim, N. Evaluation of Vertebral Bone Marrow Fat Content by Chemical-Shift Mri in Osteoporosis. *Skeletal Radiol*. (2011); **40**(5):577-85.

[153] Yeung, D.K., Griffith, J.F., Antonio, G.E., Lee, F.K., Woo, J., and Leung, P.C. Osteoporosis Is Associated with Increased Marrow Fat Content and Decreased Marrow Fat Unsaturation: A Proton Mr Spectroscopy Study. *J Magn Reson Imaging*. (2005); **22**(2):279-85.

[154] Hess, R., Pino, A.M., Ríos, S., Fernández, M., and Rodríguez, J.P. High Affinity Leptin Receptors Are Present in Human Mesenchymal Stem Cells (Mscs) Derived from Control and Osteoporotic Donors. *Journal of Cellular Biochemistry*. (2005); **94**(1):50-7.

[155] Takahashi, Y., Okimura, Y., Mizuno, I., Iida, K., Takahashi, T., Kaji, H., Abe, H., and Chihara, K. Leptin Induces Mitogen-Activated Protein Kinase-Dependent Proliferation of C3h10t1/2 Cells. *The Journal of Biological Chemistry*. (1997); **272**(20):12897-900.

[156] Thomas, T., Gori, F., Khosla, S., Jensen, M.D., Burguera, B., and Riggs, B.L. Leptin Acts on Human Marrow Stromal Cells to Enhance Differentiation to Osteoblasts and to Inhibit Differentiation to Adipocytes. *Endocrinology*. (1999); **140**(4):1630-38.

[157] Lo Celso, C., Fleming, H.E., Wu, J.W., Zhao, C.X., Miake-Lye, S., Fujisaki, J., Côté, D., Rowe, D.W., Lin, C.P., and Scadden, D.T. Live-Animal Tracking of Individual Haematopoietic Stem/Progenitor Cells in Their Niche. *Nature*. (2009); **457**(7225):92-6.

[158] Wilson, A., and Trumpp, A. Bone-Marrow Haematopoietic-Stem-Cell Niches. *Nature reviews Immunology*. (2006); **6**(2):93-106.

[159] Griffith, L.G., and Swartz, M.A. Capturing Complex 3d Tissue Physiology in Vitro. *Nat Rev Mol Cell Biol*. (2006); **7**(3):211-24.

[160] Lutolf, M.P., Gilbert, P.M., and Blau, H.M. Designing Materials to Direct Stem-Cell Fate. *Nature*. (2009); **462**(7272):433-41.

[161] Lutolf, M.P., and Hubbell, J.A. Synthetic Biomaterials as Instructive Extracellular Microenvironments for Morphogenesis in Tissue Engineering. *Nat Biotechnol*. (2005); **23**(1):47-55.

[162] Cho, E., Kutty, J.K., Datar, K., Lee, J.S., Vyavahare, N.R., and Webb, K. A Novel Synthetic Route for the Preparation of Hydrolytically Degradable Synthetic Hydrogels. *Journal of Biomedical Materials Research Part A*. (2009); **90**(4):1073-82.

[163] Jia, X., and Kiick, K.L. Hybrid Multicomponent Hydrogels for Tissue Engineering. *Macromol Biosci*. (2009); **9**(2):140-56.

[164] Lin, C.-C., and Metters, A.T. Hydrogels in Controlled Release Formulations: Network Design and Mathematical Modeling. *Adv Drug Deliv Rev*. (2006); **58**(12-13):1379-408.

[165] Peppas, N.A., Huang, Y., Torres-Lugo, M., Ward, J.H., and Zhang, J. Physicochemical Foundations and Structural Design of Hydrogels in Medicine and Biology. *Annu Rev Biomed Eng*. (2000); **2**:9-29.

[166] Lowman, A.M., and Peppas, N.A. *Hydrogels*. New York: Wiley; 1999.

[167] Tessmar, J.K., and Göpferich, A.M. Customized Peg-Derived Copolymers for Tissue-Engineering Applications. *Macromol Biosci*. (2007); **7**(1):23-39.

[168] Nicodemus, G.D., and Bryant, S.J. Cell Encapsulation in Biodegradable Hydrogels for Tissue Engineering Applications. *Tissue Eng Part B-Re*. (2008); **14**(2):149-65.

[169] Ratner, B.D., and Hoffman, A.S. Synthetic Hydrogels for Biomedical Applications. In: Andrade, J.D., editor. Hydrogels for Medical and Related Applications. Washington D. C.: American Chemical Society; 1976.

[170] Buxton, A.N., Zhu, J., Marchant, R., West, J.L., Yoo, J.U., and Johnstone, B. Design and Characterization of Poly(Ethylene Glycol) Photopolymerizable Semi-Interpenetrating Networks for Chondrogenesis of Human Mesenchymal Stem Cells. *Tissue Eng*. (2007); **13**(10):2549-60.

[171] Mano, J.F., Silva, G.A., Azevedo, H.S., Malafaya, P.B., Sousa, R.A., Silva, S.S., Boesel, L.F., Oliveira, J.M., Santos, T.C., Marques, A.P., Neves, N.M., and Reis, R.L. Natural Origin Biodegradable Systems in Tissue Engineering and Regenerative Medicine: Present Status and Some Moving Trends. *Journal of the Royal Society Interface*. (2007); **4**(17):999-1030.

[172] Peppas, N.A., Bures, P., Leobandung, W., and Ichikawa, H. Hydrogels in Pharmaceutical Formulations. *European Journal of Pharmaceutics and Biopharmaceutics*. (2000); **50**(1):27-46.

[173] Liu Tsang, V., Chen, A.A., Cho, L.M., Jadin, K.D., Sah, R.L., DeLong, S., West, J.L., and Bhatia, S.N. Fabrication of 3d Hepatic Tissues by Additive Photopatterning of Cellular Hydrogels. *Federation of American Societies for Experimental Biology Journal*. (2007); **21**(3):790-801.

[174] Peppas, N., Hilt, J., Khademhosseini, A., and Langer, R. Hydrogels in Biology and Medicine: From Molecular Principles to Bionanotechnology. *Adv Mater*. (2006); **18**(11):1345-60.

[175] James Kirkpatrick, C., Fuchs, S., Iris Hermanns, M., Peters, K., and Unger, R.E. Cell Culture Models of Higher Complexity in Tissue Engineering and Regenerative Medicine. *Biomaterials*. (2007); **28**(34):5193-8.

[176] Place, E.S., Evans, N.D., and Stevens, M.M. Complexity in Biomaterials for Tissue Engineering. *Nat Materials*. (2009); **8**(6):457-70.

[177] Davis, K.A., and Anseth, K.S. Controlled Release from Crosslinked Degradable Networks. *Crit Rev Ther Drug Carr Syst*. (2002); **19**(4-5):385-423.

[178] Drury, J.L., and Mooney, D.J. Hydrogels for Tissue Engineering: Scaffold Design Variables and Applications. *Biomaterials*. (2003); **24**(24):4337-51.

[179] Lee, K.Y., and Mooney, D.J. Hydrogels for Tissue Engineering. *Chemical Reviews*. (2001); **101**(7):1869-79.

[180] Lee, C.H., Singla, A., and Lee, Y. Biomedical Applications of Collagen. *International Journal of Pharmaceutics*. (2001); **221**(1-2):1-22.

[181] Alberts, B., Bray, D., Lewis, J., Raff, M., Roberts, K., and Watson, J.D. *Molecular Biology of the Cell*. 3rd ed. New York: Garland Publishing, Inc.; 1994.

[182] Yang, S., Leong, K.F., Du, Z., and Chua, C.K. The Design of Scaffolds for Use in Tissue Engineering. Part I. Traditional Factors. *Tissue Eng*. (2001); **7**(6):679-89.

[183] Suh, J.K., and Matthew, H.W. Application of Chitosan-Based Polysaccharide Biomaterials in Cartilage Tissue Engineering: A Review. *Biomaterials*. (2000); **21**(24):2589-98.

[184] Smidsrød, O., and Skjåk-Braek, G. Alginate as Immobilization Matrix for Cells. *Trends in Biotechnol*. (1990); **8**(3):71-78.

[185] Khademhosseini, A., Ferreira, L., Blumling III, J., Yeh, J., Karp, J.M., Fukuda, J., and Langer, R. Co-Culture of Human Embryonic Stem Cells with Murine Embryonic Fibroblasts on Microwell-Patterned Substrates. *Biomaterials*. (2006); **27**:5968-77.

[186] Thomson, R., Wake, M., Yaszemski, M., and Mikos, A. Biodegradable Polymer Scaffolds to Regenerate Organs. *Adv Polym Sci*. (1995); **122**(5):245-74.

[187] Cruise, G.M., Scharp, D.S., and Hubbell, J.A. Characterization of Permeability and Network Structure of Interfacially Photopolymerized Poly(Ethylene Glycol) Diacrylate Hydrogels. *Biomaterials*. (1998); **19**(14):1287-94.

[188] Hassan, C., and Peppas, N. Structure and Morphology of Freeze/Thawed Pva Hydrogels. *Macromol*. (2000); **33**(7):2472-79.

[189] Brink, K.S., Yang, P.J., and Temenoff, J.S. Degradative Properties and Cytocompatibility of a Mixed-Mode Hydrogel Containing Oligo[Poly(Ethylene Glycol) Fumarate] and Poly(Ethylene Glycol)Dithiol. *Acta Biomaterialia*. (2009); **5**(2):570-79.

[190] Ratner, B.D., Hoffman, A.S., Schoen, F.J., and Lemons, J.E. Biomaterials Science: An Introduction to Materials in Medicine. 2nd ed. Amsterdam: Elsevier Academic; 2004.

[191] Elbert, D.L., and Hubbell, J.A. Surface Treatments of Polymers for Biocompatibility. *Annu Rev Mater Sci*. (1996); **26**:365-94.

[192] Deible, C.R., Petrosko, P., Johnson, P.C., Beckman, E.J., Russell, A.J., and Wagner, W.R. Molecular Barriers to Biomaterial Thrombosis by Modification of Surface Proteins with Polyethylene Glycol. *Biomaterials*. (1999); **20**(2):101-9.

[193] Gombotz, W.R., Wang, G.H., Horbett, T.A., and Hoffman, A.S. Protein Adsorption to Poly(Ethylene Oxide) Surfaces. *J Biomed Mater Res*. (1991); **25**(12):1547-62.

[194] Temenoff, J.S., and Mikos, A.G. Injectable Biodegradable Materials for Orthopedic Tissue Engineering. *Biomaterials*. (2000); **21**(23):2405-12.

[195] Lutolf, M.P., and Hubbell, J.A. Synthetic Biomaterials as Instructive Extracellular Microenvironments for Morphogenesis in Tissue Engineering. *Nat Biotechnol*. (2005); **23**(1):47-55.

[196] Burdick, J.A., and Anseth, K.S. Photoencapsulation of Osteoblasts in Injectable Rgd-Modified Peg Hydrogels for Bone Tissue Engineering. *Biomaterials*. (2002); **23**(22):4315-23.

[197] Hern, D.L., and Hubbell, J.A. Incorporation of Adhesion Peptides into Nonadhesive Hydrogels Useful for Tissue Resurfacing. *J Biomed Mater Res*. (1998); **39**(2):266-76.

[198] Brandl, F.P., Seitz, A.K., Tessmar, J.K.V., Blunk, T., and Göpferich, A.M. Enzymatically Degradable Poly(Ethylene Glycol) Based Hydrogels for Adipose Tissue Engineering. *Biomaterials*. (2010); **31**(14):3957-66.

[199] Mann, B.K., Schmedlen, R.H., and West, J.L. Tethered-Tgf-Beta Increases Extracellular Matrix Production of Vascular Smooth Muscle Cells. *Biomaterials*. (2001); **22**(5):439-44.

[200] DeLong, S.A., Moon, J.J., and West, J.L. Covalently Immobilized Gradients of Bfgf on Hydrogel Scaffolds for Directed Cell Migration. *Biomaterials*. (2005); **26**(16):3227-34.

[201] Phelps, E.A., Landazuri, N., Thule, P.M., Taylor, W.R., and Garcia, A.J. Regenerative Medicine Special Feature: Bioartificial Matrices for Therapeutic Vascularization. *Proc Natl Acad Sci U S A*. (2009).

[202] Yang, F., Williams, C.G., Wang, D.A., Lee, H., Manson, P.N., and Elisseeff, J. The Effect of Incorporating Rgd Adhesive Peptide in Polyethylene Glycol Diacrylate

Hydrogel on Osteogenesis of Bone Marrow Stromal Cells. *Biomaterials*. (2005); **26**(30):5991-8.

[203] Bryant, S.J., and Anseth, K.S. Controlling the Spatial Distribution of Ecm Components in Degradable Peg Hydrogels for Tissue Engineering Cartilage. *J Biomed Mater Res A*. (2003); **64**(1):70-9.

[204] Williams, C.G., Kim, T.K., Taboas, A., Malik, A., Manson, P., and Elisseeff, J. In Vitro Chondrogenesis of Bone Marrow-Derived Mesenchymal Stem Cells in a Photopolymerizing Hydrogel. *Tissue Eng*. (2003); **9**(4):679-88.

[205] Moon, J.J., Hahn, M.S., Kim, I., Nsiah, B.A., and West, J.L. Micropatterning of Poly(Ethylene Glycol) Diacrylate Hydrogels with Biomolecules to Regulate and Guide Endothelial Morphogenesis. *Tissue Eng Part A*. (2009); **15**(3):579-85.

[206] Mahoney, M.J., and Anseth, K.S. Three-Dimensional Growth and Function of Neural Tissue in Degradable Polyethylene Glycol Hydrogels. *Biomaterials*. (2006); **27**(10):2265-74.

[207] Gunn, J.W., Turner, S.D., and Mann, B.K. Adhesive and Mechanical Properties of Hydrogels Influence Neurite Extension. *J Biomed Mater Res A*. (2005); **72**(1):91-7.

[208] Tabata, Y. Biomaterial Technology for Tissue Engineering Applications. *Journal of the Royal Society Interface*. (2009); **6 Suppl 3**:S311-S24.

[209] Zhu, J., and Marchant, R.E. Design Properties of Hydrogel Tissue-Engineering Scaffolds. *Expert Rev Med Devices*. (2011); **8**(5):607-26.

[210] Tabata, Y. Tissue Regeneration Based on Tissue Engineering Technology. *Congenit Anom*. (2004); **44**(3):111-24.

[211] Metters, A.T., Anseth, K.S., and Bowman, C.N. Fundamental Studies of a Novel, Biodegradable Peg-B-Pla Hydrogel. *Polym*. (2000); **41**(11):3993-4004.

[212] West, J.L., and Hubbell, J.A. Photopolymerized Hydrogel Materials for Drug-Delivery Applications. *Reactive Polymers*. (1995); **25**(2-3):139-47.

[213] Lutolf, M.P., Lauer-Fields, J.L., Schmoekel, H.G., Metters, A.T., Weber, F.E., Fields, G.B., and Hubbell, J.A. Synthetic Matrix Metalloproteinase-Sensitive Hydrogels for the Conduction of Tissue Regeneration: Engineering Cell-Invasion Characteristics. *Proceedings of the National Academy of Sciences USA*. (2003); **100**(9):5413-18.

[214] Hu, B.H., and Messersmith, P.B. Rational Design of Transglutaminase Substrate Peptides for Rapid Enzymatic Formation of Hydrogels. *Journal of the American Chemical Society*. (2003); **125**(47):14298-99.

[215] Hudalla, G.A., Eng, T.S., and Murphy, W.L. An Approach to Modulate Degradation and Mesenchymal Stem Cell Behavior in Poly(Ethylene Glycol) Networks. *Biomacromolecules*. (2008); **9**(3):842-9.

[216] Gobin, A.S., and West, J.L. Cell Migration through Defined, Synthetic Ecm Analogs. *FASEB J*. (2002); **16**(7):751-3.

[217] Gobin, A.S., and West, J.L. Effects of Epidermal Growth Factor on Fibroblast Migration through Biomimetic Hydrogels. *Biotechnol Prog*. (2003); **19**(6):1781-5.

[218] Yang, P.J., Levenston, M.E., and Temenoff, J. Modulation of Mesenchymal Stem Cell Shape in Enzyme-Sensitive Hydrogels Is Decoupled from Upregulation of Fibroblast Markers under Cyclic Tension. *Tissue Eng Part A*. (2012).

[219] Kloxin, A.M., Kasko, A.M., Salinas, C.N., and Anseth, K.S. Photodegradable Hydrogels for Dynamic Tuning of Physical and Chemical Properties. *Science*. (2009); **324**(5923):59-63.

[220] Fairbanks, B.D., Singh, S.P., Bowman, C.N., and Anseth, K.S. Photodegradable, Photoadaptable Hydrogels Via Radical-Mediated Disulfide Fragmentation Reaction. *Macromolecules*. (2011); **44**(8):2444-50.

[221] Kloxin, A.M., Tibbitt, M.W., and Anseth, K.S. Synthesis of Photodegradable Hydrogels as Dynamically Tunable Cell Culture Platforms. *Nat Protoc*. (2010); **5**(12):1867-87.

[222] Brink, K.S., Yang, P.J., and Temenoff, J.S. Degradative Properties and Cytocompatibility of a Mixed-Mode Hydrogel Containing Oligo[Poly(Ethylene Glycol)Fumarate] and Poly(Ethylene Glycol)Dithiol. *Acta Biomater*. (2009); **5**(2):570-9.

[223] Temenoff, J.S., Park, H., Jabbari, E., Conway, D.E., Sheffield, T.L., Ambrose, C.G., and Mikos, A.G. Thermally Cross-Linked Oligo(Poly(Ethylene Glycol) Fumarate) Hydrogels Support Osteogenic Differentiation of Encapsulated Marrow Stromal Cells in Vitro. *Biomacromolecules*. (2004); **5**(1):5-10.

[224] Nguyen, K.T., and West, J.L. Photopolymerizable Hydrogels for Tissue Engineering Applications. *Biomaterials*. (2002); **23**(22):4307-14.

[225] Ifkovits, J.L., and Burdick, J.A. Review: Photopolymerizable and Degradable Biomaterials for Tissue Engineering Applications. *Tissue Engineering*. (2007); **13**(10):2369-85.

[226] Hersel, U., Dahmen, C., and Kessler, H. Rgd Modified Polymers: Biomaterials for Stimulated Cell Adhesion and Beyond. *Biomaterials*. (2003); **24**(24):4385-415.

[227] Temenoff, J.S., Shin, H., Conway, D.E., Engel, P.S., and Mikos, A.G. In Vitro Cytotoxicity of Redox Radical Initiators for Cross-Linking of Oligo(Poly(Ethylene Glycol) Fumarate) Macromers. *Biomacromolecules*. (2003); **4**(6):1605-13.

[228] Bryant, S.J., Nuttelman, C.R., and Anseth, K.S. Cytocompatibility of Uv and Visible Light Photoinitiating Systems on Cultured Nih/3t3 Fibroblasts in Vitro. *Journal of Biomaterials Science, Polymer Edition*. (2000); **11**(5):439-57.

[229] Williams, C.G., Malik, A.N., Kim, T.K., Manson, P.N., and Elisseeff, J.H. Variable Cytocompatibility of Six Cell Lines with Photoinitiators Used for Polymerizing Hydrogels and Cell Encapsulation. *Biomaterials*. (2005); **26**(11):1211-18.

[230] Mann, B.K., Gobin, A.S., Tsai, A.T., Schmedlen, R.H., and West, J.L. Smooth Muscle Cell Growth in Photopolymerized Hydrogels with Cell Adhesive and Proteolytically Degradable Domains: Synthetic Ecm Analogs for Tissue Engineering. *Biomaterials*. (2001); **22**(22):3045-51.

[231] Biswal, D., and Hilt, J.Z. Analysis of Oxygen Inhibition in Photopolymerizations of Hydrogel Micropatterns Using Ftir Imaging. *Macromolecules*. (2009); **42**(4):973-79.

[232] O'Brien, A.K., and Bowman, C.N. Modeling the Effect of Oxygen on Photopolymerization Kinetics. *Macromol Theory Simul*. (2006); **15**(2):176-82.

[233] Chung, S.E., Park, W., Shin, S., Lee, S.A., and Kwon, S. Guided and Fluidic Self-Assembly of Microstructures Using Railed Microfluidic Channels. *Nature Materials*. (2008); **7**(7):581-7.

[234] Salinas, C.N., and Anseth, K.S. Mixed Mode Thiol-Acrylate Photopolymerizations for the Synthesis of Peg-Peptide Hydrogels. *Macromolecules*. (2008); **41**(16):6019-26.

[235] Elbert, D.L., Pratt, A.B., Lutolf, M.P., Halstenberg, S., and Hubbell, J.A. Protein Delivery from Materials Formed by Self-Selective Conjugate Addition Reactions. *J Control Release*. (2001); **76**(1-2):11-25.

[236] van de Wetering, P., Metters, A.T., Schoenmakers, R.G., and Hubbell, J.A. Poly(Ethylene Glycol) Hydrogels Formed by Conjugate Addition with Controllable Swelling, Degradation, and Release of Pharmaceutically Active Proteins. *J Control Release*. (2005); **102**(3):619-27.

[237] Polizzotti, B.D., Fairbanks, B.D., and Anseth, K.S. Three-Dimensional Biochemical Patterning of Click-Based Composite Hydrogels Via Thiolene Photopolymerization. *Biomacromolecules*. (2008); **9**(4):1084-7.

[238] Park, Y., Lutolf, M.P., Hubbell, J.A., Hunziker, E.B., and Wong, M. Bovine Primary Chondrocyte Culture in Synthetic Matrix Metalloproteinase-Sensitive

Poly(Ethylene Glycol)-Based Hydrogels as a Scaffold for Cartilage Repair. *Tissue Eng*. (2004); **10**(3-4):515-22.

[239] Hahn, M.S., Taite, L.J., Moon, J.J., Rowland, M.C., Ruffino, K.A., and West, J.L. Photolithographic Patterning of Polyethylene Glycol Hydrogels. *Biomaterials*. (2006); **27**(12):2519-24.

[240] Rivest, C., Morrison, D., Ni, B., and Rubin, J. Microscale Hydrogels for Medicine and Biology: Synthesis, Characteristics and Applications. *Journal of Mechanics of Materials and Structures*. (2007); **2**(6):1103-19.

[241] Koh, W.G., and Pishko, M.V. Fabrication of Cell-Containing Hydrogel Microstructures inside Microfluidic Devices That Can Be Used as Cell-Based Biosensors. *Anal Bioanal Chem*. (2006); **385**(8):1389-97.

[242] DeForest, C.A., Polizzotti, B.D., and Anseth, K.S. Sequential Click Reactions for Synthesizing and Patterning Three-Dimensional Cell Microenvironments. *Nat Mater*. (2009); **8**(8):659-64.

[243] Hahn, M., Miller, J., and West, J. Laser Scanning Lithography for Surface Micropatterning on Hydrogels. *Adv Mater (Weinheim, Ger)*. (2005); **17**(24):2939–42.

[244] Miller, J.S., Béthencourt, M.I., Hahn, M., Lee, T.R., and West, J.L. Laser-Scanning Lithography (Lsl) for the Soft Lithographic Patterning of Cell-Adhesive Self-Assembled Monolayers. *Biotechnology and Bioengineering*. (2006); **93**(6):1060-68.

[245] Dendukuri, D., Gu, S.S., Pregibon, D.C., Hatton, T.A., and Doyle, P.S. Stop-Flow Lithography in a Microfluidic Device. *Lab Chip*. (2007); **7**(7):818-28.

[246] Panda, P., Ali, S., Lo, E., Chung, B.G., Hatton, T.A., Khademhosseini, A., and Doyle, P.S. Stop-Flow Lithography to Generate Cell-Laden Microgel Particles. *Lab Chip*. (2008); **8**(7):1056-61.

[247] Fukuda, J., Khademhosseini, A., Yeo, Y., Yang, X., Yeh, J., Eng, G., Blumling, J., Wang, C.-F., Kohane, D.S., and Langer, R. Micromolding of Photocrosslinkable Chitosan Hydrogel for Spheroid Microarray and Co-Cultures. *Biomaterials*. (2006); **27**(30):5259-67.

[248] Liu, V., and Bhatia, S. Three-Dimensional Photopatterning of Hydrogels Containing Living Cells. *Biomedical Microdevices*. (2002); **4**(4):257-66.

[249] Hahn, M.S., Miller, J.S., and West, J.L. Three-Dimensional Biochemical and Biomechanical Patterning of Hydrogels for Guiding Cell Behavior. *Advanced Materials*. (2006); **18**(20):2679-84.

[250] Chung, S.E., Park, W., Park, H., Yu, K., Park, N., and Kwon, S. Optofluidic Maskless Lithography System for Real-Time Synthesis of Photopolymerized Microstructures in Microfluidic Channels. *Appl Phys Lett*. (2007); **91**:041106/1-06/3.

[251] Chung, K., Cho, J.K., Park, E.S., Breedveld, V., and Lu, H. Three-Dimensional in Situ Temperature Measurement in Microsystems Using Brownian Motion of Nanoparticles. *Analytical Chemistry*. (2009); **81**(3):991-99.

[252] Lee, S.A., Chung, S.E., Park, W., Lee, S.H., and Kwon, S. Three-Dimensional Fabrication of Heterogeneous Microstructures Using Soft Membrane Deformation and Optofluidic Maskless Lithography. *Lab Chip*. (2009); **9**(12):1670-75.

[253] Ling, Y., Rubin, J., Deng, Y., Huang, C., Demirci, U., Karp, J.M., and Khademhosseini, A. A Cell-Laden Microfluidic Hydrogel. *Lab on a Chip*. (2007); **7**(6):756-62.

[254] Yeh, J., Ling, Y., Karp, J.M., Gantz, J., Chandawarkar, A., Eng, G., Blumling, J., Langer, R., and Khademhosseini, A. Micromolding of Shape-Controlled, Harvestable Cell-Laden Hydrogels. *Biomaterials*. (2006); **27**(31):5391-98.

[255] Xia, Y., and Whitesides, G.M. Soft Lithography. *Annu Rev Mater Sci*. (1998); **28**:153-84.

[256] Liu Tsang, V., and Bhatia, S.N. Three-Dimensional Tissue Fabrication. *Adv Drug Deliv Rev*. (2004); **56**(11):1635-47.

[257] Xia, Y., McClelland, J.J., Gupta, R., Qin, D., Zhao, X.M., Sohn, L.L., Celotta, R.J., and Whitesides, G.M. Replica Molding Using Polymeric Materials: A Practical Step toward Nanomanufacturing. *Adv Mater (Weinheim, Ger)*. (1997); **9**(2):147-49.

[258] Albrecht, D.R., Tsang, V.L., Sah, R.L., and Bhatia, S.N. Photo- and Electropatterning of Hydrogel-Encapsulated Living Cell Arrays. *Lab on a Chip*. (2005); **5**(1):111-8.

[259] Albrecht, D.R., Underhill, G.H., Wassermann, T.B., Sah, R.L., and Bhatia, S.N. Probing the Role of Multicellular Organization in Three-Dimensional Microenvironments. *Nature Methods*. (2006); **3**(5):369-75.

[260] Anseth, K.S., Shastri, V.R., and Langer, R. Photopolymerizable Degradable Polyanhydrides with Osteocompatibility. *Nature Biotechnology*. (1999); **17**(2):156-9.

[261] Bryant, S.J., and Anseth, K.S. Hydrogel Properties Influence Ecm Production by Chondrocytes Photoencapsulated in Poly(Ethylene Glycol) Hydrogels. *Journal of Biomedical Materials Research*. (2002); **59**(1):63-72.

[262] Buxton, A.N., Zhu, J., Marchant, R., West, J.L., Yoo, J.U., and Johnstone, B. Design and Characterization of Poly(Ethylene Glycol) Photopolymerizable Semi-Interpenetrating Networks for Chondrogenesis of Human Mesenchymal Stem Cells. *Tissue Engineering*. (2007); **13**(10):2549-60.

[263] Elisseeff, J., McIntosh, W., Anseth, K., Riley, S., Ragan, P., and Langer, R. Photoencapsulation of Chondrocytes in Poly(Ethylene Oxide)-Based Semi-Interpenetrating Networks. *Journal of Biomedical Materials Research*. (2000); **51**(2):164-71.

[264] Ifkovits, J.L., and Burdick, J.A. Review: Photopolymerizable and Degradable Biomaterials for Tissue Engineering Applications. *Tissue Eng*. (2007); **13**(10):2369-85.

[265] Mann, B.K., Gobin, a.S., Tsai, a.T., Schmedlen, R.H., and West, J.L. Smooth Muscle Cell Growth in Photopolymerized Hydrogels with Cell Adhesive and Proteolytically Degradable Domains: Synthetic Ecm Analogs for Tissue Engineering. *Biomaterials*. (2001); **22**(22):3045-51.

[266] Sharma, B., Williams, C.G., Khan, M., Manson, P., and Elisseeff, J.H. In Vivo Chondrogenesis of Mesenchymal Stem Cells in a Photopolymerized Hydrogel. *Plastic and Reconstructive Surgery*. (2007); **119**(1):112-20.

[267] Underhill, G.H., Chen, A.a., Albrecht, D.R., and Bhatia, S.N. Assessment of Hepatocellular Function within Peg Hydrogels. *Biomaterials*. (2007); **28**(2):256-70.

[268] Burdick, J.A., Khademhosseini, A., and Langer, R. Fabrication of Gradient Hydrogels Using a Microfluidics/Photopolymerization Process. *Langmuir*. (2004); **20**(13):5153-56.

[269] Liu, V.A., and Bhatia, S.N. Three-Dimensional Photopatterning of Hydrogels Containing Living Cells. *Biomedical Microdevices*. (2002); **4**(4):257-66.

[270] Tsang, V.L., and Bhatia, S.N. Three-Dimensional Tissue Fabrication. *Advanced Drug Delivery Reviews*. (2004); **56**(11):1635-47.

[271] Tsang, V.L., Chen, a.a., Cho, L.M., Jadin, K.D., Sah, R.L., DeLong, S., West, J.L., and Bhatia, S.N. Fabrication of 3d Hepatic Tissues by Additive Photopatterning of Cellular Hydrogels. *The FASEB Journal*. (2007); **21**(3):790-801.

[272] Chen, C.S., Mrksich, M., Huang, S., Whitesides, G.M., and Ingber, D.E. Geometric Control of Cell Life and Death. *Science*. (1997); **276**(5317):1425-8.

[273] Choi, N.W., Cabodi, M., Held, B., Gleghorn, J.P., Bonassar, L.J., and Stroock, A.D. Microfluidic Scaffolds for Tissue Engineering. *Nature Materials*. (2007); **6**(11):908-15.

[274] Kane, R.S., Takayama, S., Ostuni, E., Ingber, D.E., and Whitesides, G.M. Patterning Proteins and Cells Using Soft Lithography. *Biomaterials*. (1999); **20**(23-24):2363-76.

[275] Khetani, S.R., and Bhatia, S.N. Engineering Tissues for in Vitro Applications. *Curr Opin Biotechnol*. (2006); **17**(5):524-31.

[276] Singhvi, R., Kumar, A., Lopez, G.P., Stephanopoulos, G.N., Wang, D.I., Whitesides, G.M., and Ingber, D.E. Engineering Cell Shape and Function. *Science*. (1994); **264**(5159):696-8.

[277] Albrecht, D.R., Underhill, G.H., Mendelson, A., and Bhatia, S.N. Multiphase Electropatterning of Cells and Biomaterials. *Lab on a Chip*. (2007); **7**(6):702-9.

[278] Hahn, M.S., Taite, L.J., Moon, J.J., Rowland, M.C., Ruffino, K.A., and West, J.L. Photolithographic Patterning of Polyethylene Glycol Hydrogels. *Biomaterials*. (2006); **27**(12):2519-24.

[279] Mapili, G., Lu, Y., Chen, S., and Roy, K. Laser-Layered Microfabrication of Spatially Patterned Functionalized Tissue-Engineering Scaffolds. *Journal of Biomedical Materials Research Part B: Applied Biomaterials*. (2005); **75**(2):414-24.

[280] Maeda, K., Onoe, H., Takinoue, M., and Takeuchi, S. Controlled Synthesis of 3d Multi-Compartmental Particles with Centrifuge-Based Microdroplet Formation from a Multi-Barrelled Capillary. *Adv Mater*. (2012); **24**(10):1340-6.

[281] Bong, K.W., Pregibon, D.C., and Doyle, P.S. Lock Release Lithography for 3d and Composite Microparticles. *Lab on a Chip*. (2009); **9**(7):863-6.

[282] Cheung, Y.K., Azeloglu, E.U., Shiovitz, D.a., Costa, K.D., Seliktar, D., and Sia, S.K. Microscale Control of Stiffness in a Cell-Adhesive Substrate Using Microfluidics-Based Lithography. *Angewandte Chemie*. (2009); **48**(39):7188-92.

[283] Cheung, Y.K., Gillette, B.M., Zhong, M., Ramcharan, S., and Sia, S.K. Direct Patterning of Composite Biocompatible Microstructures Using Microfluidics. *Lab on a Chip*. (2007); **7**(5):574-9.

[284] Chung, S.E., Park, W., Park, H., Yu, K., Park, N., and Kwon, S. Optofluidic Maskless Lithography System for Real-Time Synthesis of Photopolymerized Microstructures in Microfluidic Channels. *Applied Physics Letters*. (2007); **91**(4):041106-06.

[285] Dendukuri, D., Gu, S.S., Pregibon, D.C., Hatton, T.A., and Doyle, P.S. Stop-Flow Lithography in a Microfluidic Device. *Lab on a Chip*. (2007); **7**(7):818-28.

[286] Hwang, D.K., Oakey, J., Toner, M., Arthur, J.a., Anseth, K.S., Lee, S., Zeiger, A., J., K., and Doyle, P.S. Stop-Flow Lithography for the Production of Shape-

Evolving Degradable Microgel Particles. *Journal of the American Chemical Society*. (2009); **131**(12):4499-504.

[287] Panda, P., Ali, S., Lo, E., Chung, B.G., Hatton, T.A., Khademhosseini, A., and Doyle, P.S. Stop-Flow Lithography to Generate Cell-Laden Microgel Particles. *Lab on a Chip*. (2008); **8**(7):1056-61.

[288] Pregibon, D.C., Toner, M., and Doyle, P.S. Magnetically and Biologically Active Bead-Patterned Hydrogels. *Langmuir*. (2006); **22**(11):5122-8.

[289] Choi, N.W., Cabodi, M., Held, B., Gleghorn, J.P., Bonassar, L.J., and Stroock, A.D. Microfluidic Scaffolds for Tissue Engineering. *Nat Mater*. (2007); **6**(11):908-15.

[290] Zheng, Y., Chen, J., Craven, M., Choi, N.W., Totorica, S., Diaz-Santana, A., Kermani, P., Hempstead, B., Fischbach-Teschl, C., Lopez, J.A., and Stroock, A.D. In Vitro Microvessels for the Study of Angiogenesis and Thrombosis. *Proc Natl Acad Sci U S A*. (2012); **109**(24):9342-7.

[291] Leng, L., McAllister, A., Zhang, B., Radisic, M., and Gunther, A. Mosaic Hydrogels: One-Step Formation of Multiscale Soft Materials. *Adv Mater*. (2012); **24**(27):3650-8.

[292] Bai, L., Caplan, A., Lennon, D., and Miller, R.H. Human Mesenchymal Stem Cells Signals Regulate Neural Stem Cell Fate. *Neurochemical Research*. (2007); **32**(2):353-62.

[293] Chen, L., Tredget, E.E., Wu, P.Y.G., and Wu, Y. Paracrine Factors of Mesenchymal Stem Cells Recruit Macrophages and Endothelial Lineage Cells and Enhance Wound Healing. *PloS One*. (2008); **3**(4):e1886-e86.

[294] Ilmer, M., Karow, M., Geissler, C., Jochum, M., and Neth, P. Human Osteoblast-Derived Factors Induce Early Osteogenic Markers in Human Mesenchymal Stem Cells. *Tissue Engineering Part A*. (2009); **15**(9):2397-409.

[295] Walter, M.N.M., Wright, K.T., Fuller, H.R., MacNeil, S., and Johnson, W.E.B. Mesenchymal Stem Cell-Conditioned Medium Accelerates Skin Wound Healing: An in Vitro Study of Fibroblast and Keratinocyte Scratch Assays. *Experimental Cell Research*. (2010); **316**(7):1271-81.

[296] Maxson, S., and Burg, K.J.L. Conditioned Media Cause Increases in Select Osteogenic and Adipogenic Differentiation Markers in Mesenchymal Stem Cell Cultures. *Journal of Tissue Engineering and Regenerative Medicine*. (2008); **2**(2-3):147-54.

[297] Wang, Y., Volloch, V., Pindrus, M.A., Blasioli, D.J., Chen, J., and Kaplan, D.L. Murine Osteoblasts Regulate Mesenchymal Stem Cells Via Wnt and Cadherin

Pathways: Mechanism Depends on Cell-Cell Contact Mode. *Journal of Tissue Engineering and Regenerative Medicine*. (2007); **1**(1):39-50.

[298] Zhou, H., Mak, W., Zheng, Y., Dunstan, C.R., and Seibel, M.J. Osteoblasts Directly Control Lineage Commitment of Mesenchymal Progenitor Cells through Wnt Signaling. *The Journal of Biological Chemistry*. (2008); **283**(4):1936-45.

[299] Clabaut, A., Delplace, S., Chauveau, C., Hardouin, P., and Broux, O. Human Osteoblasts Derived from Mesenchymal Stem Cells Express Adipogenic Markers Upon Coculture with Bone Marrow Adipocytes. *Differentiation*. (2010); **80**(1):40-5.

[300] Maurin, A.C., Chavassieux, P.M., Frappart, L., Delmas, P.D., Serre, C.M., and Meunier, P.J. Influence of Mature Adipocytes on Osteoblast Proliferation in Human Primary Cocultures. *Bone*. (2000); **26**(5):485-9.

[301] Maurin, a.C., Chavassieux, P.M., and Meunier, P.J. Expression of Ppargamma and Beta/Delta in Human Primary Osteoblastic Cells: Influence of Polyunsaturated Fatty Acids. *Calcified tissue international*. (2005); **76**(5):385-92.

[302] Lecka-Czernik, B. Divergent Effects of Selective Peroxisome Proliferator-Activated Receptor- 2 Ligands on Adipocyte Versus Osteoblast Differentiation. *Endocrinology*. (2002); **143**(6):2376-84.

[303] Liu, L.-F., Shen, W.-J., Zhang, Z.H., Wang, L.J., and Kraemer, F.B. Adipocytes Decrease Runx2 Expression in Osteoblastic Cells: Roles of Pparγ and Adiponectin. *Journal of cellular physiology*. (2010); **225**(3):837-45.

[304] Maurin, a.C., Chavassieux, P.M., Vericel, E., and Meunier, P.J. Role of Polyunsaturated Fatty Acids in the Inhibitory Effect of Human Adipocytes on Osteoblastic Proliferation. *Bone*. (2002); **31**(1):260-6.

[305] Elbaz, A., Wu, X., Rivas, D., Gimble, J.M., and Duque, G. Inhibition of Fatty Acid Biosynthesis Prevents Adipocyte Lipotoxicity on Human Osteoblasts in Vitro. *Journal of Cellular and Molecular Medicine*. (2009); **14**(4):982-91.

[306] Cosgrove, B.D., Griffith, L.G., and Lauffenburger, D.A. Fusing Tissue Engineering and Systems Biology toward Fulfilling Their Promise. *Cell Mol Bioeng*. (2008); **1**(1):33-41.

[307] Nielsen, J., and Oliver, S. The Next Wave in Metabolome Analysis. *Trends Biotechnol*. (2005); **23**(11):544-6.

[308] Klingmuller, U., Bauer, A., Bohl, S., Nickel, P.J., Breitkopf, K., Dooley, S., Zellmer, S., Kern, C., Merfort, I., Sparna, T., Donauer, J., Walz, G., Geyer, M., Kreutz, C., Hermes, M., Gotschel, F., Hecht, A., Walter, D., Egger, L., Neubert, K., Borner, C., Brulport, M., Schormann, W., Sauer, C., Baumann, F., Preiss, R., MacNelly, S., Godoy, P., Wiercinska, E., Ciuclan, L., Edelmann, J., Zeilinger, K.,

Heinrich, M., Zanger, U.M., Gebhardt, R., Maiwald, T., Heinrich, R., Timmer, J., von Weizsacker, F., and Hengstler, J.G. Primary Mouse Hepatocytes for Systems Biology Approaches: A Standardized in Vitro System for Modelling of Signal Transduction Pathways. *Syst Biol (Stevenage)*. (2006); **153**(6):433-47.

[309] Albeck, J.G., MacBeath, G., White, F.M., Sorger, P.K., Lauffenburger, D.A., and Gaudet, S. Collecting and Organizing Systematic Sets of Protein Data. *Nat Rev Mol Cell Biol*. (2006); **7**(11):803-12.

[310] Aldridge, B.B., Burke, J.M., Lauffenburger, D.A., and Sorger, P.K. Physicochemical Modelling of Cell Signalling Pathways. *Nat Cell Biol*. (2006); **8**(11):1195-203.

[311] Miller-Jensen, K., Janes, K.A., Brugge, J.S., and Lauffenburger, D.A. Common Effector Processing Mediates Cell-Specific Responses to Stimuli. *Nature*. (2007); **448**(7153):604-8.

[312] Gaudet, S., Janes, K.A., Albeck, J.G., Pace, E.A., Lauffenburger, D.A., and Sorger, P.K. A Compendium of Signals and Responses Triggered by Prodeath and Prosurvival Cytokines. *Mol Cell Proteomics*. (2005); **4**(10):1569-90.

[313] Cosgrove, B.D., Alexopoulos, L.G., Hang, T.C., Hendriks, B.S., Sorger, P.K., Griffith, L.G., and Lauffenburger, D.A. Cytokine-Associated Drug Toxicity in Human Hepatocytes Is Associated with Signaling Network Dysregulation. *Mol Biosyst*. (2010); **6**(7):1195-206.

[314] Janes, K.A., and Yaffe, M.B. Data-Driven Modelling of Signal-Transduction Networks. *Nat Rev Mol Cell Biol*. (2006); **7**(11):820-8.

[315] Janes, K.A., Albeck, J.G., Gaudet, S., Sorger, P.K., Lauffenburger, D.A., and Yaffe, M.B. A Systems Model of Signaling Identifies a Molecular Basis Set for Cytokine-Induced Apoptosis. *Science*. (2005); **310**(5754):1646-53.

[316] Kharait, S., Hautaniemi, S., Wu, S., Iwabu, A., Lauffenburger, D.A., and Wells, A. Decision Tree Modeling Predicts Effects of Inhibiting Contractility Signaling on Cell Motility. *BMC Syst Biol*. (2007); **1**:9.

[317] Wu, S., Wells, A., Griffith, L.G., and Lauffenburger, D.A. Controlling Multipotent Stromal Cell Migration by Integrating "Course-Graining" Materials and "Fine-Tuning" Small Molecules Via Decision Tree Signal-Response Modeling. *Biomaterials*. (2011); **32**(30):7524-31.

[318] Hautaniemi, S., Kharait, S., Iwabu, A., Wells, A., and Lauffenburger, D.A. Modeling of Signal-Response Cascades Using Decision Tree Analysis. *Bioinformatics*. (2005); **21**(9):2027-35.

[319] Woolf, P.J., Prudhomme, W., Daheron, L., Daley, G.Q., and Lauffenburger, D.A. Bayesian Analysis of Signaling Networks Governing Embryonic Stem Cell Fate Decisions. *Bioinformatics*. (2005); **21**(6):741-53.

[320] Sachs, K., Perez, O., Pe'er, D., Lauffenburger, D.A., and Nolan, G.P. Causal Protein-Signaling Networks Derived from Multiparameter Single-Cell Data. *Science*. (2005); **308**(5721):523-9.

[321] Platt, M.O., Wilder, C.L., Wells, A., Griffith, L.G., and Lauffenburger, D.A. Multipathway Kinase Signatures of Multipotent Stromal Cells Are Predictive for Osteogenic Differentiation: Tissue-Specific Stem Cells. *Stem Cells*. (2009); **27**(11):2804-14.

[322] Guo, G., Huss, M., Tong, G.Q., Wang, C., Li Sun, L., Clarke, N.D., and Robson, P. Resolution of Cell Fate Decisions Revealed by Single-Cell Gene Expression Analysis from Zygote to Blastocyst. *Dev Cell*. (2010); **18**(4):675-85.

[323] Lenas, P., Moos, M., Jr., and Luyten, F. Developmental Engineering: A New Paradigm for the Design and Manufacturing of Cell Based Products. Part I: From Three-Dimensional Cell Growth to Biomimetics of in Vivo Development. *Tiss Eng B Rev*. (2009); **15**(4):381-94.

[324] Lenas, P., Moos, M., and Luyten, F.P. Developmental Engineering: A New Paradigm for the Design and Manufacturing of Cell-Based Products. Part Ii: From Genes to Networks: Tissue Engineering from the Viewpoint of Systems Biology and Network Science. *Tissue Eng Part B Rev*. (2009); **15**(4):395-422.

[325] Kirouac, D.C., Ito, C., Csaszar, E., Roch, A., Yu, M., Sykes, E.A., Bader, G.D., and Zandstra, P.W. Dynamic Interaction Networks in a Hierarchically Organized Tissue. *Mol Syst Biol*. (2010); **6**:417.

[326] Farahat, W.A., Wood, L.B., Zervantonakis, I.K., Schor, A., Ong, S., Neal, D., Kamm, R.D., and Asada, H.H. Ensemble Analysis of Angiogenic Growth in Three-Dimensional Microfluidic Cell Cultures. *PloS one*. (2012); **7**(5):e37333.

[327] Parsa, H., Upadhyay, R., and Sia, S.K. Uncovering the Behaviors of Individual Cells within a Multicellular Microvascular Community. *Proc Natl Acad Sci USA*. (2011); **108**(12):5133-38.

[328] Watt, F.M., and Hogan, B.L. Out of Eden: Stem Cells and Their Niches. *Science*. (2000); **287**(5457):1427-30.

[329] Baksh, D., Song, L., and Tuan, R.S. Adult Mesenchymal Stem Cells: Characterization, Differentiation, and Application in Cell and Gene Therapy. *J Cell Mol Med*. (2004); **8**(3):301-16.

[330] Hamilton, S.K., Lu, H., and Temenoff, J.S. Micropatterned Hydrogels for Stem Cell Culture. In: Roy, K., editor. *Biomaterials as Stem Cell Niche*. New York: Springer; In Press.

[331] Lenas, P., Moos, M., Jr., and Luyten, F. Developmental Engineering: A New Paradigm for the Design and Manufacturing of Cell Based Products Part Ii. From Genes to Networks: Tissue Engineering from the Viewpoint of Systems Biology and Network Science. *Tiss Eng B Rev*. (2009); **15**(4):395-422.

[332] Place, E.S., Evans, N.D., and Stevens, M.M. Complexity in Biomaterials for Tissue Engineering. *Nat Mater*. (2009); **8**(6):457-70.

[333] Lund, A.W., Yener, B., Stegemann, J.P., and Plopper, G.E. The Natural and Engineered 3d Microenvironment as a Regulatory Cue During Stem Cell Fate Determination. *Tissue Eng Part B Rev*. (2009); **15**(3):371-80.

[334] Anseth, K.S., Bowman, C.N., and Brannon-Peppas, L. Mechanical Properties of Hydrogels and Their Experimental Determination. *Biomaterials*. (1996); **17**(17):1647-57.

[335] Peppas, N., Hilt, J., Khademhosseini, A., and Langer, R. Hydrogels in Biology and Medicine: From Molecular Principles to Bionanotechnology. *Adv Mater*. (2006); **18**:1345-60.

[336] Brink, K.S., Yang, P.J., and Temenoff, J.S. Degradative Properties and Cytocompatibility of a Mixed-Mode Hydrogel Containing Oligo[Poly(Ethylene Glycol)Fumarate] and Poly(Ethylene Glycol)Dithiol. *Acta Biomater*. (2009); **5**(2):570-79.

[337] Holland, T.A., Bodde, E.W.H., Baggett, L.S., Tabata, Y., Mikos, A.G., and Jansen, J.A. Osteochondral Repair in the Rabbit Model Utilizing Bilayered, Degradable Oligo(Poly(Ethylene Glycol) Fumarate) Hydrogel Scaffolds. *J Biomed Mater Res A*. (2005); **75**(1):156-67.

[338] Park, H., Temenoff, J.S., Holland, T.A., Tabata, Y., and Mikos, A.G. Delivery of Tgf-Beta1 and Chondrocytes Via Injectable, Biodegradable Hydrogels for Cartilage Tissue Engineering Applications. *Biomaterials*. (2005); **26**(34):7095-103.

[339] Temenoff, J.S., Park, H., Jabbari, E., Sheffield, T.L., LeBaron, R.G., Ambrose, C.G., and Mikos, A.G. In Vitro Osteogenic Differentiation of Marrow Stromal Cells Encapsulated in Biodegradable Hydrogels. *J Biomed Mater Res A*. (2004); **70**(2):235-44.

[340] Shin, H., Jo, S., and Mikos, A.G. Modulation of Marrow Stromal Osteoblast Adhesion on Biomimetic Oligo[Poly(Ethylene Glycol) Fumarate] Hydrogels Modified with Arg-Gly-Asp Peptides and a Poly(Ethylene Glycol) Spacer. *J Biomed Mater Res*. (2002); **61**(2):169-79.

[341] Temenoff, J.S., Athanasiou, K.A., LeBaron, R.G., and Mikos, A.G. Effect of Poly(Ethylene Glycol) Molecular Weight on Tensile and Swelling Properties of Oligo(Poly(Ethylene Glycol) Fumarate) Hydrogels for Cartilage Tissue Engineering. *J Biomed Mater Res*. (2002); **59**(3):429-37.

[342] Burdick, J.A., Khademhosseini, A., and Langer, R. Fabrication of Gradient Hydrogels Using a Microfluidics/Photopolymerization Process. *Langmuir*. (2004); **20**(13):5153-6.

[343] Tsang, V.L., Chen, A.A., Cho, L.M., Jadin, K.D., Sah, R.L., DeLong, S., West, J.L., and Bhatia, S.N. Fabrication of 3d Hepatic Tissues by Additive Photopatterning of Cellular Hydrogels. *FASEB J*. (2007); **21**(3):790-801.

[344] Cheung, Y.K., Azeloglu, E.U., Shiovitz, D.A., Costa, K.D., Seliktar, D., and Sia, S.K. Microscale Control of Stiffness in a Cell-Adhesive Substrate Using Microfluidics-Based Lithography. *Angew Chem Int Ed Engl*. (2009); **48**(39):7188-92.

[345] Jo, S., Shin, H., Shung, A.K., Fisher, J.P., and Mikos, A.G. Synthesis and Characterization of Oligo(Poly(Ethylene Glycol) Fumarate) Macromer. *Macromolecules*. (2001); **34**(9):2839-44.

[346] McDonald, J.C., and Whitesides, G.M. Poly(Dimethylsiloxane) as a Material for Fabricating Microfluidic Devices. *Acc Chem Res*. (2002); **35**(7):491-9.

[347] Desai, S.P., Freeman, D.M., and Voldman, J. Plastic Masters-Rigid Templates for Soft Lithography. *Lab Chip*. (2009); **9**(11):1631-37.

[348] Jackman, R.J., Duffy, D.C., Cherniavskaya, O., and Whitesides, G.M. Using Elastomeric Membranes as Dry Resists and for Dry Lift-Off. *Langmuir*. (1999); **15**(8):2973-84.

[349] Ahn, S.J., Costa, J., and Emanuel, J.R. Picogreen Quantitation of DNA: Effective Evaluation of Samples Pre- or Post-Pcr. *Nucleic Acids Res*. (1996); **24**(13):2623-5.

[350] Bryant, S.J., Nuttelman, C.R., and Anseth, K.S. Cytocompatibility of Uv and Visible Light Photoinitiating Systems on Cultured Nih/3t3 Fibroblasts in Vitro. *J Biomater Sci, Polym Ed*. (2000); **11**(5):439-57.

[351] Kilambi, H., Reddy, S.K., Schneidewind, L., Stansbury, J.W., and Bowman, C.N. Copolymerization and Dark Polymerization Studies for Photopolymerization of Novel Acrylic Monomers. *Polymer*. (2007); **48**(7).

[352] Lovell, L.G., Newman, S.M., and Bowman, C.N. The Effects of Light Intensity, Temperature, and Comonomer Composition on the Polymerization Behavior of Dimethacrylate Dental Resins. *J Dent Res*. (1999); **78**(8):1469-76.

[353] Sharifi, S., Mirzadeh, H., Imani, M., Atai, M., and Ziaee, F. Photopolymerization and Shrinkage Kinetics of in Situ Crosslinkable N-Vinyl-Pyrrolidone/Poly(-Caprolactone Fumarate) Networks. *J Biomed Mater Res A*. (2007); **84A**(2):545-56.

[354] Cheung, Y.K., Gillette, B.M., Zhong, M., Ramcharan, S., and Sia, S.K. Direct Patterning of Composite Biocompatible Microstructures Using Microfluidics. *Lab Chip*. (2007); **7**(5):574-79.

[355] Bryant, S.J., Anseth, K.S., Lee, D.A., and Bader, D.L. Crosslinking Density Influences the Morphology of Chondrocytes Photoencapsulated in Peg Hydrogels During the Application of Compressive Strain. *J Orthop Res*. (2004); **22**(5):1143-9.

[356] Bryant, S.J., Chowdhury, T.T., Lee, D.A., Bader, D.L., and Anseth, K.S. Crosslinking Density Influences Chondrocyte Metabolism in Dynamically Loaded Photocrosslinked Poly(Ethylene Glycol) Hydrogels. *Ann Biomed Eng*. (2004); **32**(3):407-17.

[357] Bryant, S.J., and Anseth, K.S. Hydrogel Properties Influence Ecm Production by Chondrocytes Photoencapsulated in Poly(Ethylene Glycol) Hydrogels. *J Biomed Mater Res*. (2002); **59**(1):63-72.

[358] Ryter, S.W., Kim, H.P., Hoetzel, A., Park, J.W., Nakahira, K., Wang, X., and Choi, A.M. Mechanisms of Cell Death in Oxidative Stress. *Antioxid Redox Signal*. (2007); **9**(1):49-89.

[359] Yang, P.J., and Temenoff, J.S. Effect of Tethered Rgd on Stem Cell Retention in Fumarate Hydrogels. World Biomaterials Congress. Amsterdam, Netherlands2008.

[360] Daley, G.Q. Stem Cells: Roadmap to the Clinic. *J Clin Invest*. (2010); **120**(1):8-10.

[361] Polykandriotis, E., Popescu, L.M., and Horch, R.E. Regenerative Medicine: Then and Now--an Update of Recent History into Future Possibilities. *J Cell Mol Med*. (2010); **14**(10):2350-8.

[362] Hammoudi, T.M., Lu, H., and Temenoff, J.S. Long-Term Spatially Defined Coculture within Three-Dimensional Photopatterned Hydrogels. *Tissue Eng C Methods*. (2010); **16**(6):1621-8.

[363] Zhou, H., Mak, W., Zheng, Y., Dunstan, C.R., and Seibel, M.J. Osteoblasts Directly Control Lineage Commitment of Mesenchymal Progenitor Cells through Wnt Signaling. *J Biol Chem*. (2008); **283**(4):1936-45.

[364] Doroski, D.M., Levenston, M.E., and Temenoff, J.S. Cyclic Tensile Culture Promotes Fibroblastic Differentiation of Marrow Stromal Cells Encapsulated in Poly(Ethylene Glycol)-Based Hydrogels. *Tissue Eng A*. (2010); **16**(11):3457-66.

[365] Colter, D.C., Sekiya, I., and Prockop, D.J. Identification of a Subpopulation of Rapidly Self-Renewing and Multipotential Adult Stem Cells in Colonies of Human Marrow Stromal Cells. *Proc Natl Acad Sci USA*. (2001); **98**(14):7841-5.

[366] Vandesompele, J., De Preter, K., Pattyn, F., Poppe, B., Van Roy, N., De Paepe, A., and Speleman, F. Accurate Normalization of Real-Time Quantitative Rt-Pcr Data by Geometric Averaging of Multiple Internal Control Genes. *Genome Biol*. (2002); **3**(7):1-12.

[367] Fink, T., Lund, P., Pilgaard, L., Rasmussen, J.G., Duroux, M., and Zachar, V. Instability of Standard Pcr Reference Genes in Adipose-Derived Stem Cells During Propagation, Differentiation and Hypoxic Exposure. *BMC Mol Biol*. (2008); **9**:98.

[368] Ruijter, J.M., Ramakers, C., Hoogaars, W.M., Karlen, Y., Bakker, O., van den Hoff, M.J., and Moorman, A.F. Amplification Efficiency: Linking Baseline and Bias in the Analysis of Quantitative Pcr Data. *Nucleic Acids Res*. (2009); **37**(6):e45.

[369] Yang, C., Jenkins, L., and Burg, K.J.L. Adapted Cryosectioning Method for Hydrogels Used in Regenerative Medicine. *J Histotechnol*. (2007); **30**(3):185-85.

[370] Eriksson, L., Johansson, E., Kettaneh-Wold, N., Trygg, J., Wikstrom, C., and Wold, S. *Multi- and Megavariate Data Analysis. Part I: Basic Principles and Applications*. 2nd ed. Umea, Sweden: Umetrics AB; 2006.

[371] Martens, H., and Martens, M. *Multivariate Analysis of Quality: An Introduction*. Sussex, England, UK: John Wiley & Sons, Ltd.; 2001.

[372] Rivet, C.A., Hill, A.S., Lu, H., and Kemp, M.L. Predicting Cytotoxic T-Cell Age from Multivariate Analysis of Static and Dynamic Biomarkers. *Mol Cell Proteomics*. (2011); **10**(3):M110.003921.

[373] Henke, M., Brandl, F., Goepferich, A.M., and Tessmar, J.K. Size-Dependent Release of Fluorescent Macromolecules and Nanoparticles from Radically Cross-Linked Hydrogels. *Eur J Pharm Biopharm*. (2010); **74**(2):184-92.

[374] Nuttelman, C.R., Tripodi, M.C., and Anseth, K.S. Synthetic Hydrogel Niches That Promote Hmsc Viability. *Matrix Biol*. (2005); **24**(3):208-18.

[375] Legant, W.R., Miller, J.S., Blakely, B.L., Cohen, D.M., Genin, G.M., and Chen, C.S. Measurement of Mechanical Tractions Exerted by Cells in Three-Dimensional Matrices. *Nat Methods*. (2010); **7**(12):969-71.

[376] Legant, W.R., Pathak, A., Yang, M.T., Deshpande, V.S., McMeeking, R.M., and Chen, C.S. Microfabricated Tissue Gauges to Measure and Manipulate Forces from 3d Microtissues. *Proceedings of the National Academy of Sciences of the United States of America*. (2009); **106**(25):10097-102.

[377] Barabasi, A.L., Gulbahce, N., and Loscalzo, J. Network Medicine: A Network-Based Approach to Human Disease. *Nat Rev Genet*. (2011); **12**(1):56-68.

[378] Vidal, M., Cusick, M.E., and Barabasi, A.L. Interactome Networks and Human Disease. *Cell*. (2011); **144**(6):986-98.

[379] Vidal, M. The Reverse Two-Hybrid System. In: Bartels, P.,Fields, S., editors. *The Yeast Two-Hybrid System*. New York: Oxford University Press; 1997. p. 109-47.

[380] Ravasi, T., Suzuki, H., Cannistraci, C.V., Katayama, S., Bajic, V.B., Tan, K., Akalin, A., Schmeier, S., Kanamori-Katayama, M., Bertin, N., Carninci, P., Daub, C.O., Forrest, A.R., Gough, J., Grimmond, S., Han, J.H., Hashimoto, T., Hide, W., Hofmann, O., Kamburov, A., Kaur, M., Kawaji, H., Kubosaki, A., Lassmann, T., van Nimwegen, E., MacPherson, C.R., Ogawa, C., Radovanovic, A., Schwartz, A., Teasdale, R.D., Tegner, J., Lenhard, B., Teichmann, S.A., Arakawa, T., Ninomiya, N., Murakami, K., Tagami, M., Fukuda, S., Imamura, K., Kai, C., Ishihara, R., Kitazume, Y., Kawai, J., Hume, D.A., Ideker, T., and Hayashizaki, Y. An Atlas of Combinatorial Transcriptional Regulation in Mouse and Man. *Cell*. (2010); **140**(5):744-52.

[381] Ideker, T., and Sharan, R. Protein Networks in Disease. *Genome Res*. (2008); **18**(4):644-52.

[382] Boone, C., Bussey, H., and Andrews, B.J. Exploring Genetic Interactions and Networks with Yeast. *Nat Rev Genet*. (2007); **8**(6):437-49.

[383] Stuart, J.M., Segal, E., Koller, D., and Kim, S.K. A Gene-Coexpression Network for Global Discovery of Conserved Genetic Modules. *Science*. (2003); **302**(5643):249-55.

[384] Reynolds, A., Leake, D., Boese, Q., Scaringe, S., Marshall, W.S., and Khvorova, A. Rational Sirna Design for Rna Interference. *Nat Biotechnol*. (2004); **22**(3):326-30.

[385] Jeong, H., Tombor, B., Albert, R., Oltvai, Z.N., and Barabasi, A.L. The Large-Scale Organization of Metabolic Networks. *Nature*. (2000); **407**(6804):651-4.

[386] Stelzl, U., Worm, U., Lalowski, M., Haenig, C., Brembeck, F.H., Goehler, H., Stroedicke, M., Zenkner, M., Schoenherr, A., Koeppen, S., Timm, J., Mintzlaff, S., Abraham, C., Bock, N., Kietzmann, S., Goedde, A., Toksoz, E., Droege, A., Krobitsch, S., Korn, B., Birchmeier, W., Lehrach, H., and Wanker, E.E. A Human Protein-Protein Interaction Network: A Resource for Annotating the Proteome. *Cell*. (2005); **122**(6):957-68.

[387] Hammoudi, T.M., Rivet, C.A., Kemp, M.L., Lu, H., and Temenoff, J.S. Three-Dimensional in Vitro Tri-Culture Platform to Investigate Effects of Crosstalk between Mesenchymal Stem Cells, Osteoblasts, and Adipocytes. *Tissue Eng A*. (2012).

[388] Lage, K., Mollgard, K., Greenway, S., Wakimoto, H., Gorham, J.M., Workman, C.T., Bendsen, E., Hansen, N.T., Rigina, O., Roque, F.S., Wiese, C., Christoffels, V.M., Roberts, A.E., Smoot, L.B., Pu, W.T., Donahoe, P.K., Tommerup, N., Brunak, S., Seidman, C.E., Seidman, J.G., and Larsen, L.A. Dissecting Spatio-Temporal Protein Networks Driving Human Heart Development and Related Disorders. *Mol Syst Biol*. (2010); **6**:381.

[389] Lage, K., Hansen, N.T., Karlberg, E.O., Eklund, A.C., Roque, F.S., Donahoe, P.K., Szallasi, Z., Jensen, T.S., and Brunak, S. A Large-Scale Analysis of Tissue-Specific Pathology and Gene Expression of Human Disease Genes and Complexes. *Proc Natl Acad Sci U S A*. (2008); **105**(52):20870-5.

[390] Reverter, A., Ingham, A., and Dalrymple, B.P. Mining Tissue Specificity, Gene Connectivity and Disease Association to Reveal a Set of Genes That Modify the Action of Disease Causing Genes. *BioData Min*. (2008); **1**(1):8.

[391] Luo, X.H., Guo, L.J., Yuan, L.Q., Xie, H., Zhou, H.D., Wu, X.P., and Liao, E.Y. Adiponectin Stimulates Human Osteoblasts Proliferation and Differentiation Via the Mapk Signaling Pathway. *Exp Cell Res*. (2005); **309**(1):99-109.

[392] Ferron, M., Wei, J., Yoshizawa, T., Del Fattore, A., DePinho, R.A., Teti, A., Ducy, P., and Karsenty, G. Insulin Signaling in Osteoblasts Integrates Bone Remodeling and Energy Metabolism. *Cell*. (2010); **142**(2):296-308.

[393] Fulzele, K., Riddle, R.C., DiGirolamo, D.J., Cao, X., Wan, C., Chen, D., Faugere, M.C., Aja, S., Hussain, M.A., Bruning, J.C., and Clemens, T.L. Insulin Receptor Signaling in Osteoblasts Regulates Postnatal Bone Acquisition and Body Composition. *Cell*. (2010); **142**(2):309-19.

[394] West, J.L., and Hubbell, J.A. Polymeric Biomaterials with Degradation Sites for Proteases Involved in Cell Migration. *Macromolecules*. (1999); **32**(1):241-44.

[395] Shin, H., Jo, S., and Mikos, A.G. Modulation of Marrow Stromal Osteoblast Adhesion on Biomimetic Oligo [Poly (Ethylene Glycol) Fumarate] Hydrogels Modified with Arg-Gly-Asp Peptides and a Poly (Ethylene Glycol) Spacer. *J Biomed Mater Res A*. (2002); **61**(2):169-79.

[396] Box, G.E.P., and Cox, D.R. An Analysis of Transformations. *J Roy Stat Soc B*. (1964); **26**(2):211-52.

[397] Box, G.E.P., and Cox, D.R. An Analysis of Transformations Revisited, Rebutted. *J Am Stat Assoc*. (1982); **77**(377):209-10.

[398] Jackson, J.E. *A User's Guide to Principal Components*. New York: John Wiley; 2003.

[399] Wikstrom, C., Albano, C., Eriksson, L., Friden, H., Johansson, E., Nordahl, A., Rannar, S., Sandberg, M., Kettaneh-Wold, N., and Wold, S. Multivariate Process

and Quality Monitoring Applied to an Electrolysis Process Part I. Process Supervision with Multivariate Control Charts. *Chemometr Intell Lab*. (1998); **42**(1-2):221-31.

[400] Wold, S. Cross-Validatory Estimation of Number of Components in Factor and Principal Components Models. *Technometrics*. (1978); **20**(4):397-405.

[401] Martens, H., and Martens, M. Modified Jack-Knife Estimation of Parameter Uncertainty in Bilinear Modelling by Partial Least Squares Regression (Plsr). *Food Qual Prefer*. (2000); **11**(1-2):5-16.

[402] Patterson, J., and Hubbell, J.A. Enhanced Proteolytic Degradation of Molecularly Engineered Peg Hydrogels in Response to Mmp-1 and Mmp-2. *Biomaterials*. (2010); **31**(30):7836-45.

[403] Ideker, T., and Krogan, N.J. Differential Network Biology. *Mol Syst Biol*. (2012); **8**:565.

[404] Ducy, P., Zhang, R., Geoffroy, V., Ridall, A.L., and Karsenty, G. Osf2/Cbfa1: A Transcriptional Activator of Osteoblast Differentiation. *Cell*. (1997); **89**(5):747-54.

[405] Hwang, C.S., Loftus, T.M., Mandrup, S., and Lane, M.D. Adipocyte Differentiation and Leptin Expression. *Annu Rev Cell Dev Biol*. (1997); **13**:231-59.

[406] Kurz, D.J., Decary, S., Hong, Y., and Erusalimsky, J.D. Senescence-Associated (Beta)-Galactosidase Reflects an Increase in Lysosomal Mass During Replicative Ageing of Human Endothelial Cells. *J Cell Sci*. (2000); **113 (Pt 20)**:3613-22.

[407] da Silva Meirelles, L., Fontes, A.M., Covas, D.T., and Caplan, A.I. Mechanisms Involved in the Therapeutic Properties of Mesenchymal Stem Cells. *Cytokine Growth Factor Rev*. (2009); **20**(5-6):419-27.

[408] Salem, H.K., and Thiemermann, C. Mesenchymal Stromal Cells: Current Understanding and Clinical Status. *Stem Cells*. (2010); **28**(3):585-96.

[409] Lee, R.H., Oh, J.Y., Choi, H., and Bazhanov, N. Therapeutic Factors Secreted by Mesenchymal Stromal Cells and Tissue Repair. *J Cell Biochem*. (2011); **112**(11):3073-8.

[410] Almeida, M. Unraveling the Role of Foxos in Bone--Insights from Mouse Models. *Bone*. (2011); **49**(3):319-27.

[411] Cortizo, A.M., Sedlinsky, C., McCarthy, A.D., Blanco, A., and Schurman, L. Osteogenic Actions of the Anti-Diabetic Drug Metformin on Osteoblasts in Culture. *Eur J Pharmacol*. (2006); **536**(1-2):38-46.

[412] Zhen, D., Chen, Y., and Tang, X. Metformin Reverses the Deleterious Effects of High Glucose on Osteoblast Function. *J Diabetes Complications*. (2010); **24**(5):334-44.

[413] Gao, Y., Xue, J., Li, X., Jia, Y., and Hu, J. Metformin Regulates Osteoblast and Adipocyte Differentiation of Rat Mesenchymal Stem Cells. *J Pharm Pharmacol*. (2008); **60**(12):1695-700.

[414] Molinuevo, M.S., Schurman, L., McCarthy, A.D., Cortizo, A.M., Tolosa, M.J., Gangoiti, M.V., Arnol, V., and Sedlinsky, C. Effect of Metformin on Bone Marrow Progenitor Cell Differentiation: In Vivo and in Vitro Studies. *J Bone Miner Res*. (2010); **25**(2):211-21.

[415] Jang, W.G., Kim, E.J., Bae, I.H., Lee, K.N., Kim, Y.D., Kim, D.K., Kim, S.H., Lee, C.H., Franceschi, R.T., Choi, H.S., and Koh, J.T. Metformin Induces Osteoblast Differentiation Via Orphan Nuclear Receptor Shp-Mediated Transactivation of Runx2. *Bone*. (2011); **48**(4):885-93.

[416] Bilik, D., McEwen, L.N., Brown, M.B., Pomeroy, N.E., Kim, C., Asao, K., Crosson, J.C., Duru, O.K., Ferrara, A., Hsiao, V.C., Karter, A.J., Lee, P.G., Marrero, D.G., Selby, J.V., Subramanian, U., and Herman, W.H. Thiazolidinediones and Fractures: Evidence from Translating Research into Action for Diabetes. *J Clin Endocrinol Metab*. (2010); **95**(10):4560-5.

[417] Habib, Z.A., Havstad, S.L., Wells, K., Divine, G., Pladevall, M., and Williams, L.K. Thiazolidinedione Use and the Longitudinal Risk of Fractures in Patients with Type 2 Diabetes Mellitus. *J Clin Endocrinol Metab*. (2010); **95**(2):592-600.

[418] Meier, C., Kraenzlin, M.E., Bodmer, M., Jick, S.S., Jick, H., and Meier, C.R. Use of Thiazolidinediones and Fracture Risk. *Arch Intern Med*. (2008); **168**(8):820-5.

[419] Yaturu, S., Bryant, B., and Jain, S.K. Thiazolidinedione Treatment Decreases Bone Mineral Density in Type 2 Diabetic Men. *Diabetes Care*. (2007); **30**(6):1574-6.

[420] Grey, A., Bolland, M., Gamble, G., Wattie, D., Horne, A., Davidson, J., and Reid, I.R. The Peroxisome Proliferator-Activated Receptor-Gamma Agonist Rosiglitazone Decreases Bone Formation and Bone Mineral Density in Healthy Postmenopausal Women: A Randomized, Controlled Trial. *J Clin Endocrinol Metab*. (2007); **92**(4):1305-10.

[421] Egger, M., Davey Smith, G., Stettler, C., and Diem, P. Risk of Adverse Effects of Intensified Treatment in Insulin-Dependent Diabetes Mellitus: A Meta-Analysis. *Diabet Med*. (1997); **14**(11):919-28.

[422] Huang, P.H., Mukasa, A., Bonavia, R., Flynn, R.A., Brewer, Z.E., Cavenee, W.K., Furnari, F.B., and White, F.M. Quantitative Analysis of Egfrviii Cellular Signaling Networks Reveals a Combinatorial Therapeutic Strategy for Glioblastoma. *Proc Natl Acad Sci U S A*. (2007); **104**(31):12867-72.

[423] Pawson, T., and Linding, R. Network Medicine. *FEBS Lett*. (2008); **582**(8):1266-70.

[424] Erler, J.T., and Linding, R. Network-Based Drugs and Biomarkers. *J Pathol*. (2010); **220**(2):290-6.

[425] Lee, M.J., Ye, A.S., Gardino, A.K., Heijink, A.M., Sorger, P.K., MacBeath, G., and Yaffe, M.B. Sequential Application of Anticancer Drugs Enhances Cell Death by Rewiring Apoptotic Signaling Networks. *Cell*. (2012); **149**(4):780-94.

[426] Gregory, C.A., Ylostalo, J., and Prockop, D.J. Adult Bone Marrow Stem/Progenitor Cells (Mscs) Are Preconditioned by Microenvironmental "Niches" in Culture: A Two-Stage Hypothesis for Regulation of Msc Fate. *Sci STKE*. (2005); **2005**(294):pe37.

[427] Losick, R., and Desplan, C. Stochasticity and Cell Fate. *Science*. (2008); **320**(5872):65-8.

[428] Russell, K.C., Phinney, D.G., Lacey, M.R., Barrilleaux, B.L., Meyertholen, K.E., and O'Connor, K.C. In Vitro High-Capacity Assay to Quantify the Clonal Heterogeneity in Trilineage Potential of Mesenchymal Stem Cells Reveals a Complex Hierarchy of Lineage Commitment. *Stem Cells*. (2010); **28**(4):788-98.

[429] Pevsner-Fischer, M., Levin, S., and Zipori, D. The Origins of Mesenchymal Stromal Cell Heterogeneity. *Stem Cell Rev*. (2011); **7**(3):560-8.

[430] Krinner, A., Hoffmann, M., Loeffler, M., Drasdo, D., and Galle, J. Individual Fates of Mesenchymal Stem Cells in Vitro. *BMC Syst Biol*. (2010); **4**:73.

[431] Gaudet, S. Connecting Cell Fate Decision Networks in Hematopoeisis from the Outside In. *Mol Syst Biol*. (2010); **6**:418.

[432] Rouault, H., and Hakim, V. Different Cell Fates from Cell-Cell Interactions: Core Architectures of Two-Cell Bistable Networks. *Biophys J*. (2012); **102**(3):417-26.

[433] Kitano, H. Systems Biology: A Brief Overview. *Science*. (2002); **295**(5560):1662-4.

[434] Csete, M., and Doyle, J. Bow Ties, Metabolism and Disease. *Trends Biotechnol*. (2004); **22**(9):446-50.

[435] Csete, M.E., and Doyle, J.C. Reverse Engineering of Biological Complexity. *Science*. (2002); **295**(5560):1664-9.

[436] Huang, S. Reprogramming Cell Fates: Reconciling Rarity with Robustness. *Bioessays*. (2009); **31**(5):546-60.

[437] Paszek, P., Ryan, S., Ashall, L., Sillitoe, K., Harper, C.V., Spiller, D.G., Rand, D.A., and White, M.R. Population Robustness Arising from Cellular Heterogeneity. *Proc Natl Acad Sci U S A*. (2010); **107**(25):11644-9.

[438] Huang, S., and Wikswo, J. Dimensions of Systems Biology. In: Amara, S.G., Bamberg, E., Gudermann, T., Hebert, S.C., Jahn, R., Lederer, W.J., Lill, R., Miyajima, A.,Offermanns, S., editors. *Reviews of Physiology, Biochemistry and Pharmacology*. New York: Springer; 2007.

[439] Votteler, M., Kluger, P.J., Walles, H., and Schenke-Layland, K. Stem Cell Microenvironments--Unveiling the Secret of How Stem Cell Fate Is Defined. *Macromol Biosci*. (2010); **10**(11):1302-15.

[440] Kumar, D., Srikanth, R., Ahlfors, H., Lahesmaa, R., and Rao, K.V. Capturing Cell-Fate Decisions from the Molecular Signatures of a Receptor-Dependent Signaling Response. *Mol Syst Biol*. (2007); **3**:150.

[441] Strogatz, S.H. Exploring Complex Networks. *Nature*. (2001); **410**(6825):268-76.

[442] Liu, Y.Y., Slotine, J.J., and Barabasi, A.L. Controllability of Complex Networks. *Nature*. (2011); **473**(7346):167-73.

[443] Freeman, M. Feedback Control of Intercellular Signalling in Development. *Nature*. (2000); **408**(6810):313-9.

[444] Frankenstein, Z., Alon, U., and Cohen, I.R. The Immune-Body Cytokine Network Defines a Social Architecture of Cell Interactions. *Biol Direct*. (2006); **1**:32.

[445] Seto, S.P., Casas, M.E., and Temenoff, J.S. Differentiation of Mesenchymal Stem Cells in Heparin-Containing Hydrogels Via Coculture with Osteoblasts. *Cell Tissue Res*. (2012); **347**(3):589-601.

[446] Chung, C., and Burdick, J.A. Influence of Three-Dimensional Hyaluronic Acid Microenvironments on Mesenchymal Stem Cell Chondrogenesis. *Tissue Eng Part A*. (2009); **15**(2):243-54.

[447] Burdick, J.A., and Vunjak-Novakovic, G. Engineered Microenvironments for Controlled Stem Cell Differentiation. *Tissue Eng Part A*. (2009); **15**(2):205-19.

[448] Castano-Izquierdo, H., Alvarez-Barreto, J., van den Dolder, J., Jansen, J.A., Mikos, A.G., and Sikavitsas, V.I. Pre-Culture Period of Mesenchymal Stem Cells in Osteogenic Media Influences Their in Vivo Bone Forming Potential. *J Biomed Mater Res A*. (2007); **82**(1):129-38.

[449] Farrell, E., Both, S.K., Odorfer, K.I., Koevoet, W., Kops, N., O'Brien, F.J., Baatenburg de Jong, R.J., Verhaar, J.A., Cuijpers, V., Jansen, J., Erben, R.G., and van Osch, G.J. In-Vivo Generation of Bone Via Endochondral Ossification by in-

Vitro Chondrogenic Priming of Adult Human and Rat Mesenchymal Stem Cells. *BMC Musculoskelet Disord*. (2011); **12**:31.

[450] Jones, D.L., and Wagers, A.J. No Place Like Home: Anatomy and Function of the Stem Cell Niche. *Nat Rev Mol Cell Biol*. (2008); **9**(1):11-21.

[451] Becerra, J., Santos-Ruiz, L., Andrades, J.A., and Mari-Beffa, M. The Stem Cell Niche Should Be a Key Issue for Cell Therapy in Regenerative Medicine. *Stem Cell Rev*. (2011); **7**(2):248-55.

[452] Russell, K.C., Lacey, M.R., Gilliam, J.K., Tucker, H.A., Phinney, D.G., and O'Connor, K.C. Clonal Analysis of the Proliferation Potential of Human Bone Marrow Mesenchymal Stem Cells as a Function of Potency. *Biotechnol Bioeng*. (2011); **108**(11):2716-26.

[453] Jee, W.S., and Yao, W. Overview: Animal Models of Osteopenia and Osteoporosis. *J Musculoskelet Neuronal Interact*. (2001); **1**(3):193-207.

[454] Turner, R.T., Maran, A., Lotinun, S., Hefferan, T., Evans, G.L., Zhang, M., and Sibonga, J.D. Animal Models for Osteoporosis. *Rev Endocr Metab Disord*. (2001); **2**(1):117-27.

[455] Wagers, A.J., and Weissman, I.L. Plasticity of Adult Stem Cells. *Cell*. (2004); **116**(5):639-48.

[456] Zipori, D. The Stem State: Plasticity Is Essential, Whereas Self-Renewal and Hierarchy Are Optional. *Stem Cells*. (2005); **23**(6):719-26.

[457] Delorme, B., Ringe, J., Pontikoglou, C., Gaillard, J., Langonne, A., Sensebe, L., Noel, D., Jorgensen, C., Haupl, T., and Charbord, P. Specific Lineage-Priming of Bone Marrow Mesenchymal Stem Cells Provides the Molecular Framework for Their Plasticity. *Stem Cells*. (2009); **27**(5):1142-51.

[458] Collier, J.H., and Segura, T. Evolving the Use of Peptides as Components of Biomaterials. *Biomaterials*. (2011); **32**(18):4198-204.

[459] Iha, R.K., Wooley, K.L., Nystrom, A.M., Burke, D.J., Kade, M.J., and Hawker, C.J. Applications of Orthogonal "Click" Chemistries in the Synthesis of Functional Soft Materials. *Chem Rev*. (2009); **109**(11):5620-86.

[460] Tibbitt, M.W., and Anseth, K.S. Hydrogels as Extracellular Matrix Mimics for 3d Cell Culture. *Biotechnol Bioeng*. (2009); **103**(4):655-63.

[461] Seliktar, D., Zisch, A.H., Lutolf, M.P., Wrana, J.L., and Hubbell, J.A. Mmp-2 Sensitive, Vegf-Bearing Bioactive Hydrogels for Promotion of Vascular Healing. *J Biomed Mater Res A*. (2004); **68**(4):704-16.

[462] Ehrbar, M., Rizzi, S.C., Schoenmakers, R.G., Miguel, B.S., Hubbell, J.A., Weber, F.E., and Lutolf, M.P. Biomolecular Hydrogels Formed and Degraded Via Site-Specific Enzymatic Reactions. *Biomacromolecules*. (2007); **8**(10):3000-7.

[463] Sala, A., Hanseler, P., Ranga, A., Lutolf, M.P., Voros, J., Ehrbar, M., and Weber, F.E. Engineering 3d Cell Instructive Microenvironments by Rational Assembly of Artificial Extracellular Matrices and Cell Patterning. *Integr Biol (Camb)*. (2011); **3**(11):1102-11.

[464] Raeber, G.P., Lutolf, M.P., and Hubbell, J.A. Molecularly Engineered Peg Hydrogels: A Novel Model System for Proteolytically Mediated Cell Migration. *Biophys J*. (2005); **89**(2):1374-88.

[465] Brandl, F., Sommer, F., and Goepferich, A. Rational Design of Hydrogels for Tissue Engineering: Impact of Physical Factors on Cell Behavior. *Biomaterials*. (2007); **28**(2):134-46.

[466] Bernfield, M., Gotte, M., Park, P.W., Reizes, O., Fitzgerald, M.L., Lincecum, J., and Zako, M. Functions of Cell Surface Heparan Sulfate Proteoglycans. *Annu Rev Biochem*. (1999); **68**:729-77.

[467] Bryant, S.J., Arthur, J.A., and Anseth, K.S. Incorporation of Tissue-Specific Molecules Alters Chondrocyte Metabolism and Gene Expression in Photocrosslinked Hydrogels. *Acta Biomater*. (2005); **1**(2):243-52.

[468] Nie, T., Baldwin, A., Yamaguchi, N., and Kiick, K.L. Production of Heparin-Functionalized Hydrogels for the Development of Responsive and Controlled Growth Factor Delivery Systems. *J Control Release*. (2007); **122**(3):287-96.

[469] Elia, R., Fuegy, P.W., VanDelden, A., Firpo, M.A., Prestwich, G.D., and Peattie, R.A. Stimulation of in Vivo Angiogenesis by in Situ Crosslinked, Dual Growth Factor-Loaded, Glycosaminoglycan Hydrogels. *Biomaterials*. (2010); **31**(17):4630-8.

[470] Cai, S., Liu, Y., Zheng Shu, X., and Prestwich, G.D. Injectable Glycosaminoglycan Hydrogels for Controlled Release of Human Basic Fibroblast Growth Factor. *Biomaterials*. (2005); **26**(30):6054-67.

[471] Lim, J.J., Hammoudi, T.M., Bratt-Leal, A.M., Hamilton, S.K., Kepple, K.L., Bloodworth, N.C., McDevitt, T.C., and Temenoff, J.S. Development of Nano- and Microscale Chondroitin Sulfate Particles for Controlled Growth Factor Delivery. *Acta Biomater*. (2011); **7**(3):986-95.

[472] Lutolf, M.P., and Blau, H.M. Artificial Stem Cell Niches. *Advanced materials (Deerfield Beach, Fla)*. (2009); **21**(32-33):3255-68.

[473] Giavedoni, L.D. Simultaneous Detection of Multiple Cytokines and Chemokines from Nonhuman Primates Using Luminex Technology. *J Immunol Methods*. (2005); **301**(1-2):89-101.

[474] Liu, M.Y., Xydakis, A.M., Hoogeveen, R.C., Jones, P.H., Smith, E.O., Nelson, K.W., and Ballantyne, C.M. Multiplexed Analysis of Biomarkers Related to Obesity and the Metabolic Syndrome in Human Plasma, Using the Luminex-100 System. *Clin Chem*. (2005); **51**(7):1102-9.

[475] Lau, K.S., Juchheim, A.M., Cavaliere, K.R., Philips, S.R., Lauffenburger, D.a., and Haigis, K.M. In Vivo Systems Analysis Identifies Spatial and Temporal Aspects of the Modulation of Tnf-A-Induced Apoptosis and Proliferation by Mapks. *Science signaling*. (2011); **4**(165):ra16-ra16.

[476] Holmes, E., Wilson, I.D., and Nicholson, J.K. Metabolic Phenotyping in Health and Disease. *Cell*. (2008); **134**(5):714-7.

[477] Rinker, T., Hamilton, S.K., Bloodworth, N.C., Hammoudi, T.M., Massad, C.S., Lu, H., and Temenoff, J. Enzyme Degradable Glues for Temporal and Spatial Control in 3d Culture Systems. Biomedical Engineering Society 2012 Annual Meeting. Atlanta, GA2012.

[478] Doyle, J.C., and Csete, M. Architecture, Constraints, and Behavior. *Proc Natl Acad Sci U S A*. (2011); **108 Suppl 3**:15624-30.

[479] Doyle, J., and Csete, M. Motifs, Control, and Stability. *PLoS Biol*. (2005); **3**(11):e392.

[480] Jeon, O., Alt, D.S., Ahmed, S.M., and Alsberg, E. The Effect of Oxidation on the Degradation of Photocrosslinkable Alginate Hydrogels. *Biomaterials*. (2012); **33**(13):3503-14.

[481] Jeon, O., Powell, C., Ahmed, S.M., and Alsberg, E. Biodegradable, Photocrosslinked Alginate Hydrogels with Independently Tailorable Physical Properties and Cell Adhesivity. *Tissue Eng Part A*. (2010); **16**(9):2915-25.

[482] Jeon, O., Bouhadir, K.H., Mansour, J.M., and Alsberg, E. Photocrosslinked Alginate Hydrogels with Tunable Biodegradation Rates and Mechanical Properties. *Biomaterials*. (2009); **30**(14):2724-34.

[483] Arnau, J., Lauritzen, C., Petersen, G.E., and Pedersen, J. Current Strategies for the Use of Affinity Tags and Tag Removal for the Purification of Recombinant Proteins. *Protein expression and purification*. (2006); **48**(1):1-13.

[484] Burton, J. Substrate Analog Inhibitors of Highly Specific Proteases. *Conformationally Directed Drug Design; ACS Symposium Series*. (1984).

[485] Carter, P. Site-Specific Proteolysis of Fusion Proteins. 427 ed: ACS Publications. p. 181-93.

[486] Li, Y. Self-Cleaving Fusion Tags for Recombinant Protein Production. *Biotechnology letters*. (2011); **33**(5):869-81.

[487] Terpe, K. Overview of Tag Protein Fusions: From Molecular and Biochemical Fundamentals to Commercial Systems. *Applied microbiology and biotechnology*. (2003); **60**(5):523-33.

[488] Yang, P.J. Incorporation of Protease-Sensitive Biomaterial Degradation and Tensile Strain for Applications in Ligament-Bone Interface Tissue Engineering. Atlanta, GA: Georgia Institute of Technology; 2011.

[489] Roh, J.D., Kacena, M.A., Lopz-Soler, R.I., Coady, C.E., Troiano, N.W., and Breuer, C.K. Glycolmethacrylate Is Superior to Methylmethacrylate for Histologic Evaluation of Biodegradable Polymer Scaffolds Used for Vascular Tissue Engineering. *J Histotechnol*. (2006); **29**(4):245-52.

[490] James, R., Jenkins, L., Ellis, S.E., and Burg, K.J.L. Histological Processing of Hydrogel Scaffolds for Tissue-Engineering Applications. *J Histotechnol*. (2004); **27**(2):133-40.

[491] Webster, S.S., Jenkins, L., and Burg, K.J.L. Histological Techniques for Porous, Absorbable, Polymeric Scaffolds Used in Tissue Engineering. *J Histotechnol*. (2003); **26**(1):57-66.

[492] Ferri, G.L., Cocco, C., Melis, G.V., and Aste, L. Equipment Testing and Tuning: The Cold-Knife Cryomicrotome Microm Hm-560. *Appl Immunohistochem Mol Morphol*. (2002); **10**(4):381-6.

[493] Cocco, C., Melis, G.V., and Ferri, G.L. Embedding Media for Cryomicrotomy: An Applicative Reappraisal. *Appl Immunohistochem Mol Morphol*. (2003); **11**(3):274-80.

[494] Eriksson, L., Johansson, E., Kettaneh-Wold, N., Trygg, J., Wikstrom, C., and Wold, S. *Multi- and Megavariate Data Analysis. Part Ii: Advanced Applications and Method Extensions*. 2nd ed. Umea, Sweden: Umetrics AB; 2006.